# CVR JOURNAL OF SCIENCE AND TECHNOLOGY

Vol.No. 19, December 2020
P-ISSN 2277 - 3916

DOI 10.32377/CVRJST19
E-ISSN 2581 - 7957

CVR COLLEGE OF ENGINEERING

In Pursuit of Excellence

PATRONS

***Dr. Raghava V. Cherabuddi, President & Chairman***

***Dr. K. Rama Sastri, Director***

***Dr. K.S. Nayanathara, Principal***

***Editor*** : **Dr. K. Lal Kishore, Professor and Dean - Research, CVRCE**

***Associate Editor*** : **Dr. S. Venkateshwarlu, Professor & Head, Dept. of EEE, CVRCE**

***Technical support*** : **Mr. K. Veeranjaneyulu, Asst. Prof., Dept. of CSE, CVRCE**

***Editorial Board :***

| | |
|---|---|
| *Dr. M.V. Seshagiri Rao* | Professor & Dean-Planning & Coordination, CVRCE |
| *Prof. L.C. Siva Reddy* | Professor & Vice-Principal, CVRCE |
| *Dr. Rameshwar Rao* | Professor & Dean- Projects & Consultancy, CVRCE |
| *Dr. N.V. Rao* | Professor & Dean-Academics, CVRCE |
| *Dr. T. Muralidhara Rao* | Professor & Head, Dept. of Civil Engg., CVRCE |
| *Dr. A. Vani Vathsala* | Professor & Head, Dept. of CSE, CVRCE |
| *Dr. K. Lalithendra* | Professor & Head, Dept. of ECE, CVRCE |
| *Dr. S. Harivardhagini* | Professor & Head, Dept. of EIE, CVRCE |
| *Dr. Bipin Bihari Jayasingh* | Professor & Head, Dept. of IT, CVRCE |
| *Dr. M. Venkata Ramana* | Professor & Head, Dept. of Mech. Engg., CVRCE |
| *Dr. H.N. Lakshmi* | Professor & Head, Dept. of CSIT, CVRCE |
| *Dr. G. Bikshamaiah* | Professor & Head, Dept. of H&S, CVRCE |

***International Review Board:***

| | |
|---|---|
| *Prof. Tzung-Pei Hong* | Chair Professor, Dept. of CSI Engg., AI Research Center National University of Kaohsiung 811, Taiwan |
| *Dr. Tomonobu Senjyu* | Professor, Department of Electrical Engineering, University of the Ryukyus, Nishihara-cho, Nakagami Okinawa, Japan |
| *Dr. Masoud Mohammadian* | Assoc. Professor, Faculty of Science and Technology, University of Canberra, Australia |
| *Dr. Rubén Ruiz García* | Full Professor, Head of the Applied Optimization Systems Group, Department of Applied Statistics, Universitat Politècnica de València, Camino de Vera, Spain |
| *Dr. Ray-Hwa Wong* | Professor, Department of Mech. Engg., Hwa-Hsia University of Technology, Taipei, Taiwan |
| *Dr. Stefan Talu* | Faculty of Mech. Engineering, DMCDI, The Technical University of Cluj-Napoca, B-dul Muncii Street, No. 103-105, Cluj-Napoca, 400641, Romania |
| *Assoc. Prof. Ir. Dr. Norhaliza Abdul Wahab* | Director, Control & Mechatronics Engg. Dept., Faculty of Electrical Engineering, UTM Skudai 81310 Johor |
| *Dr. R. Venkata Rao* | Professor, Department of Mech Engg., Sardar Vallabhbhai National Institute of Technology (SVNIT), Surat, Gujarat State – 395 007, India |
| *Dr. Vijay Janyani* | Professor Dept. of ECE, Malaviya National Institute of Technology (MNIT), Jaipur - 302017 (Rajasthan) |
| *Dr. V. Prasanna Venkatesan* | Prof. & Head, Department of Banking Technology, School of Management, R.V.Nagar, Kalapet, Pondicherry University, Puducherry |

# CVR JOURNAL OF SCIENCE AND TECHNOLOGY

## Indexed by

- Google Scholar
- Directory of Research Journals Indexing (DRJI)
- Scientific Indexing Services (SIS)
- International Institute of Organised Research (I2OR)
- Scholar Impact - Journal Index
- Citefactor
- Member Crossref / DOI

***NIRF Ranking of 141 in the Country***

**Accredited by NAAC with 'A' GRADE**


## CVR COLLEGE OF ENGINEERING

(UGC Autonomous - Affiliated to JNTU Hyderabad)
Mangalpalli (V), Ibrahimpatnam (M),
R.R. District, Telangana. – 501510
http://cvr.ac.in

# EDITORIAL

It is with immense pleasure that we bring out Volume-19 of the Bi-annual CVR Journal of Science and Technology, due in December 2020. We could bring out this Volume without any delay, despite the educational institutions being closed down, for a long time, due to COVID-19 Pandemic. Normal functioning is not yet restored even now. Teaching and Research works are badly affected due to Corona Virus. Teaching is being done on-line, which has its own disadvantages. Some practical classes are to be conducted in virtual mode. This will have its own impact on quality of education.

New academic year 2020-21 has begun under these circumstances. With all such constraints, bringing out Volume-19 of CVR Journal in time was really a challenge. Editorial Team of CVR Journal thanks all the authors, contributors, reviewers and the management, for helping us, in bringing out Volume-19, with 25 research articles, in this difficult period. As all educational institutions were closed for a long time, authors and reviewers and all of us had many constraints. We have received less number of research articles this time, for selection. Hope normalcy will be restored soon.

This Volume covers research articles in the following disciplines:

**ECE – 6, EEE – 5, MECH – 9, CSE – 2, IT – 2, CIVIL – 1.**

This Volume has DOI number and e-ISSN number along with print ISSN number on the cover page. Every research article published is given DOI number and they can be accessed on-line. On-line portal is also created for the Journal. This Volume is also brought out in time, with the co-operation of all the authors and editorial team. We are thankful to the Management for supporting this activity, and permitting to publish the journal in color print, using quality printing paper.

In this issue, an interesting article on Man Machine Interface Design is published. One of the authors of this article is working as senior engineer in a reputed industry. Another article on Performance Evaluation of Switched Reluctance Motor in PV-fed Water Pump System is also published. The article on Memetic Particle Gravitation Optimization related to Wireless Networks must make interest reading. Research article on Parametric optimization of submerged arc welding using Taguchi method on P91 steel is also included in the articles. Total of 25 research articles are published in this issue. Hope these articles will generate lot of interest among researchers. Some authors from this college are collaborating with faculty of other institutions and publishing research articles.

I am thankful to all the members of the Editorial Board for their help in reviewing and short listing the research papers for inclusion in the current Volume of the journal. I wish to thank Associate Editor **Dr. S. Venkateshwarlu, HOD, EEE** for the effort made in bringing out this Volume. Thanks are due to **HOD, H & S, Dr. G. Bhikshamaiah** and the staff of English Department for reviewing the papers. I am also thankful to **Smt. A. Sreedevi, DTP Operator** in the Office of Dean Research for the preparation of research papers in Camera - Ready form.

For further clarity on waveforms, graphs, circuit diagrams and figures, readers are requested to browse the soft copy of the journal, available on the college website www.cvr.ac.in wherein a link is provided. Authors can also submit their papers through our online open journal system (OJS) www.ojs.cvr.ac.in or www.cvr.ac.in/ojs.

**Prof. K. Lal Kishore**
**Editor**

**International Review Board:**

## CONTENTS

Page No.

E-ISSN 2581 - 7957
P-ISSN 2277 - 3916

CVR Journal of Science and Technology, Volume 19, December 2020
DOI: 10.32377/cvrjst 1901

# Analysis of Switching Losses in Multilevel Cascaded H-bridge and Diode-Clamped Inverter

P. Vinod Kumar[1] and Dr. S. Venkateshwarlu[2]
[1]Assoc. Professor, CVR College of Engineering/EEE Department, Hyderabad, India
Email: p.vinodkumar@cvr.ac.in
[2]Professor, CVR College of Engineering/EEE Department, Hyderabad, India
Email: svip123@gmail.com

***Abstract:*** **Conventional two-level pulse width modulation (PWM) inverters provide good voltage and current output waveforms at the cost of high switching losses during higher frequency operations. Multilevel inverters have emerged very fast as an alternative for medium and high voltage applications. This paper presents the analysis of switching losses estimation of a nine-level cascaded H-bridge and five-level diode-clamped inverter at different switching frequencies. The analysis is also extended to find the comparison of total harmonic distortion (THD) of sine pulse width modulation (SPWM) of currents at different load power factors of cascaded H-bridge and diode-clamped multilevel inverters. This analysis can help in deciding the proper inverter based on the power ratings and area of application. As inverter plays important role in Electric Vehicles, Hybrid Electric Vehicles and Renewable Energy sources, this analysis helps in selecting the better inverter topologies with reduced switching losses.**

***Index Terms:*** **Diode-Clamped Multilevel Inverter (DCMLI), Cascaded H-Bridge Inverter (CHBI), Switching Losses, Total Harmonic Distortion (THD).**

## I. Introduction

The demand for multilevel inverters in medium and high-power applications is increasing very fast. They provide high power and voltage with improved power quality. The advancing technology needs high power rating power electronic devices with good power quality. The conventional power electronic circuit can be able to switch input and output only between two possible voltage levels, especially with DC supply. Multilevel inverters are designed to generate a sinusoidal voltage from DC input which can be split into several DC voltages using capacitors. There are three different types of topologies of multilevel inverters. The cascaded H-bridge, capacitor-clamped and diode-clamped multilevel inverters. The main aim of this topology of the multilevel inverter is to produce output waveform with less harmonic distortions without decreasing the power output and switching frequency. The number of levels of the output voltage of the multilevel inverter depends on the input DC sources. THD value decreases as the number of levels of the inverter increases. In a two-level inverter, the output voltage is produced using pulse width modulation [1]-[2]. The output voltage and current of a two-level inverter contains a lot of harmonic distortions, which decreases the quality of the output waveform. In a three-level inverter the THD of the output waveforms decreases compared to two-level inverter. This makes the use of multilevel inverters, which gives the better output voltage and currents with less THD as the levels of the inverter increases. The switching stress also decreases as the level of the inverter increases. The need of filters can be reduced by going for higher levels of the inverter with high switching frequencies. However, this will create another problem, the switching losses of the switches which decrease the circuit efficiency [3]-[4]. As the level increases the number of switches in each leg increases and as to get good output without filters the circuit should be operated at higher switching frequencies. This can be reduced by going for good modulation techniques. In this paper, analysis of switching losses for nine-level cascaded H-bridge multilevel inverter and five-level diode-clamped inverter is done with different switching frequencies. Single phase Nine-level cascaded H-bridge and five-level diode-clamped inverter contains same number of switches. As the analysis will be done on single phase inverter, the five level DCMLI can be considered as nine level inverter. The intention is to study the losses with same number of switches in both the inverters. This helps to compare the performance of inverters in switching stress perspective [5]-[6]. Sine pulse width modulation is used for the analysis. Section-II of the paper gives the details of nine-level cascaded H-bridge and five-level diode-clamped inverter. Section-III gives the details of sine PWM. Section-IV gives the details of the switching losses. Section-V gives the details of results and analysis.

## II. Cascaded & Diode-Clamped Inverters

### *A. Cascaded H-Bridge Inverter (Nine Level)*

Cascaded H-bridge multilevel inverter is developed using a full bridge circuit in series connection depending on the number of levels. Four full bridge cells are connected in series to get output as nine-levels. Nine-level cascaded inverter is shown in Figure 1.

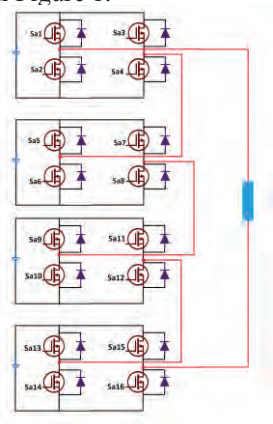

Figure 1. Nine – level CHBI

E-ISSN 2581 - 7957
P-ISSN 2277 - 3916

CVR Journal of Science and Technology, Volume 19, December 2020
DOI: 10.32377/cvrjst 1901

Cascaded H-bridge multilevel inverters are more flexible in selecting switching states compared to other types of inverters. Each bridge contains four switches, in one leg, it contains 2 switches. Four number of DC sources are needed to get a nine-level output. Sine PWM is used in generating switching pulses. Switching states of IGBTs are shown in Table 1.

TABLE I.
SWITCHING TABLE OF NINE LEVEL CHBI

| Output Voltage | Active switches |
|---|---|
| 4V | 13, 16, 12, 8, 4, 9, 5, 1 |
| 3V | 13, 16, 12, 8, 4, 9, 5 |
| 2V | 13, 16, 12, 8, 4, 9 |
| V | 13, 16, 12, 8, 4 |
| 0 | --------- |
| -V | 14, 15, 10, 6, 2 |
| -2V | 14, 15, 10, 6, 2, 11 |
| -3V | 14, 15, 10, 6, 2, 11, 7 |
| -4V | 14, 15, 10, 6, 2, 11, 7, 3 |

### *B. Diode-Clamped Multilevel Inverter (Five level)*

Five-level diode-clamped inverter is shown in the Figure 2. Each leg of the inverter contains 8 switches. Four capacitors are needed to divide the input DC supply to get five levels in the output voltage. But here four separate DC sources are considered like in case of cascaded H-bridge topology. Each leg contains clamping diodes for freewheeling action. The voltage across each device is V, and the total voltage across the leg is 4 times V.

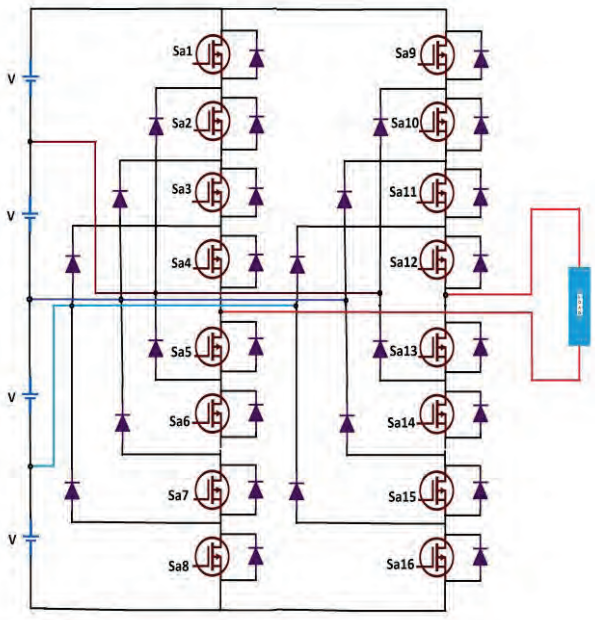


Figure 2. Five-level DCMLI

TABLE II.
SWITCHING TABLE OF FIVE LEVEL DCMLI

| Output Voltage ($V_{an}$) | $Sa_1$ | $Sa_2$ | $Sa_3$ | $Sa_4$ | $Sa_5$ | $Sa_6$ | $Sa_7$ | $Sa_8$ |
|---|---|---|---|---|---|---|---|---|
| 2V | 1 | 1 | 1 | 1 | 0 | 0 | 0 | 0 |
| V | 0 | 1 | 1 | 1 | 1 | 0 | 0 | 0 |
| 0 | 0 | 0 | 1 | 1 | 1 | 1 | 0 | 0 |
| -V | 0 | 0 | 0 | 1 | 1 | 1 | 1 | 0 |
| -2V | 0 | 0 | 0 | 0 | 1 | 1 | 1 | 1 |

## III. SINUSOIDAL PULSE WIDTH MODULATION

Sinusoidal pulse width modulation is used for inverters for generating pulses for the switches. This modulation technique compares reference sine wave with the higher frequency triangular carrier waves. Depending upon the level of the inverter, no of carrier waves required will change. In a five-level inverter generally four carrier waves are required to generate pulses to the switches and to produce five-level output. When the sine wave magnitude is greater than carrier wave, then the upper switch will be ON and when the sine wave is having lesser magnitude than carrier then the lower switch will be ON. This makes the inverter get different level in the output. Over a period of one triangular wave, the average voltage applied to the load is equal to the sine wave amplitude during this period. The modulation index is given as m=Am/Ac, where Am is the amplitude of sinusoidal wave, Ac is the amplitude of the carrier wave. By controlling the modulation index, the magnitude of the output voltage can be controlled. Higher switching frequencies produces larger switching losses, typical switching frequencies consider for power system applications are 2-15 kHz. Figure 3. shows the peak to peak nine-level inverter output waveform.

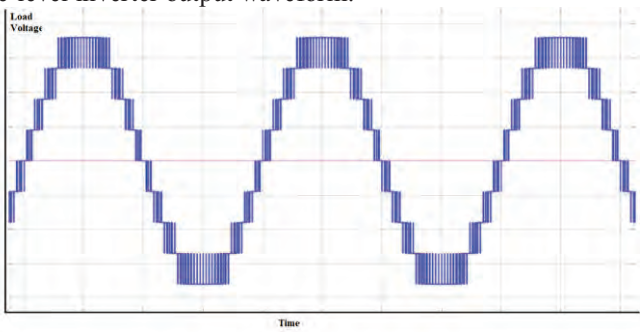


Figure 3. Nine level voltage waveform

## IV. CONDUCTION & SWITCHING LOSS CALCULATION

The total losses consist of conduction loss and the switching loss. Switching loss becomes more dominant at high frequencies. Conduction losses are directly proportional to the load current.

Conduction losses occur in the switches and the anti-parallel diodes. Conduction loss in the switches can be calculated using equation (1), and conduction loss in anti-parallel diodes can be calculated using equation 2.

$$W_{cs} = U_{CEo} * I_{Cav} + r_c * I^2_{Crms} \quad (1)$$

$$W_{cd} = U_{Do} * I_{Dav} + r_D * I^2_{Drms} \quad (2)$$

Where

$U_{CE0}$ : On state zero current collector emitter voltage
$I_{Cav}$ : Average switch current
$R_c$ : Collector emitter on state resistance
$I_{Crms}$ : RMS switch current
$U_{D0}$ : Diode approximation with a series conduction of DC voltage sources
$I_{Dav}$ : average diode current
$r_D$ : Diode on-state resistance
$I_{Drms}$ : RMS diode current

E-ISSN 2581 - 7957
P-ISSN 2277 - 3916


DOI: 10.32377/cvrjst 1901

Switching losses will occur in the switches and the anti-parallel diodes. The switching losses in the switch can be calculated using equation 3. And the switching losses in the anti-parallel diodes can be calculated using equation 4.

$$W_{SwS} = \left(E_{onSw} + E_{offsw}\right) * f_{sw} \quad (3)$$

$$W_{SwD} = \left(E_{onD} + E_{offD}\right) * f_{sw} \approx E_{onD} * f_{sw} \quad (4)$$

Where

$E_{onSw}$ : turn - on energy losses in Switch
$E_{offsw}$ : turn - off energy losses in Switch
$E_{onD}$ : turn - on energy losses in diode
$E_{offD}$ : turn - off energy losses in diode
$F_{sw}$ : Switching frequency

## V. Results and Discussions

In this paper, analysis of conduction loss & switching loss is done for nine-level cascaded H-bridge inverter and five-level diode-clamped inverter. To simulate the switching losses, a modified half bridge module is taken from Simulink. Thermal model of IGBT-diode and a simscape based heatsink are considered for switching loss analysis [7]. IGBT module no: 5SNE_0800M170100 is considered for half bridge module [8]. The thermal model of IGBT-diode is shown in figure 4. The thermal capacitance of the switch and switch to heatsink resistance are also included in the simulation. The heatsink simscape model is shown in the figure 5. The turn on loss is calculated using voltage before switching and current after switching along with the temperature at junction. The turn off loss is calculated using the current before switching and the voltage after switching along with junction temperature. Conduction losses are calculated using the saturation voltage across collector and emitter multiplied with collector current. This process of simulation of losses was done based on the lookup table taken from the MATLAB sources [7]. The analysis has been carried out at different switching frequencies such as 500 Hz, 1000 Hz, 2000 Hz and 5000 Hz. In both the inverter simulations the same number of switches and DC sources are used. The load is also common in both the cases. Simulation studies have been carried out with the specifications given in the table 3.

TABLE III.
Specifications of Simulink Model

| | |
|---|---|
| DC voltage | 1800 V x 4 sources |
| Load Power factor | 0.9 lag and 0.5 lag |
| Power | 250 KW |
| Load voltage | 5000 V - RMS |

This paper mainly concentrates on the switching performance of the two inverters while driving similar loads with the same number of switches. The levels of inverter are chosen in such a way that both should use same number of DC sources with same voltage in two cases.

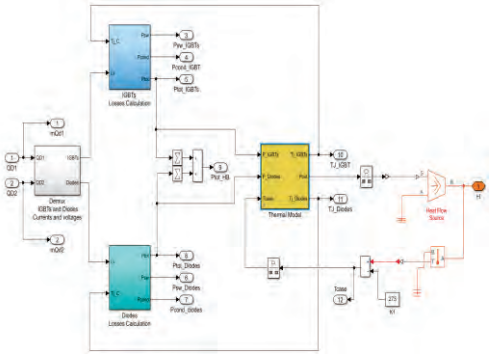

Figure 4. Thermel model of half bridge with IGBTs and diodes

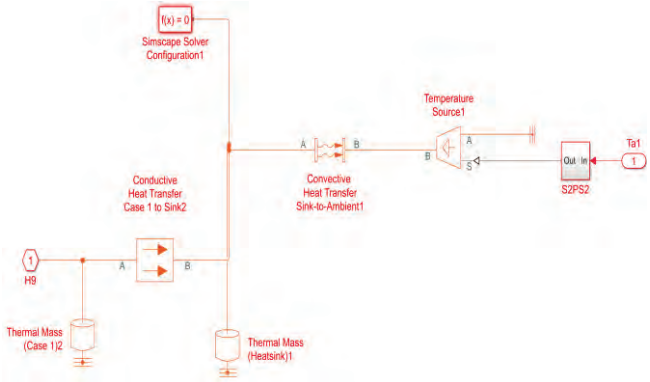


Figure 5. Simscape model of heatsink for half bridge (Two IGBTs)

### A. Nine-level Cascaded H-bridge Inverter

Nine-level cascaded H-bridge inverter is tested with sine pulse width modulation at different switching frequencies and the losses are calculated. Figure 6, Figure 7, Figure 8, and Figure 9 give the switching, conduction and total switch losses of CHB five-level inverter at 500Hz, 1000 Hz, 2000 Hz and 5000 Hz. Throughout the simulation the conduction losses remain same as the load considered here is constant. The switching losses are proportionally increasing as the switching frequencies increases. At higher frequencies, the conduction losses appear to be negligible. Figure 10 gives the graph between switching frequencies and the switching losses. Figure 11 gives the graph between switching frequencies and the Voltage THD. Figure 12 gives the graph between modulation index and the load voltage.

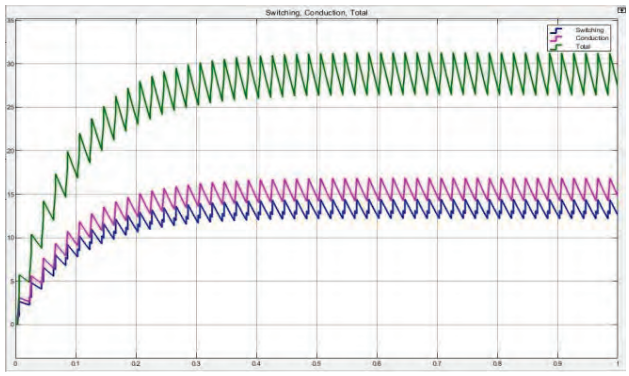


Figure 6. Losses Estimation of CHBI at 500Hz

E-ISSN 2581 - 7957
P-ISSN 2277 - 3916

CVR Journal of Science and Technology, Volume 19, December 2020
DOI: 10.32377/cvrjst 1901

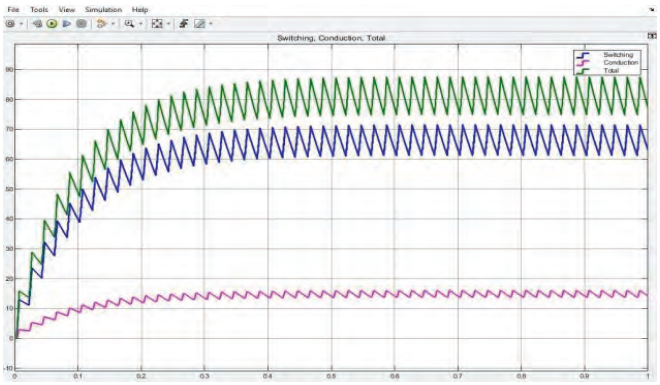


Figure 7. Losses Estimation of CHBI at 1000Hz

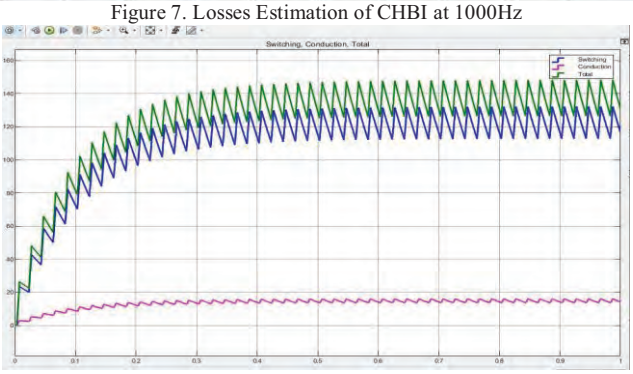


Figure 8. Losses Estimation of CHBI at 2000Hz

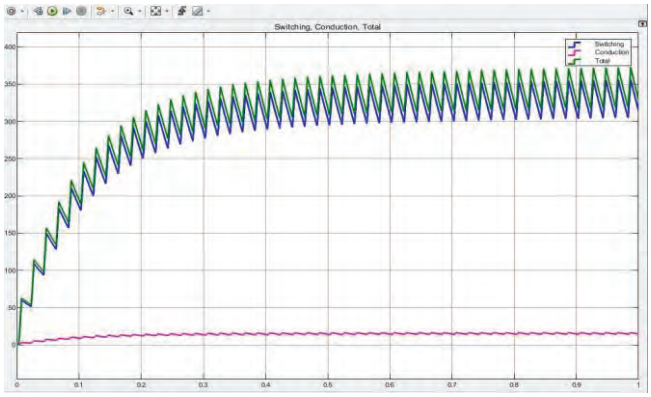


Figure 9. Losses Estimation of CHBI at 5000Hz

A similar analysis is made with 0.5 lagging load and the results are shown in the figures 10, 11 and 12. The orange color curve represents 0.5 lagging load and blue color curve represnets 0.9 lagging load.


Figure 10. Switching frequency verses switching loss for CHBI

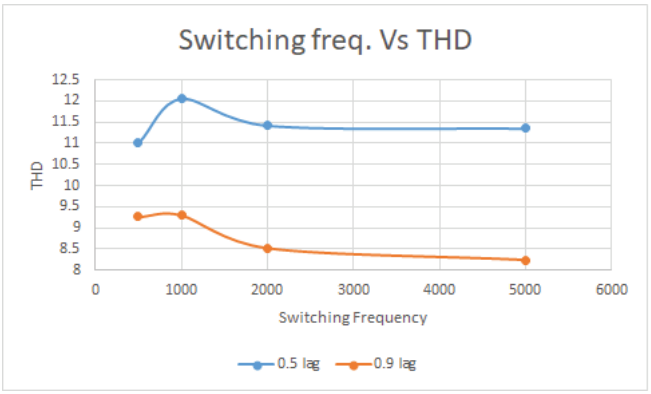


Figure 11. Swtiching frequency verses TDH of CHBI

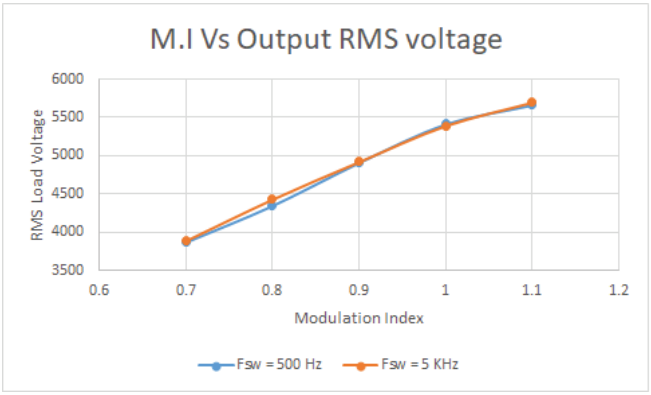


Figure 12. Modulaiton Index verses output RMS voltage of CHBI

## *B. Five-level Diode-Clamped Inverter*

Five-level diode-clamped inverter is tested with sine pulse width modulation at different switching frequencies and the losses are calculated. Figure 13, Figure 14, Figure 15, and Figure 16 gives the switching and conduction losses of diode-clamped five-level inverter at 500Hz, 1000 Hz, 2000 Hz and 5000 Hz. Figure 17 gives the graph between switching frequencies and the switching losses. Figure 18 gives the graph between switching frequencies and the Voltage THD. Figure 19 gives the graph between the modulation index and the RMS voltage.

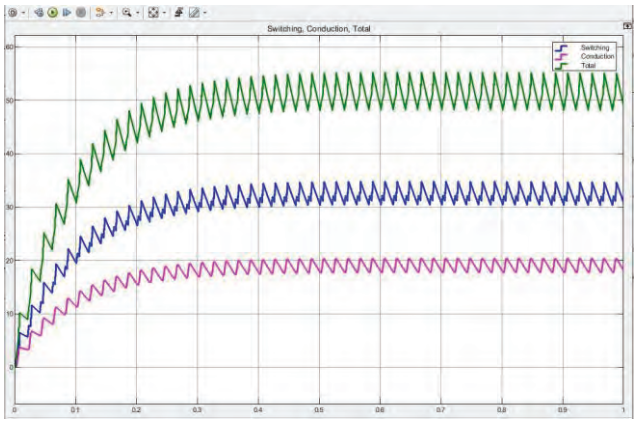


Figure 13. Losses Estimation of DCMLI at 500Hz

E-ISSN 2581 - 7957
P-ISSN 2277 - 3916

CVR Journal of Science and Technology, Volume 19, December 2020
DOI: 10.32377/cvrjst 1901

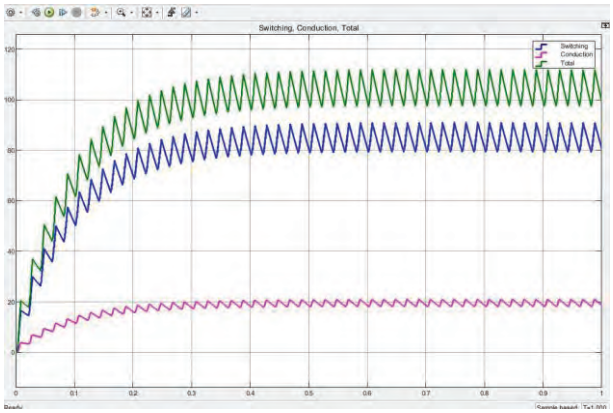


Figure 14. Losses Estimation of DCMLI at 1000 Hz

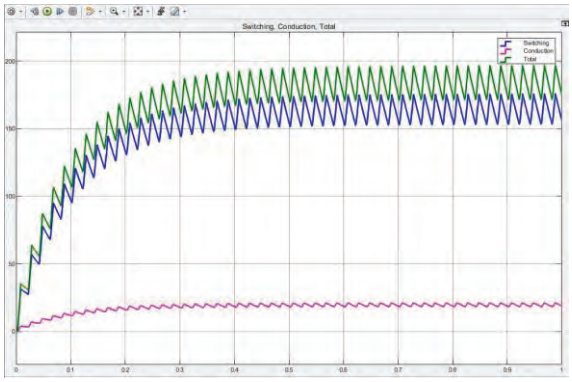


Figure 15. Losses Estimation of DCMLI at 2000 Hz

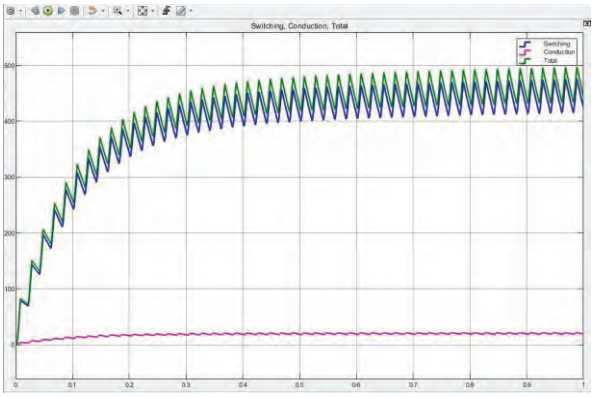


Figure 16. Losses Estimation of DCMLI at 5000 Hz


Figure 17. Switching frequency verses switching loss for DCMLI

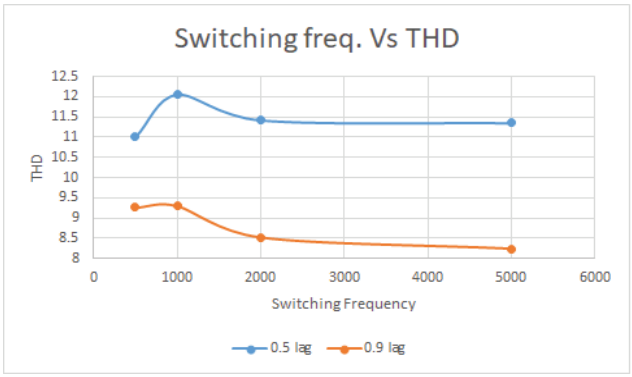


Figure 18. Swtiching frequency verses THD for DCMLI

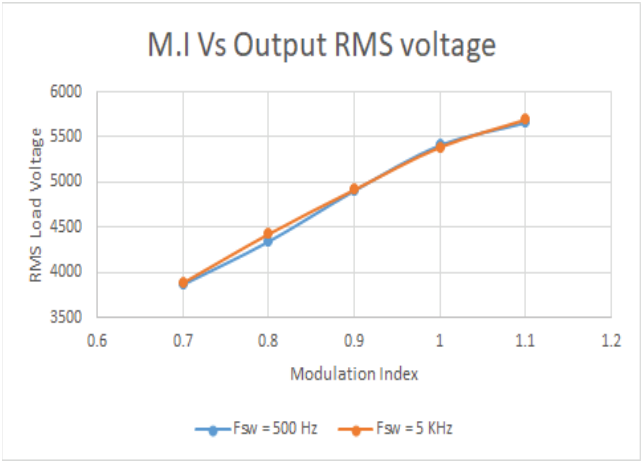


Figure 19. Modualtion index verses output voltage for DCMLI

### *C. Comparison of CHBI and DCMLI performacnce*

The comparison of CHBI and DCMLI inverters are presented here. The switching losses in DCMLI are almost 40 % higher than CHBI driving 0.9 lagging load with same DC voltage sources. Figure 20 shows the loss drop in CHBI operation.

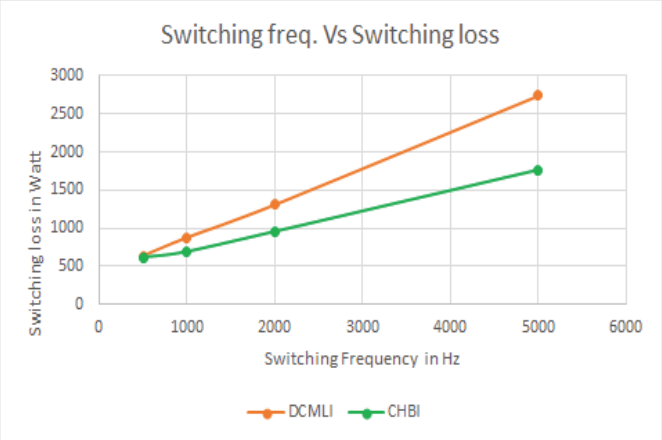


Figure 20. Loss drop in DCML inverter operation

The effect of switching frequencies over individual inverter THDs is almost constant. But when compared both

performances, THD is 90% more in CHBI. Figure 21 shows the THD Vs switching frequencies plot.

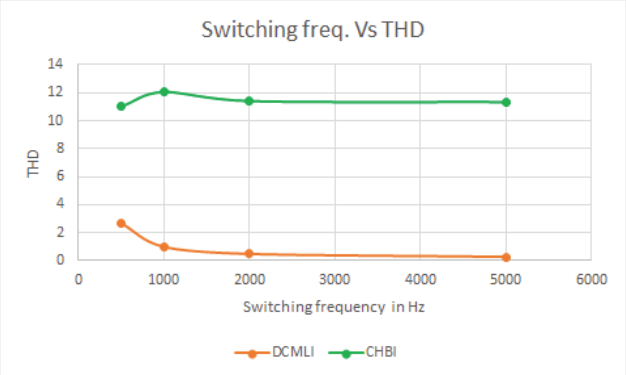


Figure 21. THD Vs Switching frequency for CHBI and DCMLI

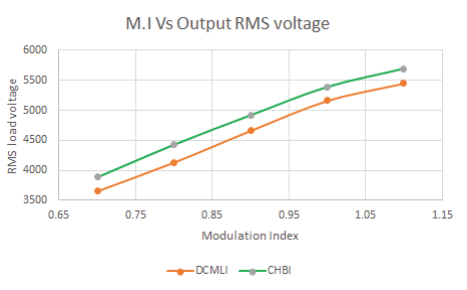


Figure 22. Load voltage Vs Mod. Index for CHBI & DCMLI

CHB Inverter produces more RMS voltage compared to DCML inverter. CHB inverter is delivering 12% more voltage to the load. Figure 22 shows the plot between modulation index Vs RMS load voltage. Switching losses occurred in CHBI and DCMLI while driving 250KW load with respect to the switching frequencies are given in the table 4.

TABLE IV.
SWITCHING LOSS COMPARISON TABLE

| Switching Frequency (Hz) | Switching Loss (W) | |
|---|---|---|
| | CHBI | DCMLI |
| 500 | 618 | 637 |
| 1000 | 696 | 877 |
| 2000 | 958 | 1311 |
| 5000 | 1765 | 2747 |

## VI. CONCLUSIONS

The main aim of this paper was to determine the losses in cascaded H-bridge inverter and diode-clamped inverter circuit in which each circuit has the same number of switches. When same number of switches are there then it is easy to compare the losses in the circuit. This helps to go for methods to reduce losses and the application of each inverter in a particular circuit. The selection of the simscape thermal model of IGBT and heatsink helped a lot in finding the switching losses of the inverters. The simulation mainly emphasized on same number of switches delivering the same amount of power between similar source and load structures. It is observed that for 0.5 lagging and 0.9 lagging loads, the DCML inverter has more switching losses providing a quality sine wave with THD 2% in its current waveform. But the CHB inverter losses are 40% less than DCML inverter with 11% THD.

## REFERENCES

[1] A. Nabae, I. Takahashi and H.A. Kagi, “A New Neutral Point Clamped PWM inverter,” IEEE Trans. Industry Application, vol.IA-17, pp. 518-523, sep/oct 9181.
[2] J. Rodriguez, J. S. Lai, and F. Z. Peng, “Multilevel Inverter: A survey of Topologies controls and applications,” IEEE Trans. Industrial Electronics vol.49, no.4, pp. 724-738, Aug.2002.
[3] Mohan Ned, Undeland T.M and Robbins W.P, “Power electronics converters applications & Design,” John Wiley & Sons, Second Edition 2007.
[4] G. Bhuvaneswari & Nagaraju, “Multilevel inverters- A comparative study,” IETE Journal of Research, vol. 51, no.2, Mar-Apr. 2005, pp. 141-153.
[5] Mohammadreza Derakhshanfar, “Analysis of different topologies of multilevel inverters,” Master Thesis, Chalmers University of Technology, 2010.
[6] Akagi H, “Multilevel Converters Fundamental circuits & Systems,” Proceedings IEEEE, 2017, vol.105, pp. 2048-2065.
[7] Mathworks.com – Loss Calculation in a 3-Phase 3-Level Inverter Using SimPowerSystems and Simscape.
[8] http\\abb.com. IGBT Module 5SNE 0800M170100.

E-ISSN 2581 - 7957
P-ISSN 2277 - 3916

CVR Journal of Science and Technology, Volume 19, December 2020
DOI: 10.32377/cvrjst1902

# Performance Evaluation of Switched Reluctance Motor in PV-fed Water Pump System with Different Controllers

Dr. M. Lakshmi Swarupa[1] and R. Naveena Bhargavi[2]
[1]Professor, CVR College of Engineering/EEE Department., Hyderabad, India
swarupamalladi@gmail.com
[2]Assoc. Professor,CVR College of Engineering/EEE Department., Hyderabad, India
bhargavi.rn5@gmail.com

***Abstract:*** **The agricultural motors need a more precise control and simple operation to have wet fields and better irrigation systems. The PV driven SRM is considered in this paper because, the robust operation and versatile speed control methods are available for this motor. The closed loop control of the motor is also tested, and a comparative analysis has been done for various controllers applied to SRM and the performance characteristics have been analyzed. The results obtained in the PID controller, Fuzzy logic Controller, SMC controller and the hybrid Fuzzy – neural controller, the closed loop control are compared to the open loop control.**

***Index Terms*****: Switched Reluctance motor (SRM), Solar PV, PID controller, fuzzy controller fuzzy-neural controller, SMC controller, agricultural pumps.**

## I. INTRODUCTION

Our nation being predominantly agriculture based and irrigation centric, advancement of technology in this area will have a vast impact on the overall production of the Crop and the amount of water utilized for harvesting. Depending on the location of the field and the ground water availability, Water has to be provided as a supplement for proper growth of the plants in most of the cases [1]. Farmers make use of electric motor pumps to bring water from deep underground onto the surface. For many decades, induction motors are being used extensively for this purpose. With the advent of new machines, there are many efficient Motors available to use for irrigation. Switched reluctance Motors can deliver high torque, which can lift water and pump to the fields.

The construction of SRM is rugged and considered to be simple in construction. The cost is less and the reliability on the performance characteristics is high. The control part of the motor needs some switching techniques to be incorporated and there is a scope to develop new methods of control mechanisms. The sensor less control technique is more predominant. Hence it has been considered in the present paper.

Several control methods are available to minimize the ripple in torque of the motor, such as designing an optimal magnetic circuit and current control techniques. Based on the modelling of the machine, it can be seen that the torque control is different to the traditional methods used and has a range of control techniques and certain assumptions are made regarding the parameters considered for SRM.

The main power conversion is done from the reluctance power available in the motor to a useful mechanical using the salient pole construction. The lack of windings and magnets on the rotor makes it more rugged and simple in construction. The cost of this motor is less compared to the traditional squirrel cage induction motors, and the maintenance different Pulse Width Modulation techniques can be applied and obtain the required torque characteristics from the motor. The power drawn by this motor must come from the regional power distribution centers. But reliability of the power is very less in rural areas of the country. Hence there is a need of a standalone power supply.

The solar Photo Voltaic based power generation has been a boom to the agricultural sector and is being extensively used for water pumping. The problem is that the nature of power supply must meet the demands of input characteristics of SRM. The DC power developed must convert to AC using an inverter circuit and fed to SRM, The PV panel shall be mounted in such a way that the shadow of panel does not disrupt solar rays falling on the panel. The power generated is directly used by the motor instead of having a storage equipment.

In this paper, different control techniques are employed, and they are tested on the SRM to understand the performance characteristics. The paper is organized as follows: Section -2 deals with the mathematical modelling of SRM. The various technique used to control the performance of the parameters are presented in section – 3. Different controllers are also tested in the system, which are presented in section – 4. The MATLAB Simulink results are presented in section – 5, followed by conclusion and references used.

E-ISSN 2581 - 7957
P-ISSN 2277 - 3916

CVR Journal of Science and Technology, Volume 19, December 2020
DOI: 10.32377/cvrjst1902

## II. Modelling of Switched Reluctance Motor

The output of SRM which we are concerned here is the instantaneous torque, given in equation

$$T_i = \frac{\delta W^1}{\delta \theta} \quad (1)$$

where W1 is the co-energy defined in equation 2.

$$W^1 = \int_0^i \varphi . di \quad (2)$$

The relationship between the flux linkage and the current at the instant rotor position $\vartheta$ is a straight line whose slope is the instantaneous inductance L. Thus,

$$\psi = L * I \quad (3)$$

and

$$W^1 = \frac{1}{2} L i^2 \quad (4)$$

Therefore, the torque is given by equation 5.

$$T = \frac{1}{2} i^2 \frac{dL}{d\theta} \quad (5)$$

The voltage equation is integrated in the form and is given as

$$\varphi = \int (v - ri) dt \quad (6)$$

## III. Control Algorithms

### A. PID controller

The Proportional Integral and Derivative control is a traditional way of driving the system towards a target setpoint. In this paper, we are using the PID controller to make the motor operate at desired torque and speed values at given point of time. This is generally a closed loop control of the system. Ziegler and Nichols method is used in the paper to find the optimum point of operation.

### B. Fuzzy Controller

This technique to control the parameters of a system and optimize the operation of a system are considered here in the paper. The fuzzy membership function values are tuned by using neural network so that the output defuzzified value is in the expected range of the user. Here the PWM modulation index shall be optimally decided by the fuzzy logic controller.

### C. Sliding Mode Controller

To control a nonlinear system, which changes the dynamics fast, a discontinuous control signal is needed. This methodology is adopted to slide along the behavior of the system randomly and to find out the best possible point to operate the system at. It has a feedback mechanism to check its position in space and has information about the next step to move. In this paper, SMC is applied and compared with the other methods.

## IV. Simulation Models and Results

### A. Model of SRM

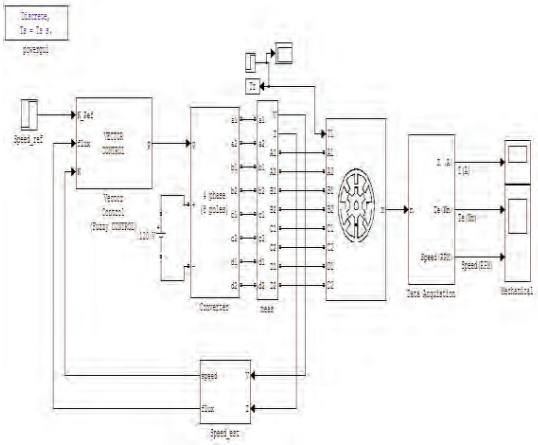

Figure 1. Simulation model of sensor less control

The SRM considered in the paper is a four phase 8 pole motor driven by a speed reference as a step function and also driven by a field excitation of 120V. The speed feedback is taken and vector-based control is implemented to have a sensor less control.

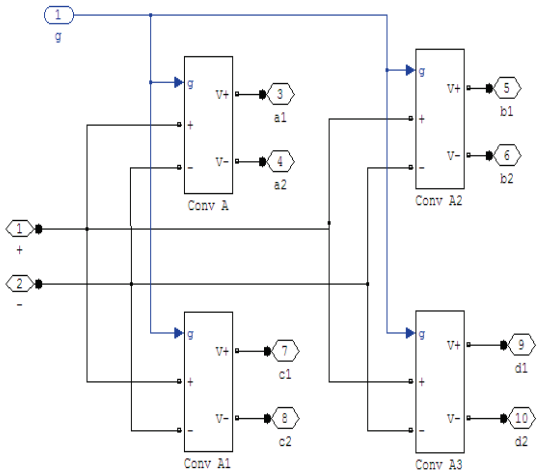


Figure 2. Converter control

E-ISSN 2581 - 7957
P-ISSN 2277 - 3916

CVR Journal of Science and Technology, Volume 19, December 2020
DOI: 10.32377/cvrjst1902

The converter used in the simulation is shown in figure 2.

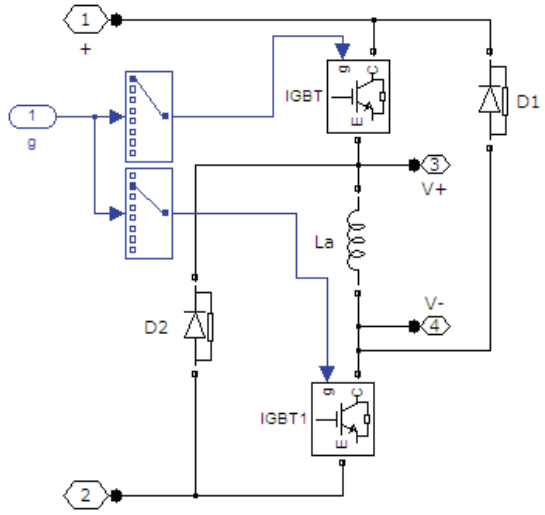


Figure 3. Subsystem of Bridge Rectifier

Figure 3 shows the circuit used for Bridge rectifier operation with IGBT as switches. A multi-port switch is connected to the gate terminals to provide specific outputs at specific points of rotations of shaft of motor.

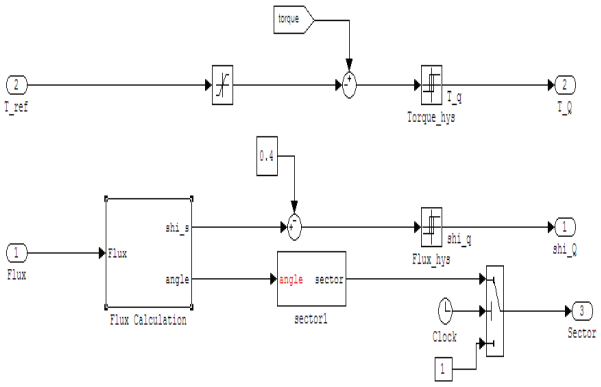


Figure 4. Subsystem of Mathematical Equations in Terms of Flux and Speed

The flux calculation along with torque of the motor helps in understanding the Q component of the torque and 'shi'. This is shown in figure 4. Figure 5 shows the flux equations to find out the angle of rotation of the shaft. This is expessed in polar format.

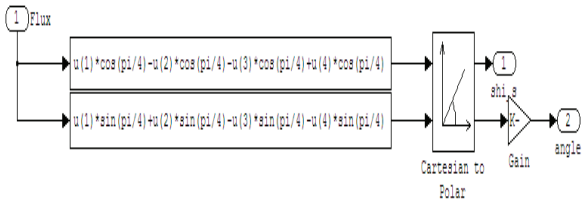


Figure 5. Equations of Flux in Polar (Angle) notation

## B. Without controller

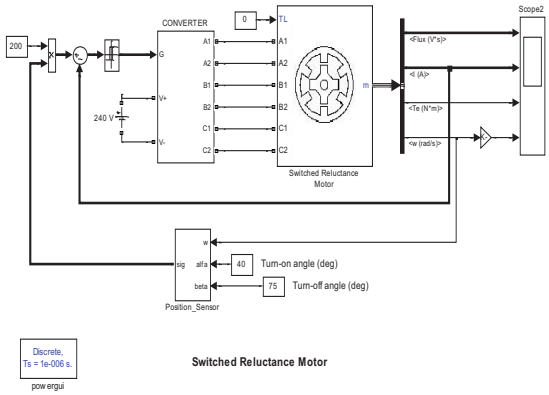


Figure 6. Simulation Model without Controller

The SRM considered in the paper without the feedback controller is shown in figure 6.

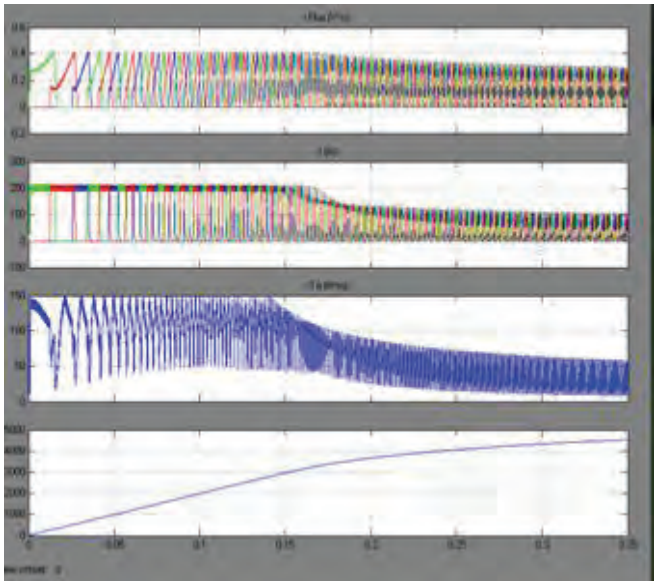

Figure 7. Flux (Wb), Current (Amps), Torque (N-M), Speed (Rpm) Versus Time (Secs) for NO Controller

Figure 7 shows that the speed of the motor is increasing significantly but is not controlled for settling at a finite value. After 0.15s, there is a certain shift in the response of torque and current.

## C. With PID controller

The error obtained due to uncontrolled operation can be overcome by introducing another controller called PID controller. The system considered is shown in figure 8, and the results obtained are shown in figure 9 respectively.

E-ISSN 2581 - 7957
P-ISSN 2277 - 3916

CVR Journal of Science and Technology, Volume 19, December 2020
DOI: 10.32377/cvrjst1902

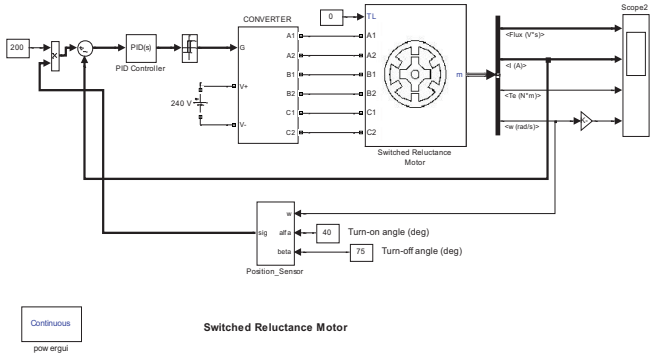


Figure 8. Simulation Model with PID Controller

The system is now tested with a fuzzy logic controller to control the speed and torque of the motor. The sample of fuzzy inference rules are shown in figure 10. There are three input and three outputs considered in the fuzzy controller. The schematic of the same is shown in figure 11.

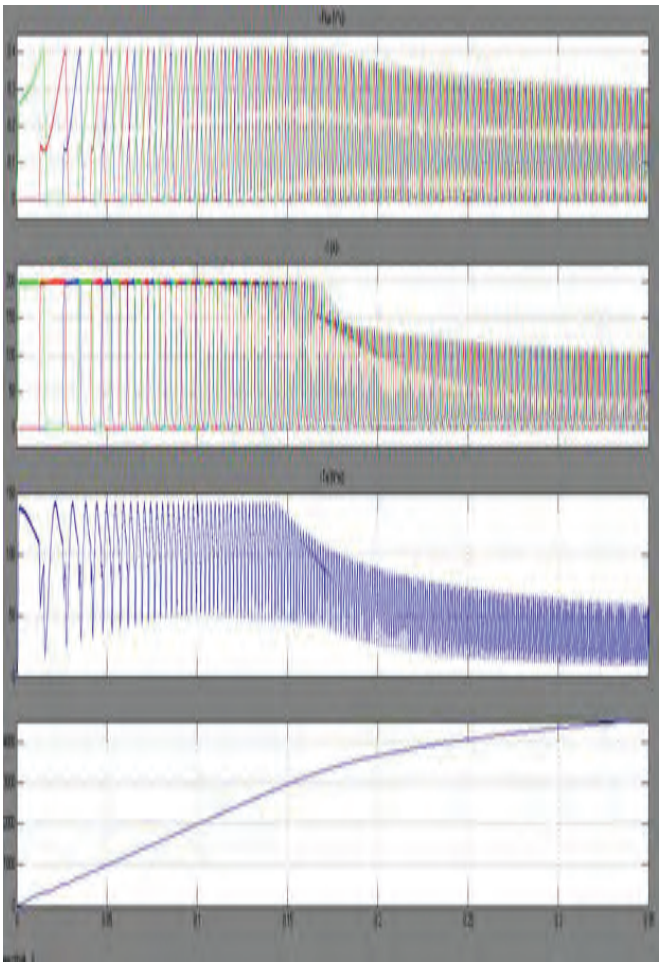

Figure 9. Flux (Wb), Current (Amps), Torque (N-M), Speed (Rpm) Versus Time (Secs) with PID Controller

### *D. With FLC*

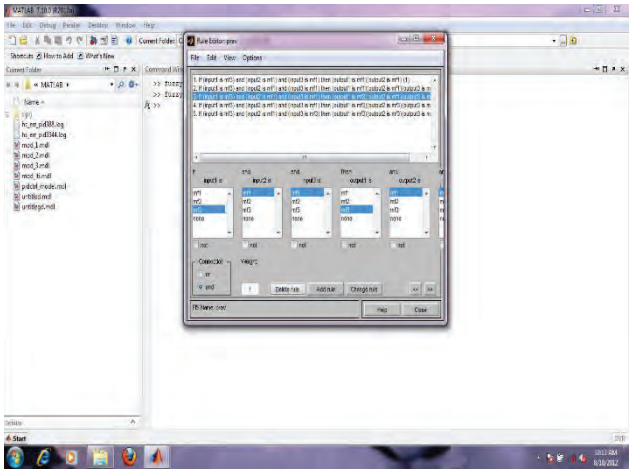

Figure 10. Fuzzy inference rules

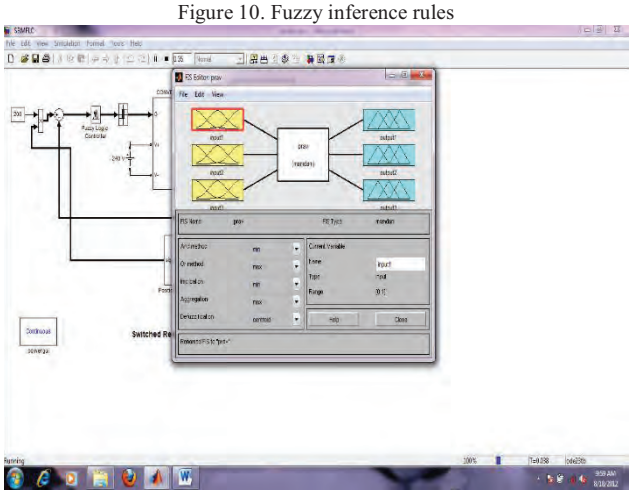

Figure 11. Fuzzy inference system rules and its implication

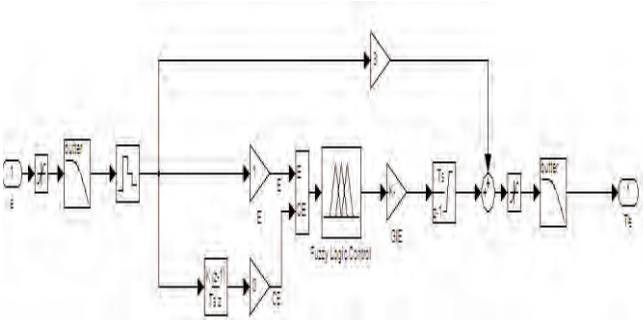

Figure 12. Subsystem of FLC Controller in SRM

Once the fuzzy rules are read, the controller is placed in the main system to give the control output to change the electrical torque as shown in figure 12. The data will be collected and presented in a subsystem of the simulation called data acquisition. This is shown in figure 13. The flux, current and

E-ISSN 2581 - 7957
P-ISSN 2277 - 3916

CVR Journal of Science and Technology, Volume 19, December 2020
DOI: 10.32377/cvrjst1902

speed parameters can be analysed in this block. The outputs obtained are shown in figures 14 and 15 respectively.

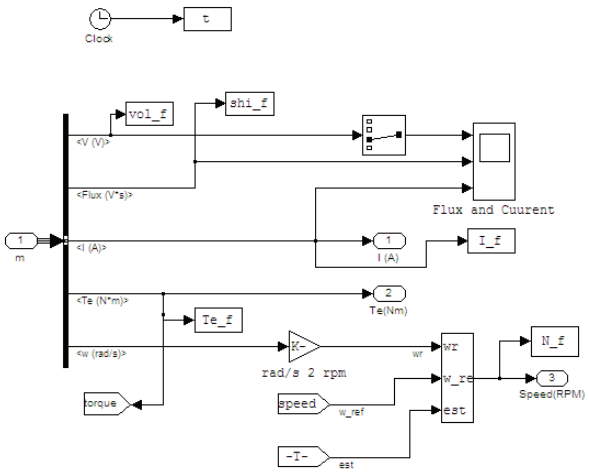


Figure 13. Subsystem of the data acquisition system

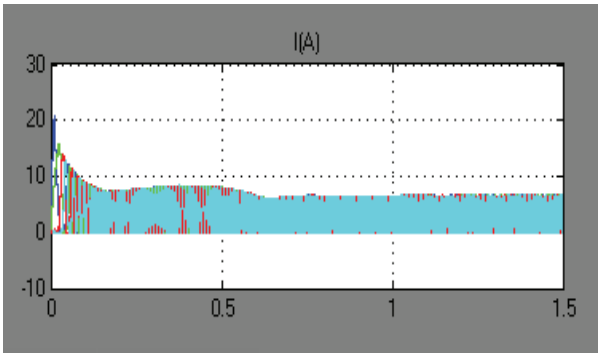


Figure 14. Current (Amps) Versus Time(secs)

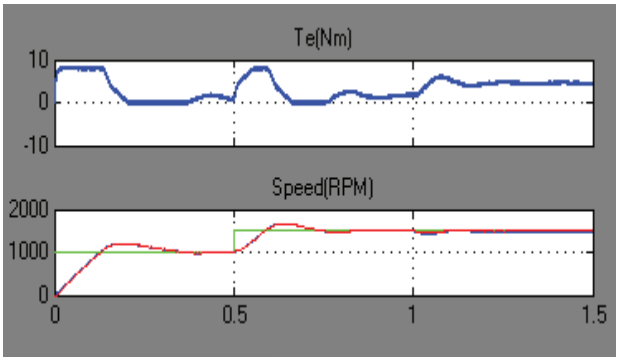


Figure 15. Torque (Nm) and Speed (rpm) Versus Time (secs)

## *E. With SMC*

SMC controller is also used to check the efficiency of the motor to be controlled for speed and torque, as required by the load. Figure 16 shows the schematic and figure 17 shows the output waveforms of speed and torque. It can be observed that the controller is successful in controlling the torque.

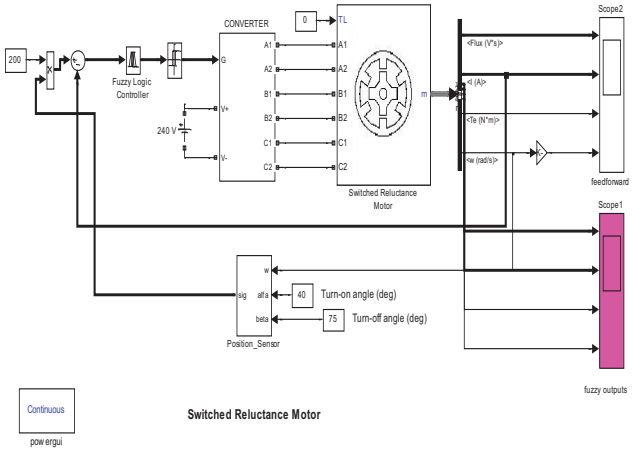


Figure 16. Simulation model with SMC controller

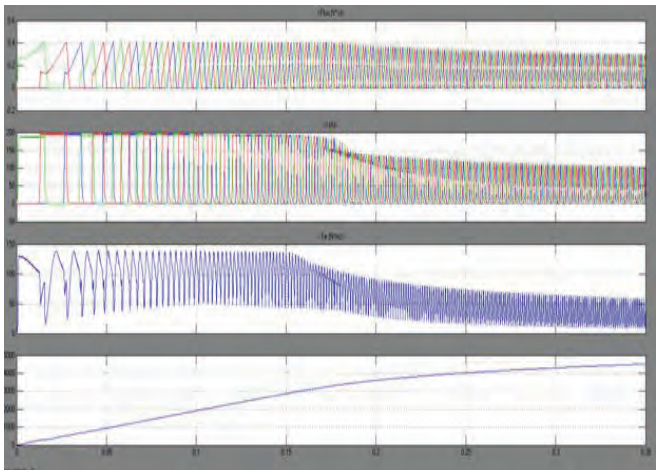

Figure 17. Flux (Wb), Current (Amps), Torque (N-M), Speed (Rpm) Versus Time (Secs) with SMC Controller

Figure 18 shows the filtering of the signal that is obtained by using the first order transfer function, that has been beneficial to analyses the signals.

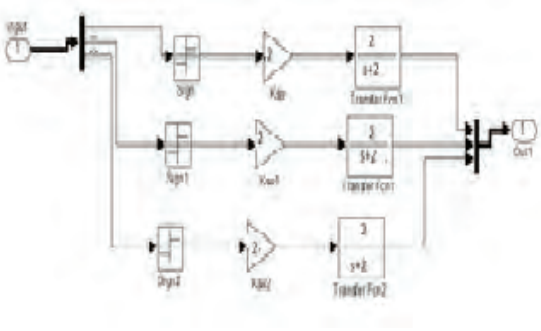

Figure 18. Filter circuit design

E-ISSN 2581 - 7957
P-ISSN 2277 - 3916


DOI: 10.32377/cvrjst1902

### F. Technical Specifications

Specifications: Phase number 4; Number of stator poles 8; 22.6° pole arc; Number of rotor poles 6; 23.0° pole arc; Maximum inductance 9.15 mH (unsaturated); Minimum inductance 1.45 mH; Phase resistance $R = 0.3\Omega$; Moment of inertia $J = 0.0027 Kg/m^2$; Friction $f = 0{,}0067$ Nm/s; Inverter voltage $V = 100$ V. Speed reference: 1500 rpm

TABLE I.
COMPARISON TABLE OF ZETA CONVERTER OF SRM WITH DIFFERENT CONTROLLERS

| Type of controller | Open loop (error) | | | Closed Loop (error) | | | Inductance (mH) |
|---|---|---|---|---|---|---|---|
| | I (A) | N (rpm) | T (N-m) | I (A) | N (rpm) | T (N-m) | |
| No controller | 0.5 | 1.5 | 50 | 0.48 | 1.4 | 548 | 0.99 |
| PID Controller | 0.45 | 1.3 | 45 | 0.425 | 1.25 | 42 | 1.42 |
| FLC Controller | 0.456 | 1.2 | 52 | 0.424 | 1.21 | 47 | 1.245 |
| SMC Controller | 0.215 | 0.9 | 35 | 0.201 | 0.99 | 31.2 | 1.016 |

### G. Analysis

The waveform of the circulating current in steady state is shown in the Figure.17. Note that this current cannot be directly measured as such and it has to be calculated. Also note that it is not perfect DC because of the inductive energy storage in the windings. The circulating current contains a ripple of mainly triple harmonics that repeats every 120◦. The performance of the SRM is mainly manifested in its speed and torque characteristics. So, the current, speed and torque error should be almost zero, and to neglect the error, controllers are used.

In switched reluctance motors (SRMs) yields minimum and maximum points in the inductance profile. Minimum and maximum inductances directly affect energy conversion capabilities of a given design. Estimating the maximum inductance is a relatively simple process, even if MW drop in the magnetic steel is not: ignored. However, minimum inductance estimation is much more difficult task due to the uncertain path of airgap magnetic field which is dominated by fringing between rotor and stator poles. A new approach is proposed in this paper to estimate minimum inductance (Lmin) of SRM. The conventional phase current-torque equation for SRM is a function of slope of inductance with respect to rotor position. Hence, an accurate value of the inductance profile is essential to compute suitable phase current, which flows into motor phase winding and produces desired torque with minimum torque ripple.

Model Predictive Control (MPC) can directly manipulate the switches of the DC-link power converter. The results of applying the sliding mode controller to a SRM give best performances and high robustness than those obtained by the application of a conventional controller (PI). The simulation results show that the proposed controller is superior to conventional controller in robustness and in tracking precision. The overshoot is less important in the case of the sliding regulator, with a best response time without increasing the overshoot. The simulation study clearly indicates the superior performance of sliding control because it is inherently adaptive in nature. It appears from the response properties that it has a high performance in presence of the plant parameters uncertain and load disturbances. It is used to control system with unknown model. The control of speed by SMC gives fast dynamic response without overshoot and zero steady-state error.

## V. CONCLUSIONS

The agricultural motors need a more precise control and simple operation to have wet fields and better irrigation systems. The PV driven SRM is hence the best combination of a motor pump, because the robust operation and speed controls are available. A comparative analysis has been done for various controllers applied to SRM and the performance characteristics have been analyzed. It is found that out of the PID controller, Fuzzy logic Controller, SMC controller and the hybrid Fuzzy – neural controller, the closed loop control has many advantages compared to the open loop control.

## REFERENCES

[1] Krishnan, R.: Switched Reluctance Motor Drivers, Modeling, Simulation, Analysis, Design, and Applications, CRC Press, Boca Rraton, London, 2001.
[2] KRISHNAN, R.: Switched Reluctance Motor Drivers, Modeling, Prentic-Hall, USA, 1994.
[3] Badari Mahayana P, Sanjeeva Reddy BR, Prasad M, Sanjay D. Design & simulation of solar DC pump in Simulink. IEEE Trans 2013;978 (1):4673–6150.
[4] Ould-Amrouche S, Rekioua D, Hamidat A. Modelling photovoltaic water pumping systems and evaluation of their CO2 emissions mitigation potential. Appl Energy 2010; 87:3451–9.
[5] Maurya VN, Diwinder Kaur A, Maurya AK, Gautam RA. Numerical simulation and design parameters in solar photovoltaic water pumping systems. Am J Eng Technol 2013; 1:01–9.
[6] Biji G. Modelling and simulation of PV based pumping system for maximum efficiency. IEEE Trans 2012.
[7] Jafar M. A model for small-scale photovoltaic solar water pumping. Renew Energy 2000; 19:85–90.
[8] Flores C, Poza F, Narvarte L. A tool to widen the possibilities of PV pumping simulation. Int J Sustain Energy 2012; 31:73–84.

[9] Velvizhi J, Subramanian DP. Performance enhancement of PV based water pumping system. Int J Innov Technol Explor Eng 2014;3(10):2278–3075.
[10] Wagdy R, Nourb MA. Optimum design of a photovoltaic powered pumping system. J Power Sources 1994;50:l–9.
[11] Argaw N. Optimization of photovoltaic water pumps coupled with an interfacing pulse width modulated dc/ac inverter power conditioning devices; 1994. p. 1165–8, (IEEE First WCPEC; December 5–9, 1994; Hawaii).
[12] Yahia B, Arab AH, Azoui B. Optimal sizing of photovoltaic pumping system with water tank storage using LPSP concept. Sol Energy 2011; 85:288–94.
[13] Kaldellis JK, Spyropoulos GC, Kavadias KA, Koronaki IP. Experimental validation of autonomous PV-based water pumping system optimum sizing. Renew Energy 2009; 34:1106–13.
[14] Zvonimir G, Margeta J. A model for optimal sizing of photovoltaic irrigation water pumping systems. Sol Energy 2007; 81:904–16.
[15] Hamidat A, Benyoucef B. Mathematic models of photovoltaic motor-pump systems. Renew Energy 2008; 33:933–42.
[16] Firatoglu Z, Yesilata B. New approaches on the optimization of directly coupled PV pumping systems. Sol Energy 2004; 77:81–93.
[17] Cuadros F, Rodrıguez FL, Marcos A, Coello J. A procedure to size solar powered irrigation (photo irrigation) schemes. Sol Energy 2004; 76:465–73.
[18] J.M. Mcknion and H.E. Lemmon, Symbolic Computer and Al Yools for a Cotton Expert System, ASAE Paper No: 85-5520, St. Joseph, MI, 1985.
[19] J. Jones, Interfacing an Expert Diagnostic Tool to Real Time Data, ASAE Paper No. 85-5522, St, Joseph, MI, 1985.
[20] Hasbini, B.A., Buchleiter, G.W., and Duke, H.R. (1991) Expert system for improved irrigation management. Proc. Int. Summer Meet. American Society of Agricultural Engineers, Albuquerque, New Mexico, June 23-26, l-17.

E-ISSN 2581 - 7957
P-ISSN 2277 - 3916

CVR Journal of Science and Technology, Volume 19, December 2020
DOI: 10.32377/cvrjst 1903

# Emulation of Ventricular Assist Devices based on Fuzzy Logic Control

B. Jhanvitha[1], K.S.V. Phani Kumar[2], and Dr. S. Venkateshwarlu[3]
[1]PG Scholar, CVR College of Engineering/EEE Department, Hyderabad, India
Email: bathula.jhanvitha@gmail.com
[2]Asst. Professor, CVR College of Engineering/EEE Department, Hyderabad, India
Email: phani5016@gmail.com
[3]Professor, CVR College of Engineering/EEE Department, Hyderabad, India
Email: svip123@gmail.com

***Abstract:*** **These days many people are suffering from different heart diseases. These heart diseases or heart failures due to some problems are one of the major reasons for the deaths of many people. To avoid these problems, they are searching for heart donors to transplant the heart. Due to the less availability of heart donors, many people are dying because of heart failure. To overcome this problem, a device needs to be developed that will support the circulatory system of the body. These devices are termed Ventricular Assist Devices (VADs). These VADs are used to help in pumping the blood from the heart to other body parts in case of heart failure. They play a key role in saving the lives of the people who are suffering from different heart diseases and the people who are at the end stage of their heart failure. In previous cases, many of the experiments were conducted on continuous flow systems. But due to some complications that are resulted during their operation these continuous flow devices are not recommended. These continuous flow devices are replaced with pulsatile flow devices which represent the flow of blood from the heart to other body parts. This pulsatile flow can be achieved by controlling the speed of the BLDC motor. To control the speed of the BLDC motor, different controllers such as PID controller and Fuzzy Logic Controllers are used efficiently, which give better results when compared to P and PI controllers.**

***Index Terms:*** **Ventricular Assist Devices; Pulsatile Flow; BLDC Motor; Fuzzy Logic Controller**.

## I. Introduction

Cardiovascular diseases are the major reasons for death all over the world. Due to fewer heart donors, Artificial Hearts (AH) are the only treatment given to cardiovascular patients. Artificial Hearts starts with design to its implantation to the human body. Artificial Hearts should pass several clinical tests that involve various redesigns and optimizations. During this process, the weight, the dimensions, and the required Electro-Magnetic Forces of the Artificial Hearts are made with perfection. In the medical terminology, there are two types of Artificial Hearts are Total Artificial Hearts and Ventricular Assist Devices. Total Artificial Hearts replaces the human heart. Ventricular Assist Devices supports the human heart. Ventricular Assist Devices allows two therapeutic strategies for heart diseases, which are called bridge to recovery and bridge to transplant. In the first strategy, the heart recovers due to the support of the Ventricular Assist Devices, and in the second strategy, it ensures the patient's survival until a donor or total artificial heart can be transplanted.

### *A. History and Background*

First, in the inception of the heart program in 1964, investigations in the field have been to develop both Total Artificial Hearts and Ventricular Assist Devices that are implantable without penetrating the skin. To meet this goal, the blood pump, electrical motor, power supply, and volume compensator should be small to fit in the human body and sufficiently durable to support the patient for a long duration. The greatest design challenges have been designed and developed of a reliable, long-lasting, internal electric supply and means of volume compensation as sac type blood pumps eject blood, an equivalent air or fluid must enter into the non-blood side of pump house which prevents a vacuum from forming. Therefore, the development of the volume compensator and the energy source for the pump motor was interdependent. The early method for volume compensation was a compliance chamber which had a variable volume of air in communication and a housing pump. The compliance chamber was a flexible sac which was placed in the chest that would allow a volume of air equal to the stock volume which makes to enter the non-blood chamber of the pump as blood was ejected. Although the compliance chamber initially worked properly within the laboratory, air losses by diffusion and development of animal tissues around the sac eventually rendered the device ineffective.

In addition to this, anticipation is made which makes the change in altitude that would affect air volume in the compliance chamber. Making air travel is impossible for the patients, to resolve this problem of the compliance chamber there is an urgent need for clinical devices Total Artificial Hearts and Ventricular Assist Devices were designed. These devices would have either direct communication with an external pneumatic drive console or an atmospheric vent, which will overcome the need for a compliance chamber. The skin has been penetrated for volume compensation, because of this reason it seemed to be more efficient to transmit electrical power through wires incorporated into the venting apparatus. To overcome the problems related to the volume compensation researchers continued to develop a method that delivers a sufficient amount of electricity to pump the blood. Total Artificial Hearts and Ventricular Assist Devices are electrically driven devices which require a continuous power supply of 8 to 12W. Conventional batteries were not capable to provide this much amount of power for more than 30 minutes and a nuclear power supply was determined to be impartial and potentially dangerous.

E-ISSN 2581 - 7957
P-ISSN 2277 - 3916

CVR Journal of Science and Technology, Volume 19, December 2020
DOI: 10.32377/cvrjst 1903

Therefore, methods for transcutaneous energy transmission were developed [1].

## II. Components used in Ventricular Assist Devices

A ventricular assist device pumps the blood from the left apex into the aorta and could be helpful in 80% of cases. Because of the risk of infection, a heart assist device has to be implantable. Therefore, we require a highly durable and reliable system which is having the smallest possible volume and weight. The left ventricular heart assist system consists of a blood pump, a centrifugal pump, a brushless D.C. motor, a solenoid, power supply, and controls.

### *A. Brushless D.C Motors used in Ventricular Assist Devices*

These are electronically commuted dc motors that don't have any brushes. The rotor of a BLDC motor is a permanent magnet but is fixed in place on the stator and the stator has a coil arrangement. These windings can be arranged by either star or delta connections. The stator must be chosen with correct ratings of voltage depending on power supply capability. As the coils do not move there is no need for brushes. Here permanent magnet rotates; the rotation is achieved by changing the direction of magnetic fields generated by surrounding stationary coils. To control the rotation, we adjust the magnitude and direction of current in the rest of the two coils.

BLDC motor works on a similar principle as conventional motors i.e., the Lorentz force law. As a result of reaction forces magnet experiences equal and opposite forces. In BLDC motors current-carrying conductor is stationary while the permanent magnet rotates. When stator coils are switched by a power supply, it becomes an electromagnet and starts producing uniform fields in the area. Due to the force of interaction between electromagnet stator and permanent magnet rotor rotates continuously. The motor produces torque because the development of attraction forces and repulsion forces the motor to move in a clockwise direction. By applying DC power to the coil, the coil will get energized and become an electromagnet. Before energizing a particular stator-winding rotor position acknowledgment is necessary. Hall Effect sensors embedded in the stator sense the rotor position. Therefore, we require a highly durable and reliable system which is having the smallest possible volume and weight. Based on the signals from the sensor controller decides which coil to energize. Low and high-level signals are generated by Hall Effect sensors whenever rotor poles pass near it. The main disadvantage of this motor is that it requires mechanical arrangements to be mounted. Moreover, these sensors are temperature sensitive, due to which the operation of the motor is limited. The reliability of the system is reduced due to excess components and wiring of the system.

1. *BLDC without Hall-effect sensors:* BLDC motors without the usage of sensors have been used in a larger amount due to their various advantages. Due to the absence of Hall Effect sensors, the action performed by this is obtained from other processes.

a. Back EMF
b. Detecting the conducting state of the diode
c. Back EMF integration
d. Detecting the harmonic voltage

From the above-mentioned methods, the detection of back EMF method is used widely. The winding's present in the motor helps in creating EMF by using Faraday's Law of Electro `Magnetic Induction. According to Lenz's law, EMF produced gives rise to a secondary magnetic field that opposes the original change in magnetic flux which helps in the running of the motor. In simpler terms, the EMF resists back EMF. Produced EMF is proportional to the angular velocity of the rotor.

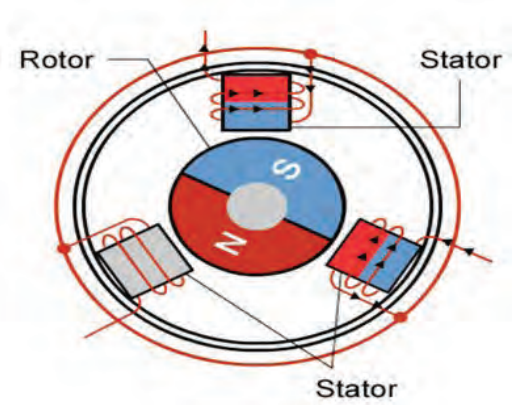


Figure 1. Brushless DC Motor

2. *BLDC motors in Ventricular Assist Devices:* The range of power in ventricular assist devices is 15W to 20 W. The motor which is used should pump 8L/min to 10L /min. The hearts have to pump a minimum of 3L/min for a bedridden patient for their survival. Pulsatile flow can be achieved using constant torque and variable systems with motor-pump in ventricular assist devices. For this application, we use Brush-Less DC motors. Generally, a mechanical circulatory support system requires low volume motor pump. BLDC motor is more preferred because of its high efficiency, reliability, smaller volume, and high torque capability [2].

### *B. Batteries used in Ventricular Assist Devices*

The rechargeable battery pack used for Ventricular Assist Devices should be as small and light as possible for its easy and effective operation. The use of rechargeable lithium cells in implantable medical devices may yield batteries that are smaller and lighter than those of Ni/Cd batteries; however, Ni/Cd cells are preferred over lithium cells because of their high discharge cycle and life cycle. The following are the corresponding characteristics of rechargeable batteries. Testing done on various batteries is shown in the figure below which is varying at a temperature of 45 degrees [3].

Various batteries were considered for supplying power to Ventricular assist devices starting from percutaneous lead cables to a Free-range Resonant Electrical Energy-Delivery (FREE-D) system. Where all of them have both advantages and disadvantages. Some of the new batteries charging systems have been evolving day by day. Such as Solar based recharging systems, Proton exchange membrane fuel cells, and Skeletal muscle energy. The evolution has been started from using battery technology to the above discussed. These emerging technologies hold promise for increasing the life

E-ISSN 2581 - 7957
P-ISSN 2277 - 3916


DOI: 10.32377/cvrjst 1903

of the battery. Out of these FREE-D systems holds good for delivering power to ventricular assist devices.

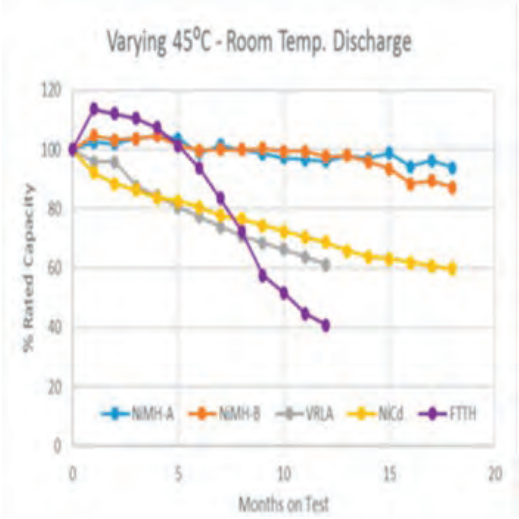


Figure 2. Comparison of various batteries

Wireless power to Ventricular assist devices is provided by FREE-D systems which make use of strong resonant coupling technology. FREE-D system achieves high power transfer efficiency up to 90% for nearly any angular orientation over a large of separation distances. They are two types of power circuits. FREE-D technology could be applied in other medical applications that require implanted batteries, such as pacemakers, implanted defibrillators, cochlear implants. Outside medicine, FREE-D technology is applied in some ideal consumer electronic applications mobile charging, electric car charging, and kitchen appliance operation. Future work for this FREE-D systems to power VADs a full characterization of relay resonators presented and the resonators to improve the system efficiency and enable single-frequency operation.

### *C. Pumps used in Ventricular Assist Devices*

In past decades therapeutic instruments have greater innovation in them and have been widely used for the treatment of cardiac arrest. In general, these instruments consist of different types of blood pumps with different pumping principles ranging from intra-aortic balloon pumps to total artificial heart (TAH). In fact, in recent years there has been more Left Ventricular Assist Devices (LVAD) than heart transplants. These devices not only sustain life but also improve the quality of life of patients with end-stage heart failure. Total Artificial Hearts usually follow Left Ventricular Assist Devices by a certain lag because it applies to fewer people.

All currently used clinically are total artificial hearts which are pulsatile. There is continuous improvement in certain areas for more physiological application of it. One of the most common adverse effects of Left Ventricular Assist Devices use is the development of right heart failure. As many as 30% of Left Ventricular Assist Devices patients exhibit some degree of right heart failure that requires prolonged in tropic support. Hence there is a need for a bi-ventricular assist device has arisen which needs a total artificial heart.

Ventricular Assist Devices includes blood pumps for its operation. In general blood pumps are categorized into two types, they are displacement pumps and rotatory pumps in which displacement pumps are used for clinic and medical purposes [4].

At present rotatory pumps which includes centrifugal pump has been widely used which works on the principle of energy transferred at larger volume with low pressure. The main advantage of this pump is better transportability, less spallation, and lower blood damage for cardiopulmonary bypass.

### *D. Controllers used in Ventricular Assist Devices*

For controlling the speed of the brushless DC motors various controllers are used nowadays. They are termed as Proportional Integral (PI), Proportional Integral Derivative (PID), Fuzzy Logic Controller (FLC), and various combinations between them. Out of various controllers, the Fuzzy Logic Controller serves as a solution for high-performance electric drives.

Due to various disadvantages of PI Controllers such as slow response, sudden change in load torque and sensitivity to gains of the controller. Because of such reasons, there has been an increasing demand for non-linear control structures such as Fuzzy Logic Controllers which are inherently robust to disturbances caused due to loads. Due to variations in load disturbances and parameters, BLDC motors being nonlinear are greatly affected.

Fuzzy Logic Controllers can model non-linear systems very effectively. It makes use of linguistic variables for the operations required. It is a very easy and feasible method for defining the characteristics of a nonlinear system during implementation and designing. Reference value and speed error value are the two main factors considered for comparing the speed of the motor. The main components of the Fuzzy Logic Controller are fuzzification, fuzzy inference defuzzification.

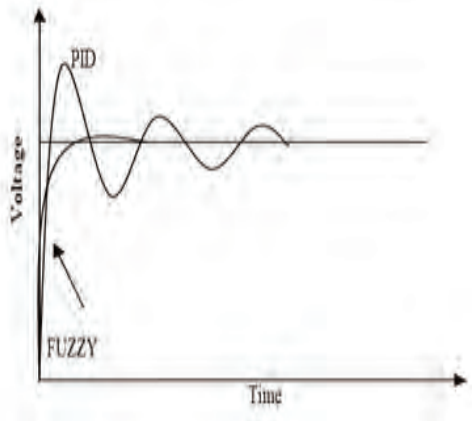


Figure 3. The response of the fuzzy controller

E-ISSN 2581 - 7957
P-ISSN 2277 - 3916


DOI: 10.32377/cvrjst 1903

## III. Experimental Evaluation of Ventricular Assist Devices

Based on the results of optimization, the prototype was constructed. The blood chamber and valves are modified. This made pumping capacity to increase from 50ml to 60ml[5].In addition to this wear, prone components such as fragile coupled gear and the ball bearings have been replaced by linear moving part, the magnetic attraction forces between stator and rotor are avoided minimizing the current supplying springs as healed a duration for more than 5years.

### *A. Working of Ventricular Assist Devices*

Blood is continuously drained from the Left Ventricular chamber via the apical inflow canal and propelled through pump housing where the magnetic field generation by a rotary pump transmits blood through the outflow graft anastomosed to the ascending aorta. A percutaneously tunneled driveline connects the external power source or the system controller to the pump. We can observe how ventricular assist devices are connected to the human body. The system controller has both manual and fixed settings that modulate pump speed, provided hazard alarms, log any device malfunction for future analysis. This device delivers 3 to 10L per min of flow at pump speeds of 6000 to 15000rpm. The batteries used here to power the device may last 12hrs before it should be recharged.

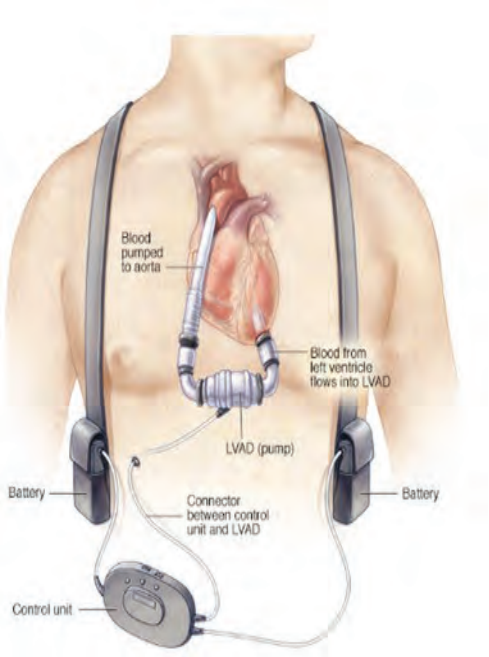


Figure 4. Ventricular assist devices are connected to the human body

Ventricular Assist Device is a centrifugal, continuous flow, implantable rotary pump currently in clinical practice. This third-generation Ventricular Assist Device operates via a hydro-magnetically levitated rotor without mechanical bearings and can deliver up to 10L/min. Elimination of the contact bearings imparts several clinically relevant structural, and theoretical advantages relative to the HM ll. Firstly by affording further miniaturization this 140g pump can be implanted between the pericardial space, thus simplifying the operative placement by eliminating the need of creating a pump pocket. This miniature size also makes the device more conducive to minimally invasive implantation techniques. The absence of mechanical contact within the pump eliminates friction and heat generation which also improves device durability. Generally, the pump is set at the range of 2400 to 3200rpm to deliver flow rates between 3 and 8L/min. The batteries which power the devices can deliver 4 to 6h of support when fully charged.

## IV. Emulation Environment

Mechanical circulatory support helps to keep their heart pumping enough blood. It acts as a supplement or replacement for the action of the failed heart. Introduction of pulsatility to the motor by varying the speed during rotation. Implementation is done using a microcontroller for the BLDC motor. In this, we are using a BLDC motor which is used to pump the blood. BLDC motor is used because of its advantages such as it as high-speed control during at high voltage and low voltage-time and it has constant torque while changing the speed of the motor.

TABLE I.
Reference Input for the Speed Controller of the Motor.

| S. No | Speed (rpm) | Time (sec) |
|---|---|---|
| 1 | 1200 | 0+ |
| 2 | 1600 | 0.2 |
| 3 | 1400 | 0.35 |
| 4 | 1300 | 0.5 |
| 5 | 1220 | 0.6 |
| 6 | 1200 | 0.7 |
| 7 | 1200 | 1 |

The power to the BLDC motor is given by a battery which is connected to the controller. Without applying any load on the motor we can control the speed of by motor which varies accordingly by using ATMEGA328p. In this paper, reference speed values of a repeating sequence block are considered which are as follows.

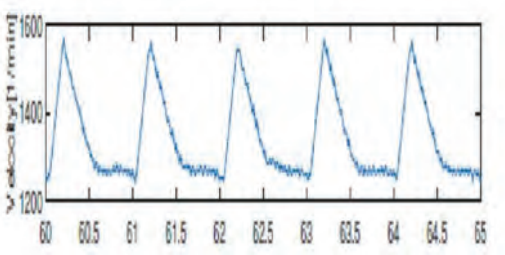


Figure 5. Reference input graph for the speed controller of the motor.

Before controlling the speed of the brushless dc motor at various speeds, we need to find out whether the motor is rotating or not. For this process, we can make use of a proximity sensor which helps in detecting an obstacle which therefore helps in finding total revolutions per minute i.e

E-ISSN 2581 - 7957
P-ISSN 2277 - 3916


DOI: 10.32377/cvrjst 1903

(rpm). Proximity sensors provide medium or low-resolution sensing, depending on the total number of pulses measured per revolution. A bolt attached to the shaft can be sensed using a proximity sensor. Revolutions per minute can be calculated by using the formula (1) given below.

$$RPM = Pulse\ Frequency * 0.1 \quad (1)$$

Whereas the number of pulses is being sensed per revolution is termed as pulse frequency.

### *A. Algorithm for Obtaining RPM using a Proximity Sensor*

STEP 1**:** First we need to set and initialize the variables such as proxy, s, Val, prev_state, current_state, count, and formula of rpm.

STEP 2: Initialize current_state as equal to the proxy.

STEP 3: Here we need to check for the condition whether current_state is not equal to prev_state are not.

STEP 4: If this condition is false again we have to go back to STEP 2.

STEP 5: If the condition is true check whether the obtained current_state is equal to one.

STEP 6: If the condition is false, go back to STEP 2.

STEP 7: If the condition is true increment the count value by 1 (count = count +1).

STEP 8: Completing the loop initializes the prev_state value is equal to the current_state value.

STEP 9: By using this formula we can calculate the rpm of the motor.

Figure 6. Finding the speed of the BLDC motor using the proximity sensor

This method produces low resolution and it acts as a major drawback. To overcome this we can make use of two bolt heads by which resolution improves but often pulses are inconsistent and they are not symmetrical. Hence we can directly control the speed of the motor by writing a code in the microcontroller.

For achieving the speed values of the above-shown Table. 1 we require a brushless dc motor, ATMEGA328p microcontroller, and a battery. The block diagram for this operation is as shown below. Here the variations in the speed can be obtained by programming ATMEGA328p. The programming is done in such a way that the motor starts running as soon as the battery is connected to the brushless dc motor. ATMEGA328p programming is described in the algorithm accordingly.

### *B. Block Diagram for Controlling the Speed*

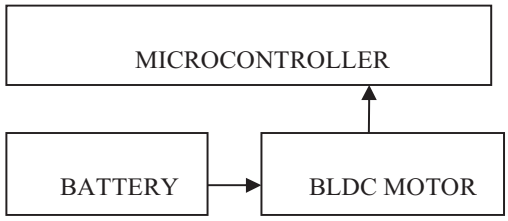


Figure 7. Block diagram for speed control of motor

### *C. Algorithm for Controlling the speed of the Motor*

STEP 1: First we have to initialize the values which we are using in this code.

STEP 2: Next step is we have to declare each input and output pin in which tells the Arduino how to configure a certain pin. In this, we also define the serial begin which is 9600 in this program which defines the baud rate from which the program will begin.

STEP 3: The next step is the void loop () where we specify the main behavior of our interactive device (Arduino). This will be repeated over and over again until you remove power from the board.

STEP 4: In this step, we use 6 different types of for loops in which it is described with different speed variations with certain delay time.

STEP 5: In the first for loop we give the different values like from 1200rpm 1600rpm for which the motor rotates at given speeds with an increment of speed for 400 rpm with the delay of 0.2 seconds.

STEP 6: In the second for loop we give the different values like from 1600rpm to 1400rpm for which the motor rotates at given speeds with the decrement of speed for 200 rpm with the delay of 0.15 seconds.

STEP 6: In the third for loop we give the different values like from 1400rpm to 1300rpm for which the motor rotates at given speeds with the decrement of speed for 100 rpm with the delay of 0.15seconds.

STEP 7: In the fourth for loop we give the different values like from 1300rpm to 1220rpm for which the motor rotates at given speeds with the decrement of speed for 80 rpm with the delay of 0.1 seconds.

STEP 8: In the fifth for loop we give the different values like from 1220rpm to 1200rpm for which the motor rotates at given speeds with the decrement of speed for 20 rpm with the delay of 0.1 seconds.

STEP 9: In the last for loop we give the different values like from 1200rpm to 1200rpm for which the motor rotates at given speeds with the constant speed with a delay of 0.3 seconds.

STEP 10: After this, the loop will end and we will come out of the loop and the program will stop.

E-ISSN 2581 - 7957
P-ISSN 2277 - 3916

CVR Journal of Science and Technology, Volume 19, December 2020
DOI: 10.32377/cvrjst 1903

### *D. Results for Controlling the Speed of the Motor*

After dumping the code into ATMEGA328p and uploading it, we can observe the rotation of the motor. The motor continues to rotate at various speeds accordingly until the loop is completely executed. We can observe the changes in the speed from the serial monitor of the microcontroller.

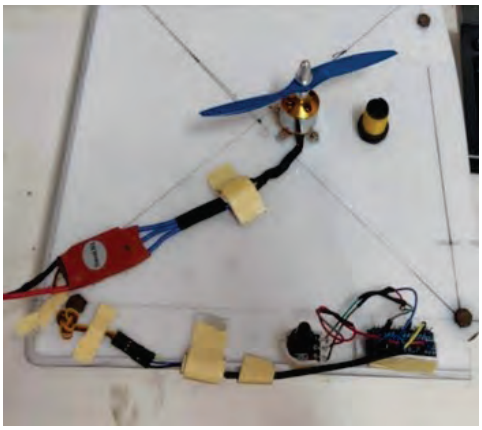

Figure 8. Prototype for controlling the speed after writing a program


Figure 9. Output values from the serial monitor

TABLE II.
ACTUAL VALUES OBSERVED IN SPEEDS OF THE MOTOR USING THE DIGITAL TACHOMETER

| S. No | Speed (rpm) | Time (sec) |
|---|---|---|
| 1 | 1205 | 0+ |
| 2 | 1602 | 0.2 |
| 3 | 1404 | 0.35 |
| 4 | 1306 | 0.5 |
| 5 | 1228 | 0.6 |
| 6 | 1209 | 0.7 |
| 7 | 1210 | 1 |

By using this procedure we could emulate the speeds of BLDC Motor to the actual graph. But we could find some errors in the speed achieved by the motor. To overcome these issues Fuzzy Logic Controller can be used. We can detect the speed of the brushless dc motor by making use of a digital tachometer. The speed values for which error has been observed are as follows.

### *E. Block Diagram using Fuzzy Logic Control for Rectifying the Errors in Speed*

Generally, for using Fuzzy Logic Control we need to calculate the errors and change in error values. Here we come across two speed values one is 'Set Value' which is the reference values considered for the variations in speed using a repeating sequence. Another speed value is termed as the 'Actual Value' which is obtained from the digital tachometer readings. Using set values and actual values we can determine the 'Error' i.e. the difference between the set value and the actual value is termed as the Error.

$$Error = Set\ value - Actual\ value \tag{2}$$

The difference between two error values at a particular instance of time is termed as a change in error.

$$Change\ in\ error = \frac{Error(2) - Error(1)}{t} \tag{3}$$

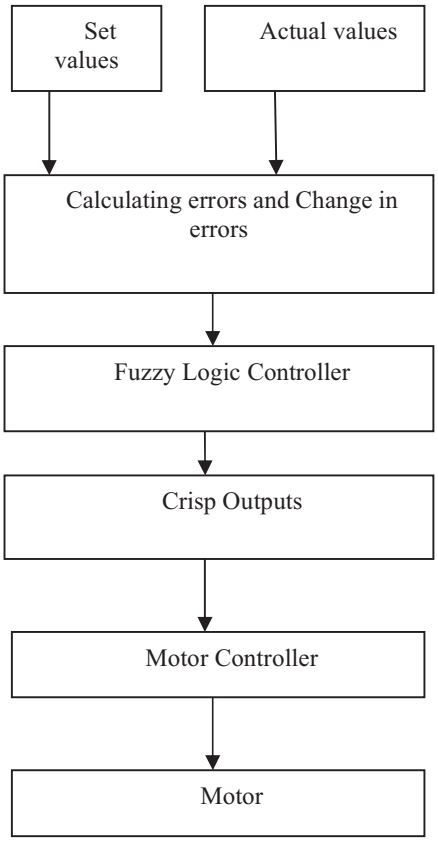


Figure 10. Block diagram for rectifying errors in speed

E-ISSN 2581 - 7957
P-ISSN 2277 - 3916


DOI: 10.32377/cvrjst 1903

### *F. Flowchart for Fuzzy Logic Controllers for Rectifying the Errors in Speed*

The fuzzy logic controller plays a vital role in the process of finding the error and change in error values until the crisp output is found.

In the process of fuzzification membership functions are applied to the measurement and the degree of membership is determined. For calculating the degree of membership we need to calculate the values of $\delta_1$ and $\delta_2$. These two values can be computed as follows.

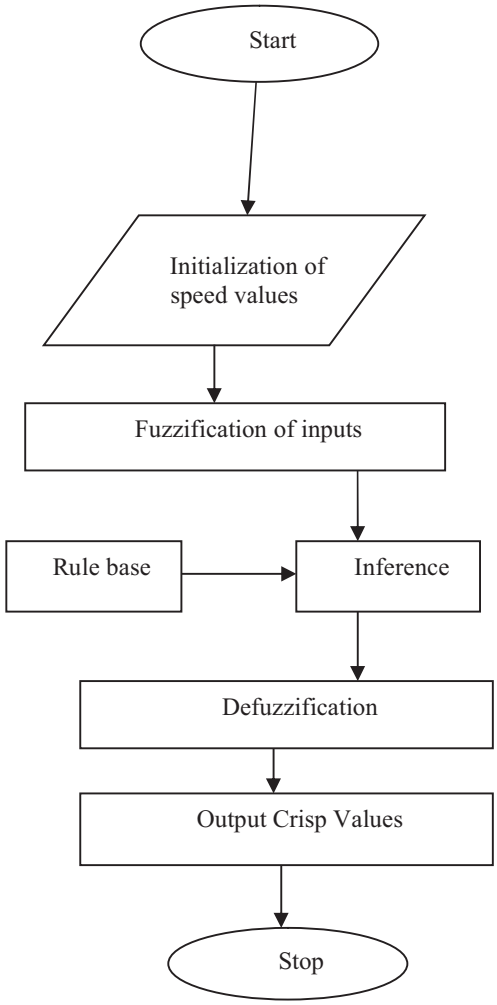


Figure 11. Flowchart for rectifying errors in speed

$$\delta 1 = x - Point1 \quad (4)$$

$$\delta 2 = Point2 - x \quad (5)$$

Point1 and Point2 are the starting and ending values i.e. first and last limits of the various membership functions. And x is the input error value. Then from equations (4) and (5), if $\delta_1 <= 0$ and $\delta_2 <= 0$, the degree of membership is considered as zero. In case if anyone of the conditions is not satisfied, we need to compute for the degree of membership in another manner using the slopes of the chosen membership function which is as follows.

$$degree\ of\ membership = \min(\delta 1 * slope1; \delta 2 * slope2; maximum\ y - axis\ limit)$$

Rule Base contains the fuzzy logic gradation of the expert's linguistic description in the form of a set of rules of how to achieve good control.

Inference engine and fuzzy inference module are the synonyms for "inference mechanism". It helps in emulating the expert's decision in applying and rendering the knowledge which helps in knowing which is best to manage the plant. This helps in evaluating the control rules which are relevant at present time and decides what input to the plant should be.

The defuzzification interface converts the conclusions obtained by the inference mechanism into the actual inputs. Converting decisions into actions is the process of defuzzification. After defuzzification output, crisp values are obtained. Defuzzification can be performed using various methods such as Center of Sums Method; Center of gravity or Centroid of Area Method; Center of Area or Bisector of Area Method; Weighted Average Method and Maxima Method again in Maxima method as First of Maxima Method; Last of Maxima Method; Mean of Maxima Method. Out of which mostly the Center of gravity method and Center of area method are used widely.

For writing a code using Fuzzy Logic Control in the microcontroller we need to follow all the above-said steps accurately. While writing the program we need to initialize the entire variable. We need to consider the rule base according to our requirements. These crisp values are fed to the motor controller and balances the errors produced. The whole process of fuzzification to defuzzification can be done by writing a code in the microcontroller depending on the changes that occurred. By using this procedure, we can eliminate the errors that occurred and emulate them to the actual graph results.

## V. Conclusions

By pulsating the speed of the motor, the pulsatile flow of the blood in mechanical circulatory devices can be achieved. According to the dimensions, weight, and simplistic control, a practicable solution is obtained by the BLDC motor. Controlling of BLDC motor's speed can be achieved using various methods as discussed above. The ripples in the speed of the motor while knowing the pulsatility in speed may cause turbulence in blood flow. So, to reduce the ripples in speed we can use various control techniques. Fuzzy-based control results in a smaller number of overall ripples get reduced increasing the performance and smaller percentage of peak overshoot in motor speed than simple PI, PID, and fuzzy, fuzzy PI are obtained by the combination of Fuzzy and PID.

## References

[1] Slaughter MS, Myers TJ. "Transcutaneous energy transmission for mechanical circulatory support systems: history, current status, and future prospects". J Card Surg 2010;25:484–9.

[2] P. Damodharan and Krishna Vasudevan, Member, IEEE on "Sensorless Brush less DC Motor Drive Based on the Zero-Crossing Detection of Back Electromotive Force (EMF) From the Line Voltage Difference" IEEE transactions on energy conversions, VOL. 25, NO. 3, September 2010.

[3] MacLean GK, Aiken PA, Adams WA, Mussiv and T. "Comparison of rechargeable lithium and nickel/cadmium battery cells for implantable circulatory support devices". Artif Organs 1994;18:331–4.

[4] Jan D. Schmitto, MD, Daniel Burkhoff, Murat Avsar, Oliver Fey, Petra Ziehme, Gwen Buechler, Axel Haverich, and Martin Strueber, From the Department of Cardiac, Thoracic, Transplantation, and Vascular Surgery, Hannover Medical School, Hannover, Germany; Department of Cardiology, Columbia University, New York, New York; and CircuLite Inc, Saddle Brook, New Jersey. On "Two axial-flow Synergy MicroPumps as a biventricular assist device in an ovine animal model"; The Journal of Heart and Lung Transplantation, Vol 31, No 11, November 2012.

[5] André Pohlmann, Marc Lebmann, Thomas Finocchiaro_, Thomas SchmitzRode_, and Kay Hameyer on "Numerical Computation Can Save Life: FEM Simulations for the Development of Artificial Hearts"; IEEE transactions on magnetics Vol. 47, No. 5, May 2011.

[6] B. Lima, Michael M., Gonzalo V. G. Stawinski. "Ventricular assist devices: The future is now". Elsevier publications on Trends in cardiovascular medicine 25 (2015).

[7] Waters BH, range resonant electrical energy delivery (FREE-D) system. Proc IEEE 2012;100:138–Sample AP, Bonde P, Smith JR. Powering ventricular assist device (VAD) with the free- 49.

[8] Steven Keeping "Controlling Sensorless, BLDC Motors via BackEMF"2013-06-19. https://www.digikey.com/en/articles/techzone/2013/jun/controllingsensorless-bldc-motors-via-back-emf

E-ISSN 2581 - 7957
P-ISSN 2277 - 3916

CVR Journal of Science and Technology, Volume 19, December 2020
DOI: 10.32377/cvrjst 1904

# Energy Management of Stand-alone Hybrid Generation System

B. Deepika[1] and Dr. R. Vijay[2]
[1]PG Scholar, CVR College of Engineering/EEE Department, Hyderabad, India
Email: deepukondru93@gmail.com
[2]Assoc. Professor, CVR College of Engineering/EEE Department, Hyderabad, India
Email: vijai.mtp@gmail.com

***Abstract:*** **This paper offers a distinct self-power composite electricity production system, which employs modern energy management methods. The energy sources such as wind farms and solar energy with battery, and diesel combustion engine alternator or fuel cell are considered for energy management, which is isolated from the trade power system. Substantial effort is laid towards the growth of real-reactive power and collapses energy management. The magnitudes and phase angles of the alternating output voltage are well-supervised in the designed composite system. In this composite power system, various energy sources are coupled at all locations on the same supply line. This results in a power system generation growth towards the standard. Furthermore, this will progress world energy security in distant regions and agricultural zones with independence on marketable power systems.**

***Index Terms:*** **standalone power system, diversion power control, hybrid wind-solar power, self-power composite electricity production system, storage battery, fuel cell.**

## I. Introduction

With the rapid rise in energy demand and rising concerns towards the environmental impact due to the high degree of reliability on fossil fuels, renewable power production and clean power techniques play a crucial role in the future tolerable power system. The dispersed non-conventional power systems and small-production systems such as solar photovoltaic array (PVA) and wind farms are offered to reduce power demand from the utility grid. Since non-conventional energies are from the organic environment, it is dependent on all seasons which make them insecure when one renewable source is applied to build a constant power system. Using a combination of multiple renewable sources such as solar and wind supplementing each other, where sunlight is available over the day, and wind energy at night in winter and summer seasons.

The combination of variable renewable resources is allowed for soft, steady, and authentic output to power grids aimed at the protection, consistency, and constancy of dispatch power, which is cheaper than investing in single non-conventional technology [1]. Recently, eco-friendly solutions are gaining importance for energy generation to overcome environmental problems, but uncertainty in nature is the main constraints of non-conventional sources to produce uninterrupted power. To overcome these disadvantages, different renewable sources such as solar PVA, wind farm, and battery are to be included. The biggest challenge of this incorporation is to control and handle the power flow [2]. The best design and performance of a connectionless PVA/fuel cell/diesel alternator energy system has been explained as follows.

The main objective is to propose an energy system with a high non-conventional fraction; low greenhouse gas discharges, and less cost of energy. The goal is to control from grid-connected fossil fuel energy system to a non-conventional and good power system [3]. Stand-alone photovoltaic (PV) systems are mostly used to produce electrical energy in agricultural areas. Migrants in PV radiation influence electrical energy produced by solar stand-alone PV systems. The PV systems strictly need energy-saving units like batteries to balance the solar energy deficiency. The batteries can store electric strength with an excessive-electricity ratio; however, their potential is constrained. Supercapacitors have a high energy density with a low-electricity density. A combination of each power storage gadget is required to be related in a suitable configuration, that it caters to the power call for and strength exceptional concerns of the sun stand-alone PV systems [4]. A Hybrid Power Storage Device (HPSD) is a promising solution for mitigating these strength fluctuations. The electricity that the HPSD additives have to deliver/absorb, the Electricity Control Method (ECM) impacts the dimensions/capacity of the Energy storage system.

Based on this consideration, sizing and ECM of a battery/supercapacitor (SC) HPSD is mutually optimized employing the use of a deep reinforcement mastering-based totally technique. The proposed technique splits the electricity between the HPSD additives so that the operational constraints are rectified. Correspondingly the electricity garage length and losses are minimized [5-6]. A techno-economic evaluation based totally on incorporating modeling, simulation, and optimization techniques is used to layout an off-grid hybrid sun PV/fuel cell power device. The major objective is to optimize the design and broaden dispatch, manage techniques of the standalone hybrid renewable electricity device to satisfy the desired electric powered load of a residential community positioned in a desert.

The results of temperature and dirt accumulation at the sun PV panels in the design and overall performance of the hybrid power machine in a wasteland location are investigated. The intention of the proposed off-grid hybrid renewable electricity system is to increase the penetration of renewable power in the power mix. Lesser the greenhouse fuel emissions from fossil gasoline combustion, and decrease the cost of power from the power structures. Simulation, modeling, optimization, and dispatch, manage

CVR Journal of Science and Technology, Volume 19, December 2020
DOI: 10.32377/cvrjst 1904

techniques were used to determine the overall performance and the cost of the proposed hybrid renewable strength machine [7].

The feasibility and ideal sizing layout of a stand-on wind/hydrogen hybrid power machine for a residence are taken into account with no connection to the electricity grid lines. The designed device ensures uninterrupted, reliable, continuous electricity to the residence at any time. The wind strength, and the considered hybrid PV-wind and the fuel cell system is a good alternative for providing the power [8,9]. Off-grid packages (i.e., users not connected to a country's primary electric grid) are assuming an increasing number of essential functions inside the future energy structures [9,10].

In contrast, almost the complete transportation region (excluding trains) may be considered as made of off-grid [11,12] structures (e.g., vehicles, trucks, planes, and ships). More typically, numerous elements contribute to a renewed interest in small-scale technology. Among them are the price and public opposition to new transmission lines and large power vegetation [13,14]. The need of reducing the vulnerability of the supply chain in centralized structures, and the elevated overall performance of small electricity technologies [15,16]. Hybrid renewable electric powered energy era devices emerge as crucial to most electrical networks and the stand-alone systems like the water pumping and telecommunication systems. Renewable resources generally required garage devices due to change in the electrical outputs in the day.

Due to an increase in the demand for the use of batteries, the charging procedure of battery gadgets needed to be properly controlled through an adaptive managed power handling machine. Fuel Cell (FC) strength plants are electrochemical devices that convert the chemical strength of a reaction directly into electricity. It generates power through an electrolytic reaction, not combustion. In a fuel cell, hydrogen and oxygen are used to generate electricity, heat, and water. Fuel cells are used nowadays in a range of applications, to provide power to homes and businesses, and for supply power to critical facilities like hospitals, supermarkets, and computer centre. These are used to move a variety of vehicles includes cars, buses, goods vehicles, excavators, trains, and more.

This paper deals with the different kinds of energy resources such as solar PVA and wind farms. As well as storage batteries, and diesel generator, or fuel cell with different types of control techniques to contribute and manage the power in off-grid. The remaining of this paper is outlined as follows: Section II describes the prototype of the hybrid system. Section III is about energy monitoring methods. The modeling and simulation results are shown in Section IV. Conclusions are presented in Section V.

## II. HYBRID ENERGY SYSTEM

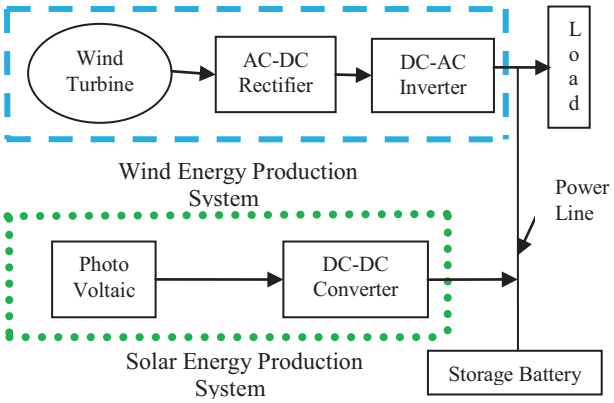


Figure 1. Hybrid energy system without backup devices.

The wind and solar systems are needed to supply the power to the load and are shown in Fig.1. But if they fail to meet the load demand, then the backup devices, i.e., storage battery and diesel generator/fuel cell are needed to supply the power to the load.

### *A. Hybrid System Configuration:*

The hybrid system consists of the following characteristics.

1) The various energy sources are interlinked in parallel.
2) Removal of diversion load by using an individual diversion energy control focused on avoiding battery excess charging.
3) A high-speed line is unnecessary for battery modern-day/voltage report data communication.
4) Extension of capacity is easy through a parallel connection of extra power sources to cope with future load growth.

Particular concentration has also been given to Phase-Locked Loop (PLL) control methods via workshop tests, and examines the performance of the current/voltage effect of input real-reactive energy parameters into an energy control network test and established suitable energy to manage the result. The proposed self-power composite electricity production system is, as shown in Fig.2.

E-ISSN 2581 - 7957
P-ISSN 2277 - 3916

CVR Journal of Science and Technology, Volume 19, December 2020
DOI: 10.32377/cvrjst 1904

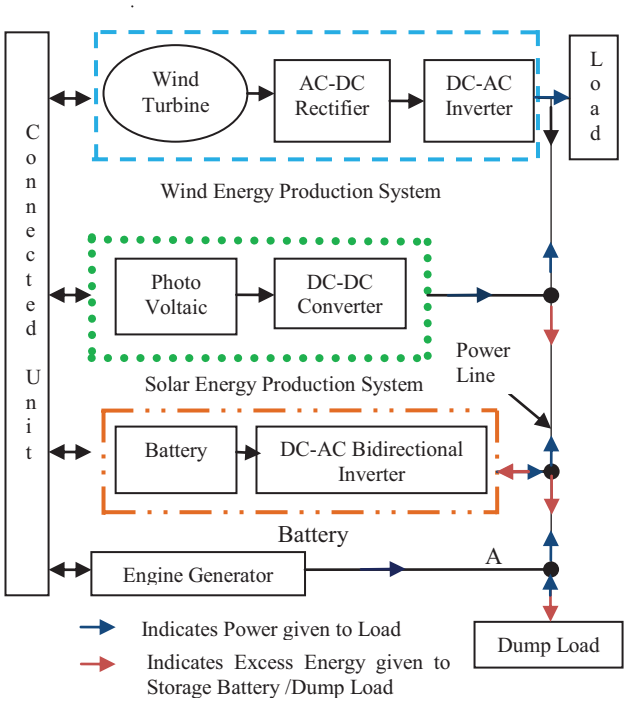


Figure 2. Hybrid energy system with backup devices.

### *B. Hybrid System Operation:*

Major operation flows of the planned hybrid system are explained below.

1) **When the leftover battery potential is satisfactory:** Engine Generator (EG) action stops, and all inverters operate in parallel. Energy excess and shortage, according to the equilibrium among the output and load are optimally used via battery charging or discharging.

2) **When the leftover battery potential is unsatisfactory:** EG and all inverters work in parallel. When the energy produced by wind and PV energy production systems is inadequate to reach load demand, EG balance for the shortage. Simultaneously, EG charges the battery through the two way inverter. This inverter improves charging energy for the battery so that EG operated at the better load factor matches with high efficiency and the following command from the monitoring unit.

## III. Hybrid Energy System Monitoring Methods

In the proposed composite system, it focused on monitor real-reactive energy on load distribution in parallel inverter operations and phase management. Through further study energy diversion control method is considered without a diversion load.

### *A. Real-Reactive Energy Balance*

The auto-master-slave control technique is applied in all inverters. When EG is in operation, the switch of each inverter is closed, and these switches are in AC-synchronized operation with all inverters that operate as slaves and with EG as the master. When EG operation stops, the switch of the battery bank two-way inverter is closed. This inverter works as a master and is under the Constant Voltage Constant Frequency (CVCF) condition. The switch of each remaining inverter that acts as a slave is closed which is shown in Fig.3. Then, the AC-synchronized operation is undergone. The proposed composite system concentrates on the method of the PLL in the real-reactive energy control.

**1) Parallel Inverters Operation:**

In this assembly a sample self-power composite electricity production system, and conducted experiments. $X_1, X_2$ *and* $X_3$ are interlinked reactors arranged in WT inverter, PV inverter, and two-directional inverters respectively. This research finds the optimal real reactive energy parameters for each inverter to improve the output under the conditions that each inverter capacity is $3kVA$ (with a power factor of 0.8) and the output voltage is single-phase $100V, 60Hz$.

**2) Phase-Locked Loop/Feedback Control Loop:**

The PLL, which acts as a phase synchronization control, is consists of a phase comparator, low-pass (LP) filter, phase shifter, multiplier, and Voltage-Controlled Oscillator (VCO). The phase comparator acts to expand the AC output voltage wave by the cosine wave pass on hence obtained from the sine wave reference passes through the phase shifter. The expanded wave is changed to DC voltage for VCO frequency control through the LP filter.

PLL consists of two control elements, the phase comparator output, and the phase reference signal which is introduced into the LP filter and shown in Fig.4. The phase comparator output is introduced as synchronization data (i.e., the difference compared to reference frequency). The phase reference signal is introduced as the amount of phase shift in inverter output voltage at the same time by balancing the synchronization in opposition to voltage in the marketable energy system. Thus, the real power changes along with the change in the phase Reference signal.

**3) Parallel Inverters Operation:**

In this construction a sample self-power composite electricity production system and conducted laboratory experiments. $X_1, X_2$ & $X_3$ are interlinked reactors arranged in WT inverter, PV inverter, and two-directional inverters respectively. The research finds the optimal real reactive energy parameters for each inverter to improve the output under the conditions that each inverter capacity is $3kVA$ (with a power factor of 0.8) and the output voltage is single-phase $100V, 60Hz$. The specification of wind & solar energy storage system, battery, the fuel cell is displayed in Table I, II, III & IV correspondingly.

E-ISSN 2581 - 7957
P-ISSN 2277 - 3916

CVR Journal of Science and Technology, Volume 19, December 2020
DOI: 10.32377/cvrjst 1904

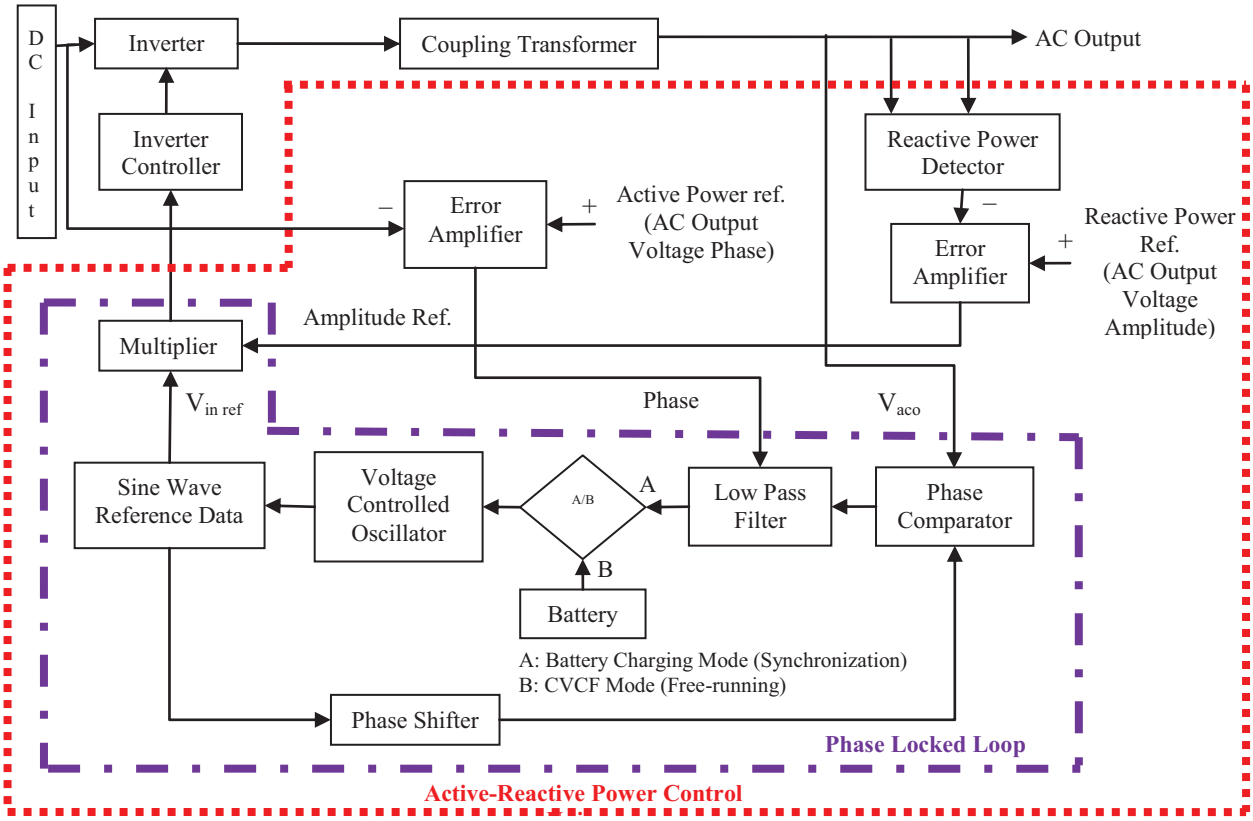


Figure 3. Basic power control block of the inverter section

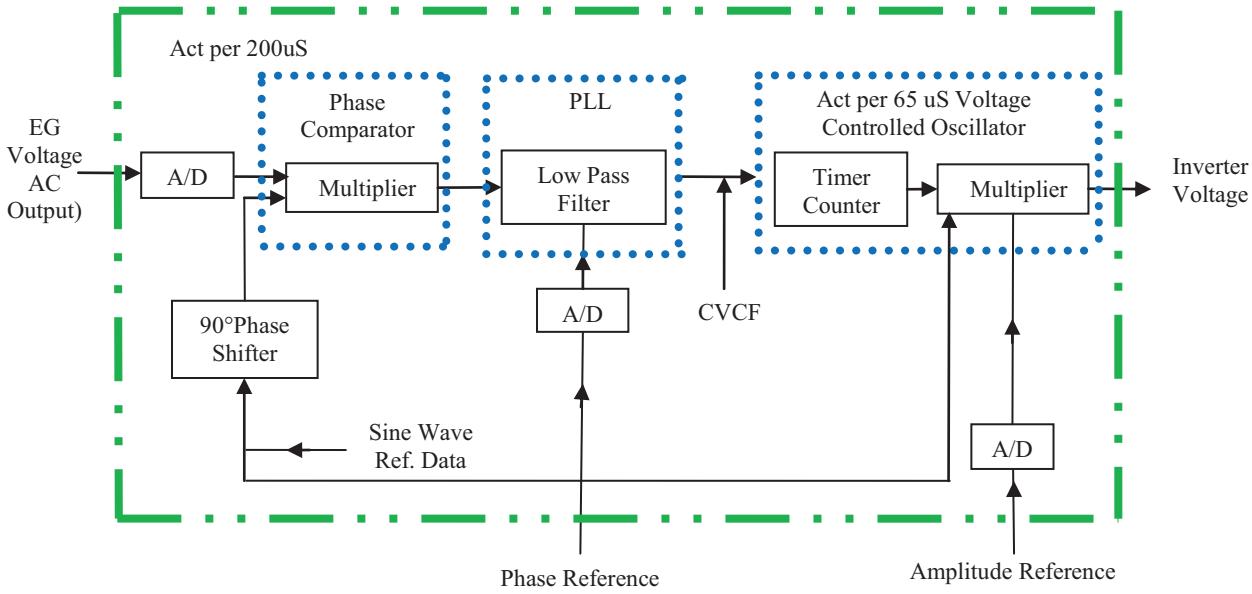


Figure 4. Phase-locked loop control

TABLE I.
SPECIFICATION OF WIND ENERGY PRODUCTION SYSTEM

| Item | Specification |
|---|---|
| ***Wind Energy*** | |
| Output Capacity | 3.5 kW |
| Output Voltage | 3-phase,3-wire AC 100V |
| ***AC-DC Converter*** | |
| Output Capacity | 3.5kW |
| Output Voltage | DC 250V |
| ***DC-AC Inverter*** | |
| Output Capacity | 3kW |
| Output Voltage | 1-phase, 2-wire, AC100V, 0.8 Power factor |

TABLE II.
SPECIFICATION OF THE SOLAR ENERGY PRODUCTION SYSTEM

| Item | Specification |
|---|---|
| ***Solar Panel*** | |
| Output Capacity | 3.41 kW |
| Open Circuit Voltage | DC 344V |
| ***DC-AC Inverter*** | |
| Output Capacity | 3kW |
| Output Voltage | 1-phase,2-wire, AC 100V, 0.8 Power factor |

TABLE III.
SPECIFICATION OF THE STORAGE BATTERY SYSTEM

| Item | Specification |
|---|---|
| ***Battery Bank Module*** | |
| Rated Voltage | DC 12V |
| Rated Capacity | 24Ah |
| ***Battery Bank Unit*** | |
| Rated Voltage | DC 288V |
| Rated Charging Voltage | DC 332.1V |
| Rated Charging Current | DC 10A |
| Connection | 24 modules connected in series in two parallel |
| ***DC-AC Bidirectional Inverter*** | |
| Output Capacity | 3kW |
| Output Voltage | 1-phase, 2-wire, AC 100V, 0.8 Power factor |

TABLE IV.
SPECIFICATION OF THE ENGINE ALTERNATOR

| Item | Specification |
|---|---|
| Output Capacity | 10kVA |
| Output Voltage | 1-phase, 2-wire, AC 100V, 0.8 Power factor |

Assume $V_{sm}$ is defined as the input side voltage and $V_r$ as the load side voltage, and the angle of phase difference is $\delta$, each of $P_{sm}$, $Q_{sm}$, $P_{rm}$, and $Q_{rm}$ is represented as follows [18], [19]:

$$P_{sm} = P_{rm} = \frac{V_{sm}V_r}{X_m}\sin\delta \quad (1)$$

$$Q_{sm} = \frac{V_{sm}^2 - V_{sm}V_r\cos\delta}{X_m} \quad (2)$$

$$Q_{rm} = \frac{V_{sm}V_r\cos\delta - v_r^2}{X_m} \quad (3)$$

Where active power is $P_{sm}$ and reactive power is $Q_{sm}$ at the sending-end active power is $P_{rm}$ and the reactive power is $Q_{rm}$ at the load-side, and the reactance of the interlinked reactor is $X_m$.

Here, $m$ indicates the number of power sources operated in parallel. It is attractive to regulate the voltage amplitude variation and the angle of phase variation to be inside the period from 5 V to 15 V, and from 5◦ to 10◦, respectively, based on the behavior of the real-reactive energy control unit as shown in Fig. 5.

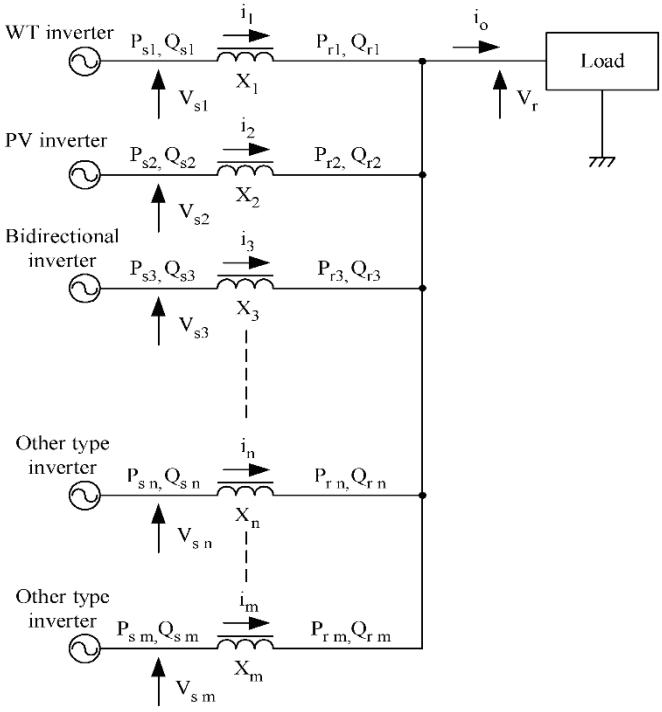


Figure 5. Operating model of parallel inverters.

E-ISSN 2581 - 7957
P-ISSN 2277 - 3916

CVR Journal of Science and Technology, Volume 19, December 2020
DOI: 10.32377/cvrjst 1904

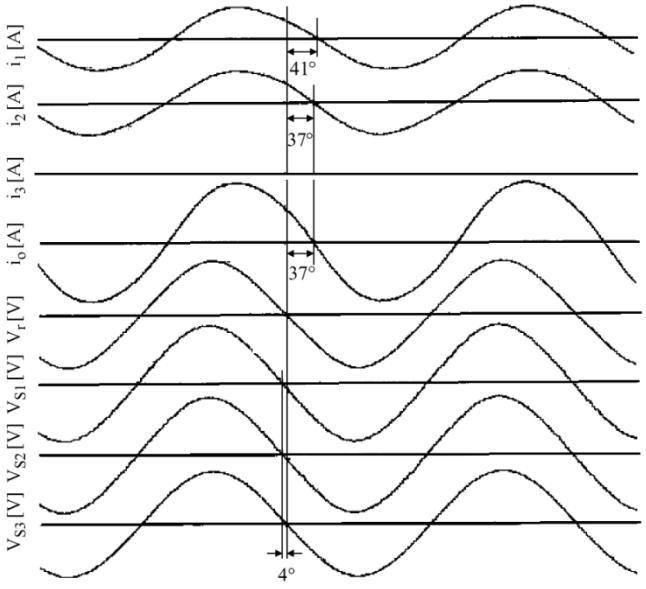


Figure 6. Each inverter current and voltage waveforms.

When $\delta$ is 7.5◦ and $V_r$ is 100 V, $V_{sm}$ becomes 109 V by using (1) and (2). The reactance of the interlinked reactor becomes 1.57 mH.

Fig.6. shows each inverter current and voltage waveforms. 50% of real energy is sent to the load by separate WT and PV inverters. Under this condition reactive energy of the battery bank, two-directional inverters became zero. The capacity of the load is $3kVA$ , and the power factor is 0.8.

The rating of each lead-acid battery module is $12V$,$24Ah$. The battery unit consists of 24 battery modules connected in series in two parallel rows. The balanced charging voltage is set as $331.2\ V$, and the charging current is set at $10A$.

### *B. Diversion power control*

The real-reactive energy control method is developed for the successful control of diversion power. When either wind power or PV power production becomes better than load, EG stops, and the 2-directional inverter as a grasp is operated underneath the CVCF situation. Then, the remaining portion obtained after removed load from production power (diversion power), is used as a charging power for the battery bank. In the course of battery charging, an advanced technique to prevent battery overcharge is required. Diversion load (e.g., resistive load or radiator), to utilize diversion power, is usually placed in parallel with the battery or AC output.

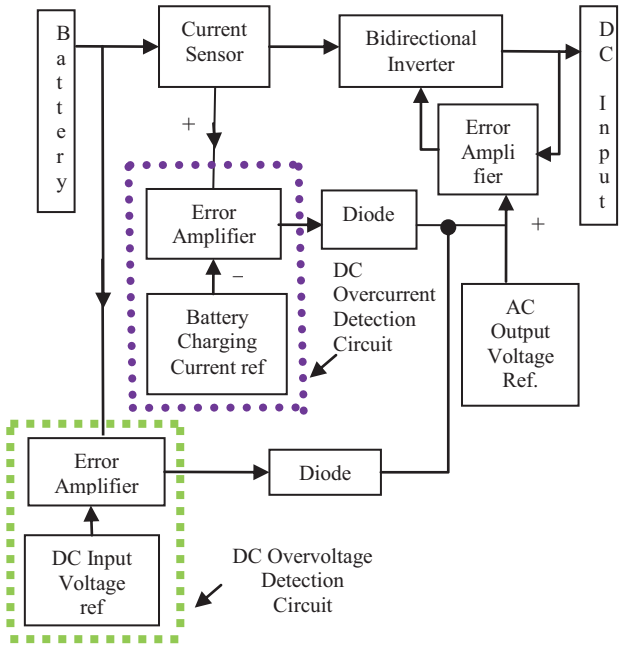


Figure 7. Bidirectional inverter dump power control

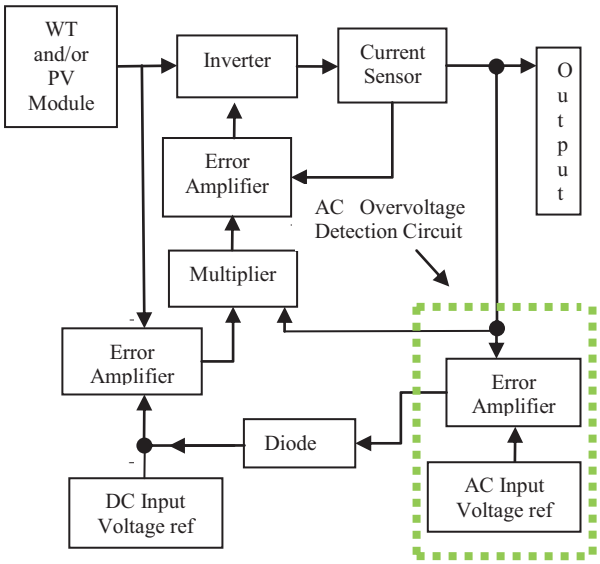


Figure 8. WT and PV inverters dump power control

The diversion power changes continuously, it is challenging to adjust the diversion load by simply input diversion load, because this hinders flexible control of battery charging. To stabilize both the charging current and voltage of the battery bank, the improved matchless advanced dump power control method is factorized by diversion energy guidelines without any diversion load and their difference is shown in Fig.7 & 8. This method allows for immediate response to diversion energy as well as a decrease in unwanted diversion power control, contributes to more successful use of natural energy.

E-ISSN 2581 - 7957
P-ISSN 2277 - 3916

CVR Journal of Science and Technology, Volume 19, December 2020
DOI: 10.32377/cvrjst 1904

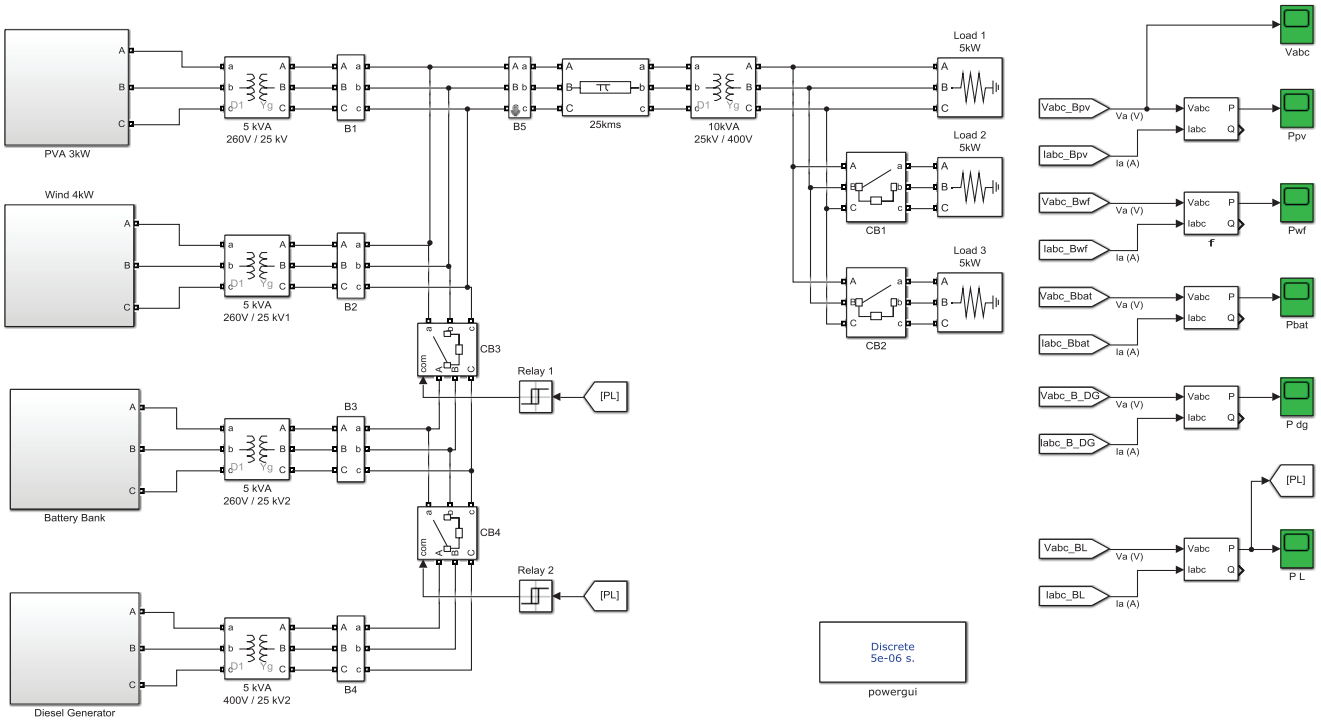


Figure 9. Simulation diagram of the hybrid power system with PVA, wind farm, battery, diesel generator.

## IV. Simulation Results and Discussions

The simulation diagram of the hybrid power system is shown in Fig.9. The proposed hybrid system consists of four energy sources such as PVA, wind farm, storage battery, and diesel generator. The solar PVA and wind farm are directly connected to the load through a transmission line, whereas the battery and diesel generator is connected to the transmission line through a circuit breaker (CB). For every system, the $5kVA$ rating of the transformer is used to step up the voltages. All the above four systems are operated in parallel by synchronizing their phase angles and magnitudes.

The synchronization is done by using the Synchronous Reference Frame (SRF) controller. The SRF controller has been implemented in all four systems to maintain synchronization. In this system total, three loads are introduced. Each load consumes 5kw power, i.e., the total power consumed by the load is $15kW$ . Hence, it is needed to supply the $15kW$ power to the load by synchronizing all the four sources. The results of different energy systems are simulated in a MATLAB environment as shown below.

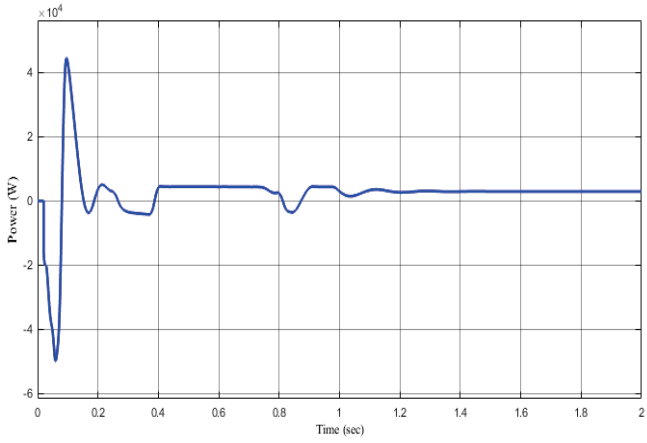


Figure 10. Solar PVA output power.

The PVA generates $3kW$ power, but the power given to the load is $2.650kW$ only. The $350W$ power is lost due to the conversion and transformation losses in the system. The above graph shows the solar output power, initially, transients are present in the system. Then the system came into a stable state and supply $2.650kW$ to the load as shown in Fig.10.

E-ISSN 2581 - 7957
P-ISSN 2277 - 3916

CVR Journal of Science and Technology, Volume 19, December 2020
DOI: 10.32377/cvrjst 1904

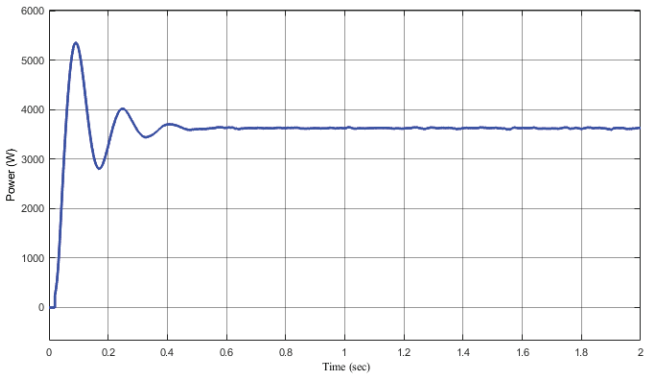


Figure 11. Windfarm output power

The actual power generated by the wind farm is $4kW$, but due to losses the power injected into the load is only $3.30kW$. The remaining $700W$ power is lost due to the rotating parts of the wind turbine. The Permanent Magnet Synchronous Generator (PMSG) is used in the wind energy system. Initially, there are transients in the system, then the system came into a stable position and supplies $3.30kW$ to the load. The simulation result is shown in Fig.11.

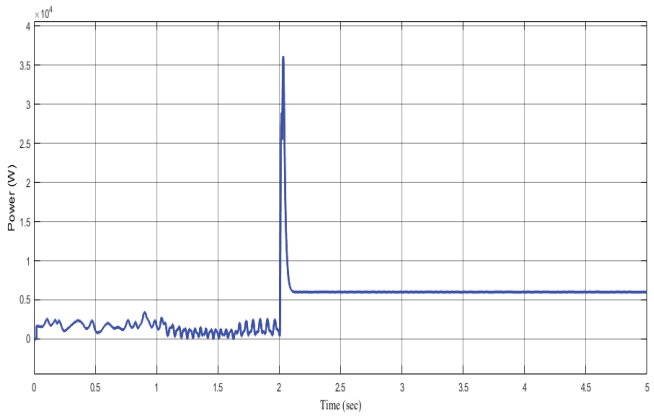


Figure 12. Storage battery output power

The lead-acid battery is used with the rating of $E = 450V$ with the capacity of 24 Ampere hours (Ah). There are two states in the battery i.e, charging and discharging state. The Fig.12. shows there is a transient (harmonics) in the starting and the negative part of the graph shows the charging of a battery and the positive part shows the discharging of a battery. If the State of Charge (SoC) is 80% it indicates the discharging of a battery and 10% indicates the charging of a battery.

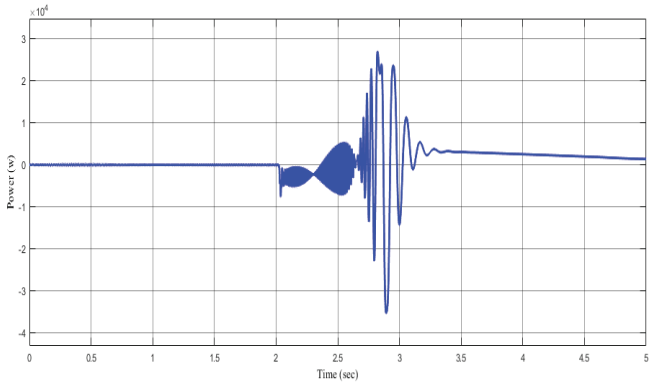


Figure 13. Diesel generator output power

The diesel generator generates only $2kW$ to the load. It is used as a backup device. Initially, there are transients in the system then it becomes the stable state and supplies power to the load shown in Fig.13. It is a non-renewable energy resource. The cost of fuel is high, so, instead of using diesel, one more renewable energy source i.e, the fuel cell is introduced.

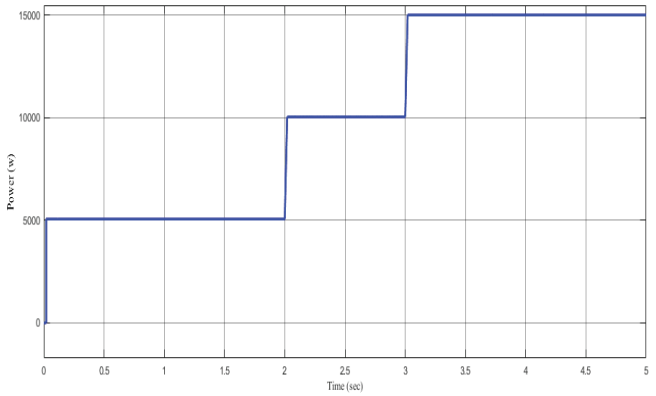


Figure 14. Load output power

In Fig.14, three loads are added each load consists of $5kW$. Depends upon the load demand the renewable energy sources are activated. If the first load demand is $5kW$ then PVA and wind farm supplies power to the load. If the second load is added into the system, then the total load demand is $10kW$. Then the power supplied by the wind farm and solar didn't sufficient to meet the load demand. Hence the storage battery supplies the power to the load demand. If the third load is added then the power supplied by these three devices is not sufficient. Hence in this situation, all the four energy sources are activated and supply power to meet the load demand.

E-ISSN 2581 - 7957
P-ISSN 2277 - 3916

CVR Journal of Science and Technology, Volume 19, December 2020
DOI: 10.32377/cvrjst 1904

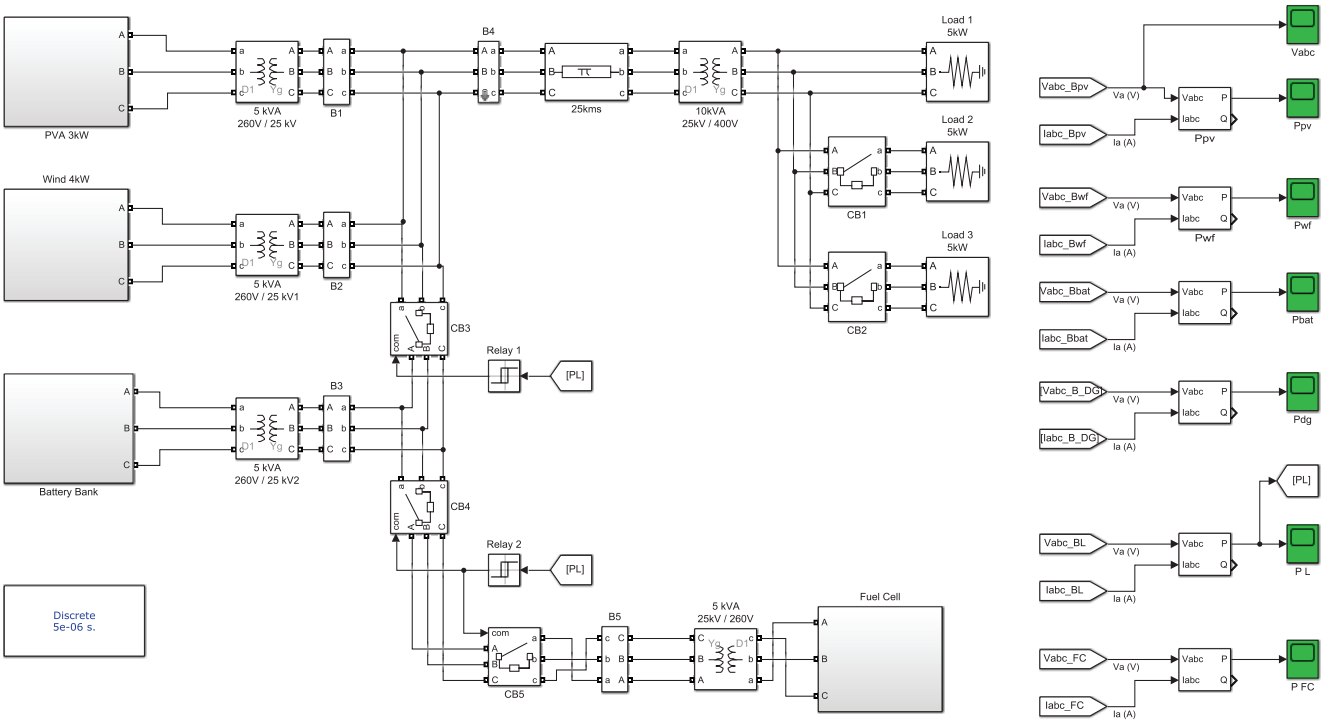


Figure 15. Simulation diagram of hybrid power system with PVA, windfarm, battery & fuel cell

The Fig.15. shows the simulation diagram of four energy sources, but all these are renewable energy sources only. But in the simulation diagram Fig.9. there is one diesel generator (non-renewable energy source) is connected. Here diesel generator is detached and fuel cells are introduced to reduce the cost so that the system efficiency is improved.

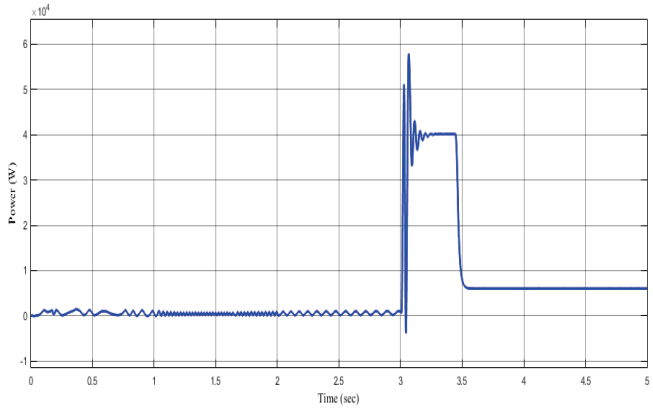


Figure 16. Fuel cell output power

The fuel cell generates $6kW$ this power is supplied to the load when PVA, wind farm, and the storage battery is not able to fulfill the load demand. The effective use of fuel cells is also presented in the paper for optimal operation.

## V. Conclusions

This paper is equipped with a self-power composite electricity production system, comprised of PLL and diversion energy control. The diversion energy control allows for the arrangement of a return path in this system, there is no need for a devoted ultra-speed line to deliver battery storage voltage and current information. If the energy line is used as a medium for the transfer of data, the line voltage magnitude is used as the transfer of data. So, there is no usage of a fiber optic communication line or the energy line transporter system via which harmonic signals are applied to the energy line. Moreover, neither the diversion load nor diversion load control device is required. Under the proposed diversion energy control, management of output is done without the battery fully charging, and effective use of excess energy is made possible. This furnishes to the extension of battery life and comprehension of a less-price system. The system, via the AC system interlinked, has allowed the stretchy expansion of the system in the future. Energy sources together with EG have interconnected flexibly any location with the same energy line, and the energy quality constant is maintained by controlling the phase and magnitude of the AC output voltage. It is estimated that this composite system with natural energy makes use of a variety of power control techniques, is validated. With the above-considered system without the connection from the main grid, i.e., in the off-grid, the battery and 6 kW fuel cells can improve the stability of the system. In the same off-grid time, the SoC is 80%, which means that the battery and fuel cell is fully utilized thus maintaining efficiency. The system will also help other developing countries in context protection through an appeal on remote islands with no dependence on marketable energy systems.

## REFERENCES

[1] M.Uzunoglu, & M.S.Alam, "Dynamic modeling, design, and simulation of a combined PEM fuel cell and ultracapacitor system for stand-alone residential applications," *IEEE Transactions on Energy Conversion*, vol.21, no.3, pp.767-775,2006.

[2] N.A.Ahmed, M.Miyatake, & A.K.Al-Othman, "Power fluctuations suppression of stand-alone hybrid generation combining solar photovoltaic/wind turbine and fuel cell systems," *Energy Conversion and Management*, vol.49, no.10, pp.2711-2719, 2008.

[3] S.K. Kim, J.H. Jeon, C.H. Cho, J.B. Ahn, and S.H. Kwon, "Dynamic modeling and control of a grid-connected hybrid generation system with versatile power transfer," *IEEE Trans. Ind. Electron.*, vol. 55, no. 4, pp. 1677–1688, Apr. 2008.

[4] W.Li, G.Joos, and J.Belanger, "Real-time simulation of a wind turbine generator coupled with a battery super capacitor energy storage system," *IEEE Trans. Ind. Electron.*, vol. 57, no. 4, pp. 1137–1145, Apr. 2010.

[5] K.Karakoulidis, K.Mavridis, D.V.Bandekas, P.Adoniadis, "Techno-economic analysis of a stand-alone hybrid photovoltaic-diesel–battery-fuel cell power system," *Renewable Energy*, vol.*36*, no.8, pp.2238-2244, 2011.

[6] A.I.Bratcu, I.Munteau, S.Bacha, D.Picault, and B. Raison, "Cascaded dc–dc converter photovoltaic systems: Power optimization issues," *IEEE Trans. Ind. Electron.*, vol. 58, no. 2, pp. 403–411, Feb. 2011.

[7] E.Dursun, & O.Kilic, "Comparative evaluation of different power management strategies of a stand-alone PV/Wind/PEMFC hybrid power system," *International Journal of Electrical Power & Energy Systems*, vol.34, no.1, pp.81-89, 2012.

[8] M.Rezkallah, A.Chandra, D.R.Rousse, H.Ibrahim, "Control of small-scale wind/diesel/battery hybrid standalone power generation system based on fixed speed generators for remote areas," In *IECON 2016-42nd Annual Conference of the IEEE Industrial Electronics Society,* vol.*42,* pp.4060-4065, 2016.

[9] V.Raviprabakaran, & R.C.Subramanian, "Enhanced ant colony optimization to solve the optimal power flow with ecological emission,". *International Journal of System Assurance Engineering and Management*, vol.9*,* no. 1, pp.58-65, 2018.

[10] S.Das, & A.K.Akella, "Power flow control of PV-wind-battery hybrid renewable energy systems for stand-alone application," *International Journal of Renewable Energy Research (IJRER)*, vol.8, no.1, pp.36-43, 2018.

[11] R.Vijay, "Quorum sensing driven bacterial swarm optimization to solve practical dynamic power ecological emission economic dispatch," *International Journal of Computational Methods,* vol.15, no. 03,pp. 1850089-24 ,2018.

[12] A.F.Bendary, & M.M.Ismail, "Battery charge management for hybrid PV/wind/fuel cell with storage battery," *Energy Procedia*, vol.162, pp.107-116, 2019.

[13] A.Amar Bensaber, M.Benghanem, A.Guerouad, & M.Amar Bensaber, "Power flow control and management of a Hybrid Power System," *Przegląd Elektrotechniczny*, vol. 9, no.1, pp.189-190, 2019.

[14] A.Shaqour, H.Farzaneh, Y.Yoshida, & T.Hinokuma, "Power control and simulation of a building integrated stand-alone hybrid PV-wind-battery system," in Kasuga City, Japan. *Energy Reports*, vol.6, pp.1528-1544, 2020.

[15] V.Raviprabakaran, "Optimal and stable operation of microgrid using enriched biogeography based optimization algorithm," *Journal of Electrical Engineering*, vol.17, no. 4, pp.1-11, 2018.

[16] C.Ghenai, T.Salameh, & A.Merabet, "Technico-economic analysis of off grid solar PV/Fuel cell energy system for residential community in desert region," *International Journal of Hydrogen Energy*, vol.45, no.20, pp.11460-11470, 2020.

E-ISSN 2581 - 7957
P-ISSN 2277 - 3916

CVR Journal of Science and Technology, Volume 19, December 2020
DOI: 10.32377/cvrjst 1905

# Considerations to Achieve Pulsatility for Left Ventricular Assist Devices through BLDC Motor by Open Loop Control System

Yenumula Vinod Kumar[1], Dr. S.Venkateshwarlu[2], Dr. Anil Kumar Puppala[3] and Phani Kumar K.S.V[4]
[1]PG Scholar, CVR College of Engineering/EEE Department, Hyderabad, India.
Email: yenumulavinod123@gmail.com
[2]Professor, CVR College of Engineering/EEE Department, Hyderabad, India.
Email: svip123@gmail.com
[3]Professor, Geethanjali College of Engineering and Technology/EEE Department, Hyderabad, India.
Email: apuppala@gmail.com
[4]Asst. Professor, CVR College of Engineering/EEE Department, Hyderabad, India.
Email: phani5016@gmail.com

***Abstract:*** **Ventricular Assist Devices (VADs) and Total Artificial Heart (TAH) are used to replace the diseased heart and play a major role in saving the lives of the people. Left Ventricular Assisting Devices are the mechanical circulatory devices which play a key role in assisting patients who are suffering from different heart problems. In earlier stages, pulsatile flow devices are used, and later they are switched to continuous-flow devices. Though these devices have several advantages they have reported several complications during working. To avoid these complications, several trails were being conducted. In this paper, the work is done on achieving the pulsatility in Ventricular Assisting Devices. The open-loop control system has been implemented which is used to get different speeds of the BLDC motor to achieve the pulsatile flow in the device. The results are compared to the earlier experiment results and are tabulated.**

***Index Terms:*** **Left Ventricular assisting devices, pulsatile flow, BLDC motor control, percutaneous cables.**

## I. Introduction

In the past few years, cardiac diseases are the main reasons for the death of many people. Due to less availability of heart donors, many people who are suffering from heart disease who are waiting for the replacement of their hearts with normal hearts are dying. To overcome this problem, there is a need for developing a device that will support the circulatory system of the body. There is an ongoing development of these circulatory devices and heart replacement devices from the past 62 years [1]. The step towards the development of Mechanical Circulatory Devices (MCD) [2] has been started in 1957 and the field of MCD is the first introduced in 1964 [3-4]. From the past few decades, there are many deaths recorded due to heart failure. This motivated many of the engineers to develop MCDs. Mechanical circulator support devices are used to help in pumping the blood from the heart to other parts of the body in case of heart failure. These devices are used in two different therapy systems which are called bridge to recovery and bridge to transplant. In the first strategy, the heart recovers due to the support of Ventricular Assist Devices, and in the second strategy it ensures the patients' survival until a donor or total artificial heart can be transplanted. In the inception of the heart program in 1964 investigations have been conducted to develop the Total Artificial Heart [5] and Ventricular assisting Devices that are implantable inside the body without causing any damage to the skin. To implant these devices in patients' body, they have to undergo many clinical trials that involve various designs and different optimizations. During this process, it is needed to design these devices in such a way that they must fit the body without any problems and the weight and dimensions of these devices must be considered properly to implant into the patients' body. To meet this requirement, the blood pump, electric motor, the power supply should be small and these electric motors and blood pumps must be designed in a size such that they can be easily fit into the human body and sufficiently durable to support the patient for a longer duration and have a good performance efficiency. In the previous cases, many of the experiments were conducted on continuous flow systems. Due to many advantages of these systems such as ease of control and smaller in size they have been implemented in the body as a mechanical support system. Despite their advantages, continuous-flow devices have been reported several complications in providing a pulsatile flow of blood which resulted in several problems such as frequent hospitalization, etc., To overcome this problem, many of the experiments have been recently conducted to achieve the pulsatile nature which is the natural working of the heart. It is possible to achieve pulsatile flow by changing the speed of the motor & pump at the rate of native heart rate [6-7]. To get the different speed levels of the motor, there is a need to control the speed using some controlling action. In the present paper, an open-loop control system to control the speed of the BLDC motor is being used.

## II. Literature Review

Gregory K. MacLean, Peter A. Aiken, William A. Adams, Tofy Mussivand (1994) conducted a study between Ni/Cd and lithium cells which are used for implantable medical devices. In this process, they have used 2 different

E-ISSN 2581 - 7957
P-ISSN 2277 - 3916

CVR Journal of Science and Technology, Volume 19, December 2020
DOI: 10.32377/cvrjst 1905

rectangular prismatic Ni/Cd cells and 5 different rechargeable lithium cells and determined at $37^0$c temperature [8].

E. Okamoto, K. Tomoda, K. Yamamoto (1994) talked about a highly efficient, totally implantable assisting pump device, and also compact which has a motor-driven assisting pump. The volume of the pump which they have is used is 350ml, and its controller is 210ml. The outflow of the pump is 5.8 L/min which is obtained against a mean after-load of 100 mm Hg [9].

P J Ayre, N H Lovell, J C Woodard (2003) studied the effects of pulsatile and non-pulsatile flows using in vitro mock loops, and acute (N = 3) and chronic (N = 6) ovine experiments. An estimation of average flow in its algorithm was derived from the RMS pump impeller speed and RMS input power using the non-pulsatile and pulsatile mock loops. By using this algorithm, it has been estimated the flow in a rotary blood pump without implanting additional invasive sensors [10].

Allen Cheng, Christine A. Williamitis, and Mark S. Slaughter (2014) compared between continuous flow and pulsatile flow devices are considered and they have explained the advantages and disadvantages of different devices [11].

A. K. Puppala, V. Sonnati, and S. Gangapuram suggested a few materials for additive manufacturing. They thought that additive manufacturing would increase the performance of VADs. They reviewed a few materials like Ti-6A1-4V, Co-Cr-Mo, Co-Ni-Cr-Mo which would be suitable for applications related to the heart [12].

## III. Working of Left Ventricular Assist Devices

Before knowing the working of LVADs the functioning of the heart is described. The heart is a muscular organ which is used to pump the blood continuously throughout the body. The heart is a muscular organ that consists of four chambers; they are, namely, the right and the left atrium and the right and the left ventricle. These chambers of the heart work together by contracting and relaxing alternatively in pumping blood throughout the body. The below figure describes the structure and functioning of the heart.

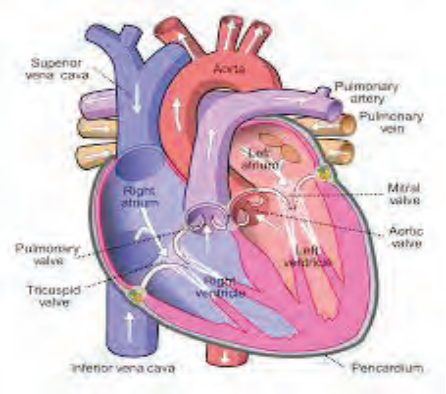


Figure 1. Structure and functioning of heart

After knowing the functioning of the heart, the working of Ventricular Assisting Devices which are used to assist the heart failure is presented. These devices are placed inside the body and are connected between the apex of the left ventricle to the aorta which is considered the main artery of the heart which is used to carry the oxygenated blood to the entire body. Blood is continuously sent from the left Ventricular Assisting chamber via the apical inflow canal and propelled through a pumping house where the magnetic field generation by a rotary pump transmits blood through the outflow graft to the ascending aorta. A percutaneously tunnelled driveline connects the external power source or the systems controller to the pump. The figure shown below indicates how the left Ventricular Assisting Devices (VADs) are connected to the human body.

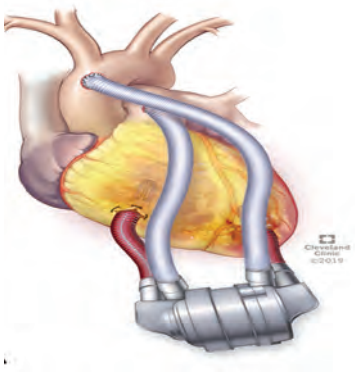

Figure 2. The Left Ventricular Assist Device connected to heart with controller and battery assembly

The system controller is the main component that is placed outside the body has both manual and fixed settings that modulate the speed of the pump, provided alarms where there is any malfunction in the device for future analysis. These Ventricular Assisting Devices deliver 4 to 8L per minute of blood at different speed levels. The VAD has a centrifugal, pulsatile flow, implantable rotary pump currently in clinical practice. This Ventricular Assisting Device operates via a hydro-magnetically levitated rotor without mechanical bearings and can deliver up to 4.5 to 5L/min of blood through the heart.

## IV. Design of LVADs

### *A. Internal Structure of the LVAD*

The design of the LVAD [13] is considered below. The design of the LVAD must be done in such a way that it must be small in size and be able to fit inside the body. The design of the LVAD requires different components like a pump which consists of motor, inlet and outlet valves, impeller unit, and housing which is used as a covering for these parts of the pump. Before designing the LVAD, there is a need to know how the LVAD internal structure looks like.

E-ISSN 2581 - 7957
P-ISSN 2277 - 3916

CVR Journal of Science and Technology, Volume 19, December 2020
DOI: 10.32377/cvrjst 1905

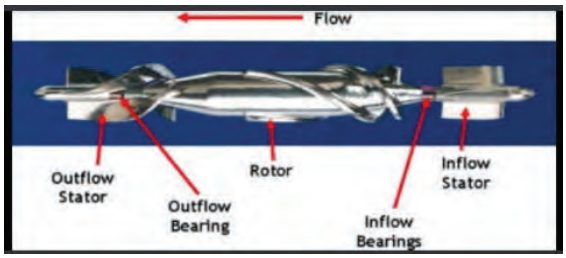


Figure 3. Internal structure of LVAD pump

The above diagram represents how the pump of the LVAD looks internally. It consists of an inflow stator from where blood enters the pump from the inlet valve. It is connected to the rotor of the motor with a shaft and bearings for free rotation of the inflow stator. This will rotate when the rotor starts rotating and it is used to drive the flow of blood inside the pump. After this inlet stator, there is a rotor that is known as the impeller unit of the pump which consists of a blade on it. This impeller unit is used in this system because the impeller is a rotating part of the pump which is able to convert mechanical energy given by the motor into power of the pump output which is fluid output by rotation. After the rotor, it consists of an outflow stator which is also connected to the rotor with the help of outflow bearings. This will allow blood to flow smoothly from the pump to the outlet valve. The Figure 4 represents the entire internal structure of the LVAD which has the inlet and the outlet valves. The inlet valve is connected at the apex of the left ventricle from where the oxygenated blood will enter from the right ventricle. From this inlet valve, blood enters the pump of the device.

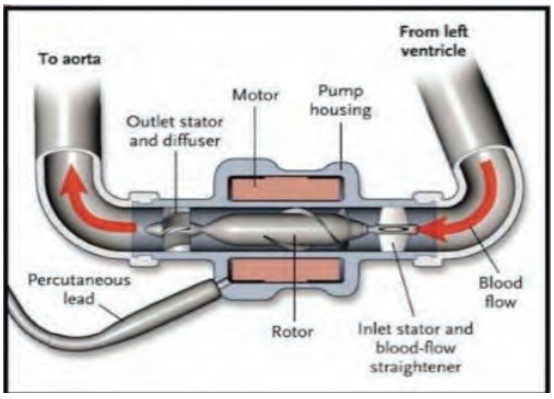


Figure 4. Internal structure of the LVAD with the inlet and the outlet valves

The outlet valve is connected to the Aorta which is considered the main artery of the heart which will deliver the oxygenated blood to the entire body. From the output side of the pump, blood will enter the outlet valve and from there, blood will enter the aorta. This outlet valve is connected to the pump with the help of strain relief. This strain relief is also referred to as bend relief that is required because it gives mechanical strength to the valve when the load is applied to the valve. By considering this requirement, a small device, which is totally implanted inside the body [14] has been designed.

### *B. The BLDC Motor*

In the above section, the internal structure of the LVAD is described. From the above discussion, it is clear that the pump which is present in the LVAD is the key component in which the motor is present and due which blood is allowed to flow from the LVAD to the entire body. The motor is an important part of the pump which should be very small in size and can be fit inside the pump. During this study, there is a use of the BLDC motor. The construction of the BLDC motor is as if the construction of the PMSM. The invention of the brushed DC motor was done in the 19th century. These DC motors consist of brushes and the commutator assembly. Due to these brushes, there is friction along with the rotating commutator segments which will lead to power loss and this will make the motor as low power motor. Another disadvantage of a brushed DC motor is the resistance of the sliding brush contact which will lead to a voltage drop in the motor circuit which is also known as brush drop that will consume the energy. So, considering the above disadvantages of the brushed DC motor, the alternate motor is made which is known as brushless DC motor. These BLDC motors came into existence around the 1970s.

Figure 5. The BLDC motor with Electronic Speed Controller

The above figure represents the BLDC motor which is considered for testing purposes in this study. The BLDC motor is synchronous motors that are powered by DC electricity with the help of an inverter circuit which produces AC electricity as output which is used to drive each phase of the motor as a closed-loop controller. A Brushless DC motor has a commutation process done using a microcontroller. These motors use a hall-effect sensor which is used to determine the position of the rotor shaft. To rotate the BLDC motor, the stator windings must be energized in a particular sequence. The commutation circuit which is present inside the motor must know the position of the rotor to energize the correct winding. To do this, the BLDC motor consists of a hall-effect sensor. In a three-phase motor, there are three hall sensors present in it. When there is a moment of rotor magnetic poles near the hall sensor, it will produce a signal indicating there is a pole

E-ISSN 2581 - 7957
P-ISSN 2277 - 3916

CVR Journal of Science and Technology, Volume 19, December 2020
DOI: 10.32377/cvrjst 1905

passing near the sensor. Based on these combinations, the determination of the position of the rotor and according to the position, the energized stator windings can be done.

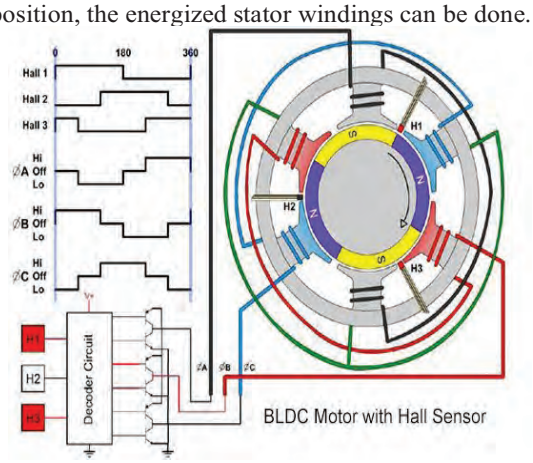


Figure 6. BLDC motor with hall sensors

This is the basic working of a BLDC motor using a hall-effect sensor. In the VADs, the most commonly used motor is the BLDC motor. This is because the BLDC motor has several advantages over many other motors and the requirements for the VADs are met by the BLDC motor. Generally, the power ratings of TAH and VADs are in the range of 8W to 20W and the duration of these devices is around 2 years [15]. In this study, for testing of motor, A2212/1000kV motor is used which has 7V to 12V input voltage and 0.5A of no-load current. From the study of the functioning of the heart, it is clear that the heart must pump around 5 to 6 litres of blood per minute. So, this BLDC motor should be able to pump 5litres of blood in one minute which can be done by adjusting the speed of the motor. The pulsatile flow of blood can be achieved maintaining constant torque at variable speeds with the motor-pump set which is used in TAH and VAD. This is another reason to use the BLDC motor in these devices. In a brushed DC motor, it consists of brushes for delivering current. If this motor is used for a longer period of time the brushes will worn out and they will produce sparking which is not allowed. So, in order to overcome this problem, the BLDC motor is used which doesn't have brushes which will remove the sparking effect. The BLDC motor also has many advantages like high torque to weight ratio, increase in reliability, it has less noise compared to the brushed DC motor, and a longer lifetime. So, the BLDC motor is an ideal choice for TAHs and VADs.

### *C. Experimental Setup Controlling the Speed of the BLDC Motor by Potentiometer*

After studying the internal structure of the LVAD, it is clear that it uses the motor inside the pump which is used for the flow of blood through the heart. Before implanting the BLDC, motor inside the pump for designing the LVAD, the speed of the motor must be controlled and verified that when the power supply is given to the motor, it must rotate at the desired speed. The speed of this motor can be tested using different components like Arduino nano, potentiometer, and proximity sensor.

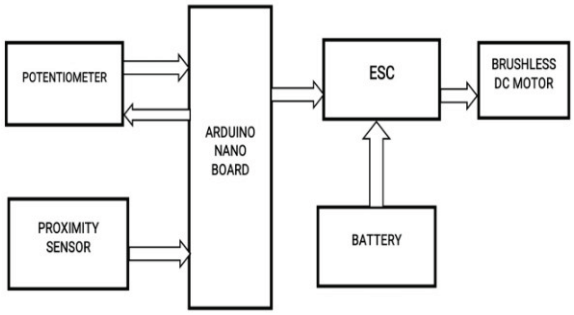


Figure 7. Block diagram of the BLDC motor with potentiometer and proximity sensor.

The above figure represents the block diagram of the BLDC motor connection to find the speed of the motor. In this first phase, the motor is controlled manually using a potentiometer which has potentiometer is a three-terminal device and it is generally a voltage divider to measure voltage or electric potential. These instruments are commonly used to control electrical devices mainly to control the speed of the motors. It consists of a sliding contact, when it is rotated, it will increase or decrease the resistance value through which the voltage can be limited, and ultimately, the speed of the motor can also be controlled. Another device that is taken into consideration is the proximity sensor. A proximity sensor is a device that is used to sense the presence of objects which are closer to it without any physical contact between the object and the sensor. A proximity sensor will emit an electromagnetic field that looks for changes in the field and returns that change to it. This sensor is used to detect the obstacle when it enters the field. The proximity sensor returns the signals in the form of 0s and 1s. If there is no obstacle detected, it will return the value as 0 and if there is any obstacle is detected, it will return the value as 1. A battery is also shown in the block diagram. In this study, Lipo battery of rating 11.1V, 2200mAh is used to give power supply to the motor. The other component, it is being used i.e. Arduino nano which consists of a microcontroller to do operations using the nano-board. The program which is used to rotate the motor and is used to control the speed of the motor using a potentiometer is written and dumped in this Arduino Nano board.

### *D. Algorithm for analysing speed of rotation:*

- Set and initialize the variables such as proxy, s, Val, prev_state, current_state, count.
- Initialize current_state is equal to proxy.
- Check for the condition of current_state is not equal to prev_state.
- If the condition is false again go back to STEP 2.
- If the condition is true check where the obtained current_state is equal to one.
- If the condition is false again go back to STEP 2.

E-ISSN 2581 - 7957
P-ISSN 2277 - 3916

CVR Journal of Science and Technology, Volume 19, December 2020
DOI: 10.32377/cvrjst 1905

- If the condition is true increment the count value by 1 (count = count +1).
- After completing the loop initialize prev_state value is equal to current_state value.

The above algorithm describes how the code is written in the Arduino board to rotate the motor and also used to detect the speed of the motor. The BLDC motor is connected with the nano board with the help of Electronic Speed Control (ESC). The ESC is an electronic circuit that is used to control and regulate the speed of the motor. This will follow a speed reference signal which is used to energize the coils at particular instants of time. In the ESC, it consists of MOSFETS as a switch and if the BLDC motor has Hall sensor, it will send signals which represent the position of the rotor. In another case, if a BLDC motor without a hall sensor is used using back-emf, it will send the signals which represent the position of the rotor. According to the position of the rotor, the respective pair of switches will get closed and the remaining switches will be in off mode.

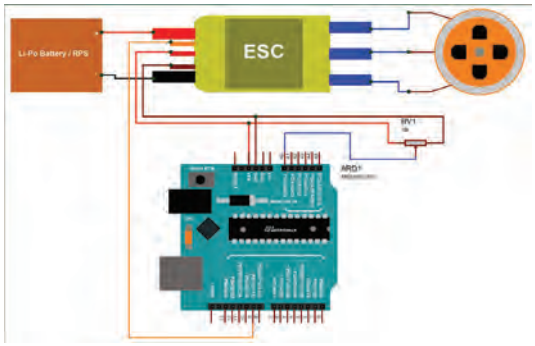


Figure 8. Experimental setup to find the speed of the BLDC motor using proximity sensor

The above figure represents the experimental setup to find the speed of the BLDC motor using the proximity sensor. When the power supply through the battery is given to the motor, it will start rotating. A small piece of paper or wire is attached at the tip of the motor which can be detected by the sensor. While the motor is rotating the piece of paper or wire also starts rotating. This is taken as an obstacle for the proximity sensor and whenever it detects the piece, it will send the signal and the value of count is increased. By using this count value which will appear on the serial monitor, the speed of the motor can be determined.

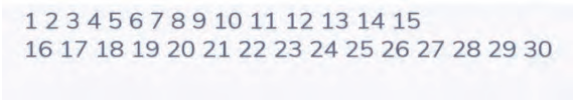


Figure 9. Serial monitor output for speed control of motor

By considering the values in the serial monitor after 30sec, the speed of the motor (SPEED = value we get on the serial monitor after 30sec) can be calculated. By using a potentiometer, the speed of the BLDC motor can be varied and this can be done by varying the potentiometer nob manually.

### *E. Open Loop Control System*

From the above, it is seen that how the speed of the BLDC motor can be controlled manually using a potentiometer and the speed of the motor can be determined the proximity sensor. In the above system, there is manual control of the motor is considered. But, when the motor is used in the design of the LVAD which is placed inside the body, the speed of the motor must be automatically controlled to achieve a pulsatile nature flow of blood. So, this is the reason the open-loop control system is considered in this study.

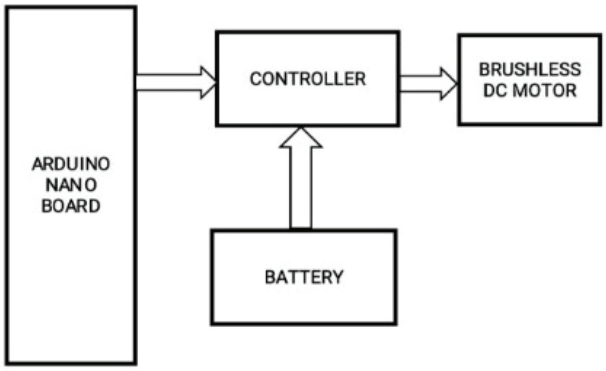


Figure 10. Block diagram for open loop control system

The above figure represents the block diagram for the automatic speed control of the motor using an open-loop control system. In this Arduino nano, a controller (ESC), the BLDC motors, a battery that powers the BLDC motor used.

### *F. Algorithm for open loop control:*

- Initialize the values of proxy, value, count and declare them as integers.
- set proxy value as input parameter, the motor attached pin value, baud rate of serial monitor.
- check whether the value of count is not equal to 2.
- If the condition is true the loop begins. The motor speeds will increase from 1200 to 1600 and the motors rotates at that speed for 0.2 sec.
- In the next step the speed of motor will reduce from 1600 to 1400 and the motor will rotate at that speed for 0.15 sec.
- Again, the motor speed is reduced from 1400 to 1300 and will rotate for 0.15 sec.
- From that speed the speed will get further reduced to 1220 and the motor will rotate for 0.1 sec.
- In the last step the motor will gain the starting speed which is 1200 and rotate for 0.4 sec.
- After completing this loop, the count value is increased and again, it goes to STEP 3.
- The loop will continue until the value count is equal to 2. After this the loop will end and we will come out of the loop and the program will stop.

E-ISSN 2581 - 7957
P-ISSN 2277 - 3916

CVR Journal of Science and Technology, Volume 19, December 2020
DOI: 10.32377/cvrjst 1905


Figure 11. The output values obtained from serial monitor for an open loop system

From the above figure, it is observed in the serial monitor that the speed values of the motor which is varying in certain intervals of the time.

So, this is how the speed of the motor can be varied which is used to design the Ventricular Assisting Devices that are used to pump the blood in a pulsatile manner which represents the normal functioning of the heart. The speed of the motor is varied in an open-loop control system to achieve the pulsatile flow of blood. Due to these variations in the speed of the motor the blood which is pumped from the LVAD will resemble the normal heart pumping.

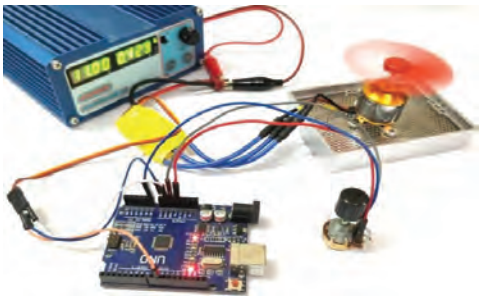

Figure.12. Experimental setup for an open loop control system

The above diagram represents the experimental setup of an open-loop control system. By this setup, the required code is written and dumped in the nano board and the speed of the motor at different intervals of the time is recorded and are verified with the previous results.

## V. Batteries Used and Power Transferred for Ventricular Assisting Devices

The rechargeable battery pack is used for Ventricular Assisting Devices. The batteries which give power supply to the LVAD must be easy and effective in operation. The use of rechargeable lithium cells in implantable medical devices may yield batteries that are smaller and lighter than those of Ni/Cd batteries, however, Ni/Cd cells are less preferred than lithium batteries because of its high discharge cycle and life cycle. Various batteries were considered for supplying power to Ventricular Assisting Devices (VADs). In the recent days, Lithium-ion batteries have more advantages like low discharge rate, high power supply, and less weight when compared to different batteries. So, in the recent studies in giving power supply to the LVAD Lithium-ion batteries are used. Two 14V lithium-ion battery packs were used to give power supply. These battery packs are connected to the controller and it will supply the power to the motor which is implanted inside the body.

To give power to the motor, there is a need to develop a connection between battery packs and the motor. Here, there are the percutaneous cables [16] which are used to transmit the electrical energy from a battery source which is located outside the body to the motor which is present inside the body. These types of cables are passed through the skin and which will give power to the implanted motor.

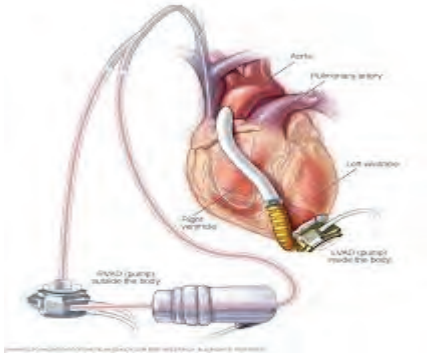

Figure 13. Percutaneous cable type transmission

## VI. Experimental Results

This paper implemented an open-loop control system to achieve the pulsatile speed in the BLDC motor (hall sensor-based) which is placed inside the pump which is used to design the LVAD.

The experimental results for the open-loop control system are obtained for different levels of speed at different intervals of time and are tabulated as below.

TABLE I.
Different Levels of Speed at Different Intervals of Time

| S. No | Speed (rpm) | Time (sec) |
|---|---|---|
| 1 | 1200 | 0+ |
| 2 | 1600 | 0.2 |
| 3 | 1400 | 0.35 |
| 4 | 1300 | 0.5 |
| 5 | 1220 | 0.6 |
| 6 | 1200 | 0.7 |
| 7 | 1200 | 0.1 |

These levels of speed are considered from the previous results and are used in the present work to get the pulsatile flow of blood. This work is done by using Arduino nano through which the open-loop operation is done and made to rotate the motor at different levels of speed. These levels of speed of the motor which are varied during particular intervals of time are plotted in the graph and the output of the graph obtained is shown below.

The peak in the graph is observed because initially, the heart is in a contraction state in which the blood is pumped from the left ventricle to the aorta with some pressure. Hence, the open-loop system is set up for initial speed to be high. After that, the heart will go into a relaxation state in which the heart is slowly relaxed. Due to this, speed is slowly reduced and made constant.

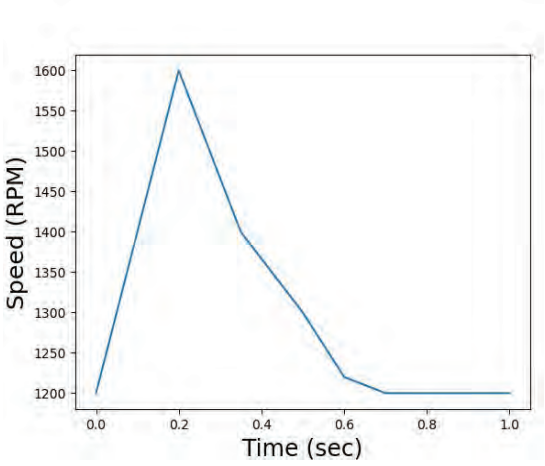


Figure 14. Pulsatile speed obtained with the BLDC motor using open loop control system

## VII. Conclusions

The weight, dimensions, and simplicity in control of the speed of the BLDC motor offer a practical solution for VAD. Control of the speed of the motor can be achieved by using different methods. While hall sensor-based operation for speed control is suitable for the devices. In the present paper, an open-loop control system is used to achieve the various levels of speed of the motor at different intervals of time. By using this open-loop system, pulsatile flow of blood is obtained which resembles the normal functioning of the heart.

Although this open-loop system is easy to implement, it has certain disadvantages. If there is no disturbance in the system, this open-loop system will work normally. But, if there are any disturbances in the system, it will affect the speed of the motor. Ripples will occur due to the disturbances present in the system. These ripples may lead to an uneven flow of blood inside the body. So, for the future, a closed-loop control system can be used to overcome this type of problem. The speed of the motor is fed back to the controller and this controller will compare the fed back speed and the original speed in which the motor has to rotate and reduce the error in the speed signal. Due to this, the speed of the motor can be controlled at the desired speed.

## References

[1] Benedikt A. Pelletier, Yvonne M. Blaszczyk, Patrick Carstens, Gonzalo Alvarez, Felix Lamping, Marco Laumen, Thomas Finocchiaro, and Ulrich Steinseifer on “Novel Optical Position Sensing for Miniaturized Applications and Validation in a Total Artificial Heart” IEEE transaction on biomedical engineering, VOL. 63, NO. 3, MARCH 2016.

[2] James F. Antaki, Richard K. Wampler, Kormos. M. “Mechanical circulatory support. A companion to Heart disease”. Elsevier Saunders 1995.

[3] Leslie mertz on “From artificial kidneys to artificial heart and beyond”;14 IEEE Pulse May 2012.

[4] Sean Pinney .P, on “Left Ventricular Assist Devices: The Adolescence of a Disruptive Technology” Journal of Cardiac Failure Vol. 21 No. 10 2015.

[5] T. Vakhtang, S. Phillips “Update in Artificial Heart Technology: Are We there yet?” Artificial Organs Vol 40., No.12,2016.

[6] Francis D. Pagani on “The quest towards the Holy Grail of mechanical circulatory support”; The Journal of Thoracic and Cardiovascular Surgery, September2015.

[7] R. Basanth, Anil K. Puppala “Considerations for Introducing Pulsatility in Continuous flow Ventricular Assist Devices by Modulation of Motor Speed,” IEEE International Conference on Innovative Technologies in Engineering 2018 (ICITE OU).

[8] Gregory K. MacLean, Peter A. Aiken, William A. Adams, Tofy Mussivand “Comparison of rechargeable lithium and nickel/cadmium battery cells for mechanical circulatory support devices”. ASAIO J 1994; 18:33–4.

[9] E Okamoto, K Tomoda, K Yamamoto, “Development of a compact, highly efficient totally implantable motor-driven assist pump system.” Artificial Organs 1994; 18(12):911–917.

[10] P J Ayre, N H Lovell, J C Woodard “Non-invasive flow estimation in an implantable rotary blood pump: A study considering non-pulsatile and pulsatile flows.” Physiol MEA 2003; 24:179–189.

[11] Allen Cheng, Christine A. Williamitis, and Mark S. Slaughter on “Comparison on continuous flow and pulsatile flow left ventricular assist devices: is there an advantage to pulsatility” Ann Cardiothorac Surg. 2014 Nov.

[12] Puppala A. K., Sonnati, V., & Gangapuram, S. (2020, March). “Additive Manufacturing for VADs and TAHs-a Review.” In *Journal of Physics: Conference Series* (Vol. 1495, No. 1, p. 12021). IOP Publishing.

[13] Praveen Kumar C, Neeth Antony A on “Designing and Modelling A Ventricular Assistive Device” IOSR Journal of Electrical and Electronics Engineering, Volume 11, April 2016.

[14] S. Takatani, Kazunobu Ouchi, M. Nakamura “Miniature, Totally implantable, permanent, Electromechanical pulsatile VAD system.” ASAIO J 2000 - Volume 46.

[15] William L. Holman, David C. Naftel, Chad E. Eckert, Robert L. Kormos, Daniel J. Goldstein, and James K. Kirklin, on “Durability of left ventricular assist devices: Interagency Registry for Mechanically Assisted Circulatory Support (INTERMACS)”; The Journal of Thoracic and Cardiovascular Surgery. August 2013.

[16] R. Basanth, Anil K. Puppala “Review of power delivery techniques and sources of power for VAD’s and TAH’s,” IEEE international Conference on innovative Technologies in Engineering 2018 (ICITE OU).

E-ISSN 2581 - 7957
P-ISSN 2277 - 3916

CVR Journal of Science and Technology, Volume 19, December 2020
DOI: 10.32377/cvrjst 1906

# Man Machine Interface Design using Hardware Programming for Performance Enhancement

Dr. T. Harinath[1] and Dr. K. Lal Kishore[2]
[1]Senior Manager, ECIL/Hyderabad, India
Email: harnath.t@gmail.com
[2]Professor, CVR College of Engineering/ECE Department, Hyderabad, India
Email: lalkishorek@gmail.com

***Abstract*: Existing Embedded Systems are designed using a microprocessor. Design methodology of the embedded system depends on the architecture of the microprocessor used. Architecture of these embedded system designs have total dependence on the architecture of the microprocessor used. Study and analysis of various embedded system designs for the past thirty years revealed that there are several other design, development and manufacturing related issues with the microprocessor based designs like speed of processing, power consumption, excessive utilization of silicon, etc. Objective of this paper is to critically examine the design requirements for Man Machine Interface Logic, which is an embedded system and ascertain the issues in the existing designs. Hardware Programming, an innovative conceptual solution is proposed to overcome the issues observed by designing an embedded system without using any microprocessor. Design approach and design methodology based on Hardware Programming have been presented. Concepts of designing Man Machine Interface logic using Hardware Programming have been elaborated. Comparative Analysis is provided to ensure both the qualitative and quantitative improvement in performance. Performance is gauged in terms of both qualitative and quantitative parameters.**

***Index Terms:* Embedded System, Protocol Analysis, Architecture, Silicon Utilization, Latency, Man Machine Interface, Hardware Programming**

## I. Introduction

### *A. Man Machine Interface*

Man Machine Interface (MMI) logic is a subsystem used in an electronic system for incorporating control, status, system and storage operations. These operations facilitate user in selecting different sets of parameters among the available groups for carrying out different activities without any design changes, whether hardware or software [1], [2]. In other words, MMI logic is meant for incorporating programmability feature to an embedded system. MMI logic itself is an independent embedded system. Transfer of information to and from the system is through interfaces [3]. MMI has five types of interfaces. They are input interface, output interface, I/O interface, system interface and memory interface. Collection of control information is through input interface from input devices like keypad. Display of output status information is through output interface to output devices like Liquid Crystal Display (LCD), Light Emitting Diodes (LED). Bidirectional flow of information is through I/O interfaces using I/O devices like Universal Asynchronous Receiver Transmitter (UART). Non-volatile storage of control and configuration data is done non-volatile memory like Serial Peripheral Interface (SPI) Flash memory using storage interface. Passing on the user fed control data and collection of system related status information is through system bus. UART is used for system bus. SPI is used for memory interface. Design methodology for MMI design is similar to any other embedded design. The factors to be concentrated on while designing MMI with a microprocessor are: Processing capabilities, Memory requirements, Data transfer mechanism, Integration with rest of the system and Clock requirements [4], [5].

Study and Analysis of various embedded systems design for the past 30 years have lead to the categorization of embedded systems design into following types:

- Embedded System using Hard Processor
- Embedded System using Soft Processor
- Embedded System using Multi-Core Hard Processor
- Embedded System using Multiple Processors
- Embedded System using Micro Controller
- Embedded System using embedded hard processor on Field Programmable Gate Array (FPGA) and reconfigurable logic on the same FPGA
- Embedded System using Digital Signal Processor
- Combination of two or more of the above

The Trends being followed in latest embedded system design are:

- System Design with Multiple – Processors and Multi Core Processors [6], [7], [8].
- System Design with Micro Controllers and Peripherals on same chip
- Hardware/ Software Co-Design
- Heterogeneous Embedded System Design
- FPGA based Embedded System Design [9], [10], [11].
- Single Bit Processor based System [12].
- Distributed Co-operative Design Method [13], [14].
- Power – Delay Reduction, Memory Efficient Techniques
- Dynamic Profiling [15].

### *B. Issues in Existing Embedded Systems*

Several issues have been observed in embedded system design with respect to the design, performance, reliability and productivity in industrial application perspective. A list of the issues is given below.

- Architectural Dependence
- Multiple Skill Set Requirement
- Sequential Execution of Instructions

E-ISSN 2581 - 7957
P-ISSN 2277 - 3916

CVR Journal of Science and Technology, Volume 19, December 2020
DOI: 10.32377/cvrjst 1906

- Speed of Processing
- Large Memory Requirement
- Additional Resources Requirement
- Stringent Clock Requirement
- Excessive Utilization of Silicon
- High Power Consumption
- Design Complexity
- Huge Cost of Development
- Production / Manufacturing related issues

### C. *Possibilities of Replacing Microprocessor*

Design of an embedded system revolves around the architecture of the microprocessor used. Main activities of an embedded system are classified into three parts, namely receiving the data input, processing the data and sending the output data. Data input is collected from different input sources. Received data received is processed by the pre-programmed algorithms and results are stored in memory. These processed outputs are sent out to output devices. For example, in case of a software defined radio, base band signal is received through a Coder Decoder (CODEC), various algorithms like modulation, filtering, etc are run on the base band signal received. Samples of modulated and filtered Intermediate Frequency (IF) are sent out to the Radio Frequency (RF) circuitry for further processing. In order to effectively implement the above three functions, a microprocessor is used.

The functions performed by the microprocessor used in an embedded system are: Accessing and controlling peripherals, scheduling events, processing of interrupts, managing memory, receiving data, executing algorithm, processing data and sending data. Microprocessor plays a supporting role in an embedded system and an embedded system can be designed with same specifications using different types of microprocessors / microcontrollers / digital signal processors. Hence, the focus of embedded system must be on receiving the inputs, computation of the algorithms and transmitting the processed data to the external world. If all the activities being executed by the microprocessor are implemented with some other logic or mechanisms, Microprocessor can be successfully replaced or avoided in the design of an embedded system.

## II. MMI Design using Hardware Programming based Design Methodology

Hardware Programming based design methodology is an innovative technique to design an embedded system without using any microprocessor, but realizing the logic as well as driver applications using hardware programming with Hardware Description Language (HDL) like VHDL or Verilog HDL [16], [17], [18], [19]. This design methodology is applied for MMI logic that can be used in software defined radio project. This can be used in any other systems as well, for example, networking applications, nuclear applications and so on, with very minor changes. Figure1 illustrates the application of MMI in a system. As presented in the diagram, P1 is input interface. P2a and P2b are output interfaces, P3 is I/O interface. P4 is system interface and P5 is Memory interface.

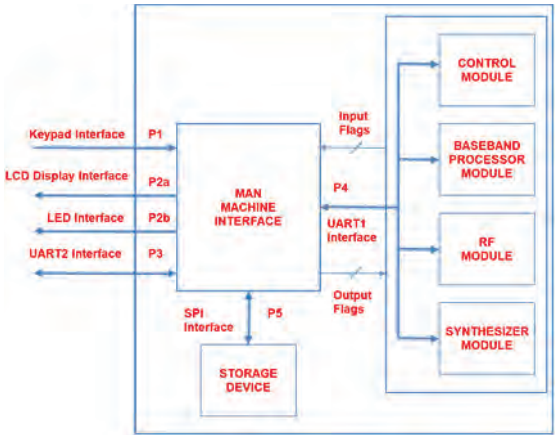


Figure1. Application of Man Machine Interface

### A. *Identification of Activities*

Activities of MMI Logic to be designed are:

- ✓ To ascertain the data entered through Keypad
- ✓ To provide appropriate messages on LCD Display
- ✓ To restrict the user access through passwords management
- ✓ To collect the user configuration data through asynchronous serial interface
- ✓ To authenticate the data access through asynchronous serial interface
- ✓ To provide replies to user through asynchronous serial interface
- ✓ To store user configuration data in non-volatile memory through synchronous serial interface
- ✓ To configure the system based on the user configuration data through asynchronous serial interface as system bus
- ✓ To collect the status information of entire system using system bus
- ✓ To provide user friendly menu driven operations
- ✓ To facilitate for erasure or modification of the configuration data based on the user commands
- ✓ To prepare preset channels for user convenience (A preset channel is a group of parameters and this entire group can be selected with a single key stroke)

### B. *Dividing System into Functional Modules*

In order to realize the functions identified above, logic of MMI module is divided into the following functional modules.

a) Clock generation logic
b) Keypad interface logic
c) LCD display interface logic
d) LED interface logic
e) Key processing logic
f) Serial peripheral interface logic
g) UART1 receiver logic
h) UART1 transmitter logic
i) UART1 driver logic
j) UART2 receiver logic
k) UART2 transmitter logic
l) UART2 driver logic
m) Passwords Management logic

Modules (g), (h) and (i) are integrated to form UART1 logic. Modules (j), (k) and (l) are integrated to form UART2 logic. MMI logic design using hardware programming is shown in Figure 2. As shown in the figure, modules are categorized into peripheral modules, algorithm modules and clock & control modules. All the modules are independent in working and do not require microprocessor for its working. Keypad Interface Module, UART1 Receiver and UART2 receiver are input peripheral modules, LCD interface, LED interface, UART1 Transmitter and UART2 transmitter modules are output peripheral modules. UART1 Driver, UART2 Driver module and Passwords Management Module are algorithm modules. SPI interface module is an I/O peripheral module. Clock generation module and Key processing logic work together as clock and control module. Key processing logic performs control operations (i.e. generating required control signals) and also does the processing of the keypad interface output signals.

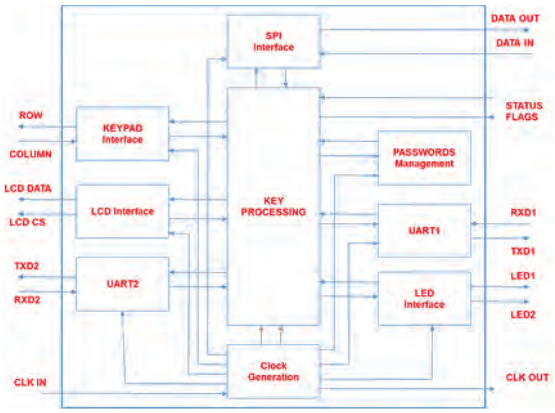


Figure 2. MMI Design using Hardware Programming

## C. *Identifying the Events of Functional Modules*

Figure 3a through Figure 3h depict the events executed by various modules of MMI logic.

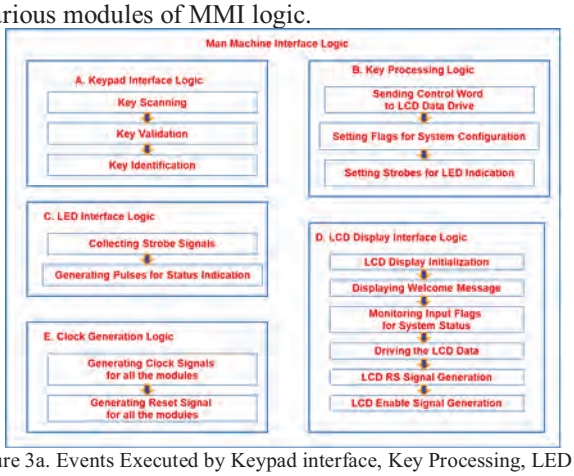


Figure 3a. Events Executed by Keypad interface, Key Processing, LED Interface, LCD Display Interface and Clock Generation Logics of MMI

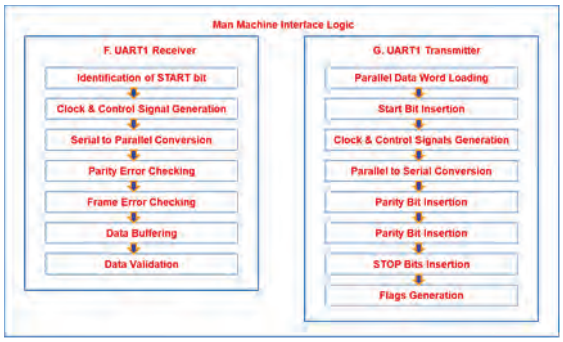


Figure 3b. Events Executed by UART1 Receiver & UART1 Transmitter Logics of MMI

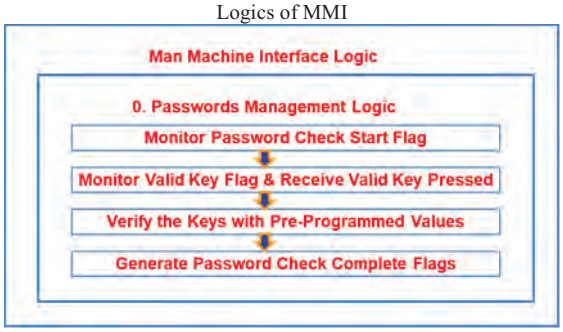


Figure 3c. Events Executed by Passwords Management

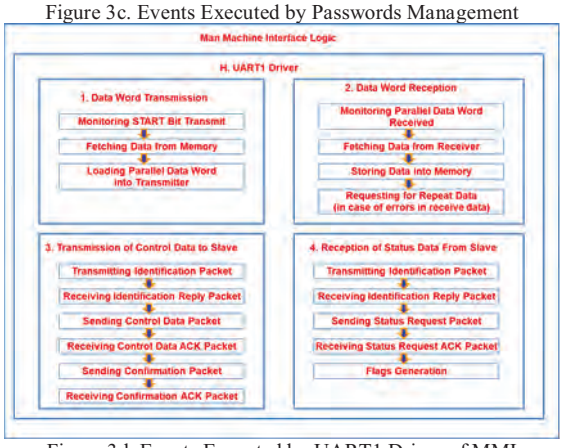


Figure 3d. Events Executed by UART1 Driver of MMI

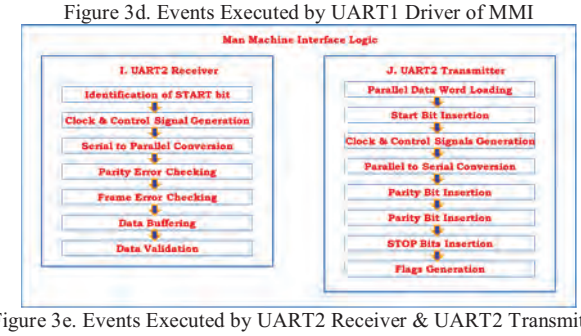


Figure 3e. Events Executed by UART2 Receiver & UART2 Transmitter Logics of MMI

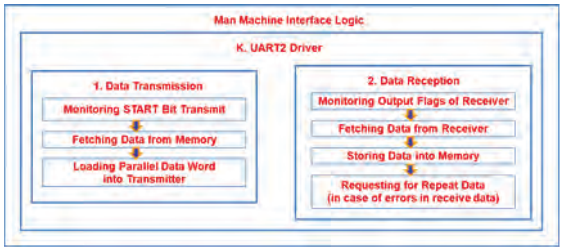


Figure 3f. Events Executed by UART2 Driver Logic of MMI

E-ISSN 2581 - 7957
P-ISSN 2277 - 3916

CVR Journal of Science and Technology, Volume 19, December 2020
DOI: 10.32377/cvrjst 1906

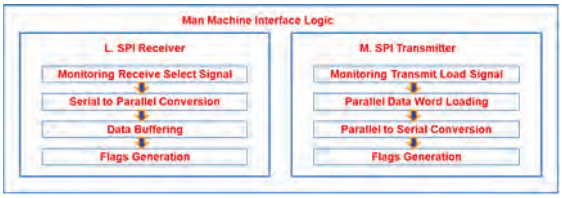


Figure 3g. Events Executed by SPI Receiver and SPI Transmitter Logics of MMI


Figure 3h. Events Executed by SPI Driver Logic of MMI

### *D. Analysis of Protocol*

Protocol analysis is to be done for getting the particulars of sources & destinations of data, packet transfer information, and extraction & insertion of data in packet structures. MMI gets inputs from different sources. Key pressed information coming from keypad, Configuration data or algorithm related data from UART2, System related information from different slave devices through UART1, and Configuration data stored in non-volatile memory fetched through SPI interface are the various inputs to MMI logic. Processed data is given as output to multiple destinations. Messages related to control and status information are sent to LCD display. Status information is given to LEDs for continuous glowing or blinking of LEDs. Configuration data available in the system is given on demand through UART2. Reply messages to user queries are also given through UART2. Configuration data and control data are given to multiple slave devices of the system through system bus. Configuration data is loaded into non-volatile memory through SPI interface. Selective data is given to the appropriate modules inside the MMI logic for processing and computation of algorithms. Transfer of data from various sources to different destinations is done in many methods. Key press data is passed on in the form of logic levels on rows and columns. Different packet structures are used for Configuration UART and System bus UART. Configuration UART is for point to point communication. Figure4 shows the details of packets exchanged in the process of getting configuration data. System bus UART is used in point to multi point configuration. MMI is configured as the master and other system modules as slave devices. Master device only initiates communication. The details of packets exchanged for system bus communication to pass on control data / configuration data / algorithm related data / status information is shown in Figure5. Non-volatile memory access is through SPI interface, wherein MMI is master and Non-Volatile memory is slave. Different commands are sent by Master along with address to write data into memory, to read data from memory, to erase sectors and to bulk erase operations etc., Slave select is active, i.e., at logic level low till the communication between master and slave devices taking place.

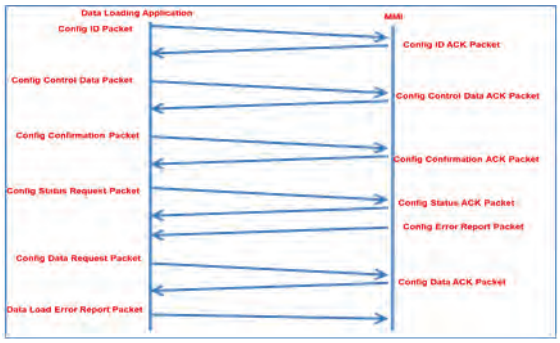


Figure 4. Data Loading into MMI

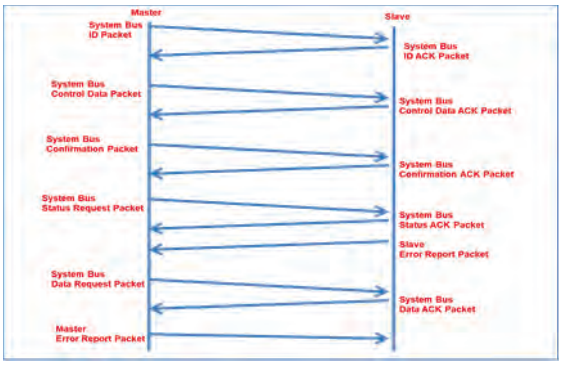


Figure 5. Flow of Packets through System Bus

### *E. Generation of Clock and Timing Signals*

In order to ensure that all the events are executed at predictable time intervals, all the modules are designed to operate in synchronous mode. To avoid ambiguities, events are started or completed at known intervals of time. Single clock input is sufficient for MMI logic. All the other clock signals required for different modules are generated in clock generation module. A clock of 32.768 MHz clock is given as input. Some of the clocks required for internal operations of different modules are generated within those respective individual modules. Timing signals also are derived within those respective individual modules.

### *F. Receiving Data*

The input data streams points must be analyzed for type of data, its availability, format and destinations for the data transfer between modules within MMI. Keypad interface logic provides valid key press output, corresponding row data and validation flag. This information is made available to key processing logic. UART1 receiver provides valid data output (in data words) and valid data flag to UART1 Driver. UART2 receiver generates valid data words received and valid data flag for UART2 Driver module. Receiver of SPI module generates parallel data output along with corresponding flags for the master driver of SPI to take up further processing of data packets.

### G. Setting of Flags

Status of different operations is given in the form of setting Flags by individual modules. This will enable the concerned modules to initiate further activities. Key processing module performs control activities of MMI in addition to the processing of keys pressed to invoke certain events. Different operations selected through Keypad are: to allow data reception from UART2, to verify and authenticate the incoming data, to transfer algorithm related data from one segment to the other within the same non-volatile memory, to set configuration data for a selected operation of the system, to erase the configuration data, to ascertain status, to print control and status messages on LCD display etc. Keypad entries are not accepted during the process of transactions with non-volatile memory. Configuration data from UART2 is communicated through the exchange of a series of packets. Different flags are set to indicate the successful extraction of required data and information about errors in the received data. These flags are used to enable storage of data or to transmit data through system bus. UART1 data is analysed to monitor the status of different slave devices on system bus. Respective flags are set or reset accordingly. These flags are used for status indication on LCD display or LEDs. SPI Flags related to the status of data transfer and data erase operations being carried out with non-volatile memory are used for the purpose of displaying appropriate messages on LCD and also for initiating certain activities by the system.

### H. Storage of Data

For performing data storage, points to be analysed are: data to be stored in Random Access Memory (RAM), data to be stored in Non-Volatile Random Access Memory (NVRAM), processing of NVRAM data, organization of RAM data and organization of NVRAM data. Configuration data, algorithm related data and preset channels data are stored in NVRAM. Initially with power ON or after reset operation, configuration and algorithm related data available in NVRAM is fetched and loaded into different segments of the RAM built with block RAMs of FPGA. Then flags are set accordingly to make system work as per the settings. Non-volatile memory is accessed through synchronous mode. Initially, configuration data is stored in RAM and after receiving the confirmation command from user, this data is dumped into NVRAM. Display messages are fixed and are stored as ASCII data in Read Only Memory designed with the look up tables of FPGA.

### I. Processing of Data

Incoming data packets are processed to get the actual data. In MMI logic – keys, configuration and algorithm related data, stored data and status information are processed by different algorithm modules. Outcome of these algorithms are: To authorize the user in choosing parameters for different operations (through two-level passwords), to extract data for use in the system, to select the message to be displayed on LCD, to set / reset flags related to the status of slave devices of the system and so on.

### J. Transferring the Processed Data

After processing the data, it should be made available at output peripheral modules and I/O peripheral modules. Data transfer through UART2 is done by exchange of different packets. These data packets contain a few keywords in addition to the actual data. UART2 transmitter will transmit data in serial fashion according to the protocol. Flags indicating the status regarding start bit transmit, transmit process in progress are monitored to avoid data overwrite and also to ensure error free transmission. Control data packets are shared with different modules of the system through UART1. As master slave configuration is adopted, transfer of data to slave devices will be done one after the other in a sequence with proper care. Similarly, status is collected from slave modules in a sequence by giving commands sequentially. With power on or with reset, status is obtained from slave devices by giving appropriate control commands. Later, exchange of control and status data is done depending on user demands through keypad. Flags of UART1 transmitter are continuously monitored by UART1 driver for smooth transfer of data. Data loading into non-volatile memory takes place through SPI interface depending on the user commands. Master driver of SPI interface logic arranges data as per the frame structure. Address and type of operations must be indicated clearly in their respective fields of the data frames. Slave select must be asserted low for the entire duration of data transfer.

### K. Enabling / Disabling the Logic

To reduce power consumption, selective enabling / disabling of the logic is done in the following ways.

- To restrict unwanted operations by providing control signals to the concerned logics
- To shut down unused logic at any instant by supplying control signals to the concerned logics.
- To gate the clocks to ensure that clocks are not supplied to unused modules at any point of time.

## III. Implementation of MMI Logic using Hardware Programming

XILINX Software ISE Design Suite 14.5 is used for various design activities of MMI like Design entry, Simulation, Implementation (Translate, Mapping and Place & Route), Programming File Generation, and Configuration of the Device. MMI logic is realized using SPARTAN 3AN XC3S1400AN device. The same MMI logic could be successfully ported on XC3S1600E device and different other devices of Virtex5 and Virtex6 families from XILINX and also on ALTERA devices like Cyclone II and Stratix Family FPGA devices. Device utilization summary of MMI logic is given in Figure 6. As shown in Figure 6, MMI logic consumed 1548 numbers of Slice Flip-Flops, 2520Nos of Occupied Slices and 4553Nos of 4-input LUTs and 16Nos of Block RAMs. Table-1 gives the summary of synthesis results of various modules used in MMI logic.

E-ISSN 2581 - 7957
P-ISSN 2277 - 3916

CVR Journal of Science and Technology, Volume 19, December 2020
DOI: 10.32377/cvrjst 1906

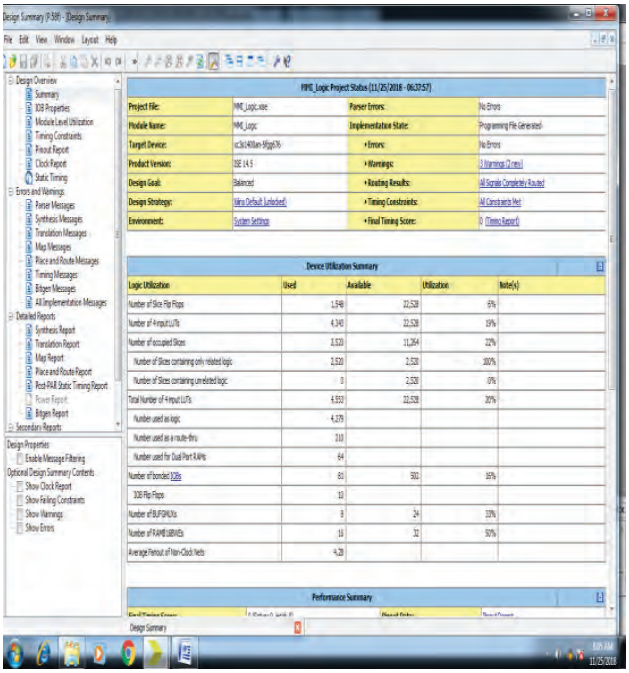

Figure 6. Device Utilization Summary for MMI

TABLE I.
SUMMARY OF SYNTHESIS RESULTS

| Module | No of I/O pins | Occupied Slices | 4-i/p LUTs | Block RAM | Power | |
|---|---|---|---|---|---|---|
| Clock Generation | 12 | 15 | 19 | - | 65mW | |
| Keypad Interface | 15 | 24 | 32 | - | 67mW | |
| Key Processing | 137 | 370 | 701 | - | 71mW | |
| LCD Display Interface | 27 | 99 | 195 | - | 66mW | |
| LED Interface | 12 | 16 | 30 | - | 65mW | |
| UART1 Receiver | 12 | 33 | 23 | - | 66mW | |
| UART1 Transmitter | 14 | 24 | 40 | - | 65mW | |
| UART1 Driver | 106 | 184 | 339 | - | 66mW | |
| UART1 | 88 | 245 | 401 | - | 70mW | |
| UART2 Receiver | 12 | 53 | 33 | | 68mW | |
| UART2 Transmitter | 14 | 24 | 40 | - | 65mW | |
| UART2 Driver | 83 | 553 | 1004 | 8 | 70mW | |
| UART2 | 65 | 641 | 1078 | 8 | 76mW | |
| SPI Interface | 75 | 960 | 1824 | 8 | 71mW | |
| Passwords Management | 74 | 246 | 468 | - | 68mW | |
| Man Machine Interface | 81 | 2520 | 4553 | 16 | 106mW | |

## IV. BENEFITS OF MMI DESIGN USING HARDWARE PROGRAMMING

The benefits observed in MMI designed using Hardware Programming based design methodology are as given below [20].

- Focus is shifted to Interface, rather than the architecture of microprocessor
- Hardware Design Skills are sufficient
- Concurrent Execution of Events
- High Speed of Processing
- Low Latency of the System
- Reduction in Memory Requirements
- Elimination of Unwanted Additional Resources
- Single Clock Source is Sufficient
- Logical Resources are effectively utilized
- Reduced Power Consumption
- Simplified Design Methodology
- Low Cost of Development
- Effective Solutions for the issues being faced in Production / Manufacturing

Intel, Motorola family microprocessors and different families of DSPs from Analog Devices & Texas are considered for making comparison analysis explained in following sub-sections.

### *A. Reduction of Logical Resources*

Traditional MMI logic based on microprocessor design requires Microprocessor, Program memory, RAM, Non-Volatile memory, UART Controller (configuration), SPI Controller (Non-Volatile memory), SPI Controller (system bus), Keypad read register, Keypad write register, LCD register, LCD display, LEDs, Keypad and Crystal oscillators to supply clock. All these components are needed for any microprocessor based design, be it a hard processor or a soft processor in an FPGA. If soft processor is used, logical resources of FPGA are consumed by the soft core of the processor. That soft core can cover some of the peripherals. If embedded processor (a built in component of FPGA) is used, then resources consumed within the FPGA are fixed, but resources available for logic realization are not consumed by the processor. Soft processors like Micro blaze, Nios, Pico blaze and ARM controllers etc. consume lot of logic resources that are more than one thousand slice registers and LUTs. These various devices used are actually meant for general purpose applications. Hence, customization with software programming is to be done to use them as per the user requirements of the system. Some of the features of peripheral devices as well as the processor may not be even used in some applications. Hence, those logic resources are not used and will go waste or sometimes might consume power. Hardware Programming is a customized design to effectively utilize the resources [21]. The peripherals are implemented as required and consume less logic resources. Unnecessary logic will not be used. Hardware programming model for MMI designed is a continuation of System on Chip concepts and consumes minimum logic resources as given below:

- FPGA, to implement all the logic on it

- Configuration memory for FPGA for storage of configuration data related to resources and interconnections among them. This memory can also be used to store configuration data of the system permanently
- Keypad to enter user commands
- LCD display to the display of messages
- LEDs for indicating status

The entire MMI logic implemented had consumed around 2500 Slices Registers only. Hence, there is a huge savings by virtue of customization due to the hardware programming design methodology.

### *B. Reduction of Clock Requirements*

Processor based system is designed using built-in peripherals on the microprocessor chip and also using ASICs for some of the peripherals. These peripherals require clocks of some specific frequencies. Microprocessor also works with clock within certain range of frequency. Hence multiple clock sources are required. Whereas in the case of hardware programming based design, a single clock source is used to derive different clock sources required to make the logic modules operate at different frequencies appropriate to the transfer and computation of data through various interfaces. MMI has used only one clock of 32.768MHz. All the clock signals required for different modules are derived from the single clock source.

### *C. Reduction of Memory Requirements*

Hardware Programming based embedded systems do not require any specific program memory and data memory as microprocessor is not used. Block RAMs of FPGAs are configured as synchronous DPRAMs for effective storage of required data. Hence very less number of memory locations are required. MMI logic has used only sixteen numbers of Block RAMs compared to Megabytes of memory required in case of processor based systems. This has lead to the improvement in execution time also.

### *D. Reduction of Power Consumption*

As the number of components used is very less, the logic resources are very optimized and most importantly the unused logic at any time is shut down or disabled selectively, power consumption is drastically reduced. With the advent of latest technology programmable devices that have very thin silicon wafers, operating voltages have come down and hence the power consumption will still be reduced significantly. Data sheets of microprocessor indicate power consumption of microprocessor as a few hundreds of mill watts; MMI logic has consumed only a few tens of mill watts.

## V. CONCLUSIONS

Hardware Programming based design methodology is used for the design of man machine interface logic and it can be considered as an alternative design methodology for embedded systems. As this design methodology does not require a microprocessor, the issues related to the microprocessor are overcome successfully. The design approach of modular structure makes the design simple and facilitates the designer in extending or modifying the design with ease. These Hardware Programming concepts can be extended for design of various systems being used in several industrial applications.

## REFERENCES

[1] Wang Yue Sheng, Gu Xiao Lei, Wand Liang, “Design of Human Machine Interface of Metal Detector Machine based on µC/OS-III and emWin”, 34th Chinese Control Conference (CCC), 2015, DOI: 10.1109/ChiCC.2015.7261013.

[2] Khan G.N, Jin M, “Hardware Software Co-design of a Safety-Critical Embedded Computer System for an Automatic Endoscope”, Canadian Conference on Electrical and Computer Engineering (CCECE), 2002, DOI: 10.1109/CCECE.2002.1013019, pp 657-662.

[3] Ajay Kumar Singh, Ankitha Taneja, “Frequency allocation in software defined radio using smart cards”, Electronics for You, Oct-2008 Vol 40, No.10, pp-108.

[4] T. Harnath, K. Lal Kishore, “Development of Customized Interrupt Controller Logic”, International Journal on VLSI Design and Communication Systems, 2015, Vol 3, Issue 10, IJVDCS7951-248, pp 1446-1449

[5] Kristanian Blomquist, “Using nV SRAMs to super charge flash memory devices in data logging applications”, Embedded systems design, Dec-2008, Vol 21, No.12, pp-18.

[6] Gereon Fuhr, Seyit Halil Hamurcu, Diego Pal, Thomas Grass, Rainer L, “Automatic Energy-Minimized Hardware/ Software Partitioning for FPGA Accelerated MPSoCs”, IEEE Embedded Systems Letters (Early Access), 2019, DOI: 10.1109/LES.2019.2901224.

[7] Ionut Radoi, Florin Rastoceanu, Daniel-Tiberius Hritcu, “Data Transfer Methods in FPGA based Embedded Design for High Speed Data Processing Systems”, International Conference on Communications (COMM), 2018, DOI: 10.1109/ICComm.2018.8484792.

[8] Mahamudul Hassan, Sheikh Md Rabiul Islam, “Design and Implementation of Pre-Processing Chip for Brain Computer Interface Machine”, International Conference on Robotics, Electrical and Signal Processing Techniques (ICREST), 2019, DOI: 10.1109/ICREST.2019.8644230.

[9] Fateh Boutekkouk, “Soft Intellectual Properties (IPS) Integration for System on Chip (SOC) Design”, International Conference on Research Methodologies in Electronic Devices and Circuits, 2012, DOI: 02.EDC.2012.1.1, pp 101-106.

[10] Shaila S Math, Veerabhadrayya Math, “Design and Analysis of XILINX verified AMBA Bridge for SOC systems”, Lecture series in Computer Science, 2013, DOI: 03.LSCS.2013.2.535, Vol.2 pp 32-37.

[11] Parthasarathy T.R, Venkatakrishnan N, Balamurugan K, “Analysis of partitioning between ARM and FPGA on Performance Characteristics”, IEEE International Conference on Advanced Communication Control and Computing Technologies (ICACCCT), 2012, DOI: 10.1109/ICACCCT.2012.6320745, pp 78-82.

[12] Jayasanthi Ranjith M.E, Muniraj N.J.R, “VLSI Implementation of Memory Efficient Single Bit Processor for Industrial Control Applications”, International Journal on Recent Trends in Engineering and Technology, 2010, DOI: 01.IJRTET.4.4.76, Vol 4, Issue 4, pp 29-31.

[13] Sikun Li, Zhihui Xiong, Tiejun Li, “Distributed Cooperative Design Method and Environment for Embedded System”, Proceedings of the Ninth International Conference on Computer Supported Cooperative Work in Design, 2005, DOI: 10.1109/CSCWD.2005.194316, pp 956-960.

[14] Kopetz Hermann, "The Complexity Challenge in Embedded System Design", 11th IEEE International Symposium on Object Oriented Real Time Distributed Computing (ISORC), 2008, DOI: 10.1109/ISORC.2008.14, pp 3-12.
[15] Mahendra Vucha, Rajendra Patel, Arvind Rajawat, "Dynamic Profiling Methodology for Rescue Optimization in Heterogeneous Computing System", Elsevier Science and Technology, 2013, DOI: 03.elsevierst.2013.1.7, Vol 1, pp 41-46.
[16] T. Harnath, K. Lal Kishore, "Development of Customized Asynchronous Serial Transceiver", Proceedings of 48th CST Infrastructure, Computer Society of India, 2013, pp 41-46
[17] T. Harnath, K. Lal Kishore, "Development of Customized Synchronous Serial Transceiver", International Journal of VLSI and Embedded Systems, 2014, Vol 5, ISSN: 2249-6556, Article 06364, pp 1054-1060
[18] T. Harnath, K. Lal Kishore, "Development of Customized System Bus Transceiver", International Journal of VLSI and Embedded Systems, 2014, Vol 5, ISSN: 2249-6556, Article 06370, pp 1066-1073
[19] T. Harnath, K. Lal Kishore, "Development of Customized Input Output Processor", International Journal on VLSI Design and Communication Systems, 2014, Vol 2, Issue 10, IJVDCS3313-197, pp 1069-1074
[20] T. Harnath, K. Lal Kishore, "Hardware Programming to Improve Embedded System Performance", 33rd Indian Engineering Congress, 2018, Technical Volume, pp 352-358
[21] T. Harnath, K. Lal Kishore, "Hardware Programming as an alternative for Embedded System", International Journal on VLSI Design and Communication Systems, 2016, Vol 4, Issue 5, IJVDCS9724-70, pp 0357-0362

E-ISSN 2581 - 7957
P-ISSN 2277 - 3916

CVR Journal of Science and Technology, Volume 19, December 2020
DOI: 10.32377/cvrjst 1907

# Improved Directivity for Multi-Layer Configured Microstrip Directional Coupler using ANSYS

R. Prakash Kumar[1] and G. Santhosh Kumar[2]
[1]Asst. Professor, CVR College of Engineering/ECE Department, Hyderabad, India
Email:prakash.rachmagdu@gmail.com
[2]Asst. Professor, CVR College of Engineering/ECE Department, Hyderabad, India
Email: santhoshemwave@gmail.com

***Abstract:*** **Directivity of microstrip directional coupler is measured based on its scattering parameters and coupling factor, directivity and isolation factor. Directivity of the microstrip directional coupler is very low, to overcome these problems many methods were applied like lumped capacitor, lumped inductor, implementing wiggling edges. In this paper we introduce a compensation method to improve directivity, i.e. multilayer configuration. This method valid for tight and closed loop structures. Proposed method is designed by using HFSS software and experimental results will show, multilayer configuration is the best suitable method to improve directivity of directional coupler.**

***Index Terms:*** **Microstrip directional coupler, directivity, ANSYS software.**

## I. Introduction

Microstrip directional coupler [1]-[4] has four ports, designing and implementation made on the parameters of insertion loss, isolation loss and coupling loss [5]. In directional coupler to improve directivity, one of the ports has to be terminated and these devices used to detect forward and reverse power. If the input power ($P_i$) is given in port 1, power received at port 2 is received power ($P_r$), power received at port 4 i.e coupled port is given by forward coupled power ($P_f$) and the power received at port 3 is back power ($P_b$), but in ideal case $P_b$=0. From these powers in directional coupler, some factors like coupling factor, directivity and isolation factor. To design any type of antenna, these factors have to be considered for practical considerations:

- Coupling factor $C=10\log(\frac{P_i}{P_f})$
- Directivity $D=10\log(\frac{P_f}{P_b})$, in practical case to develop directivity $P_b$ value has to be low.
- Isolation factor $I=10\log(\frac{P_i}{P_b})$ or $10\log(\frac{P_r}{P_f})$

Microstrip directional couplers are widely used in radar, optical, fiber communications. Directional couplers make good performance while transmitting signals from transmitter to receiver. In RF industry [6], microstrip antennas are made of very cost effective and leakage problem at receiver is null. The manufacturing and designing of microstrip type [7] directional efficiency is very high whereas the directivity is very poor. To improve directivity [8] of microstrip directional coupler, many compensation methods are available, connecting lumped components at the ends of the antenna, dielectric overlay [9] on coupler lines, wigging coupled edges and multilayer configuration [10]. In these methods, multilayer configuration makes important factor. Multilayer configuration can be designed using two-line [11] and three-line layers. Design procedure of multilayer configuration is based on statistical and numerical values. Conventional microstrip couplers are practical sampling devices and can be used to detect either forward or reverse power in practice because one of the coupled ports is usually terminated with lumped element for compensation to improve the directivity. This problem can be overcome using three-line microstrip couplers and have one of the ports of the coupled lines as forward signal detection while terminating the other port of the same-coupled line with a lumped element for compensation of the mismatch for directivity improvement. Then, other coupled line can be used for reverse signal detection and same technique can be applied to improve the directivity. The use of three-line microstrip couplers as reflectometers. However, the design of three-line microstrip directional couplers in the literature again is based on the use of odd and even mode impedance design charts.

To increase the directivity, it has been proposed to design a tightly coupled microstrip directional coupler. In this paper, the directional coupler [12] is operated in the bandwidth limited from 5GHz to 12GHz and has coupling factor of 60dB. Another important way to increase the directivity compared to the previous papers is through matched termination of the ports. In this paper, it has been implemented two-line microstrip directional coupler [13] with closed form. The dual line directional coupler is designed with the parameters like operating frequency, thickness of copper patch and substrate, port impedances. In this paper, it has been analyzed the results and statistical analysis is made on curve fitting method. The analysis of simulation, statistical and graphical methods are present in this paper.

This paper organizes as follows; Section II describes literature survey, Section III gives the information about Method of analysis. Section IV describes simulation results. Section V describes conclusion and future scope.

## II. Literature Survey

This section gives paper description on the previous papers.In [14], authors descirbe branch guide directional couplers analysis of synthetic technique to extract

E-ISSN 2581 - 7957
P-ISSN 2277 - 3916

CVR Journal of Science and Technology, Volume 19, December 2020
DOI: 10.32377/cvrjst 1907

butterworth characterstics by Chebyshev ripple characterstics. Microstrip directional couplers designed using Cohn's slotline in a combination with a microstrip was designed, an octave wide (2-4 GHz) magic tee [15] designed with simulation results. In [16], authors give information about accurate and simple model to transition between probe fed microstrip antenna and microstrip circuit in back to back configuration. In [17], authors designed antenna for wireless communication systems with H-shaped coupling slots on the grounded metal plane. In [18], authors designed microstrip antenna with the quasi-cross-shaped aperture is excited by a U-shaped and an M-shaped microstrip feedline, which leads to two orthogonal polarizations to improve directivity.

## III. Method of Analysis

In this section, the simulation designing and implementing methods of dual line micro strip directional coupler is given:

The designing procedure of dual line directional coupler is shown in figure 1 and 2. The design procedure requires port impedance, type of material, operating frequencyin MHz, coupling level in dBs and dielectric constant. Table 1 shows the operating specifications of dual line microstrip directional coupler. The physical construction of two strip directional coupler or cross sectional view of coupled microstrip lines is shown in figure 2. The configuration of two line is specified by parameters like W/h shape ratio and s/h spacing ratio. In the design of two line micro strip filters and couplers depend on W/h ratio (corrected shape ratio), s/h ratio (shape ratio), characterstic impedence in even mode impedence ($Z_{oe}$) , odd mode impedence ($Z_{oo}$) and length (L) of the substrate plays important role.

TABLE I.
DESIGNING PHYSICAL SPECIFICATION OF DUAL LINE MICROSTRIP DIRECTIONAL COUPLER

| Type of material | Operating frequency | Port impedance | Coupling level |
|---|---|---|---|
| FR4 | 250 MHz | 50 | -15 |

| Sides | Width | Length | height |
|---|---|---|---|
| 48.9mm | 100mm | 128.8mm | 3.048mm |

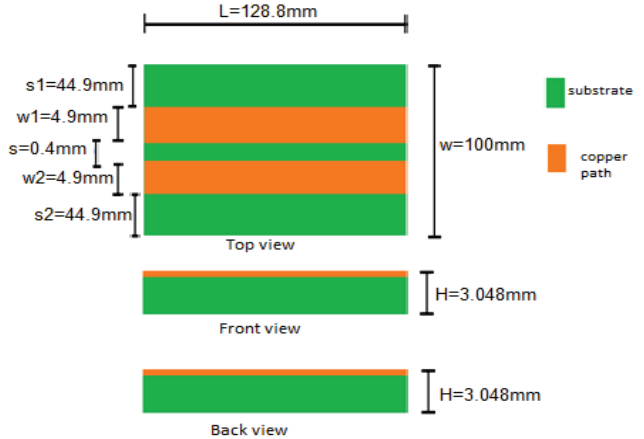


Figure 1. Top, front and back view of dual line directional coupler.

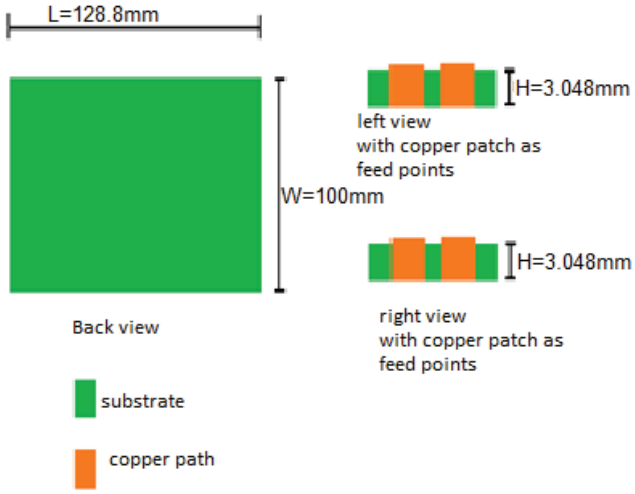


Figure 2. Back, Left and Right view of dual line directional coupler.

The first step for designing procedure is to find even and odd mode impedances, equation 1 and 2 ,

$$Z_{oe} = Z_o \sqrt{\frac{1 + 10^{C/20}}{1 - 10^{C/20}}} \quad (1)$$

$$Z_{oo} = Z_o \sqrt{\frac{1 - 10^{C/20}}{1 + 10^{C/20}}} \quad (2)$$

Where $Z_o$ is port impedance, C is coupling value in dB, after finding even and odd impendences, next step is to find spacing and shape ratios. $(W/h)_e$ and $(W/h)_o$ are the shape ratios of even and odd mode.

Shape ratio

$$W/h = \frac{8\sqrt{\left[\exp\left(\frac{R}{4.24}\sqrt{\epsilon_r + 1}\right) - 1\right]^{\frac{7 + 4/\epsilon_r}{11}}}}{\left[\exp\left(\frac{R}{4.24}\sqrt{\epsilon_r + 1}\right) - 1\right]} \quad (3)$$

Where $R = \frac{Z_{oe}}{2}$, $R = \frac{Z_{oo}}{2}$

Spacing ratio

$$\frac{s}{h} = \frac{2}{\pi} \cosh^{-1}\left[\frac{\cosh\left[\frac{\pi}{2}(W/h)\right] - 2}{\cosh\left[\frac{\pi}{2}\left(\frac{W}{h}\right)^1_{so}\right]}\right] \quad (4)$$

Where $\left(\frac{W}{h}\right)^1_{so}$ is modified term for shape ratio for odd mode geometry.

E-ISSN 2581 - 7957
P-ISSN 2277 - 3916

CVR Journal of Science and Technology, Volume 19, December 2020
DOI: 10.32377/cvrjst 1907

Then next step is to find length of the coupler and it is found by,

$$l = \frac{\gamma}{4} \quad (5)$$

where $\gamma$ is wavelength of the antenna

the effective permitivity constant of dual line couple structure is given by

$$\varepsilon_{eff} = \left[\frac{\sqrt{\varepsilon_{effe}} + \sqrt{\varepsilon_{effo}}}{2}\right]^2 \quad (6)$$

$\varepsilon_{effe}$ and $\varepsilon_{effo}$ are even and odd mode primitivities. With these parameters, it can be a design dual core microstrip directional coupler.

## IV. Simulation Results

In this, it has been presented simulation and analysis results for different cases for two-line micro strip directional coupler. Teflon is considered substrate material [19] and dielectric constant is 2.8. The base design has been considered at -15dB coupling loss and 250MHz operating frequency. Physical dimensions for two strip directional coupler are shown in figure 3. These physical dimensions are analyzed in MATLAB software GUI [20]. Many other parameters like s/h spacing, W/h shape (in eq. W/h), even mode capacitance (Ce) and odd mode capacitance (Co) with dielectric constant, length are considered and analyzed using ANSYS software.

After all physical results are known and obtained by ANSYS software [21]. In this material (teflon), the thickness is 100 millis. With this thickness, spacing between materials is 63.9 millis and width is 95.9 millis. By considering tolerance, these values are considered 65 millis and 100 millis. The layout of two line microstrip had been shown in figure 2.

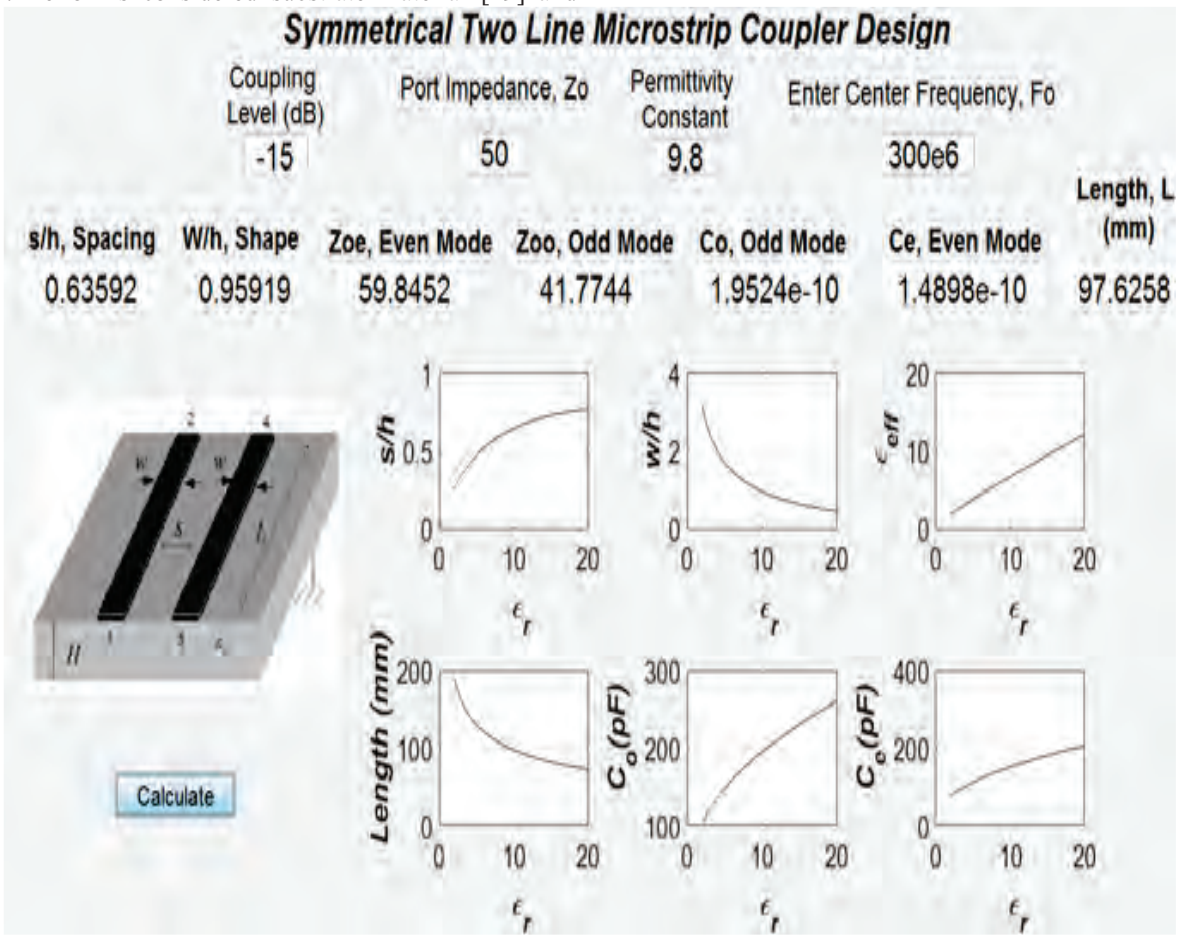


Figure 3. Teflon substrate two strip directional coupler.

In designing of directional coupler for different types of losses has been analyzed. Port losses for all ports scattering parameters has been analyzed here. Directivity, isolation and coupling losses are also considered with different parameters. Figures 4-10 show all the losses of dual line micro strip coupler. For the analysis of results in this paper, it has been considered ANSYS software and parameters are shown in table 1.

From the simulation results port loss for self port i.e $S_{11}$, $S_{22}$, $S_{33}$ and $S_{44}$ are given by -28.6dB, -44dB, -27.5dB and -40.4 dB respectively. Coupling loss and isolation loss is -12dB and -24.5dB. where the important parameter for developing the directivity is -34.75dB which is very good parameter in designing the micro strip antennas. The main advantage of multi layer configurations is improving

E-ISSN 2581 - 7957
P-ISSN 2277 - 3916

CVR Journal of Science and Technology, Volume 19, December 2020
DOI: 10.32377/cvrjst 1907

directivity. In this paper, it is shown that directivity of two layer micro strip antenna is improved significantly.

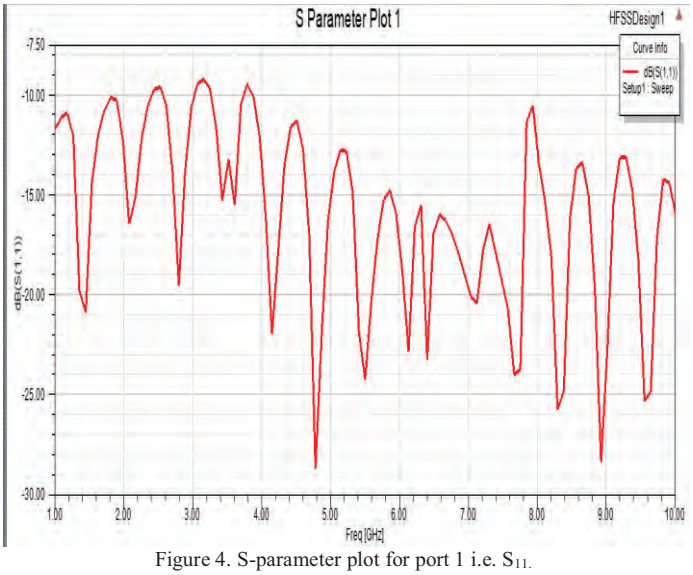


Figure 4. S-parameter plot for port 1 i.e. $S_{11}$.

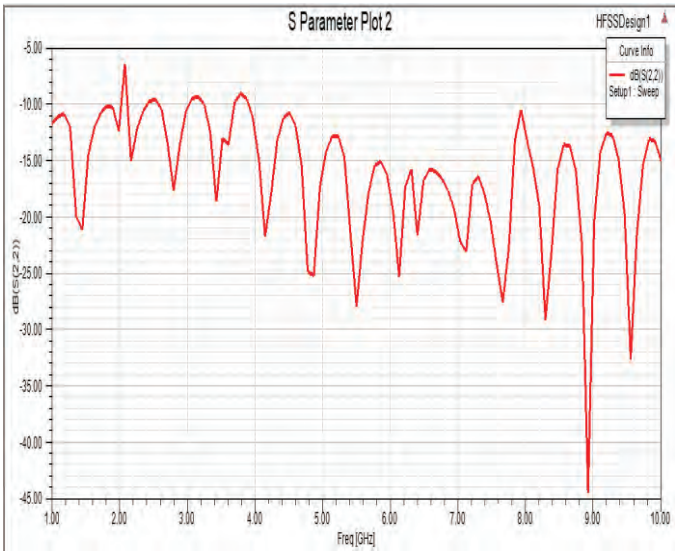


Figure 5. S-parameter plot for port 2 i.e. $S_{22}$.

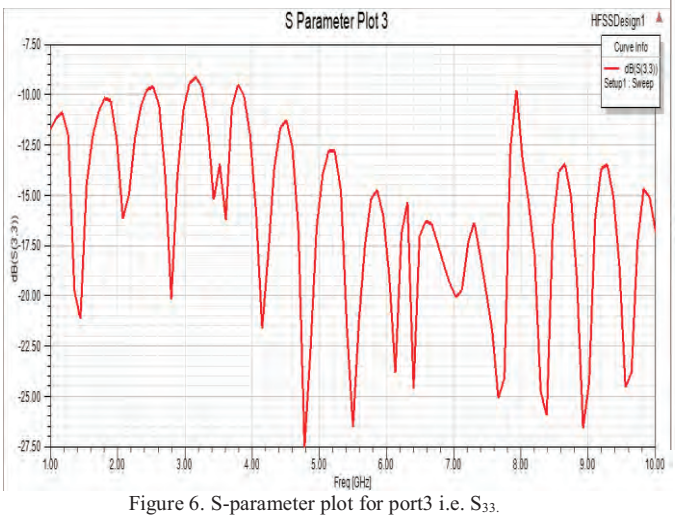


Figure 6. S-parameter plot for port3 i.e. $S_{33}$.

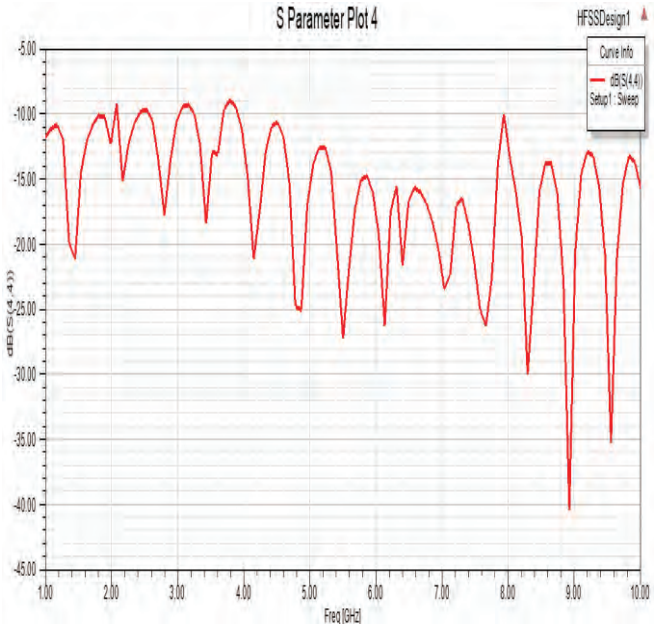


Figure 7. S-parameter plot for port 4 i.e. $S_{44}$.

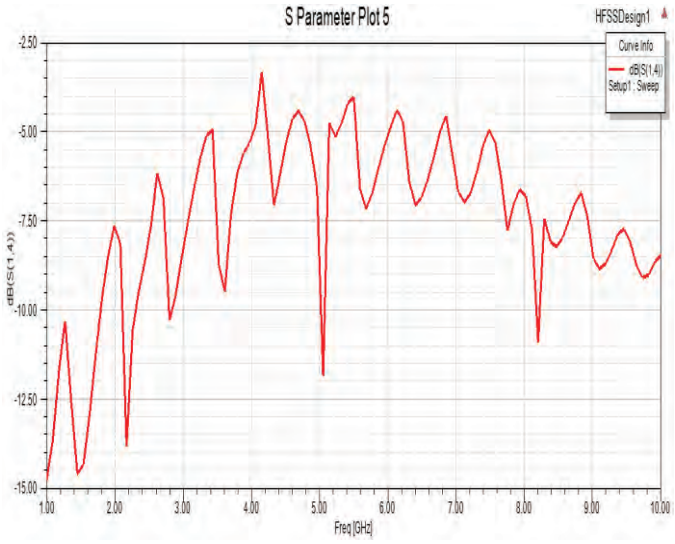


Figure 8. S-parameter plot for coupling loss between port 1 and port 4

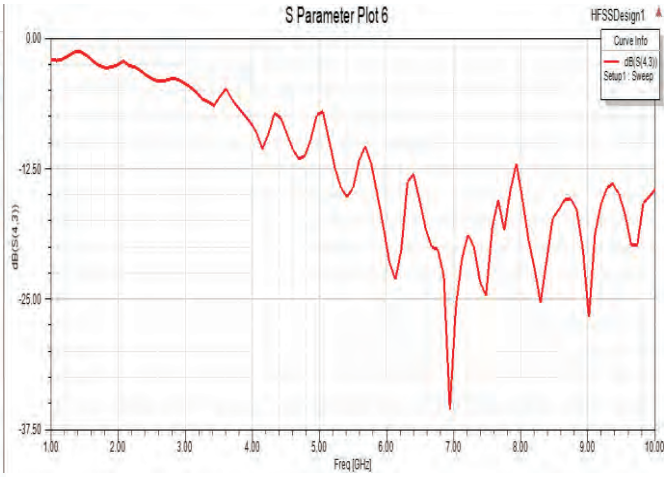


Figure 9. S-parameter plot for directivity between port 4 and port 3.

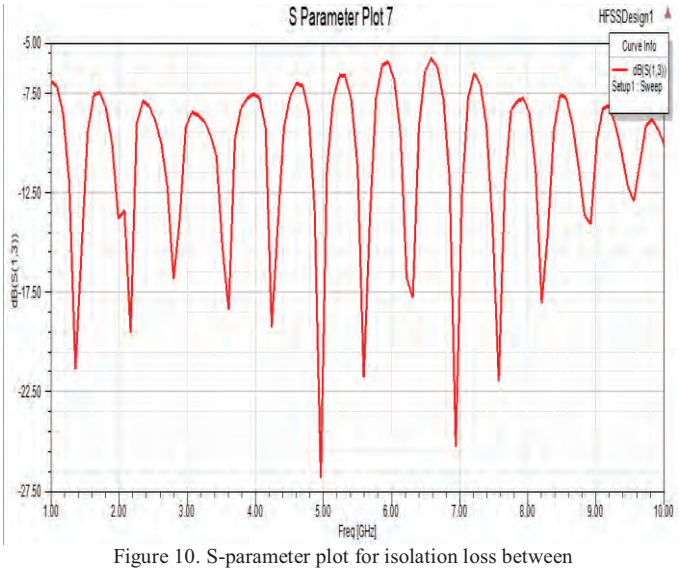


Figure 10. S-parameter plot for isolation loss between port 1 and port 3.

Once all the parameters are given to the model, then simulation starts with ANSYS software. While simulating the thickness of the material is 100mm, length is 128.8 mm and side width of 48.096 were considered. Figure 7 shows the coupling loss between 1 and 4 port, from the graph, it can be analyzed that as the frequency is increasing the coupling loss is reducing. Where as the directivity loss is also becoming low at 7GHz point. From these results, it can be made the statement that it is the best suitable method for improve directivity.

## V. Conclusion and Future Scope

In this paper, it has been introduced a compensation method to improve directivity, i.e. multilayer configuration. This method is valid for tight and closed loop structures. The proposed method is designed using ANSYS software and experimental results showed that multilayer configuration is the best suitable method to improve directivity of directional coupler.

In this paper, this work is limited to dual layer configuration, in future this method may get extension to three layer and multi-layer configuration.

## References

[1] K. Shibata, K. Hatori, Y. Tokumitsu and H. Komizo, "Microstrip Spiral Directional Coupler," in IEEE Transactions on Microwave Theory and Techniques, vol. 29, no. 7, pp. 680-689, Jul. 1981.

[2] F. C. de Ronde, "A New Class of Microstrip Directional Couplers," G-MTT 1970 International Microwave Symposium, Newport Beach, CA, USA, 1970, pp. 184-189.

[3] M. Dydyk, "Accurate design of microstrip directional couplers with capacitive compensation," IEEE International Digest on Microwave Symposium, Dallas, TX, 1990, pp. 581-584 vol.1.

[4] Jeong-Hoon Cho, Hee-Yong Hwang and Sang-Won Yun, "A design of wideband 3-dB coupler with N-section microstrip tandem structure," in IEEE Microwave and Wireless Components Letters, vol. 15, no. 2, pp. 113-115, Feb. 2005.

[5] Lung-Hwa Hsieh and Kai Chang, "Compact, low insertion-loss, sharp-rejection, and wide-band microstrip bandpass filters," in IEEE Transactions on Microwave Theory and Techniques, vol. 51, no. 4, pp. 1241-1246, April 2003.

[6] K. Sakakibara, Y. Suzuki, Y. Imade and N. Kikuma, "Rotman-lens-feeding double-layer low-profile multibeam millimeter-wave microstrip antenna using bow-tie waveguide microstrip connections," 2016 IEEE Asia-Pacific Conference on Applied Electromagnetics (APACE), Langkawi, 2016, pp. 167-169.

[7] A. A. Deshmukh, A. Parvez, P. Verma, A. Desai, P. Kadam and K. P. Ray, "Space fed ring microstrip antenna array with stacked rectangular microstrip antenna feed," 2016 IEEE Annual India Conference (INDICON), Bangalore, 2016, pp. 1-5.

[8] F. Monà, E. S. Sakomura and D. C. Nascimento, "Microstrip-to-Probe Fed Microstrip Antenna Transition," 2018 IEEE International Symposium on Antennas and Propagation & USNC/URSI National Radio Science Meeting, Boston, MA, 2018, pp. 1521-1522.M. Young, *The Techincal Writers Handbook.* Mill Valley, CA: University Science, 1989.

[9] M. M. Fahmi, J. A. Ruiz-Cruz, K. A. Zaki and A. J. Piloto, "Multilayer Multi-Section Broadband LTCC Stripline Directional Couplers," 2007 IEEE/MTT-S International Microwave Symposium, Honolulu, HI, 2007, pp. 173-176.

[10] P. Mondal and S. K. Parui, "Multi-mode resonator based asymmetric broadband 10dB directional coupler," 2018 3rd International Conference on Microwave and Photonics (ICMAP), Dhanbad, 2018, pp. 1-2.

[11] X. Xingyu and M. A. Abou-Khousa, "Miniaturized 3D directional coupler for compact monostatic microwave imaging systems," 2016 16th Mediterranean Microwave Symposium (MMS), Abu Dhabi, 2016, pp. 1-4.

[12] A. K. Tiwari, S. Awasthi and R. K. Singh, "A Leaky-Wave Antenna With Improved Directivity and Scanning Range," 2018 5th IEEE Uttar Pradesh Section International Conference on Electrical, Electronics and Computer Engineering (UPCON), Gorakhpur, 2018, pp. 1-5.

[13] S. Jun-Yu et al., "High-directivity single- and dual-band directional couplers based on substrate integrated coaxial line technology," 2013 IEEE MTT-S International Microwave Symposium Digest (MTT), Seattle, WA, 2013, pp. 1-4.

[14] A. Giménez, J. Verdú and P. De Paco Sánchez, "General Synthesis Methodology for the Design of Acoustic Wave Ladder Filters and Duplexers," in IEEE Access, vol. 6, pp. 47969-47979, 2018, doi: 10.1109/ACCESS.2018.2865808.

[15] F. C. de Ronde, "A New Class of Microstrip Directional Couplers," G-MTT 1970 International Microwave Symposium, Newport Beach, CA, USA, 1970, pp. 184-189, doi: 10.1109/GMTT.1970.1122803.

[16] D. F. Monà, E. S. Sakomura and D. C. Nascimento, "Microstrip-to-Probe Fed Microstrip Antenna Transition," 2018 IEEE International Symposium on Antennas and Propagation & USNC/URSI National Radio Science Meeting, Boston, MA, 2018, pp. 1521-1522, doi: 10.1109/APUSNCURSINRSM.2018.8609140.

[17] Z. Chen, X. Dai and G. Luo, "A new H-slot coupled microstrip filter-antenna for modern wireless communication systems," 2018 International Workshop on Antenna Technology (iWAT), Nanjing, 2018, pp. 1-3, doi: 10.1109/IWAT.2018.8379131.

[18] H. Li, L. Kang, F. Wei, Y. Cai and Y. Yin, "A Low-Profile Dual-Polarized Microstrip Antenna Array for Dual-Mode OAM Applications," in IEEE Antennas and Wireless Propagation Letters, vol. 16, pp. 3022-3025, 2017, doi: 10.1109/LAWP.2017.2758520.

[19] Aastha, A. Kaur, A. S. Dhillon and E. Sidhu, "Performance analysis of microstrip patch antenna employing Acrylic, Teflon and Polycarbonate as low dielectric constant substrate

materials," 2016 International Conference on Wireless Communications, Signal Processing and Networking (WiSPNET), Chennai, 2016, pp. 2090-2093.

[20] T. Seki, N. Honma, K. Nishikawa and K. Tsunekawa, "Millimeter-wave high-efficiency multilayer parasitic microstrip antenna array on teflon substrate," in IEEE Transactions on Microwave Theory and Techniques, vol. 53, no. 6, pp. 2101-2106, June 2005.

A. R. Alavizadeh, A. Zargari and W. R. Grise, "The application of ANSYS software in analyzing and predicting thermal behavior," Proceedings: Electrical Insulation Conference and Electrical Manufacturing and Coil Winding Conference (Cat. No.99CH37035), Cincinnati, OH, USA, 1999, pp. 583-588, doi: 10.1109/EEIC.1999.826274.

E-ISSN 2581 - 7957
P-ISSN 2277 - 3916

CVR Journal of Science and Technology, Volume 19, December 2020
DOI: 10.32377/cvrjst 1908

# Smart Mirror Design using Raspberry Pi

K. Arun Kumar[1], K. Uday[2] and K. Veeranjaneyulu[3]
[1]Asst. Professor, CVR College of Engineering/ECE Department, Hyderabad, India
Email: arun.katkoori@gmail.com
[2]Asst. Professor, CVR College of Engineering/EIE Department, Hyderabad, India
Email: kaparthiuday@gmail.com
[3]Asst. Professor, CVR College of Engineering/CSE Department, Hyderabad, India
Email: kveeru876@gmail.com

***Abstract:*** **Information is needed to integrate smart mirror technology and into one's daily schedule. As the mirror is in place, the user will get interaction and information during their routines like weather data, day highlights, daily schedule, motivational quotes. Data can be viewed in the mirror during routines, which saves the user time. This paper provides a working prototype, i.e. design and development of a smart mirror using Raspberry Pi 3 for the home environment and for commercial use in various industries. Since the microcontroller unit is 'ON' all day, it heats up, which is fixed using a cooling fan. To display information in the mirror, the setup is provided with a network connection, which displays the latest information. Look at the acrylic sheet through the mirror for the entire setup display is placed on the back. If the mirror is useful for this purpose, imagine that it would be very useful. The device looks like a normal mirror but with a screen inside. It collects real-world machine data such as location-based latest news and headlines, weather reports and local time display. Smart mirror makes life easier by saving time.**

***Index Terms:*** **Raspberry Pi 3, Acrylic sheet, Smart mirror.**

## I. Introduction

Over the past few years, technology has become an important and indispensable part of our daily routine. As technology is rapidly evolving, people expect to become more productive and e-centric in their daily activities. The use of smart phones, tablets, laptops and other similar devices has provided tools that help people stay productive and most importantly time efficient.[1] The design is to introduce a multipurpose mirror that is intended to fill in as both enrichment and data source. With a single glance at the mirror, there will be basic information on what to wear based on the weather forecast for the day or how much time they have left if they want to arrive on time for their intended destination.

Interactive computing, with embedded devices connected to wireless, is used in a variety of everyday activities, changing and improving living standards. Based on these interactive computing and communication technologies, now many devices have emerged. Multimedia intelligence can provide convenient, secure and personal services everywhere. This makes convenient for many users whether for domestic or for industries. It is used as Design and development of interactive multimedia futuristic smart mirror with artificial intelligence for ambient home environment, as well as commercial uses in various industries.

Smart mirror provides an effortless experience that allows the user to walk and is usually greeted with information that they need another device. The use of smart mirror is to increase their productivity by saving user time.

## II. Literature Survey

There are significantly more products than actual products. Some may blame it on the fact that the smart home is still a growing market and is limited by manufacturing costs without making products available from everyday consumers. The fact that there are more products shows interest in developing a more affordable and functional smart mirror.[2] however, even if the actual products developed by a company are distributed on features, they are still in the development stage or are already considered a viable competitor at a much higher price. Few of them are—

### i) Interactive Mirror

Touch the built-in touchscreen mirror to keep the user interactive.[3] Unlike our smart mirror, only one point of touch is detected because it mimics a mouse.

### ii) Magic Mirror

Magic mirror utilizes TV with mirror. By using Microsoft Kinect, it can track movement of the person who interact, and voice is also recognized.[4]

### iii) The Android-powered Mirror

In this, the LCD screen secured with hazy intelligent glass is utilized to make the mirror. The mirror contains applications, for examples, climate, news, weight, temperature and water stream [5]. Water stream is an intriguing expansion and is brilliant at helping water preservation.

### iv) Memomi

Memory mirror is abbreviated as Memomi. It is another innovative mirror on the rundown. At present accessible is magic mirror, otherwise it is called as Memomi [6]. It is being utilized as a substitution for changing areas in shops that sell garments. Clients can collaborate with the mirror through the versatile application.

E-ISSN 2581 - 7957
P-ISSN 2277 - 3916


DOI: 10.32377/cvrjst 1908

TABLE I.
SUMMARY OF EXISTING METHODS

| S.No. | Author's Name | Year of publication | Title of the paper | Limitations |
|---|---|---|---|---|
| 1 | Tataina Lashina | 2004 | Intelligent bathroom. In European Symposium on Ambient Intelligence (EUSAI'04), Eindhoven, Netherlands, | Accepts limited amount of data. Neither camera nor the other sensors suggest the features of a smart object. |
| 2 | L.Ceccaroni and X. Verdaguer | 2004 | Magical mirror: multimedia, interactive services in home automation | Web services are not used and lack of human interaction. |
| 3 | Seraku | 2012 | Seraku's smart wash Basin | Cost is more because additional sensors are required to track the hands position and motion. |
| 4 | Franco Chiarugi | 2016 | Wize Mirror - a smart, multisensory cardio-metabolic risk monitoring system | This mirror doesn't use any client acknowledgment; however the interface can be redone through a PDA application that is likewise used to control some other home components. |

The summary of existing methods is shown in above table I. In contrast with the works depicted over, proposed work is diverse in that we intend to build up a working framework for offering types of assistance in the home climate dependent on web server principles and off-the-rack innovation, where the savvy reflect is the interface to get to or control different information takes care of, different data administrations.

TABLE II.
COMPARISON OF PROPOSED MIRROR WITH EXISTING MIRRORS

| Feature | Interactive mirror | Magic mirror | Android-powered mirror | Memomi | Proposed mirror |
|---|---|---|---|---|---|
| OS | Windows 10 | Linux OS | Android | Customized | Raspbian OS |
| App Requirement | No | No | No | Yes | Yes |
| Touchscreen | No | No | Yes | Yes | No |
| Weather update | Yes | No | Yes | Yes | Yes |
| Automatic sleep | No | Yes | No | No | Yes |
| Social networking | Yes | No | Yes | Yes | Yes |

## III. PROPOSED METHOD

The proposed technique means to give users an intuitive interface for streamlined and customized services in the solace of the home of the user. It is smart and easy to use arrangement as a mirror that likewise goes about as a gateway to intelligent services. For example, multimedia and news sources are among others.

**PC Specifications**:

A computer is used in smart mirror, which takes the input data from the various peripherals. It is made up of a mini ITX Intel motherboard. This motherboard has the features like- USB ports, HDMI port and audio ports, etc. Intel i3 processor with graphics card included. The following table II gives the hardware specifications for this computer.

The motherboard with 4GB of DDR3 RAM as well as 64GB strong state drive. Finally, a 380-watt power supply used the PC. A scale down iTX PC case housed all the parts referenced and gave fitting air cooling to the hardware. Each of these parts contains the planned temperature guideline framework to give the greatest security against temperature and stickiness harm to the hardware.

TABLE III.
SPECIFICATIONS OF A PC

| | |
|---|---|
| Motherboard | mini ITX Intel |
| RAM | 4GB |
| CPU | Intel i3 |
| Solid State Drive | 64GB |
| Power Supply | 380 watts |

**System Requirements:**

To control the mirror, the microcontroller is used, and the segments utilized should be powered by a 5V power gracefully.

The framework utilized in the mirror

- Should have the option to interface with a Wi-Fi interface just as a PC show.
- Should have the option to take user contribution to program the user's location and switch what information is being shown on the auxiliary screen [7].
- Hardware components should fit inside the mirror size [8].

The total system will likewise be mounted on a wall, so there should be an edge assembled that can uphold this weight. Also, the system utilized in the mirror should have the option to interface with a Wi-Fi interface just as numerous LCD shows. The Wi-Fi should have the option to work inside a home, so it should be sufficiently touchy to get the signal from a home Wi-Fi switch. [9]

### *A. Design*

Hardware part mainly consists of:

- Raspberry Pi
- Power Supply
- Monitor
- Wi-Fi
- Cooling Fan

E-ISSN 2581 - 7957
P-ISSN 2277 - 3916

CVR Journal of Science and Technology, Volume 19, December 2020
DOI: 10.32377/cvrjst 1908

Raspberry Pi is also known as, RPi. It is a progression of little single-board PCs created in the UK by the Raspberry foundation to advance educating of essential software engineering in schools and in some nations.

Raspberry Pi3 board uses +5V USB power supply. The general purpose I/O(GPIO) pins of RPi board can just securely draw 16mA. The HDMI port uses 50mA, the camera module requires 250mA. The keyboard's and mouse's current range is 100mA to 1000mA.

The monitor is used to display the data, which is connected to Raspberry Pi board. Wi-Fi is commonly a locally situated switch. It fetches up to date information such as weather forecasting, news, etc.

Cooling Fans are utilized to draw cold air from an external perspective, remove warm air from within, and move air through heat sink to cool the element. These fans normally come in standard sizes and available in 3-pin and 4-pin connectors. These are used to cool in PCs and the microcontroller., which runs continuously.

The CPU of Raspberry Pi is indicated to run between 40° C to 85°C. if that CPU temperature surpasses 82°C, at that point the CPU's clock speed will be eased back until the temperature dips under 82°C.

The Block diagram for designing hardware is as shown in the figure1.

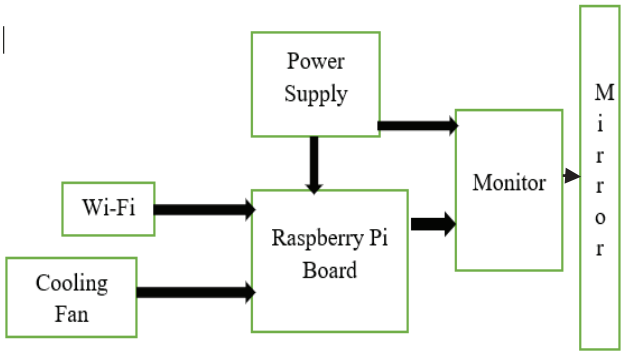


Figure 1. Hardware setup for Smart Mirror

Figure 2 shows the prototype of smart mirror. Setting up LCD and connecting it to the Raspberry pi 3. Connecting Installation of Frame around LCD and placing Acrylic Sheet in front of LCD. [10]

Next step in the design of smart mirror is software setup. It includes Booting up the Raspberry pi-3 and Configuring the modules for all features. E.g.: Calendar, Weather, NEWS etc. [11] Booting is a start-up sequence that starts the operating system of a computer when it is turned on. A boot sequence is the initial set of operations that the computer performs when it is switched on. Every computer has a boot sequence.

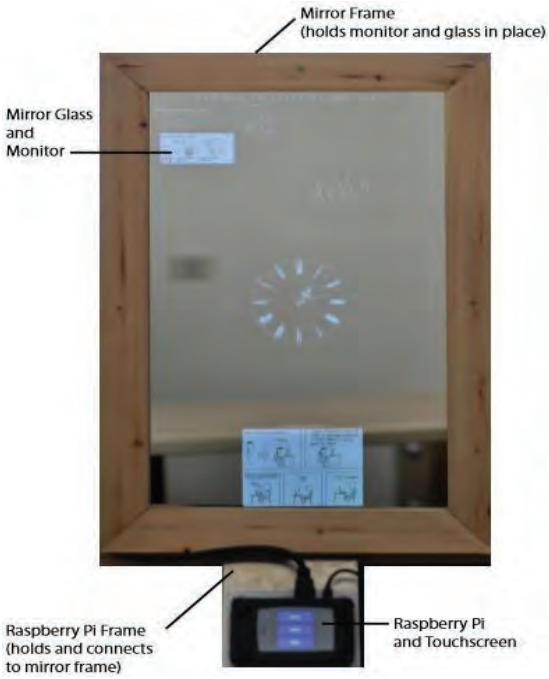


Figure 2. Smart Mirror prototype

The properties that can be configured are:

TABLE IV.
CONFIGURATION PROPERTIES

| Choice | Definition |
|---|---|
| Port | The smart mirror server running port and its default value is 8000. |
| Address | Interface IP address that accepts connections. The default address is local host, which prevents the built-in webserver from being exposed to machines on the local network. To expose to other machines, use 0.0.0.0. |
| IPWhiteLis t | It gives the list of IPs that allowed to access the proposed smart mirror. The default address is "127.0.0.1, "::ffff:127.0.0.1", "::1", which is only from the local host. Also configure IP ranges with subnet masks "127.0.0.1", "127.0.0.1/24" (or) "127.0.0.1","192.168.2.1", "127.0.0.1/24", "192.168.0.100". |
| Zoom | It allows the user to scale mirror contents with a given zoom factor. The default value is 1. |
| Language | It gives the language of interface. |
| TimeZone | A form of time notation is used. The possible values are 12 hours or 24 hours format. Default value is 24 hours. |
| unit | Unit used in default weather modules. The possible values are imperial or metric. Default is metric. |
| module | It gives the array of active modules. These modules must have objects in range. |
| customCSS | It gives the path. The default is css/custom.css |
| elctronOpti ons | This function is used to configure the browser screen size and position i.e. fullscreen, width, height, etc. |

E-ISSN 2581 - 7957
P-ISSN 2277 - 3916

CVR Journal of Science and Technology, Volume 19, December 2020
DOI: 10.32377/cvrjst 1908

The following modules are open source modules. They installed by default.

- Clock
- Calendar
- Present Weather
- Weather Forecast
- Email
- News Feed
- Compliments

**Clock:**

It is open source module. It gives information about current date and time. The information will be updated real time.

There are some properties to be configured like time Format, display Seconds, clock Bold, show Period, show Date, show Week, date Format, display Type, time zone, seconds Color, etc.

**Calendar:**

The "calendar" module displays events from a public and is also open source. It is also capable of combine multiple calendars.

The properties configured are:
Calendars, date Format, date End Format, show End, time Format, full Day Event Date Format, urgency, etc.

**Present Weather:**

This module shows the current climate, including the windspeed, the dusk or dawn time, the temperature and a symbol to show the current conditions**.** This one is also an open source.

The configuration options are- url, symbol, color, repeating Count Title, maximum Entries, maximum Number of Days Auth, symbol Class, title Class, time class, etc.

**Weather Forecast:**

This weather module shows the climate forecast for coming week, including a symbol to show the current conditions, the base temperature and the greatest temperature.

The configuration options are-location, locationID, units, roundTemp, degreeLabel updateInterval,animationSpeed, timeFormat, showPeriod, showPeriodUpper, showWindDirection, showWindDirectionAsArrow, showHumidity, showIndoorTemperature, onlyTemp, lang, etc. Figure 3 shows the weather forecast of last 5 days.

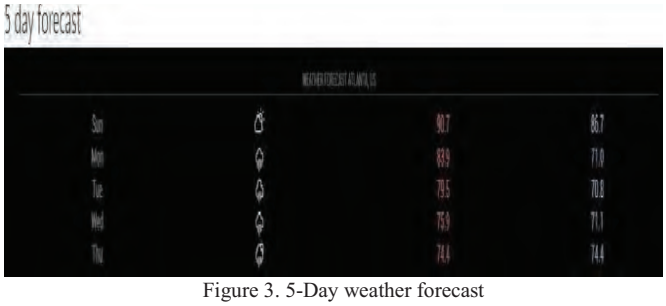


Figure 3. 5-Day weather forecast

**EMAIL:**

This module displays emails on smart mirror and listens for new incoming emails. When a new email is received, the mirror is updated to display it.

The configuration options are user, password, host, post, tls, authTimeout, numberOfEmails, maxCharacters, fade, etc.

**Newsfeed:**

This is one of the open source modules and it shows news features dependent on the RSS channel. Looking through news features happens time sensitive however can likewise be constrained by sending news source explicit warnings to the modules. Collaborating with the module, warning systems permits to send notices to the newsfeed module.

The configuration options are- showSourceTitle, showPublishDate, showDescription, wrapTitle, maxNewsItem, startTags, endTags, scrollLength, logFeedWarnings, etc.

**Compliments:**

This module shows a random compliment on the mirror. The configuration options are- up date Interval, fade Speed, compliments, remote File, classes, morning Start Time, morning End Time, afternoon Start Time, afternoon End Time, etc.

### *B. Performance measures*

By using following functions, the performance of proposed smart mirror is computed.

- **ShowToast (msg, dur)-** gives a message on the bottom part of the screen during the indicated duration.
- **ShowAlert (title, msg,IDalert)-** gives the alert message that the user can select using gesture input with alert ID.
- **SetTitle (title)-** sets the status bar message.

An API was used which is made by Google, has 50 query a day limit but it is the best one available. To use the API the user, need to make an HTTP POST request with 20000-bit rate.

### *C. Results*

This section provides the results of smart mirror. Figure 4 shows current date, current weather status information, and all calendar events. Figure 5 is smart mirror output which gives clock, calendar, email notifications, weather forecasting, compliments, etc.

E-ISSN 2581 - 7957
P-ISSN 2277 - 3916


DOI: 10.32377/cvrjst 1908

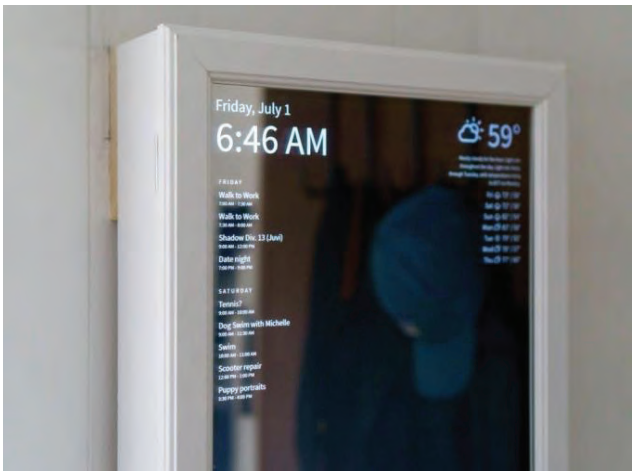


Figure 4. Calendar events

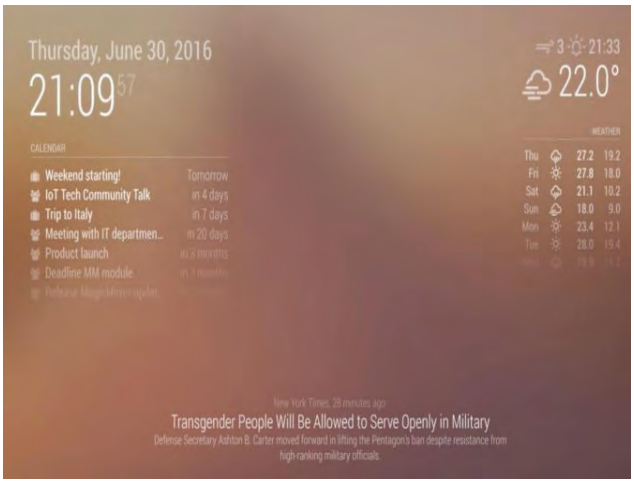


Figure 5. Smart Mirror output shows Time, Date, Weather, Notifications etc.

## IV. Conclusions

A smart mirror is planned which gives normal communication among clients and the surrounding home administrations. The mirror display is given by an LED monitor which shows all the essential data which are helpful for the client. This mirror also gives a picture-in-picture sub-display to encourage the presentation of services, for example, maps, recordings through youtube. By and large, the model gives an effectively extendable structure that can be used to give significantly greater usefulness to the user. This work will be extended in future (by examining how the surrounding context of the user) and so as to offer ideal assistance encounters in the home climate.

## References

[1] K. Arun Kumar, R. Satya Prakash, M. Vinod Kumar Reddy, "ARM Based Smart Living System using Brain Computer Interface", CVR Journal of Science & Technology, Volume 18, page no.49-54, June.2020.

[2] Dabiah A. Alboaneen, Dalia Alsaffar, Alyah Alateeq, Amani Alqahtani, Amjad Alfahhad, Bashaier Alqahtani, Rahaf Alamri, Lama Alamri, "Internet of Things Based Smart Mirrors: A Literature Review", Computer Applications & Information Security (ICCAIS) 2020 3rd International Conference on, pp. 1-6, 2020.

[3] Tatiana Lashina. Intelligent bathroom. In European Symposium on Ambient Intelligence (EUSAI'04), Eindhoven, Netherlands, 2004.

[4] L. Ceccaroni and X. Verdaguer. Magical mirror: multimedia, interactive services in home automation. In Proceedings of the Workshop on Environments forPersonalized Information Access - Working Conferenceon Advanced Visual Interfaces (AVI 2004), pages 10-21, New York, NY, USA, 2004. ACM Press.

[5] http://www.theverge.com/2012/5/10/3013168/seraku-android-mirror-prototype-hands-on.

[6] Memomi MemoryMirror",Memomi MemoryMirror, 2017. [Online]. Available: http://memorymirror.com/

[7] Preeti Pannu Vaibhav Khanna, Yash Vardhan, Dhruva Nair, ―Design and Development of a Smart Mirror Using Raspberry PI‖, IJEEDC, Volume-5, Issue 1, January 2017

[8] D.K. Mittal, R. Rastogi, A Comparative Study and New Model for Smart Mirror, International Journal of Scientific Research in Research Paper. Computer Science and Engineering Vol.5, Issue.6, pp.58-61, December (2017) M. Young, The Technical Writer's Handbook. Mill Valley, CA: University Science, 1989.

[9] Nadaf R.A., Hatture S., Challigidad P.S., Bonal V.M. (2019) Smart Mirror Using Raspberry Pi for Human Monitoring and Home Security. In: Luhach A., Jat D., Hawari K., Gao XZ., Lingras P. (eds) Advanced Informatics for Computing Research. ICAICR 2019. Communications in Computer and Information Science, vol 1076. Springer, Singapore.

[10] Sadeta KULOVIC and Belma RAMIC-BRKIC, "DIY Smart Mirror", Advanced Technologies, Systems, and Applications II, 2018.

[11] Y. Sun, L. Geng and K. Dan, "Design of Smart Mirror Based on Raspberry Pi," *2018 International Conference on Intelligent Transportation, Big Data & Smart City (ICITBS)*, Xiamen, 2018, pp. 77-80.

E-ISSN 2581 - 7957
P-ISSN 2277 - 3916

CVR Journal of Science and Technology, Volume 19, December 2020
DOI: 10.32377/cvrjst 1909

# Solar Power Elegant Irrigation System by using IoT Technology

Rajagopal K[1] and P. Rajashekar Reddy[2]
[1]Asst. Professor, CVR College of Engineering/ECE Department, Hyderabad, India
Email: rajgopalsushma@gmail.com
[2]Asst. Professor, CVR College of Engineering/ECE Department, Hyderabad, India
Email: raju.sheker@gmail.com

***Abstract:*** **It has actually been discovered that PV system is the very best remedy for remote farming system as well as for demands such as water pumping for plants. It provides the information of a solar-powered computerized watering system that gives the specific quantity of water called for depending upon the dirt wetness, therefore lessening the waste of water. A network of sensing unit nodes is utilized to accumulate the moisture and also temperature level of the dirt which is sent to a remote terminal. Making use of Solar Panel, the solar power will certainly be transformed into electric power as well as conserves in to batteries. When the sunlight increases and radiates, the photovoltaic panel will certainly soak up the power of the sunlight as well the power will certainly maintain in the battery. Photo resistors like LDR (Light Dependent Resistors) positioned on the photovoltaic panel which aids in tracking optimum strength of sunshine. This monitoring activity of the panel is attained by installing the photovoltaic panel on the tipped electric motors. This tipped electric device revolves the placed panel according to signal attained from the set Arduino family Arduino controller. Dirt wetness sensing unit is put inside dirt to pick up the dampness problems of the dirt. Based upon wetness sensing unit worth, the water pump is turned on and also off instantly.**

***Index Terms*****: LDR, Solar PV system, GSM, IoT Technology, Soil moisture sensor, SMS.**

## I. Introduction

A solar energy pumping system technique requires taking appropriate account of the reality that is needed for watering system as inflow of water differs throughout the year. Solar-powered systems are being preferred for usage in creating nations rather than various other sources of power due to the fact that they are very long lasting and can show long-lasting financial advantages. Solar energy water pumping systems can be one of the most suitable remedy for grid separated country places in inadequate nations where the degree of solar radiation is exceptionally high. The solar PV panels have actually shown in time their capacity to dependably create enough power straight from solar radiation to power animals as well as solar watering systems. Solar water pumps show their effective usage mostly in little range or area based watering areas, as big range watering needs big quantities of water which subsequently calls for a solar PV range exceptionally huge in dimension [1]. As the water perhaps called for just throughout some components of the year, a big PV variety would certainly offer excess power which isn't always called for, hence making the system in effective. Leak watering is fabricated technique of providing water to the origins of the plant. It is additionally called mini watering. Since the past couple of years there is a fast development in this system. The customer connects with the central device with SMS. The systematized system connects with the system via SMS which will certainly be gotten by the GSM module [2]. here we are using sim800 GSM module. We need to insert SIM card in this module. The GSM module sends this information to Arduino microcontroller which constantly gets the information from sensing units in Arduino programming codes. After handling, this information is shown on the LCD. Hence basically whenever the system gets the activation command from the customer it inspects all the area problems as well as provides comprehensive responses to the customer and also awaits an additional activation command to begin the electric motor. The electric motor is managed by an easy adjustment in the inner framework of the starter [3].

Various watering systems are utilized nowadays to decrease dependence of rainfall. Because of the absence of power and also management issues, in the guidebook monitor watering system often times plants are completely dry or swamped with water. So to prevent this trouble sensing unit base watering system is made use of. With hands on experience, the system helps farmers typically regulate the electrical motors observing the dirt, plant as well as climate condition by checking out the websites. Dirt wetness sensing unit base watering system guarantees appropriate dampness degree in the dirt for expanding plants in all period. In this system, sensing unit picks up the dampness material of dirt as well as appropriately switches over the pump electric motor on or off [4]. Dirt wetness sensing unit is used locate the dirt problem whether the dirt is damp or completely dry. If dirt is completely dry the pump electric motor will certainly pump the water till the area is damp which is constantly checked by the Arduino controller. The major benefit of dirt wetness sensing unit is to make certain exact dimensions and also farmer does not need to see his ranch to run the pump. At the same time, utilizing GSM strategy Arduino controller is sending out message on cellphones of farmers concerning motor condition.

E-ISSN 2581 - 7957
P-ISSN 2277 - 3916

CVR Journal of Science and Technology, Volume 19, December 2020
DOI: 10.32377/cvrjst 1909

## II. LITERATURE SURVEY

Nowadays, although watering systems are utilized in farming area to minimize dependence of rainfall, the majority of them are either managed by hand or having actually time managed automation.

In these sorts of systems water is put on in an area on the basis definite number of periods which calls for high workforce for tracking as well and it lowers the area effectiveness. On top of that, this repaired period procedure causes over watering than the real plant demand as well as under watering when plants called for a lot more water in their height durations. Retardation of plant development price, late blooming and also decrease of plant harvest are the significant occasions created as a result of water shortage. Furthermore, over watering in the origin areas causes disease of the origin areas as well as greenery, extra price for farmer, throwing away of water and also time waste. Likewise, salinity of the dirt can be enhanced by continual supply of excess water. Watering of crops requires. Solar power for power generation is important to take on the present power crisis. One of the significant weak points of the set panel planetary system is that as a result of turning off the sunlight, it is unable to remove optimum power from the sunlight. The entire surveillance system has 2 components: a cordless sensing unit network as well as surveillance facility. Sensing unit nodes, the controller node, dirt wetness sensing units, watering pipeline, spray watering as well as watering control shutoff were released in crop-growing areas, the structure of the surveillance system was displayed in Fig. ZigBee or any kind of WSN network was embraced in mesh network geography. In order to satisfy the network insurance coverage and to lower the node power usage and also the cost at the exact same time, we picked a percentage of sensing unit nodes as routers, to finish the information celebration and also directed information from various other devices to the planner. As well as the majority of the sensing unit nodes work as incurable gadgets, just accumulate information as well as sent out to the router or near the planner; A control board reaches the sensing unit nodes to offset controller node, information purchase can be continuing at regular times, control shutoff can be available to understand the watering when getting watering command. Wireless sensing unit network that includes sensing unit nodes, directing nodes as well as organizer node are dispersed into all the areas of the surveillance locations. All nodes are powered by solar power. Nodes utilize modular layout, the 3 type of nodes utilize typical core components, and also various nodes with various expansion components [5]. The temperature level as well as moisture sensing unit gathered temperature level as well as moisture details; transmitting nodes was in charge of directing interaction as well as forwarding information; the organizer node obtains information from transmitting node and sent to the host computer system display facility via RS232 serial bus. The tracking facility can videotape real-time dirt dampness and web content publishing from all nodes compute plant watering water demand according to the plant physiology particularly in various development phases. The outcome results to pass on by cordless sensing unit network, control opening and also closing time of shutoff, so regarding recognize the remote automated modification and also control for watering [6].

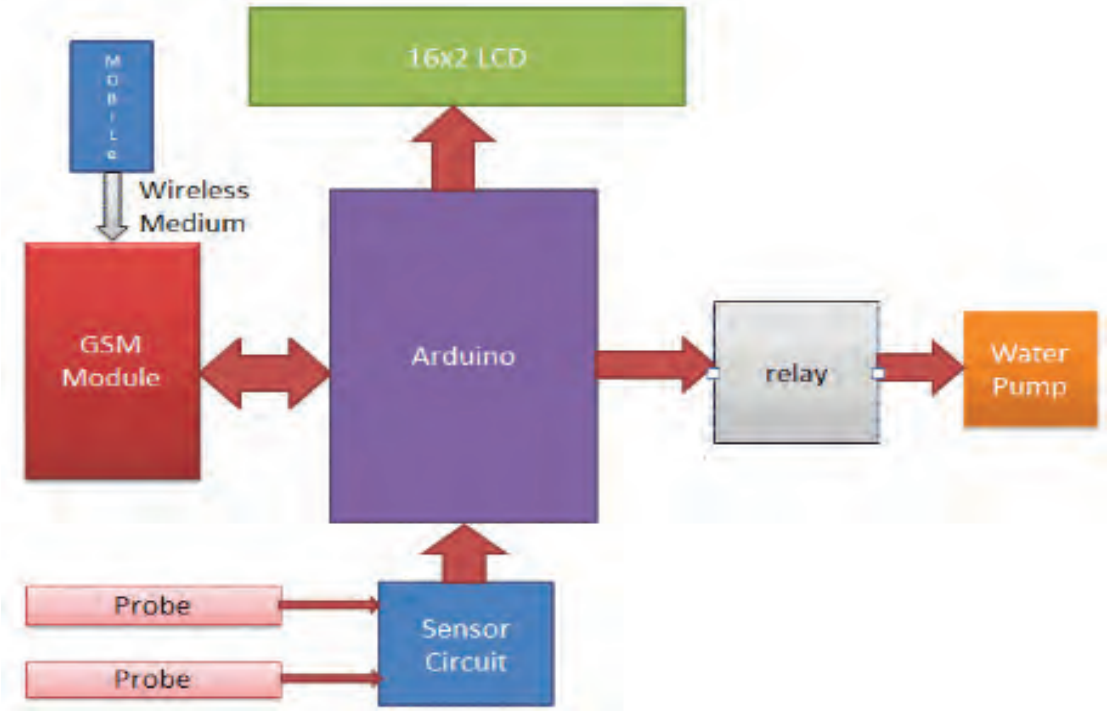


**Fig.1. Model diagram for development.**

E-ISSN 2581 - 7957
P-ISSN 2277 - 3916

CVR Journal of Science and Technology, Volume 19, December 2020
DOI: 10.32377/cvrjst 1909

## III. Methodology

Suggested watering system contains 2 almost all, solar pumping and also automated watering component. Photovoltaic panel bills the battery via cost controller. From the battery, supply is provided to the electric motor straight in this job. Right here the picking up circuit regulates the electric motor. The sensing units utilized are dirt wetness sensing unit, temperature level & moisture sensing unit. The sensing unit identifies the worth of dirt dampness, temperature level & moisture at various factors in the area. Arduino controller according to pre-set worth contrasts the gauged worth. Based upon the mistake in between the pre-set and also gauged worth, electric motor ON/OFF problem is regulated. The solar batteries that we see are additionally called photovoltaic or PV cells, which transform sunshine straight right into power. A photovoltaic panel pumps electrical energy right into a battery that saves it, yet the photovoltaic panel has no control over just how much it does or exactly how the battery gets it. The cost controller (fee regulatory authority) located in between the photovoltaic panel and also the battery manages the voltage as well as the existing as well as basically stops billing task temporally when required. The terms moisture as well as wetness are not compatible. Moisture describes the water web content in gases such as in the environment. Dampness is the water web content in any kind of strong or fluid. It includes a linking probe, which is put down in the dirt. Dampness sensing unit is made use of to pick up the dampness of the dirt as well as sends out the signals to the controller. If the dampness degree gets to the listed below the pre-set worth, after that the water is sent out to the area. These sensing units have no relocating components, they are specific, never ever wear, do not require calibration, job under several ecological problems, as well as correspond in between sensing units and also analyses. Furthermore, they are not pricey and also rather simple to utilize.

Figure 2. Soil moisture sensor.

Currently transferring to the 2nd component of the task, the power produced with the photovoltaic panel will certainly be sent out to a DC battery. The battery will certainly keep the power for more applications. Currently we are linking a water pump to the battery to make sure that the electric motor ought to operate on the power created by the photovoltaic panel. In this system the water will be an automated one that suggests the pump will provide the water just when the land requires it. In order to accomplish this job, we are taking advantage of dirt dampness sensing unit as well as a GSM component. The dirt wetness sensing units will certainly be put inside the area, and also it will certainly be linked to the Arduino controller. The dampness sensing unit will certainly be constantly noticing the wetness material of the dirt as well as sending it to the Arduino controller, where wetness web content worth will certainly be compared to predefine degree. Currently whenever the wetness degree comes to be much less than the predefined degree, Arduino controller will certainly send out a command to trigger the water pump. Very same time Arduino controller will certainly trigger GSM component, which will certainly send out a comments message to individual, mentioning that the "Pump on". After the electric motor gets going and also begins providing water to the area; at the same time the wetness sensing unit will certainly be picking up the wetness web content as well as sending out the information to the Arduino controller. Because the area is obtaining supply of water currently the dampness degree of the area will certainly begin boosting, this boost in the wetness material will certainly once again will certainly be compared to a predefined wetness degree. When it will certainly get to the predefined dampness degree, pump will immediately off. Once again GSM component will certainly send out comments message mentioning that "Pump off". This water pump additionally functions by hand by pushing the trick.

Figure 3. GSM module.

**NodeMCU (ESP8266)**

NodeMCU is an open-source Lua based firmware and advancement board, as shown in figure 2. exceptionally focused on IoT based Applications. It incorporates firmware that sudden spikes in demand for the ESP8266

E-ISSN 2581 - 7957
P-ISSN 2277 - 3916

CVR Journal of Science and Technology, Volume 19, December 2020
DOI: 10.32377/cvrjst 1909

wi-fi SoC from Expressive Systems and equipment, which depends on the ESP-12 module. The NodeMCU ESP8266 improvement board accompanies the ESP-12E module containing an ESP8266 chip having Tensilica Xtensa 32-cycle LX106 RISC microchip [2]. This chip underpins RTOS and works at 80MHz to 160 MHz movable clock recurrence. NodeMCU has 128 KB RAM and 4MB of Flash memory to store information and projects. Its high preparing power with in-assembled wi-fi/Bluetooth and Deep Sleep Operating highlights. It is shown in figure 4.

Figure 4. Node MCU

## IV. Operation and Results

In the suggested system solitary axis solar radar is utilized for the watering in addition to GSM. 4 LDR's are put on photovoltaic panels assists to track optimum strength of sunshine and also assists to gather even more power. Created electrical energy is kept in DC battery which is utilized to pump the water for watering system. The analog worth from LDR sensing units and also dirt wetness sensing unit are transformed in to electronic worth by utilizing ADC Converter. The electronic worth after that was given to Arduino controller as an input. Arduino controller is interfaced with DC Pump, LCD and GSM Module. When moisture material of dirt will certainly be low, pump will certainly begin immediately and also farmers can obtain the info on his mobile via GSM component.

Figure 5. Hardware kit image.

The suggested system manages quantity of water usage for watering in the farming areas. Hence it minimizes extreme stress on farmers to pay added water toll on water. Along with this regulated watering likewise conserve added price for water pumping, decreases the transportation and also circulation losses in the area degree. In addition, power intake on water pumps can be decreased by effective water allotment based upon the plant water demand. This solar energy automatic watering system does not need male power for procedure. This smart system can discover the dirt wetness problems and also carry out instantly based upon predefined wetness problems.

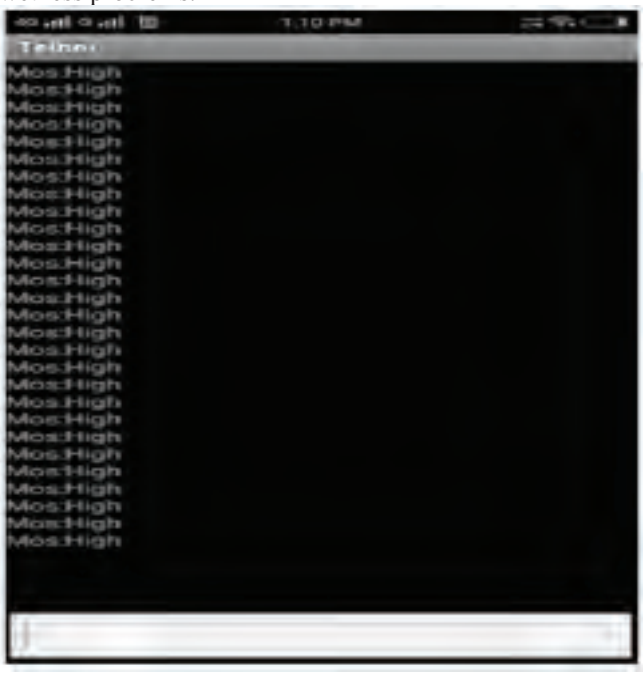


Figure 6. Output results.

## V. Conclusions

In this paper, a solar energy sensing unit base automated watering design is recommended. We developed this version thinking about affordability, integrity, alternating resource of electrical power as well as automated control. As the recommended design is immediately managed, it will certainly assist the farmers to effectively water their areas. The version constantly makes certain the adequate degree of moisture in the dirt. Hence, this system prevents over watering, under watering, leading dirt disintegration and also minimizes the wastefulness of water. Solar energy gives adequate quantity of power to drive the system. To conquer the requirement of power as well as to alleviate the watering system to the crops, the suggested version can be an ideal choice. Solar power for watering is cost-competitive with standard power resources for little, remote applications, if the complete system layouts and also Utilization timing is very carefully thought about and also arranged to utilize the solar power as successfully as feasible.

## REFERENCES

[1] Y.Erdem, L.Arin, T.Erdem, S.Polat, M.Deveci, H.Okursoy, andH. T. Gültas, "Crop water anxiousness index for examining watering schedulingof drip irrigated broccoli (Brassica oleracea L. var. italica),"Agricult. Water Manag., vol. 98, no. 1, pp. 148-- 156, Dec. 2010.

[2] Vishal Dineshkumar Soni 2018. "Artificial Cognition for Human-robot Interaction." International Journal on Integrated Education. 1, 1 (Dec. 2018), 49-53. DOI:https://doi.org/10.31149/ijie.v1i1.482.

[3] Khan T, Tanzil S M, Rahman R as well as additionally Alam S M, 'Design along with Construction of an Automatic Solar Tracking System', IEEE 6th International Conference on Electrical as well as likewise Computer Engineering ICECE 18-20, 2010.

[4] Luthra S K, Kaledhonkar M J, Singh O P in addition to Tyagi N K, 'Design in addition to development of an automobile watering System', Elsevier Science B. V. - Agricultural Water Management, Volume 33: 169-181, 1997.

[5] Hair A, Arif S M, Shaikh S along with Shaikh S, 'Solar Panel Tracking System for GSM Based Agriculture System', International Journal of Engineering as well as additionally Advanced Technology (IJEAT), Volume 2, Issue 5, June 2013.

[6] Vishal Dineshkumar Soni 2018. Prediction of Stock Market Values using Artificial Intelligence, International Journal of Advanced Research in Electrical, Electronics and Instrumentation Engineering, Vol. 7, Issue 4, April 2018.

[7] Sanjukumar as well as likewise Krishnaiah R V, 'Advance Technique for Soil Moisture Content Based Automatic Motor Pumping for Agriculture Land Purpose', International Journal of VLSI along with Embedded Systems - IJVES, Volume 4, Article 09149, September 2013.

[8] [Seal B, Shirke O, Shewale S, Sirsikar An in addition to Hankare P,'Solar Based Automatic Irrigation System', International Journal of Research in Advent Technology, Volume 2, Number 4, April 2014.

[9] I. Ahmad and K. Pothuganti, "Design & implementation of real time autonomous car by using image processing & IoT," 2020 Third International Conference on Smart Systems and Inventive Technology (ICSSIT), Tirunelveli, India, 2020, pp. 107-113, doi: 10.1109/ICSSIT48917.2020.9214125.

[10] I. Ahmad and K. Pothuganti, "Smart Field Monitoring using ToxTrac: A Cyber-Physical System Approach in Agriculture," 2020 International Conference on Smart Electronics and Communication (ICOSEC), Trichy, India, 2020, pp. 723-727, doi: 10.1109/ICOSEC49089.2020.9215282.

[11] Vishal Dineshkumar Soni. (, 2018). Internet of Things based Energy Efficient Home Automation System. International Journal of Innovative Research in Science Engineering and Technology, 7(3), 2924-2929. Doi:10.15680/IJIRSET.2018.0703148.

E-ISSN 2581 - 7957
P-ISSN 2277 - 3916

CVR Journal of Science and Technology, Volume 19, December 2020
DOI: 10.32377/cvrjst 1910

# FPGA Implementation of CORDIC – I using Redundant Arithmetic

Niharika Chaudhary[1] and T. Subha Sri Lakshmi[2]
[1]PG Scholar, CVR College of Engineering/ECE Department, Hyderabad, India
Email: niharikaodf@gmail.com
[2]Asst. Professor, CVR College of Engineering/ECE Department, Hyderabad, India
Email: subha.sri@cvr.ac.in

***Abstract:*** **This paper provides high speed, low power consumption, and less area utilization of the Coordinate Rotation Digital Computer (CORDIC) Algorithm for digital signal processing applications. Here methodology is built on a multiplexer-based, that is used to accomplish the fast and efficient hardware on FPGA for sine and cosine values. A 6-stage CORDIC is calculated by four arrangements scheduled i.e., Unrolled CORDIC and MUXes based CORDIC with and without pipelining up to three stages. The proposed architecture has adders, subtractors, and shifters. Shifters are replaced with multiplexers up to 3-stages. All remaining adders and subtractors are traded with Redundant Arithmetic. A 16-bit CORDIC algorithm is designed to achieve the sine and cosine function values by using VIVADO 20.1. Comparisons are performed between Unrolled CORDIC structure and MUXes based CORDIC structure for sine and cosine values in terms of timing and power consumed. MUXes based CORDIC structure attains high operating frequency, less area utilization, and low power consumption for hardware implementation.**

***Index Terms:*** **CORDIC Algorithm, Rotation Mode, Multiplexer, Pipelining, Redundant Arithmetic, Unrolled CORDIC**

## I. Introduction

In 1956 the CORDIC algorithm was presented by Jack Volder while building a real-time navigator [1]. CORDIC is simple and efficient because requires only addition, subtraction, shifting of bits, and a lookup table. Sine and Cosine can be derived from any complex functions. These functions are used in a wide range of applications such as DSP, wireless communication, biometrics, robotics, etc. CORDIC method is castoff to generate hardware that performs sine and cosine calculations. CORDIC is used in a wide variety of elementary transcendental functions involving exponentials, logarithms, and square roots. Thereafter it was polished by Walter and others. In this algorithm, the angle is broken into the sum of angles and micro rotated by predefined angles. The CORDIC algorithm is implemented in the FPGA platform because the speed and computational power of ASICs are merged with the resilience of microprocessors [3]. CORDIC algorithm is castoff in various applications such as calculators, mathematical coprocessor units, clock recovery circuits, waveform generators. The iterative architecture provides hardware implementation with minimum size and throughput as a trade-off, while parallel and pipelined CORDIC architecture offers high – speed and high-throughput computation.

CORDIC algorithm comprises diverse architectures for mapping into hardware. These are grouped as folded and unfolded (as shown in figure 1). These operations are done by the knowledge of three iterative calculations [14]. First method architecture of folded implemented by copying every difference equation of CORDIC into time multiplexing and hardware. In a single functional unit, all these operations are done, so it will provide a trading area for speed [16]. It can be categorized into two kinds; folded bit-serial and folded word-serial architectures. It will check the functional unit implementation logic for every one bit or word of CORDIC in each iteration

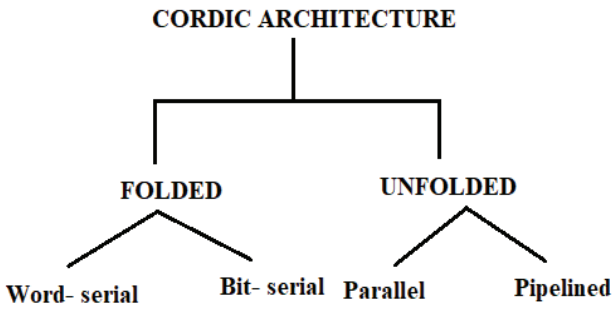


Figure 1. Nomenclature of CORDIC

Cordic is an iterative method of performing the microrotations for arbitrary angles using shifts and addition [1]. This MUXes based approach shows high speed and hardware efficient CORDIC, which can be used for DSP applications. A reconfigurable CORDIC can be operated in both rotation and vectoring mode. In this paper, only the rotation mode is discussed.

Nevertheless, the number of micro rotations is a serious downside of the critical path delay, the micro-rotation increases propagation delay In this paper, proposed CORDIC architecture the adders, subtractors, and shifters are replaced by multiplexers and redundant Arithmetic. CORDIC is designed in Unrolled CORDIC, pipelined Unrolled CORDIC, and MUXes based CORDIC up to 3 stages with and without pipelining. Replacement of the multiplexer and Redundant Arithmetic in the place of adders and shifters minimize the area of utilization on an FPGA, which intern reduces the power consumption, and surges the speed of operation.

This paper provides a prototype for implementing unrolled and pipelined architectures.

E-ISSN 2581 - 7957
P-ISSN 2277 - 3916

CVR Journal of Science and Technology, Volume 19, December 2020
DOI: 10.32377/cvrjst 1910

## II. CORDIC ALGORITHM

The CORDIC programs on an iterative process that executes vector rotations by representing them as arbitrary angles by the application of shift and add operations [3]. The generalized rotation transform from the results of the Volder algorithm is given below [4].

$$f \sin \beta + r \cos \beta = r' \quad (1)$$

$$f \cos \beta - r \sin \beta = f' \quad (2)$$

This Cartesian plane switches by the angle β, as publicized in figure 2.

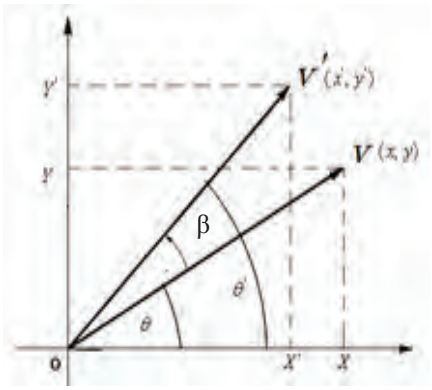


Figure 2. CORDIC angle rotation by $\varphi$.

The above equations can readapt as:

$$[\, r + f \tan \beta \,] \cos \beta = r' \quad (3)$$

$$[\, f - r \tan \beta \,] \cos \beta = f' \quad (4)$$

These rotations of angles are forced such that $\tan \beta = \pm 2^{-i}$. This will decrease tangent multiplication by the simple shift operation. By the execution of elementary rotations alternative rotation of arbitrary angles is managed. Through a sequence of micro-rotations of elementary angles ($\varphi_i$) CORDIC rotations are achieved. By decomposing β into elementary rotations in a sequence style the micro-rotations is achieved:

$$\beta = \Sigma \varphi_i \quad (5)$$

By using these we can form simple iterative rotations

$$[r_i + f_i \tan \varphi_i \,] \cos \varphi_i = r_{i+1} \quad (6)$$

$$[f_i - r_i \tan \varphi_i \,] \cos \varphi_i = f_{i+1} \quad (7)$$

From trigonometric identities we have:

$$\cos \varphi_i = 1/ (1+\tan^2 \varphi_i)^{1/2} \quad (8)$$

Substituting equation (8) in equation (6) and (7) we have:

$$r_{i+1} = [\, r_i + f_i \tan \varphi_i \,] / (\, 1 + \tan^2 \varphi_i \,)^{1/2} \quad (9)$$

$$f_{i+1} = [\, f_i - r_i \tan \varphi_i \,] / (1 + \tan^2 \varphi_i \,)^{1/2} \quad (10)$$

To guarantee that tangent multiplication reduced to a small shifting operation, the rotation angles obtained from the following relation:

$$\text{Tan } \varphi_i = \pm 2^{-i} \quad (11)$$

Here i represent the total number of iterations. And $\tan \varphi_i$ is traded in above equation by substituting equation (12) in (9) and (10), we have:

$$r_{i+1} = [\, r_i + f_i \,.k_i.\, 2^{-i}].J_i \quad (12)$$

$$f_{i+1} = [\, f_i - r_i \,.k_i.\, 2^{-i}].J_i \quad (13)$$

Here,

$1/ (1+2^{-2i})^{1/2} = J_i$, denoted as scale of constant.

$k_i = \pm 1$, where $k_i$ is decision function.

The constant scale value from obtained equations of vector rotation is eradicated by a shift-add algorithm. In the system, the product term $J_i$'s is applied. Through the use of iterations in infinite times this product value has a range up to 0.6073. Rotation algorithm gain is represented as $A_n$ where,

$$A_n = \Pi [1+2^{-2i}]^{1/2} \quad (14)$$

The gain is unevenly equal to 1.647 for infinite iterations. However, this gain is calculated with the support of the total number of iterations, and also it depends on the compound rotation angle is discrete by a sequence of elementary rotations in the way of the direction. These sequences are denoted as decision vectors. And all these vectors, are used for the angular calculation system, depending on the values of binary arctangents. Translations are completed utilizing a look-up table among the angular system and any other systems. For each iteration, an enhanced conversion technique is employed by adding subtractor and adder unit to it for elementary rotation angles. The above angles are expressed by an appropriate angular unit. A small lookup table supplies the angular values, and also we can use hardwired, depending on the suitable implementation.

Accumulator angle is added to the third value of difference equation to CORDIC algorithm:

$$z_i - \varphi_i = Z_{i+1}$$

$$Z_{i+1} = z_i - k_i \tan^{-1} (2^{-i})$$

E-ISSN 2581 - 7957
P-ISSN 2277 - 3916


DOI: 10.32377/cvrjst 1910

Hence, the CORDIC micro-rotation equations are inscribed as:

$$x_{i+1} = x_i - y_i . 2^{-I}.k_i \quad (15)$$

$$y_{i+1} = y_i + x_i . 2^{-I}.k_i \quad (16)$$

$$z_{i+1} = z_i - k_i \tan^{-1} ( 2^{-i} ) \quad (17)$$

## III . CORDIC MODES

The CORDIC algorithm is divided into two modes. Rotation mode is the one [15], in which the input vector value is rotated by a specified angle. The second one is Vectoring mode where the input vector is rotated to the x-axis.

### *A. Rotation Mode*

In this mode, some favored rotation angle is set by the angle accumulator. The trigonometric, hyperbolic, or some other transcendental values are found through these rotation angles as the argument. Angle accumulators will take care of the rotation decision. Here, the decision is made and evaluated at every rotation.

CORDIC equations in this model are written as:

$$l_i - h_i . 2^{-I}.k_i = l_{i+1}$$

$$h_i + l_i . 2^{-I}.k_i = h_{i+1}$$

$$t_i - k_i \tan^{-1} ( 2^{-i} ) = t_{i+1}$$

Here,

$$k_i = -1 \quad \text{if } t_i < 0 \text{ +1, else}$$

n iterations after it produces the following results:

$$t_n = 0$$

$$[y_1 \cos z_1 + x_0 \sin z_1] An = H_n$$

$$[x_1 \cos z_1 - y_1 \sin z_1 ] An = L_n$$

### *B. Vectoting Mode*

In vectoring mode, the input vector of the CORDIC rotator is circled through whichever angle is essential to align the resultant vector with the *x*-axis. The outcome of the vectoring operation is a scaled magnitude of the original vector (the *x* component of the result) and rotation angle. At every rotation, the vectoring function works by minimizing the *y* component of the residual vector. The sign of the residual *y* component is used to determine which direction to rotate next. If the angle accumulator is initialized to zero, it holds the traversed angle at the end of the iterations.

A CORDIC equation in vectoring mode follows:

$$q_{j+1} = q_j - m_j . w_j . 2^{-j}$$

$$m_{j+1} = m_j + q_j . w_j . 2^{-j}$$

$$f_{j+1} = f_j - w_j \tan^{-1} ( 2^{-j} )$$

Here,

$$w_j = +1 \quad \text{if} \quad m_j < 0 \text{ -1, else}$$

*n* iterations after it produces following results:

$$q_n = A_n (q_0^2+m_0^2)^{1/2}$$

$$f_n = \tan^{-1}(m_0 / q_0) + F_0$$

$$m_n = 0$$

## IV. REDUNDANT ARITHMETIC

In implementations as the computations always start from the most significant bit (MSB). Redundant number systemAdders play a major role in CORDIC and due to carry propagation in adders the delay increases rapidly and slows down the speed of operation so that, move on to Redundant Arithmetic to decrease the delay and increase the speed of operation. The conservative tasks like subtraction, multiplication, and addition produce carry-propagation chains. A redundant number scheme was announced to resolve this problem [10]. The redundant number scheme improves the arithmetic operations speed. This method is used for sign processing and additional applications. When the reconversion and conversion circuitry shares the information among all the function units, this method also saves the area in VLSI and also power dissipation, due to these two reasons system will become more effective. Redundant number systems (RNS) suitable for numerically intensive applications. RNS can prevent or captures the carry propagation, by generating parallel adders with the delay of constant value; it won't depend on the operand word-length. This will be produced in an RNS format by using low latency results. RNS can improve performance in mathematically intensive applications. However, the implementation of an arithmetic circuit is expensive because for each symbol multiple bits are required. These circuits will eliminate carry propagation, by giving near-constant addition delay, regardless of the operand width. The Redundant number system (RNS) has a unique property of "carry-free" addition which makes them beneficial in implementations as the computations always start from the most significant bit (MSB).

### *A. Carry- Free Addition Radix-2*

Redundant number representations limit the carry propagation to a few bit positions and are usually independent of word length W. This carry free propagation feature enables fast addition

The logic implementation is varied because the algorithm for signed binary digit addition is not unique. By using two binary unsigned numbers, it can perform the radix-2 operation, one bit is negative and another bit is positive and

E-ISSN 2581 - 7957
P-ISSN 2277 - 3916

CVR Journal of Science and Technology, Volume 19, December 2020
DOI: 10.32377/cvrjst 1910

it can be represented as [11]

$$X = X^{+} - X^{-} \quad (18)$$

$x_i^+$ and $x_i^-$ are both negative as well as positive numbers these bit values are 0 and 1, $x_i$ should vary {1,0,1}, all these values are given in Table I.

TABLE I.
REDUNDANT NUMBER SYSTEM OF RADIX-2

| $x^+$ | $x^-$ | X | $X = x^+ x^-$ |
|---|---|---|---|
| 0 | 0 | 0 | 00 |
| 0 | 1 | -1 | 01 |
| 1 | 1 | 1 | 10 |
| 1 | 1 | 0 | 11 |

### *B. Hybrid addition Radix-2*

In this hybrid operation, the 2 input operands are a redundant signed-digit representation and conventional unsigned number. The output operand obtained is in redundant signed-digit representation. For The signed-digit number addition $X_{<2.1>}$ is considered which is a radix-2 operation, where 2 indicates the radix-2 job, and 1 indicates the largest digit value and an unsigned conventional number Y.

$$X_{<2.1>} + Y = S_{<2.1>} \quad (19)$$

In 2 steps we can get an added value. Here 1st step all the bits are in parallel positions i ($0 \le i \le W-1$), W being the word length. The intermediary sum $p_i = x_i + y_i$ is calculated, it ranges between {1, 0, 1, 2}. This addition can be

$$x_i + y_i = p_i = 2t_i + u_i, \quad (20)$$

Table II summarizes hybrid radix-2 addition, in that table $t_i$ denotes transfer digit and it varies value from 0 or 1, and it is also represented as $t_i^+$ and $u_i$ denotes interim added sum and it varies the values either 1 or 0, and it is also represented as $u_i^-$.

TABLE II.
SUMMARIZES THE DIGIT SETS INVOLVED IN HYBRID RADIX-2 ADDITION

| Digit | Binary Code | Radix 2 Digit Set |
|---|---|---|
| $x_i$ | $x_i^+ - x_i^-$ | {1,0,1} |
| $y_i$ | $y_i^+$ | {0,1} |
| $p_i = x_i + y_i$ | ..... | {1,0,1,2} |
| $u_i$ | $-u_i^-$ | {1,0} |
| $t_i$ | $t_i^+$ | {0,1} |
| $s_i = u_i + t_{i-1}$ | $s_i^+ - s_i^-$ | {1,0,1} |

The most significant interim sum digit $u_w$ has a value zero, the same as the least significant transfer digit $t_{-1}$.

The digit sum $s_i$ is designed by linking $t^+_{i-1}$ and also $u_i^-$, which is one of the single-digit in the second step:

$$s_i = t^+_{i-1} - u_i^-. \quad (21)$$

Replacing the corresponding binary codes from Table 2 in (3a) we get:

$$x_i^+ - x_i^- + y_i^+ = 2t_i^+ + u_i^- \quad (22)$$

These all operations are performed by using type-1 full adder [12], it is nothing but plus-plus-minus adder (PPM) [13] as shown in figure 3. The four-digit hybrid radix-2 adder is shown in figure 4.

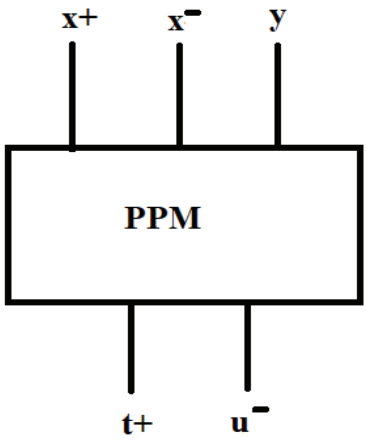


Figure 3. Hybrid Radix 2 PPM Adder

E-ISSN 2581 - 7957
P-ISSN 2277 - 3916

CVR Journal of Science and Technology, Volume 19, December 2020
DOI: 10.32377/cvrjst 1910

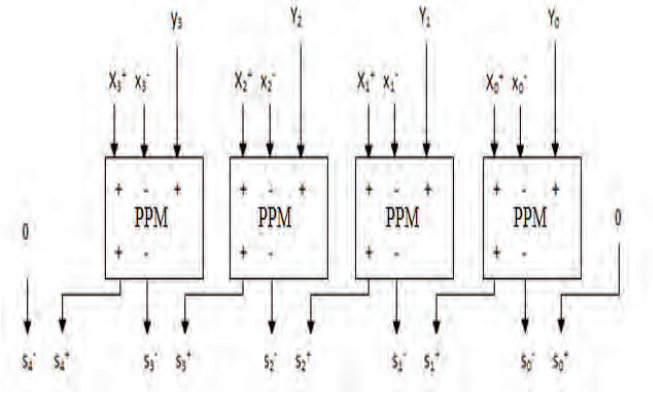


Figure 4. Four Digit Hybrid Radix-2 Adder

### C. Hybrid Radix-2 subtraction

MMP subtractor does subtraction on a redundant binary signed digit number system. To draw high-speed systems this subtractor shown in Figure 5 is beneficial as it permits "borrow free" subtraction. It carries out subtraction of a redundant number x where, x = x- and x+ to an unsigned binary number y, resulting in another redundant number expressed by an interim sum $b^-$ and a transfer digit $t^+$. the input bits are defined as x+, x-, y $\varepsilon$ {0,1}, and the output bits are $b^-, t^+ \varepsilon$ {0,1}.

The following operations are performed by subtractor:

$$x - y = x^+ - x^- - y \Rightarrow$$

$$b^- - 2t^+ \quad (23)$$

where x is a redundant number expressed as

$$x = x^+ - x^-$$

Therefore,

$$x^+ - x^- - y = b^- - 2t^+ \quad (24)$$

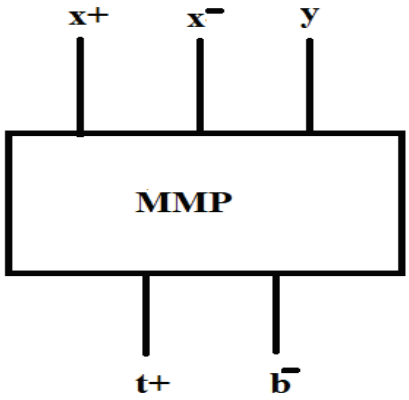


Figure 5. Hybrid Radix 2 MMP Subtractor

The interim sum $b^-$ and the transfer digit $t^+$ is stated by the following Boolean expression using the Truth table:

$$b^- = (x^+)'(x^-)y' + (x^+)'(x^-)y + (x^+)(x^-)'y' + (x^+)(x^-)y$$

$$t^+ = (x^+)'(x^-)y' + (x^+)(x^-)'y' + (x^+)'(x^-)y + (x^+)(x^-)y$$

After simplification of the above equations, a new the equation for the interim sum $b^-$ and the transfer digit $t^+$ is

$$b^- = x^+ \overline{\oplus}\, x^- \overline{\oplus}\, y$$

$$t^+ = x^+ \cdot (x^+ \oplus x^-) + y(x^+ \overline{\oplus}\, x^-) \quad (25)$$

## V. Unrolled Cordic Algorithm

CORDIC algorithm calculates the sine and cosine values of input angles concurrently in rotation mode. Figure 6 shows the unrolled CORDIC. It carries redundant adders, and subtractors, and shifters respectively. The subtraction or addition of angle succeeded based on the MSB of the previous angle in every rotation of the vector. The right shifts for division are executed by shift registers. Initially, for sine and cosine angles $x_i$=1 and $y_i$= 0. These initial values are shifted by i bits, where i= {1,2,3,4,5,6} which is divided by 1,2,4,6,8,16,32 at each stage. Discrete sine and cosine values range from -1 to 1 [18].

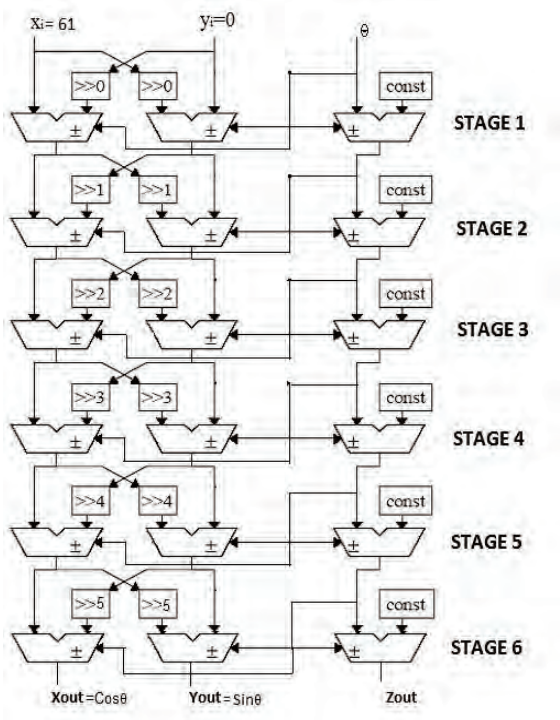


Figure 6. Construction of general unrolled CORDIC

As initial conditions has the outcome of discrete sine and cosine values varying from -1 to 1, so the fractional values are realized in FPGA by -100 to 100. $z_i$ is varied for every clock pulse to generate sine and cosine values. The rest values are computed by using the quadrature symmetry property of sine and cosine waves.

E-ISSN 2581 - 7957
P-ISSN 2277 - 3916

CVR Journal of Science and Technology, Volume 19, December 2020
DOI: 10.32377/cvrjst 1910

## VI. Pipelined Unrolled Cordic Algorithm

Pipelining is an implementation technique where a bundle of data processing instructions is overlapped. These instructions are given in a series. The pipeline process maximum frequency of operation in CORDIC. The architecture of the pipelined unrolled CORDIC is shown in Figure 7 [19,20].

Enlarged area and N-clock delays are the disadvantages of pipeline architecture. Hence, several pipelined registers and their positions are computed repetitively.

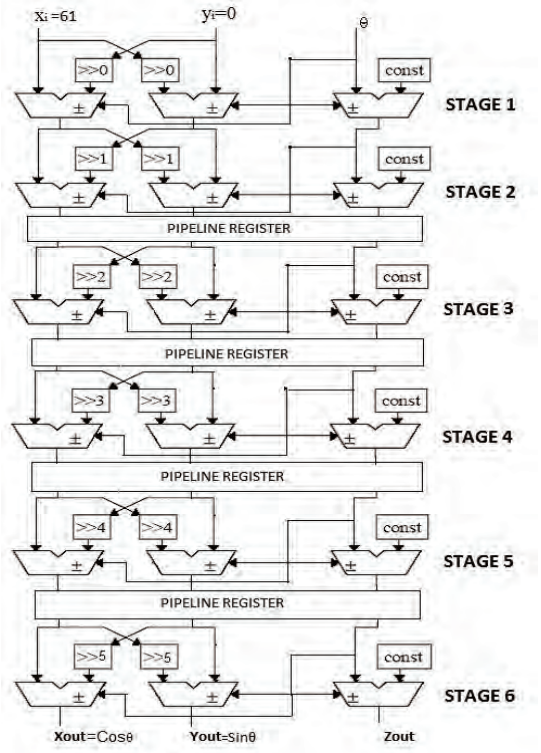


Figure 7. The architecture of Pipelined unrolled CORDIC

Four intermediate stages of pipelined registers are used to get optimized output.

## VII. Multiplexer Based Unrolled Cordic Algorithm

CORDIC architecture's area is reduced via multiplexer [20]. A multiplexer is used in the place of three stages in general unrolled CORDIC. The output is equal to $X_i$ as $Y_i$=0 in the first stage in original unrolled CORDIC architecture so the 1st stage's output is given as:

$$Y_1 = X_i = 61$$
$$X_1 = X_i = 61$$
$$Z_1 = Z_i - 45 \quad (26)$$

In the first iteration stage, $Z_1$ is calculated by subtraction since $Z_i$ is always positive as it varies from 0 to 90.

If $Z_1$ is positive, then the second stage output is described as

$$Y_2 = Y_1 - (X_1/2) = (X_1/2) = 31$$
$$X_2 = X_1 + (Y_1/2) = 3X_1/2 = 91 \quad (27)$$

If $Z_1$ is negative, then the second stage output is

$$Y_2 = Y_1 + (X_1/2) = 3X_1/2 = 91$$
$$X_2 = X_1 - (Y_1/2) = X_1/2 = 31 \quad (28)$$

Figure 8 shows two multiplexers used for the second stage.

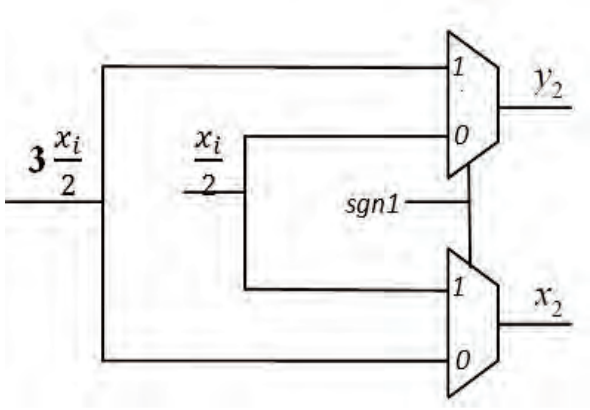


Figure 8. 2 multiplexers used for the second stage

Equivalently, by using 4 multiplexers the third stage is implemented with the following equation. $Z_2$ is computed by the formula

$$Z_{n+1} = \theta - \sum_{i=0}^{n}\theta_i = \theta - \sum_{i=0}^{n} arc\ tan\left(\frac{1}{2^n}\right) \quad (29)$$

For the third stage multiplexers, the above equation is used as the selection line input of the multiplexer.

For $Z_1$ = positive , $Z_2$ = positive

$$Y_3 = Y_2 + (X_2/4) = (3X_1/2) + (X_1/8) = 13X_1/8 = 99$$
$$X_3 = X_2 + (Y_2/4) = (3X_1/2) - (X_1/8) = X_1/8 = 7 \quad (30)$$

For $Z_1$ = negative , $Z_2$ = positive

$$Y_3 = Y_2 + (X_2/4) = (X_1/2) + (3X_1/8) = 7X_1/8 = 99$$
$$X_3 = X_2 + (Y_2/4) = (3X_1/2) - (X_1/8) = 11X_1/8 = 83 \quad (31)$$

For $Z_1$ = positive , $Z_2$ = negative

$$Y_3 = Y_2 - (X_2/4) = (3X_1/2) - (X_1/8) = 11X_1/8 = 83$$
$$X_3 = X_2 + (Y_2/4) = (3X_1/2) + (X_1/8) = 7X_1/8 = 53 \quad (32)$$

For $Z_1$ = negative, $Z_2$ = negative

$$Y_3 = Y_2 - (X_2/4) = (X_1/2) + (3X_1/8) = X_1/8 = 7$$
$$X_3 = X_2 + (Y_2/4) = (3X_1/2) + (X_1/8) = 13X_1/8 = 99 \quad (33)$$

The area is minimized as adders with 2:1 multiplexers are swapped up to the 3rd stage. There is an exponential increase in multiplexers i.e, 6,14,30 multiplexers for 3, 4, and 5stages as adders and shifters are replaced with mux. The fixed values expand due to the growth in multiplexers. The deletion of the 5th stage needs thirty muxes with sixteen

E-ISSN 2581 - 7957
P-ISSN 2277 - 3916

CVR Journal of Science and Technology, Volume 19, December 2020
DOI: 10.32377/cvrjst 1910

fixed values. On that occasion, utilizing a ROM is more effective.

The CORDIC-I algorithm runs on rotation mode whose input is $Y_i$=0 and $X_i$=1. The equation to used is

$$f_{i+1} = k_i . [ f_i - r_i . d_i . 2^{-i}]$$

$$r_{i+1} = k_i . [ r_i + f_i . d_i . 2^{-i}]$$

At this time, $k_i$ is the scaling factor with 0.611 is multiplied with the input $X_i$= 1 Discrete sine and cosine values are varied from -100 to 100 for FPGA realization.

Equations 30-33 are solved by taking input $X_i$= 61 and Y= 0.

The obtained values are

- P = $x_i$ /8 = 8
- Q = 11 $x_i$ /8 = 84
- R = 7 $x_i$ /8 = 53
- S = 13 $x_i$ /8 = 99

Figure 9 shows the architecture of unrolled CORDIC based on 2:1 mux.

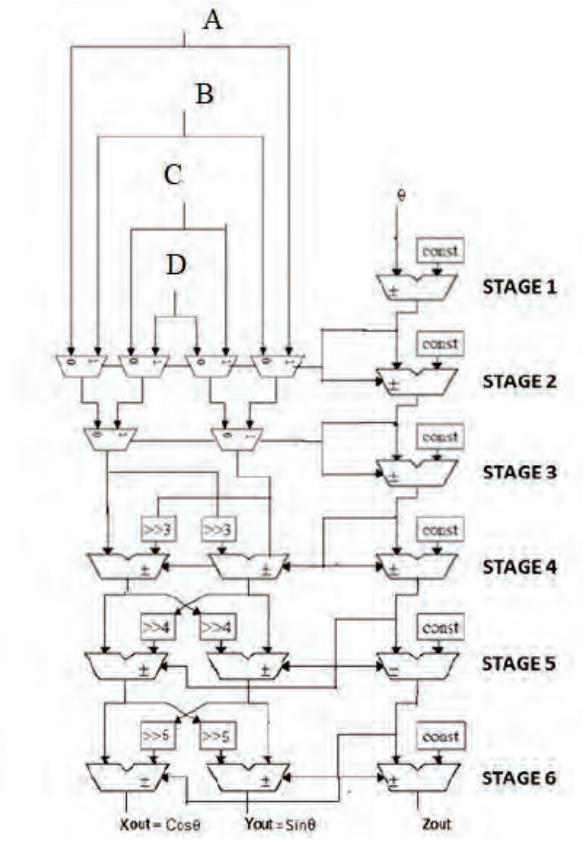


Figure 9. The architecture of unrolled CORDIC with MUX

## VIII. Multiplexer Based Pipelined Unrolled Cordic Algorithm

The multiplexer based pipeline CORDIC utilizes the same computation as used for unrolled CORDIC with a multiplexer. Architecture is shown in Figure 10.

Here, subtractors, adders, and shifters are swapped up to 3 stages with a multiplexer.

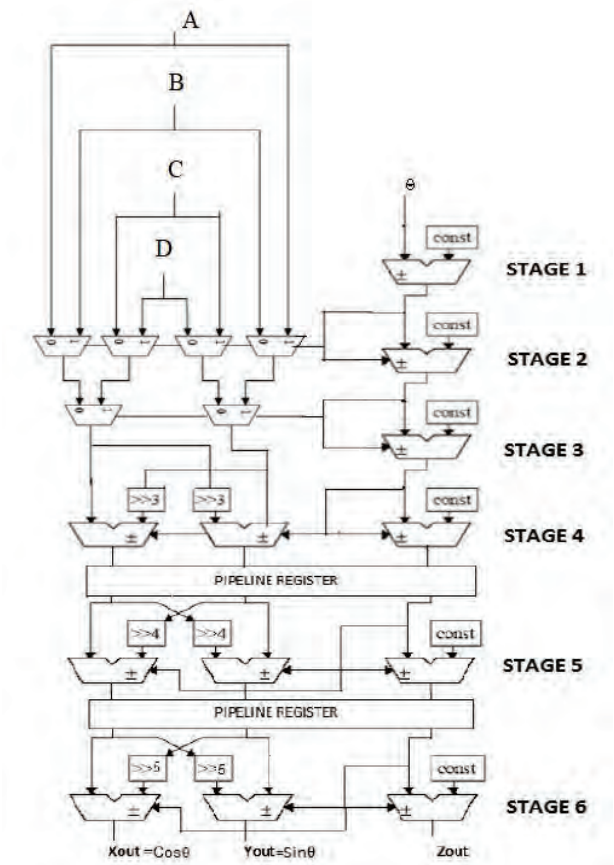


Figure 10. The architecture of Pipelined unrolled CORDIC with MUX

## IX. Results

An 8-bit CORDIC for constructing sine and cosine function with and without pipelining based on Unrolled and multiplexer based CORDIC. The initial design entry is finished using VERILOG. The core is implemented with the following synthesis description:

- Design Entry: VERILOG
- Synthesis and Simulation: VIVADO 18.1
- Platform: FPGA
- Family: Zynq-7000
- Target board: xc7z020clg484-1
- Optimization area: Power

Figure 11 is the implemented result of the Unrolled CORDIC architecture schematic obtained from the tool.

In Figure 12 “clk” is the input signal along with x, y, and z is the angle which is 60. “sin” is discrete sine values, “cos” is the discrete cosine values and “zout” is the microrotation

E-ISSN 2581 - 7957
P-ISSN 2277 - 3916

CVR Journal of Science and Technology, Volume 19, December 2020
DOI: 10.32377/cvrjst 1910

angle obtained as output. The addresses are the stored predefined values of the CORDIC angles.

Calculation of zout : $60^0 - 45^0 = 15^0$
$15^0 - 27^0 = -12^0$
$12^0 + 14^0 = 2^0$
$2^0 - 7^0 = -5^0$
$-5^0 + 4^0 = -1^0$
$-1^0 + 2^0 = 1^0$

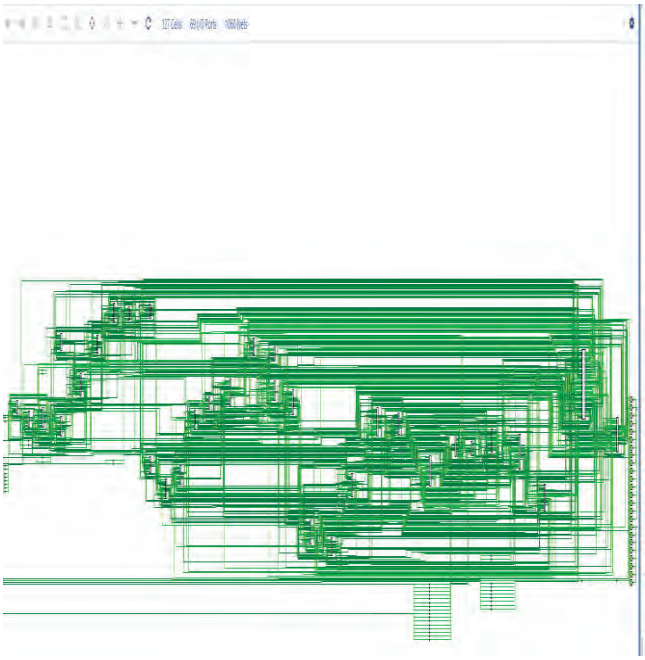

Figure 11. Schematic of Unrolled CORDIC

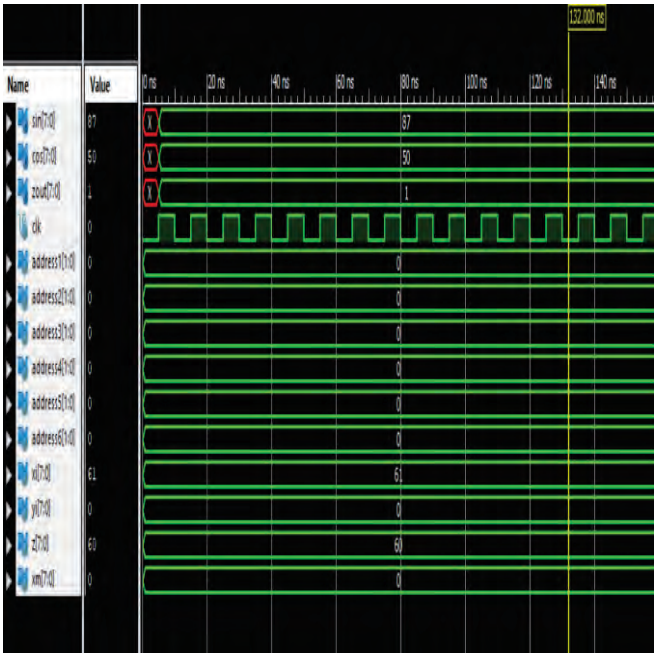


Figure 12. Simulation Result of Unrolled CORDIC

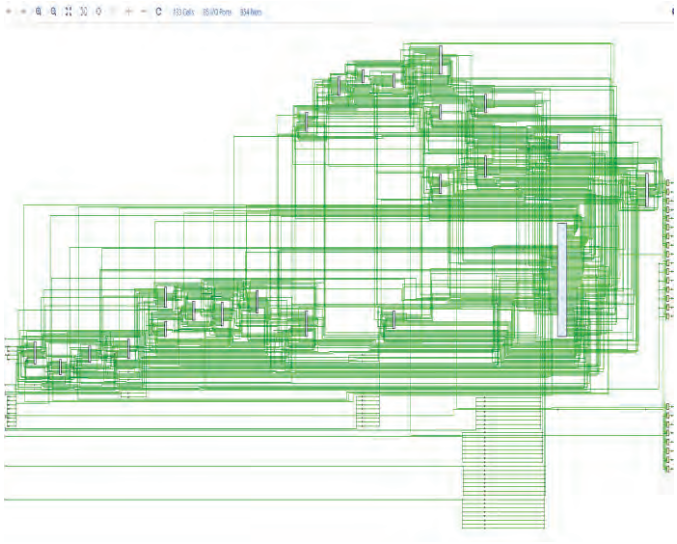

Figure 13. Schematic of Pipelined Unrolled CORDIC

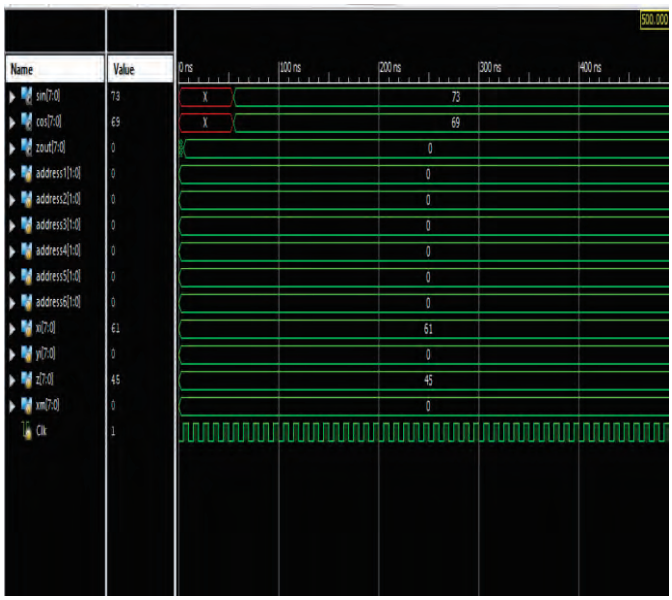


Figure 14. Simulation Result of Pipelined Unrolled CORDIC

Figure 13 is the implemented result of the pipelined unrolled CORDIC architecture schematic obtained from the tool.

In Figure 14 “clk” is the input signal along with x, y, and z is the angle which is 45. “sin” is discrete sine values, “cos” is the discrete cosine values and “zout” is the microrotation angle obtained as output.

The addresses are the stored predefined values of the CORDIC angles.

Figure 15 is the implemented result of unrolled CORDIC using MUXes schematic obtained from the tool.

In Figure 16 “clk” is the input signal along with x, y, and z is the angle which is 45. “sin” is discrete sine values, “cos” is the discrete cosine values and “zout” is the microrotation angle obtained as output.

The addresses are the stored predefined values of the CORDIC angles.

E-ISSN 2581 - 7957
P-ISSN 2277 - 3916

CVR Journal of Science and Technology, Volume 19, December 2020
DOI: 10.32377/cvrjst 1910

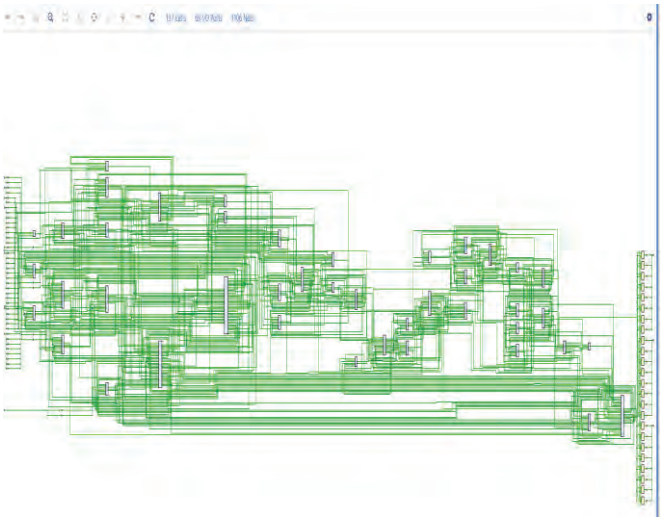

Figure 15. Schematic of Unrolled CORDIC using MUXes

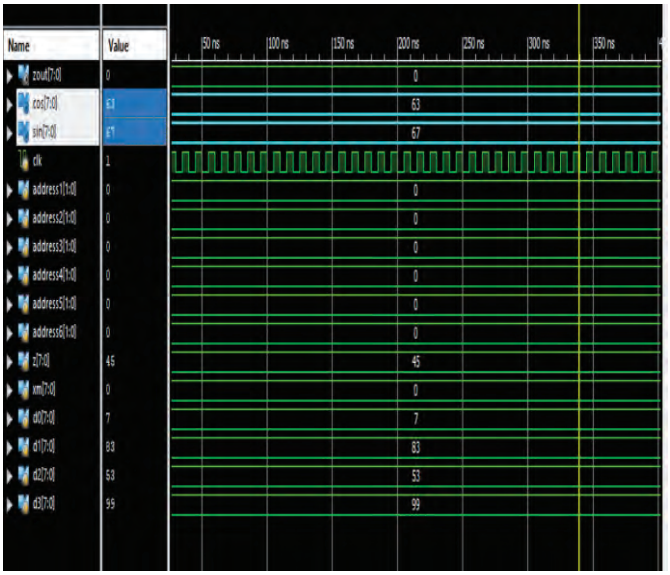


Figure 16. Simulation Result of Unrolled CORDIC using MUXes

Figure 17. Schematic of Pipelined Unrolled CORDIC using MUXes

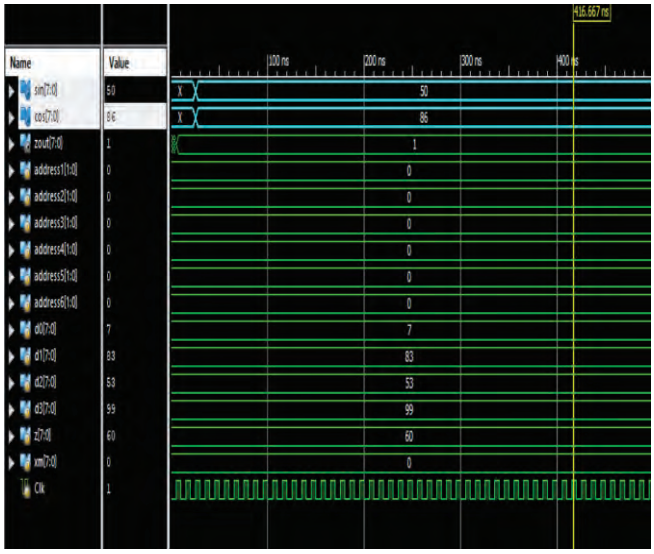


Figure 18. Simulation Result of Pipelined Unrolled CORDIC using MUXes

Figure 17 is the implemented result of pipelined unrolled CORDIC using with MUXes schematic obtained from the tool. In Figure 18 “clk” is the input signal along with x, y, and z is the angle which is 60. “sin” is discrete sine values, “cos” is the discrete cosine values and “zout” is the microrotation angle obtained as output.

The addresses are the stored predefined values of the CORDIC angles.

TABLE III.
COMPARISON OF FOUR SCHEMES BASED ON RESULTS OBTAINED IN VIVADO IMPLEMENTATION

| | SIN 60 | COS 60 | SIN 45 | COS 45 | No.of Slices used (Area) | Power (W) | Off set Timing (nS) |
|---|---|---|---|---|---|---|---|
| Unrolled CORDIC Without Mux | 50 | 87 | 73 | 69 | 580 | 48.6 | 60.21 |
| Unrolled CORDIC With Mux | 50 | 86 | 63 | 67 | 427 | 43.1 | 53.42 |
| Pipelined CORDIC Without Mux | 50 | 87 | 69 | 73 | 594 | 42 | 53.59 |
| Pipelined CORDIC With Mux | 50 | 86 | 63 | 67 | 414 | 38.7 | 53.51 |

CVR Journal of Science and Technology, Volume 19, December 2020
DOI: 10.32377/cvrjst 1910

In this paper proposed algorithm achieves high speed, less hardware implementation, and less power consumption on FPGA. Table III shows a comparison of all four architectures in terms of area and power. The area and power are reduced because the adders, subtractors, and shifters are replaced with the multiplexer up to 3 stages. This lessens the complexity of architecture by which it runs faster and efficiently. Thus, the decrease in area is shown in Table III as the number of slices.

## X. Conclusions

This paper discusses 8-bit CORDIC using the Unrolled and multiplexer-based architectures with and without pipelining for generating the sine and cosine values. A 6-stages CORDIC is implemented with unrolled CORDIC, pipelined CORDIC general, and Multiplexer based architecture up to 3 stages. From the results observations, it is found that the multiplexer-based approach operates on only 11% of the total area when compared with without MUXes which uses 16%. Therefore, 25% of the circuitry can be detached when 3 stages are eliminated. In terms of Power, the pipelined Unrolled CORDIC MUXes based utilizes only 39% of the total power available on FPGA. The pipelined Unrolled CORDIC based on MUXes has a maximum frequency of 88.75MHz which is relatively good as compared with others. As shown in Table III, the pipelined Multiplexer built CORDIC algorithm decreases equally area and power but increases the speed of operation. Swapping the multiplexer in the place of adders, subtractors, and shifters up to 3 stages and replacing the adders and subtractors of all 6-stages with Redundant Arithmetic reduces area utilization and power consumption on FPGA and increase the speed of operation. Henceforth, built on a user-defined application, any one of the 4 methodologies can be selected.

## References

[1] B. Khurshid, G.M.Rather and N.Hakim, “Performance Comparison of Non-redundant and Redundant FPGA based Unfolded CORDIC Architectures, “in International Journal of Electronics and Communication Technology, vol. 3, issue 1 pp 85-89, March 2012.

[2] Volder J. E., “The CORDIC trigonometric computing technique”, IRE Trans. Electronic Computing, Volume EC-8, pp 330 - 334, 1959.

[3] Walther J. S., “A unified algorithm for elementary functions,” in Proceedings of the AFIPS Spring Joint Computer Conference, pp. 379–385, May 1971.

[4] Walther J. S., “The story of Unified CORDIC,” Journal of VLSI Signal Processing, vol. 25, no. 2, pp. 107–112, 2000.

[5] Andraka R, “A survey of CORDIC algorithms for FPGA based computers,” FPGA ’98, ACM/SIGDA International Symposium on Field Programmable Gate Arrays, pp 191-200.

[6] De Lange A. A. J., Van der Hoeven A. J., Deprettere E. F., and Bu J., “Optimal floating-point pipeline CMOS CORDIC processor,” Proceedings of the IEEE International Symposium on Circuits and Systems (ISCAS ’88), vol. 3, pp. 2043–2047, June 1988.

[7] Despain A. M., “Fourier transform computers using CORDIC iterations,” IEEE Transactions on Computers, vol. 23, no. 10, pp. 993–1001, 1974.

[8] Ahmed H. M., Delosme J. M., and Morf M., “Highly concurrent computing structures for matrix arithmetic and signal processing,” Computer, vol. 15, no. 1, pp. 65–82, 1982.

[9] Cavallaro J. R. and Luk F. T., “CORDIC arithmetic for an SVD processor,” Journal of Parallel and Distributed Computing, vol. 5, no. 3, pp. 271–290, 1988.

[10] Lee J. A. and Lang T., “SVD by constant-factor-redundant-CORDIC,” Proceedings of the 10th IEEE Symposium on Computer Arithmetic, pp. 264–271, June 1991.

[11] Meyer A., Watzel R., Meyer U., and Foo S., “A parallel CORDIC architecture dedicated to compute the Gaussian potential function in neural networks,” Engineering Applications of Artificial Intelligence, vol. 16, no. 7-8, pp. 595– 605, 2003.

[12] Kang C. Y. and Swartzlander E. E., “Digit-pipelined direct digital frequency synthesis based on differential CORDIC,” IEEE Transactions on Circuits and Systems I, vol. 53, no. 5, pp. 1035–1044, 2006.

[13] Antelo E., Lang T. and Bruguera J. D., “Very-High Radix CORDIC Rotation Based on Selection by Rounding,” Journal of VLSI Signal Processing, Kluwer Academic Publishers, Netherlands, Vol.25, 141.153, 2000.

[14] Delosme M. J.,Lau C. Y. and Hsiao S. F., “Redundant Constant-Factor Implementation of Multi-Dimensional CORDIC and Its Application to Complex SVD,” Journal of VLSI Signal Processing, Kluwer Academic Publishers, Netherlands, Volume 25, pp 155.166, 2000.

[15] Choi J. H., Kwak J. H. and Swartzlander, Journal of VLSI Signal Processing, Kluwer Academic Publishers, Netherlands, Volume 25, 2000.

[16] Meggitt J. E., “Pseudo division and pseudo multiplication processes” IBM Journal, vol. 6, no. 2, pp. 210–226, 1962.

[17] Deprettere E., Dewilde P., and Udo R., "Pipelined CORDIC Architecture for Fast VLSI Filtering and Array Processing," Proc. ICASSP'84, 1984, pp. 41.A.6.1- 41.A.6.4.

[18] M. Chinnathambi, N. Bharanidharan, and S. Rajaram, "FPGA implementation of fast and area efficient CORDIC algorithm," 2014 International Conference on Communication and Network Technologies, Sivakasi, 2014, pp. 228-232.

[19] P. Nilsson, "Complexity reductions in unrolled CORDIC architectures," 2009 16th IEEE International Conference on Electronics, Circuits, and Systems - (ICECS 2009), YasmineHammamet, 2009, pp. 868-871.

[20] V. Naresh, B. Venkataramani and R. Raja, "An area efficient multiplexer based CORDIC," 2013 International Conference on Computer Communication and Informatics, Coimbatore, 2013,pp.1-5.

E-ISSN 2581 - 7957
P-ISSN 2277 - 3916

CVR Journal of Science and Technology, Volume 19, December 2020
DOI: 10.32377/cvrjst 1911

# Implementation of Optimized FIR Filter using Reversible Logic

E. Janaki Ram[1] and S.Swetha[2]
[1]PG Scholar, CVR College of Engineering/ECE Department, Hyderabad, India
Email: janakiram.emani@gmail.com
[2]Asst. Professor, CVR College of Engineering/ECE Department, Hyderabad, India
Email: swetha.sillveri@gmail.com

***Abstract:*** **The Finite Impulse Response (FIR) filter is extensively used in mobile and wireless applications. Low power and low complexity FIR filters architectures are essential to implement these applications. For signal processing applications, FIR Filter is the most frequently used hardware block. The performance enhancement in the FIR filter is a great challenge. In this paper, two different but effectual methods have been implemented in Xilinx software to improve the performance metrics in terms of speed, area and power.**

**The first FIR filter is implemented using a normal architecture. The second type of FIR filter is based on Pipelined Technique. In this technique, throughput is enhanced by utilizing the retiming effectively. Due to this performance also increases gradually. Implementing the FIR Filter using Reversible Vedic Multiplier with both adders i.e. Reversible Carry Look Ahead Adder and Reversible Carry Select Adder can optimize the performance in terms of Power, Delay and utilization. The proposed architecture is implemented using IP Integrator in Xilinx Vivado by utilizing the ZYNQ Zed Board which can be used for DSP Applications.**

***Index Terms:*** **Carry Look Ahead Adder, Carry Select Adder, FIR Filters, Pipelining, Reversible Logic and Vedic Design**

## I. Introduction

FIR filters typically utilized in various applications like biomedical, communications and control because of their stability and linear phase properties. FIR filters have simple and regular structures in correlation with IIR filters which are easy to implement on hardware.

A digital filter is programmable, i.e. a function stored within the processor's memory determines its operation compared to analog filter. The analog filter features are temperature dependent and focus on drift. These problems are not faced by digital Filters, and they are highly stable both in time and temperature.

A Filter is also used to get the filter output with a chain of delays, multipliers, and adders. FIR Filter functions are based on existing and former values of input.

In CMOS VLSI design, Power optimization is often done at various abstraction levels. In 1973, C. H. Bennett concluded that "no energy would be dissipated from a system as long because the system was ready to return to its initial state from its final state no matter what occurred in between." It made us understand that, a reversible gate can shrink power dissipation.

In Reversible logic, system drives in both forward and backward which causes input from output and vice versa. It can recess the process at any stage and return to any point in computation history. There is individual mapping among the input and output signals due to same number of inputs and outputs

Reduction of heat generation and power loss will be attained by decreasing the garbage outputs and constant inputs which upsurges overall circuit performance by using individual inputs and outputs [1].

## II. Reversible Gates

### A. Introduction

In VLSI parameters like area, speed and power play a vital role as per the emerging technology. By utilizing reversible logic gates having equal number of inputs and outputs can shrink the power consumption and energy leakage which made feedback unessential in the circuit. Due to irreversible gates, the energy carried by the source is altered into heat with every single bit of loss [1].

### B. Cost Metrics of Reversible Logic Gates:

1. **Gate Cost:** It indicates the essential number of gates to analyze the cost of a circuit.
2. **Quantum Cost:** It is the accumulation of elementary quantum gates of the circuit.
3. **Ancilla Input:** Transformation of reversible circuit from an irreversible circuit using essential additional inputs are denoted as Ancilla inputs (AI).
4. **Input:** The number of input or wires (n) including ancillary input will assist to estimate design methodology performance.
5. **Garbage Output:** Reversibility of the circuit can be maintained by placing avoidable outputs of the entire circuit into a single output which could be left unused.

The above factors illustrate a straight connection with the area/size and complexity of the circuit which enhances the power dissipation and physical cost [1].

### C. Types of Reversible Logic Gates:

Various Reversible gates exist at present. Some of the reversible logic gates are shown below that are used in the proposed design:

a. *Feynman gate*: 2X2 Feynman Gate mainly utilized for fan-out purposes. It achieves complementing and XOR operations are shown in fig 1(a). It is also called a CNOT gate. Quantum cost of this gate is 1.

*b.* *Peres gate*: It is a 3*3 reversible gate i.e., it has three inputs and outputs. The depiction of Peres gate is shown in fig 1(b). Quantum cost is 4.

*c.* *Fredkin gate*: It is a 3*3 reversible gate i.e., it has three inputs and three outputs. The depiction of the Fredkin gate is shown in fig 1(c). Quantum cost is 5. Fredkin gate can be designed as Multiplexer.

*d.* *BME gate*: It is a 4*4 reversible gate i.e., it has four inputs and four outputs. The depiction of BME gate is shown in fig 1(d). The quantum cost is 5[2].

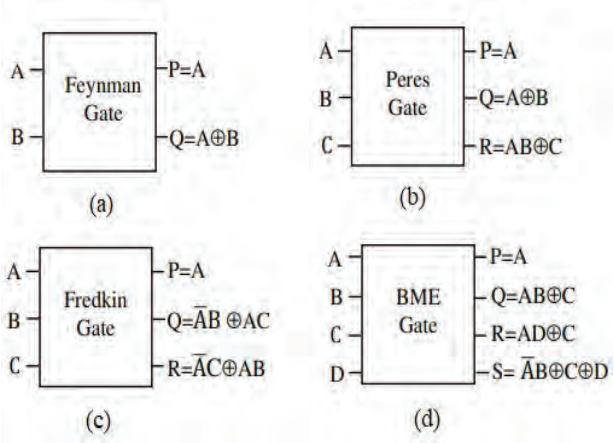


Figure 1. Reversible Gates

## III. FIR Filter

The objective of a FIR filter is to realize the coefficients and filter order that match certain necessities. Computation of discrete convolutions i.e. input signal with a known signal is termed as FIR Convolution.

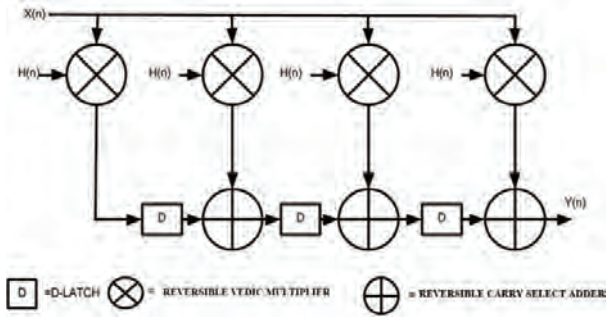


Figure 2 . Reversible FIR Filter

In Direct form FIR filter, length of critical path upsurges with increase in length of filter. The pipelining and parallel processing application will attain growth in input data processing rate or throughput and critical path reduction.

Therefore, it would be more efficient to introduce pipeline filters which improve power and critical path delay along with high throughput than standard filters.

The proposed filter 1 access carry look-ahead adder and proposed filter 2 access carry select adder with carry look-ahead adder for all additions [3].

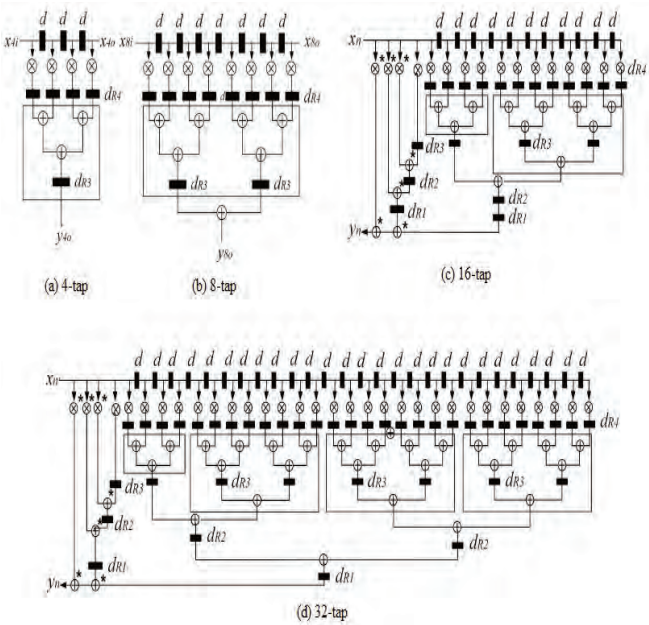


Figure 3. Pipelined FIR Filter

## IV. Vedic Multiplier and Adder

In reversible VM, the BME gate and the Peres gate in Fig.4 are substituted with the AND gates and HA in Fig.3. The first BME gate pass in the number of p0, the multiplication of LSB x0 and y0. The two BME gates each have 2 garbage outputs. The inputs to the PERES gate are one of the outputs of both the BME gate and the sum s1, s2 and s3 are attained[4].

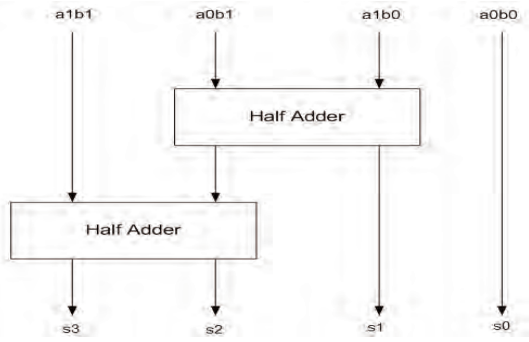


Figure 4. 2-bit Vedic Multiplier

Generating faster partial products can be accomplished using BME gate than the usual Vedic multiplier. In the existing architecture of Vedic multiplier using carry look ahead adder[5], OR gate was added to increase the accuracy and throughput of the output which was specified in below Fig6.

E-ISSN 2581 - 7957
P-ISSN 2277 - 3916

CVR Journal of Science and Technology, Volume 19, December 2020
DOI: 10.32377/cvrjst 1911

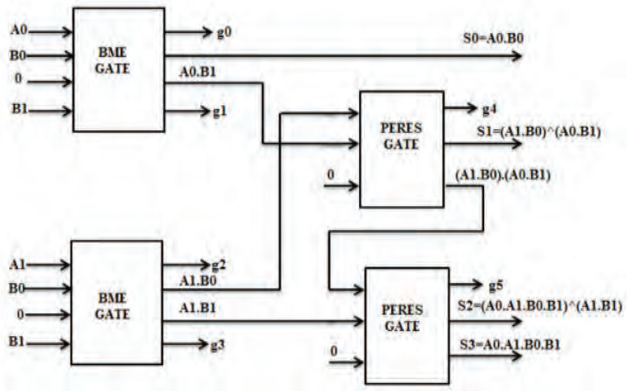


Figure 5 : Reversible Vedic Multiplier

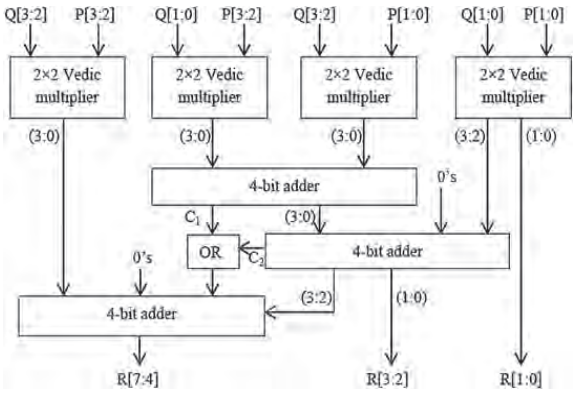


Figure 6. 4-bit Vedic Multiplier

The operation of the above Vedic multiplier is specified as follows. The delay would be reduced by the synchronized partial products measurement. Here, as shown in Fig.5, 4X4 Vedic multipliers can use 2X2Vedic multipliers for generation of partial product. For the partial product addition produced, three adders of 4 bits each are used.

The OR operation achieves the carry output of the first two Adders and its output is set to the next Adder. Where appropriate, zero inputs are pre-arranged for certain adders.

The next adder has two zero inputs along with carry acquired from the former adder. In the above block diagram, the Adders organization is seen, which will diminish the computational time so that the delay can be reduced. Process in Fig.6 for 8-bit VM. It's similar to the VM 4-bit [6].

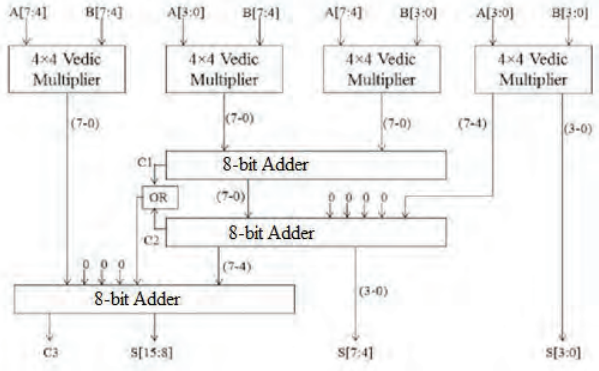


Figure 7. 8-bit Vedic Multiplier

Carry Look-ahead Adder is the fastest adder related to other Adders. It controls the propagation delay, which ascends through addition, by consuming more complex hardware circuitry. The Block diagram of 4-bit Carry Look-ahead Adder is as follows.

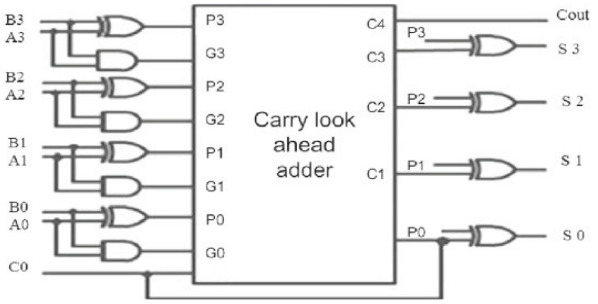


Figure 8. Block Diagram of 4-bit Carry Look-ahead Adder

Carry Look Ahead Adder is aimed for better output as shown in Fig.8 by using reversible gates, i.e., Peres gate for carry propagate, carry generate and sum and Feynman gate for carry. Parameters such as quantum cost, complexity of hardware and power consumption are enhanced compared to traditional and previous current models[7].

The carry look-ahead adder can also be used as a borrow look-ahead subtractor by inserting four Feynman gates at the input terminal [7].

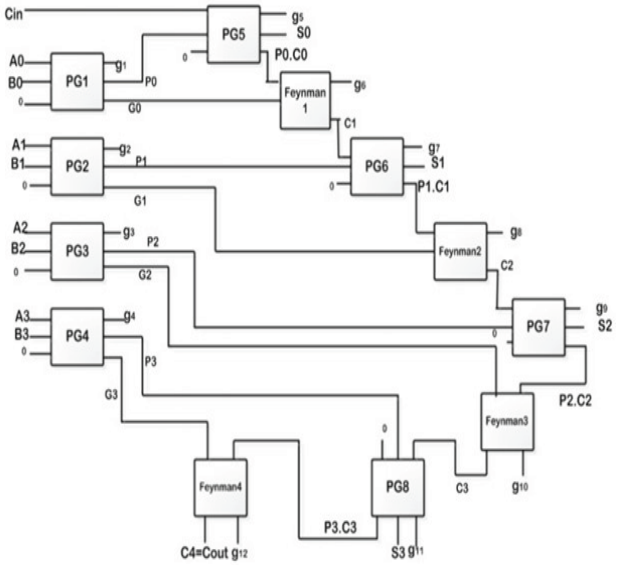


Figure 9. Reversible Carry Look ahead Adder

We need Carry Select Adder, which is speedier than remaining current adders, to succeed arithmetic operations as quickly as possible. Fig.9. reflects the Carry Select Adder block diagram using reversible gates.

Carry select adder was implemented in this paper using Reversible Carry look Ahead Adder, Reversible Multiplexer using Fredkin gate and D-Latch to compensate for parameters of area , delay and power.

The Reversible Carry Select Adder protocol is as follows.

E-ISSN 2581 - 7957
P-ISSN 2277 - 3916

CVR Journal of Science and Technology, Volume 19, December 2020
DOI: 10.32377/cvrjst 1911

In the first step, Adder and D-Latch are simultaneously operated using the enable signal with the values 0 and 1 respectively. In the second stage, a multiplexer is fed as inputs with outputs from the adder and latch and carries output from the previous one as a select line[8].

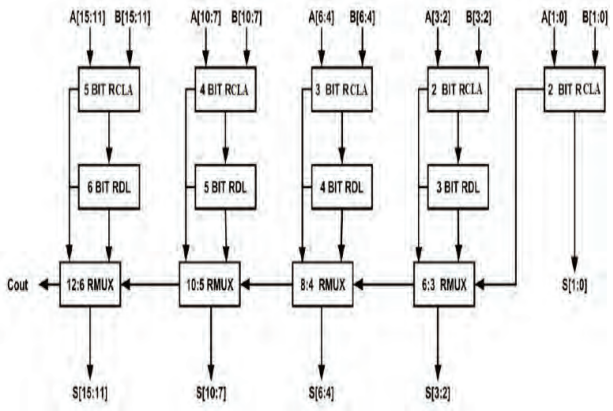


Figure 10. Reversible CSLA using D-latch

## V. Design Analysis

These methods are validated for the target device of the Zynq Zed board FPGA. The techniques are simulated and synthesized in Xilinx Vivado software using IP Integrator.

FIR filter was implemented using Carry look ahead Adder and Carry Select Adder in both architectures i.e., Normal and Pipelined. Compared to normal RTL implementation, IP Integrator can optimize parameters like power, delay and utilization.

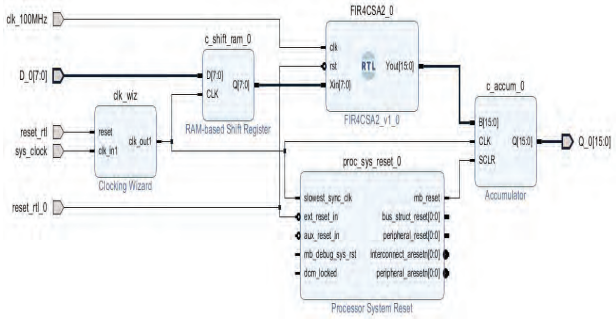


Figure 11. Reversible FIR FILTER using IP Integrator

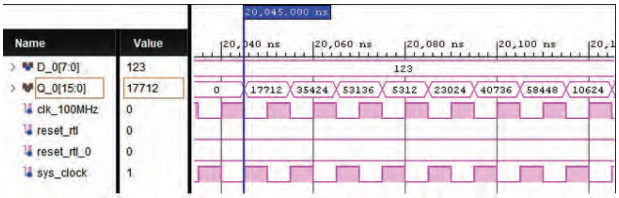


Figure 12. Simulation of 32-tap FIR Filter

The above figure 12 shows Simulation Results of 32-tap FIR Filter using IP BLOCKS and D_0, clock, reset are inputs and Q_0 is output.

## VI. Results and Discussion

Experimental results of FPGA performances of VD-CLA-FIR and VD-CSLA-FIR method are as follows.

TABLE I.
Normal Architectutre of Reversible VD-CLA-FIR Filter

| FIR FILTER N-TAP | POWER (mW) | DELAY (ns) | FREQUENCY (MHz) | UTILIZATION | |
|---|---|---|---|---|---|
| | | | | LUT (53200) | FF (106400) |
| 4 | 243.867 | 2.652 | 141.023 | 39 | 73 |
| 8 | 247.944 | 2.280 | 135.263 | 151 | 76 |
| 16 | 247.884 | 2.375 | 137.3060 | 150 | 88 |
| 32 | 294.52 | 2.415 | 137.3249 | 149 | 88 |

TABLE II.
Pipelined Architectutre of Reversible VD-CLA-FIR Filter

| FIR FILTER N-TAP | POWER (mW) | DELAY (ns) | FREQUENCY (MHz) | UTILIZATION | |
|---|---|---|---|---|---|
| | | | | LUT (53200) | FF (106400) |
| 4 | 243.962 | 2.578 | 141.203 | 54 | 73 |
| 8 | 245.923 | 2.542 | 136.724 | 127 | 74 |
| 16 | 247.384 | 2.653 | 142.5516 | 186 | 97 |
| 32 | 249.918 | 2.48 | 137.3437 | 219 | 105 |

TABLE III.
Normal Architectutre of Reversible VD-CSLA-FIR Filter

| FIR FILTER N-TAP | POWER (mW) | DELAY (ns) | FREQUENCY (MHz) | UTILIZATION | |
|---|---|---|---|---|---|
| | | | | LUT (53200) | FF (106400) |
| 4 | 244.274 | 2.652 | 141.037 | 61 | 73 |
| 8 | 247.584 | 2.458 | 138.1215 | 144 | 76 |
| 16 | 247.384 | 2.325 | 138.6577 | 142 | 88 |
| 32 | 247.333 | 2.415 | 132.2401 | 143 | 87 |

TABLE IV.
Pipelined Architectutre of Reversible VD-CSLA-FIR Filter

| FIR FILTER N-TAP | POWER (mW) | DELAY (ns) | FREQUENCY (MHz) | UTILIZATION | |
|---|---|---|---|---|---|
| | | | | LUT (53200) | FF (106400) |
| 4 | 244.139 | 2.650 | 143.2660 | 60 | 73 |
| 8 | 245.933 | 2.406 | 138.3700 | 131 | 74 |
| 16 | 248.17 | 2.371 | 137.3060 | 189 | 97 |
| 32 | 248.166 | 2.345 | 135.5564 | 193 | 98 |

The results listed in the tables 1-4, depicts the performance metrics. Those are frequency, power, Delay and utilization of the different efficient FIR filter architectures.

In this, the operating frequency of the pipelining FIR Filter is comparatively high and delay along with power consumption of this architecture is more optimized than the normal architecture

Compared to Carry Look Ahead Adder, Carry Select Adder was enhanced the performance of FIR Filter in terms of frequency, delay and utilization.

It is confirmed that pipelined FIR Filters had achieved high throughput along with less utilization than normal FIR Filters. When a number of taps is incremented, the

CVR Journal of Science and Technology, Volume 19, December 2020
DOI: 10.32377/cvrjst 1911

difference can be witnessed between the architectures and adders.

## VII. Conclusions

In this paper, two types of efficient VLSI architectures required for digital signal processing are designed with different implementation techniques.

Several types of full adders i.e., Carry Look Ahead Adder and Carry Select Adder are involved for the implementation of 4-bit and 8-bit Vedic Multiplier and FIR Filter. All these are executed using Reversible Logic Gates which have condensed the power, delay and area along with utilization parameters.

The Normal architecture of FIR filter using both CLA and CSLA are discussed. The results of CSLA in comparison with CLA make it clear that the CSLA Architecture method reduces the power consumption with the additional area and optimized speed.

The second method called pipelined technique has been applied in FIR Filter to enhance the throughput. There is an increase in power consumption, area and delay along with operating frequency respectively, when compared to the normal FIR Filter.

Despite of normal RTL Implementation, IP Integrator had optimized the architecture in terms of parameters like Power, Delay and Area.

## REFERENCES

[1] Ashutosh Kumar Singh, Masahiro Fujita and Anand Mohan, "Design and Testing of Reversible Logic," Springer Singapore, pp. 3-11, 2020.

[2] Md. Belayet Ali, Md. Mosharof Hossin and Md. Eneyat Ullah, “Design of Reversible Sequential Circuit Using Reversible Logic Synthesis”, International Journal of VLSI design and Communication Systems (VLSICS) Vol.2, No.4, December 2011.

[3] Pramod Patali and Shahana Thottathikkulam Kassim, “High throughput FIR filter architectures using retiming and modified CSLA based adders” IET Circuits Devices Syst., 2019, Vol. 13 Iss. 7, pp. 1007-1017.

[4] S.Prema, Ramanan.S.V, R.Arun Sekar and Rajan Cristin “High Performance Reversible Vedic Multiplier Using Cadence 45 nm Technology”, International Journal of Innovative Technology and Exploring Engineering (IJITEE) ISSN: 2278-3075, Volume-8 Issue-7 May, 2019.

[5] M. Sumalatha , P.V. Naganjaneyulu and K. Satya Prasad ," Low power and low area VLSI implementation of vedic design FIR filter for ECG signal de-noising" in Microprocessors and Microsystems, vol. 71, Elsevier 2019.

[6] C. Durgadevi, M. Renugadevi, C. Sathyasree, R.Chitra, “Design of High Speed Vedic Multiplier Using Carry Select Adder”, International Journal Of Engineering Research and Technology (IJERT) NCIECC – 2017, Volume 5 – Issue 09,2017.

[7] Rahmati, M., Houshmand, M. and Houshmand Kaffashian, M. “Novel designs of a carry/borrow look-ahead adder/subtractor using reversible gates”, J Comput Electron 16, 856–866 (2017).

[8] R. Arun Sekar and S. Sasipriya, "Implementation of FIR filter using reversible modified carry select adder," in Recent Research Challenges in Intelligent Techniques, Big Data and Internet of Things (ITBDIOT2018), Wiley Online Library on, vol. 31, Issue 14, 25 July 2019.

E-ISSN 2581 - 7957
P-ISSN 2277 - 3916

CVR Journal of Science and Technology, Volume 19, December 2020
DOI: 10.32377/cvrjst 1912

# Proficient Machine Learning based Scheme for Classifying User Reviews

Dr. M. Deva Priya[1] and T. Akash[2]
[1]Assoc. Professor, Sri Krishna College of Technology/CSE Department, Coimbatore, Tamil Nadu, India
Email: m.devapriya@skct.edu.in
[2]UG Scholar, Sri Krishna College of Technology/CSE Department,Coimbatore, Tamil Nadu, India
Email: akashthiruvenkatam@gmail.com

***Abstract:*** **Each user represents his view on a product or issue using several aspects or features. A user's opinion may be conveyed based on diverse levels of positivity or negativity. In this paper, a proficient technique is propounded for categorizing customer reviews taken from Twitter dataset. The features are extracted using Bag of Words (BoW) algorithm and the information is categorized using modified Support Vector Machine (SVM) and ensemble classification. Further, the results are optimized using BAT algorithm which improves the classification accuracy. It is notable that the scheme proposed offers better accuracy, precision, recall and involves less time.**

***Index Terms:*** **Text mining, Bag of Words (BoW) algorithm, Support Vector Machine (SVM), ensemble classification, Twitter dataset**

## I. Introduction

Users exhibit their views on the social media and other related applications about a particular topic. They either grant their support or non-support [1]. These views and opinions collectively form a huge volume of data with huge dimensions and velocities [2]. The data from social media constituting a huge volume is processed for exposing the views of the users [3]. Many researchers have concentrated on using huge volumes of data to describe, estimate and predict human insights and features of important areas of applications [4]. In the data available over the internet, about 82% are text and hence text analysis plays a dominant role in the process of expounding views, emotions and sentiments of users [5].

Sentiment analysis, well-known as opinion mining is appropriate for measuring the users' sentiments connected to a subject by examining their views and posts on the social media [6]. The polarities of posts are classified into emotions that include positive feedback, negative feedback and similar ones [7]. Sentiment analysis or opinion mining is involved in observing sentiments of people. Internet is a collection of sentiments. People post their views on social media including forums, blogs and other sites. Social media includes reviews about different issues, news and products etc., People update their views through the internet. Sentiment analysis deals with categorization of these reviews based on the opinion as positive or negative.

Sentiment analysis is categorized into lexicon and machine learning analysis.

- ✓ Lexicon analysis emphases on computing the degree of polarity of a particular content based on the words' semantic positioning or the phrases seen in the document. This method does not consider the context of investigation [8].
- ✓ Machine learning based sentiment analysis is based on constructing models collected from the training dataset. These data are labeled for measuring the degree of orientation of the document. This scheme is extensively used in the method of opinion collection for evaluating the satisfying sentiments relating to a topic in the data. This method can be applied to items, themes, folks, events and services in varied domains [9, 10]. This method of analysis yields extremely variable accuracies.

These methods do not seem to be successful due to issues in the semantic positioning of words that varies based on the context. Deep learning based schemes may be used in opinion mining to effectively estimate users, emotions, sentiments, likes and dislikes.

The learnt information is shared among users through tools like chats, forums, comments etc., of social media. The information on such websites is direct and is unstructured and fuzzy. In everyday debates, the users do not focus on spelling, grammar and sentence forms prompting diverse types of ambiguities. Phrase mining focuses on removing phrases from a text corpus which is good in quality and has diverse downstream applications like extraction and retrieval of information, building of taxonomy and modeling topics.

Opinion mining is highly employed in very recent years. Studies which are not optimal for offering better precision rate focus on the precision rate of feature reviews and extraction of opinion words. With the development of textual data available on the Internet, automatic text classification is a reasonable solution for organizing information and managing knowledge. Feature selection is the rudimentary phase in statistical text classification, which is significantly based on the term weighting methods.

The amount of observations in a class of imbalanced data is considerably rarer in another class leading to significant focus in the area of data mining. As multi-class imbalanced learning is hardly specified, it emphases on binary imbalanced cases.

In this paper, a model is propounded to classify user reviews posted on social media. Features are extracted using the Bag of Words (BoW) algorithm. Classification is performed using Support Vector Machine (SVM) algorithm and ensemble classification. The results are optimized using the BAT Algorithm.

E-ISSN 2581 - 7957
P-ISSN 2277 - 3916

DOI: 10.32377/cvrjst 1912

## II. Related Work

This section discusses about the researches of authors done in feature extraction, classification and optimization of mining texts.

### A. Feature Extraction

Supervised Protein-Protein Interaction Extraction (PPIE) deals with richly selected features and kernels yielding high accuracy [11]. Features and kernels focus on the domain knowledge and analysis of natural language. This converts a supervised model into a costly, heavy and fragile one. Additionally, the representation methods like one-hot encoding and vector space model do not keep the semantic likeness between words. The instance representation architecture of PPIE includes word representation, vector configuration and feature choice to reduce manual intervention.

In the study of Salloum et al (2017) [12] textual data from Facebook is analyzed to determine interesting information and represent in diverse ways. The posts are extracted using diverse mining techniques and examined which shows that the Fox news is the mostly used channel with maximum on Facebook, followed by CNN and ABC News respectively.

The methods which exist for phrase mining rely on multifaceted, skilled linguistic analyzers, and so likely have an unacceptable performance on text quantities of novel areas and genres with exclusive adjustment. The state-of-the-art models and even data-driven models are not fully automatic. This is due to the requirement of human experts for scheming rules or classifying phrases. Shang et al (2018) [13] have proposed Auto Phrase which is suitable for all languages until a general knowledge base is available, while benefiting from a POS tagger. In contrast to other methods, this method is efficient and can be extended to model single-word phrases.

### B. Classification

Text classification which is vital in information retrieval is applied to categorize documents into a collection of predefined groups. Numerous practices are available to classify data and many researches have dealt with English text classification. Classification is done using Support Vector Machine (SVM) algorithm, Modified SVM algorithm and Ensemble Classification.

#### i. Support Vector Machine (SVM) algorithm

Machine learning techniques are mostly used for extracting text. SVM is the best supervised learning method used in text classification. Ramesh & Sathiaseelan (2015) [14] have proposed Advanced Multi Class Instance Selection based Support Vector Machine (AMCISSVM) to increase the effectiveness of SVM. The performance of AMCISSVM is analyzed by relating it with Multi-class Instance Selection (MCIS) which shows high accuracy to multi-datasets and Neighbourhood Property based Pattern Selection (NPPS) algorithm.

The healthcare industry gathers enormous amount of healthcare data that is not extracted to find the concealed information for efficient analysis and decision making. Discovery of concealed patterns and relationships frequently goes inactive. Latest data mining schemes can assist and offer solution to deal with these circumstances. Data mining schemes play a dominant role in domains like text, graph, medical, multimedia and web mining. Vijayarani et al (2015) [15] have predicted kidney ailments by using SVM and Artificial Neural Network (ANN). The proposed scheme offers better accuracy and involves less execution time. It is also seen that the performance of ANN is better in contrast to SVM.

Nowadays, news is posted in blogs and social networks and the major role of text mining is to classify the news posted. Dadgar et al (2016) [16] have dealt with classifying news based on their popularity, country and time. The authors have propounded a classification scheme using Term Frequency-Inverse Document Frequency (TF-IDF) and SVM. It involves pre-processing of text, extracting features related to TF-IDF and classification based on SVM. The scheme is analyzed for BBC and diverse news group datasets.

Few works have focused on Arabic text classification. Mohammad et al (2016) [17] have discussed about three famous techniques used to classify data which are applied to Arabic datasets. This study uses fixed quantity of documents for training and testing and shows that SVM yields better performance.

Networking messages, news and reviews of products involve much effort in extracting opinions and sentiments from natural language. Rana & Singh (2016) [18] have dealt with sentiment orientation by taking the positive and negative sentiments from reviews of films. The scheme uses Naive Bayes Classifier (NBC), Linear SVM and synthetic words followed by Synthetic words approach to provide better accuracy.

The studies by Ali et al (2016) [19] are based on NBC, SVM, K-Nearest Neighbours (KNN) and classical ontology which are not suitable for categorizing feature reviews into better levels of polarity. Moreover, the prevailing classical ontology-based systems are not capable of retrieving distorted information from reviews and hence provide pitiable results. They have proposed a classification scheme for identifying features and semantic knowledge based on SVM and Fuzzy Domain Ontology (FDO) for hotel dataset. SVM is used to remove inappropriate reviews (noises) and FDO is used for finding the polarity of features. The mixture of FDO and SVM improves the precision rate.

Power load forecasting shows time and spatial distribution of upcoming power loads. The accuracy directly manipulates the trustworthiness of the power system. Niu & Dai (2017) [20] have propounded Empirical Mode Decomposition-Grey Relational Analysis-Modified Particle Swarm Optimization-Least Squares Support Vector Machine (EMD-GRA-MPSO-LSSVM) load predicting model which uses a de-noising method merging empirical mode decomposition and Grey Relational Analysis (GRA) to deal with the actual load series. It shows the processed results of modified Particle Swarm Optimization (PSO) and Least Square-SVM (LS-SVM).

#### ii. Modified SVM algorithm

In the work done by Jadav & Vaghela (2016) [21], primarily, the dataset is pre-processed to convert unstructured reviews into structured ones. Lexicon based

method is involved to change structured review into a numerical score. The dataset is pre-processed using feature selection and semantic analysis. Stop word removal, stemming, POS tagging and computation of sentiment score using SentiWordNet dictionary are carried out in the pre-processing step. The opinions are classified either as positive or negative. SVM categorizes reviews wherein, RBF kernel SVM is adapted using hyper parameters. Optimized SVM offers better results when compared to SVM and NBC.

Sabbah et al (2017) [22] have proposed improved frequency-based term weighting mechanism namely, Mtf, Mtfidf, TFmIDF, and mTFmIDF. The propounded term weighting schemes consider the quantity of missing terms by operating the weight of existing terms. Moreover, from the results, it is understood that by using SVM and KNN for classification, better results can be obtained when compared to the weighting schemes like TF, TFIDF and Entropy.

Non-informative sequence features and class disparity in the training data are some of the issues faced. To focus on these issues, Abidine et al (2018) [23] have propounded a new scheme based on an amalgamation of Principal Component Analysis (PCA), Linear Discriminant Analysis (LDA) and the modified weighted SVMs. Initially, the dominating features are retrieved using LDA and added to the set. An appropriate sequence feature set joint with the modified WSVM based on criterion classifier offers better development and efficacy over existing methods.

### *iii. Ensemble Classification*

Ensemble method uses diverse models for better performance. Ensemble methods are widely used in areas like statistics, machine learning and computational intelligence. Ren et al (2016) [24] have reviewed conventional and advanced ensemble methods. The ensemble methods are categorized into traditional methods like bagging, boosting and random forest, negative correlation learning methods, decomposition methods, fuzzy methods, multi-objective optimization based schemes, multiple kernel learning schemes and deep learning based schemes. Deviations, developments and typical applications are examined.

Yijing et al (2016) [25] have dealt with imbalanced data using an adaptable algorithm. The imbalanced data differs in its balanced ratio, number of classes and performance of classifiers for diverse datasets. The authors have proposed Adaptive Multiple Classifier System (AMCS) to manage multi-class imbalanced learning that builds a difference between huge amounts of imbalanced data. It includes feature selection, resampling and ensemble learning chosen discriminatively for different types of data. The adapting principle of selecting components from the pool is inspected through empirical analysis. To confirm the efficiency of AMCS, AMCS with several advanced algorithms are compared.

Pan et al (2017) [26] have propounded an ensemble framework that associates spectral and spatial information that are in diverse scales. It is based on the idea that by merging separate learners, ensemble learning can offer improved generalization than an individual learner. Single learners are chosen using joint spectral-spatial features produced from diverse scales. Hierarchical Guidance Filtering (HGF) and matrix of Spectral Angle Distance (Msad) are used to build an ensemble model. These methods are combined using a weighted ensemble strategy. The spatial contextual information is reclaimed in each hierarchy. With increase in the hierarchy, the pixel spectra become smooth, and the spatial features are improved. HGF offers a series of classifiers. Consequently, Msad aids in computing the variety of training samples in every hierarchy.

Ensemble-based methods are extensively utilized for categorization of data streams. They offer better performance when compared to single learners while being significantly simple to organize real-world applications. Ensemble algorithms are used in data stream learning by combining it with drift identification algorithms and including dynamic updates like choosy removal or inclusion of classifiers. Gomes et al (2017) [27] have performed data stream ensemble learning by studying over 60 algorithms. Significant aspects such as grouping, variety and lively updates are methodically presented. Open-source tools and research challenges related to ensemble learning are also included.

Artificial Neural Networks (ANNs) are used to perform a diversity of machine learning functions like image identification, semantic segmentation and machine translation. Few studies have fully examined collections of ANNs. Ju et al (2018) [28] have examined extensively used ensemble methods comprising of unweighted averaging, majority voting, Bayes Optimal Classifier and Super Learner for image identification with Deep Neural Networks (DNNs). Many experiments with these algorithms are performed using diverse model checkpoints in a single training process, networks with similar structure but trained many times and the ones with varied structure. It is seen that the super learner offers better performance.

Sentiment analysis aids in examining opinion and sentiments prevalent in texts. The opinion mining methods are based on sentiment lexicon that includes a collection of predefined keywords. Opinion mining demands appropriate sentiment words to be mined beforehand and faces a challenge in categorizing sentences that entail an opinion without using sentiment keywords. Kang et al (2018) [29] have proposed a sentiment analysis that is based on text-based Hidden Markov models (TextHMMs) for text categorization making use of word sequences in training texts on behalf of predefined sentiment lexicon. It is essential to know text patterns that represent sentiments in ensemble TextHMMs. The hidden variables in TextHMMs are found using semantic cluster information and considering the co-occurrence of words. The sentiment orientation of sentences by fitted TextHMMs is computed, and to replicate diverse patterns, an ensemble of TextHMM-based classifiers is applied.

## *C. Optimization*

Optimization is carried out using BAT algorithm. Heraguemi et al (2016) [30] have proposed a cooperative multi-swarm bat algorithm for Association Rule Mining (ARM) that mimics bat-inspired algorithm reformed to rule learning problem (BAT-ARM). This involves loss of

communication among bats that reduce the examination of search space. It has an efficient rule generation procedure leading to perfect local search. It sustains a good trade-off between diversification and intensification. Cooperative methods are introduced among the swarms that reveal their competence in multi-swarm optimization algorithm. Alomari et al (2017) [31] have propounded a filter method named Minimum Redundancy Maximum Relevancy (MRMR) and a wrapper method, Bat Algorithm (BA) for gene selection in microarray dataset. MRMR is involved in finding the most significant genes in gene expression data, and BA is used to find the most edifying gene subset from the reduced set produced by MRMR. The wrapper method based on SVM method with 10-fold cross-validation serves as an evaluator of the BA. Alomari et al (2017) [32] have designed a Bat-Inspired algorithm for gene selection for classifying cancer using microarray datasets. Microarray data involves irrelevant, repeated and noisy genes. Gene selection problem deals with finding the most relevant genes taken from microarray data to precisely identify cancer. There are two stages in gene selection namely, filter stage that uses MRMR method, and wrapper stage that involves BA and SVM.

## III. Pre-Processing

Pre-processing of data taken from Twitter includes stop word removal, tokenization and normalization.

### *A. Stop Word Removal*

Stop words are the most frequently used words like ‘a, the, an, in. The search engine ignores them while searching and extracting them based on the query. Removing them reduces the processing time. In the natural language, stop words are removed before processing of text. The most common stop words that support text mining include prepositions, articles and pronouns.

### *B. Tokenization*

Tokenization deals with splitting a sequence of strings into tokens which include words, keywords, phrases, symbols etc., Characters like punctuation marks may be discarded and meaningful keywords are identified. In short, it is the process of delineating and categorizing sections of a string. The words in a sentence are explored and consistency is established.

### *C. Normalization*

Normalizing words deals with the process of dropping words to their roots. This depends on the nature of the text taken for analysis. The stems are not challenging if they do not become a part of human interaction.

## IV. Feature Extraction

Features are taken from the token obtained from the previous phase using the Bag of Words (BoW) algorithm.

### *A. Bag Of Words*

The Bag of Words (BoW) algorithm finds its effective use in Information Retrieval (IR) and Natural Language Processing (NLP). The text including sentences is taken as a bag of words, preserving their diversity but excluding their grammar and order of words. It also finds its application in Computer Vision (CV) [33].

It is widely used in classification of documents where the rate of word occurrence is taken as the predominant feature taken for classifier training. It is referred in a linguistic framework designed for distributional structure [34]. BoW is also widely used to generate features. Once the words in the text are added to bags, diverse measures can be taken to describe the text. Out of all the features considered, the commonly seen feature is ‘frequency’ which gives the total number of times a word is found in the document.

Lists are constructed to keep in store the frequencies of all dissimilar words. The order of words as seen in the document is not preserved in the list. This is an important aspect in BoW. This form of demonstration enables it to be applied in email filtering [33]. Nevertheless, frequencies of words that appear in the document do not seem to be the best form of demonstration. Familiar words including ‘the’, ‘a’ and ‘to' are seen to be the ones with greater frequency. This count creates an illusion that the words with high frequency are the most important. To deal with this issue, the frequencies are normalized by assigning weights to words by the inverse of document frequency.

Further, to support classification, supervised substitutes are designed to find the label for the class label. Finally, binary weighting can be used to find the frequencies for problems that are executed in the WEKA software [35]. BoW is used in different types of text mining which includes constructing a classification system involving text that contains tweets, short articles etc., The text is categorized and labelled as positive or negative. A bag containing unigrams and a vector comprising of words seen in the text are built. The text in the training set is considered repeatedly, and ‘1’ is marked in the row vector conforming to the word it holds. The feature size is reduced so as to improve the computation speed and performance of classification by applying different feature selection techniques.

## V. Classification

The customer reviews are classified into positive, negative and neutral reviews using modified SVM algorithm and ensemble classification.

### *A. Modified Support Vector Machine (Svm) Algorithm*

Support Vector Machine (SVM) algorithm is the most appropriate classification algorithm used in text mining. It is a supervised Machine Learning (ML) algorithm that is widely in classification and outlier detection along with problems related to regression.

SVM finds hyperplanes and forms groups based on patterns. The hyperplane with the highest margin is chosen as the best. SVM is also used in classifying text and image, recognizing hand-writing, detecting faces and analyzing bio sequences. SVM is capable of both linear and non-linear data. It maps the training data to higher dimensions and segregates tuples belonging to each class. With non-linear mapping to a high dimension, data is divided using a

E-ISSN 2581 - 7957
P-ISSN 2277 - 3916


DOI: 10.32377/cvrjst 1912

hyperplane found using vectors and margins. SVMs consume more training time but are accurate as they are less subject to overfitting in contrast to other methods.

**Step 1:** Initialize the population size, crossover probability, mutation probability
**Step 2:** Categorize the dataset using SVM and calculate the accuracy rate, that is the fitness function offered by the BAT algorithm
**Step 3:** Frame the fitness function which is the optimization goal
**Step 4:** Set the Population
**Step 6:** Choose the operation and compute the fitness in population and predictive rate for unidentified data
**Step 7:** Execute Crossover
**Step 8:** Implement Mutation
**Step 9:** Compute the fitness value again and move to Step 2

### *B. Ensemble Classification*

Ensemble learning aids in improving the results of Machine Learning (ML) by joining several models. This method yields a better performance in contrast to a single model. A set of classifiers learn and then cast their vote. The predictive accuracy is improved but it is challenging to understand them [36]. It is useful in solving statistical, computational and representational problems. It is not essential to find more precise models, but build models with errors. Ensemble models built to perform classification can misclassify initially.

There are different methods of building ensembles.

- Maximum Vote
- Bagging and Random Forest (RF)
- Chance Injection
- Feature choice Ensembles
- Error Correcting Output Coding (ECOC)

The algorithm is shown below.

**Step 1:** Form the test set ‘T’ using ‘n’ documents in ‘X’
**Step 2:** Form the training set ‘TR’ using the residual documents in ‘X’
**Step 3:** for every classifier in ‘C’
Train the classifier using the categorized documents in ‘T’
Use the trained classifier to categorize the documents in ‘S’
Store the resultant labels in the particular class
**Step 4:** for every ‘o’ in the range 1 to s
for every ‘j’ in the range 1 to s
for every ‘b’ in the range 1 to k
for every ‘i’ in the range b+1 to k
if(class[b,o] == class[i,j])
if(M[o,j]==0)
M[o,j]=1;
else
M[o,j]=M[o,j]*2;
**Step 5:** ‘m’ is fed into the k-means algorithm to form document clusters
**Step 6:** Apply SVM-linear algorithm on ‘T’ for document categorization
**Step 7:** Select the classes conforming to the clusters by finding the class attained in the preceding step

## VI. Optimization

The classification results are optimized using BAT algorithm.

### *A. Bat Algorithm*

BAT, founded by Yang (2010) [37] is a meta-heuristic algorithm used in global optimization. The animals with the capacity to echolocate produce calls to the surrounding and pay attention to the echoes that come from diverse objects adjacent to them. Based on this characteristic, the BAT algorithm was built to mimic the characteristics of micro bats. Varying emission rates and intensity of noise are considered [38].

It is assumed that the bats fly arbitrarily at a velocity with changing wavelength and noise. As bats find their prey, they modify the frequency, volume of noise and Pulse Emission Rate (PER). Local random walk is performed to carry out the search. Just as the bats go in search of the prey, the best solution is selected once the criteria to stop the process are satisfied. Frequency is tuned to regulate the vibrant characteristics of a swarm of bats. Investigation and deployment are monitored by the tuning algorithm.

## VII. Results and Discussion

This section discusses about the implementation done to extract features, classify and optimize them. Reviews are evaluated qualitatively and quantitatively. From the results, it is evident that the propounded system outperforms the existing systems. This novel method is proposed to deal with user reviews. It yields better accuracy and involves less time period in contrast to the existing methods and algorithms. Figure 1 shows the dataset taken as input loaded for experimentation.

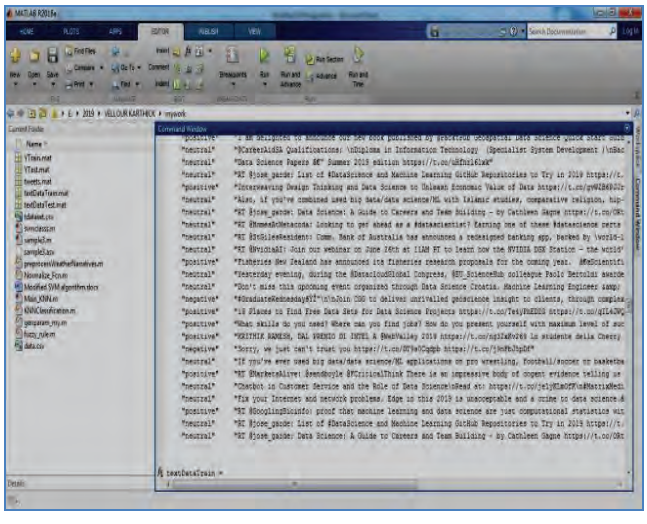

Figure 1. Input Dataset

Figure 2 shows the process of tokenization.

E-ISSN 2581 - 7957
P-ISSN 2277 - 3916

CVR Journal of Science and Technology, Volume 19, December 2020
DOI: 10.32377/cvrjst 1912

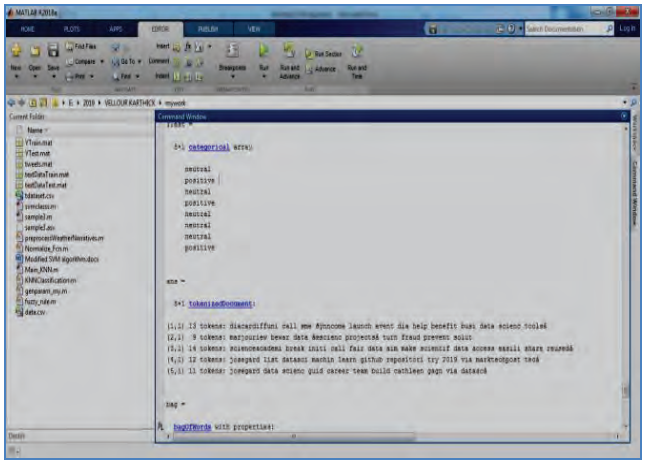

Figure 2. Text Preprocessing Tokenization

Figure 3 shows how Bag of Words (BoW) algorithm is applied for feature extraction.

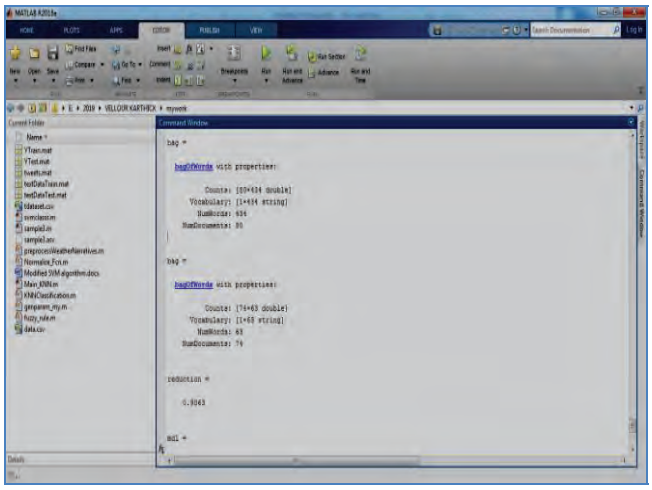

Figure 3. Bag of Words Detection

Figure 4 shows the Confusion matrix.

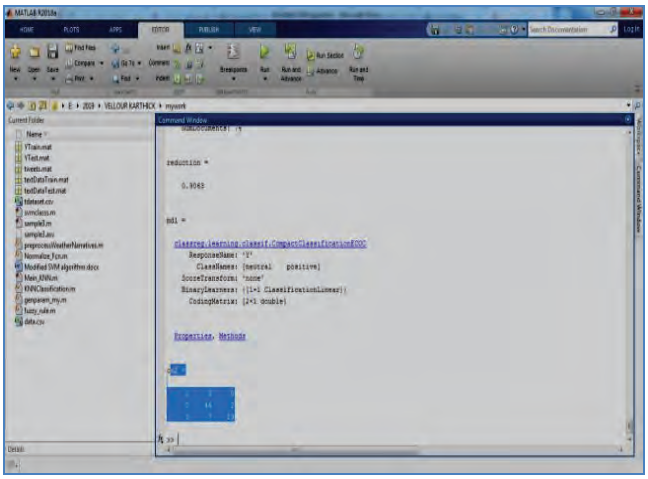

Figure 4. Classification Confusion Matrix

Figure 5 shows the count of positive and negative words.

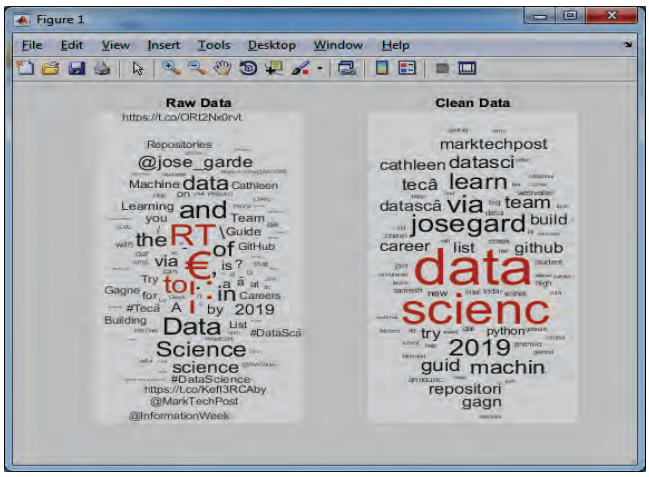


Figure 5. Word Count based on Positive and Negative Words

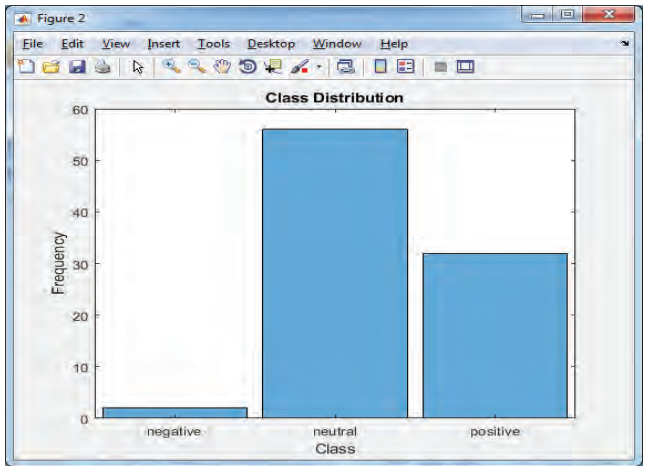


Figure 6. Classification

Figure 6 and Figure 7 show the classification classes and results respectively.

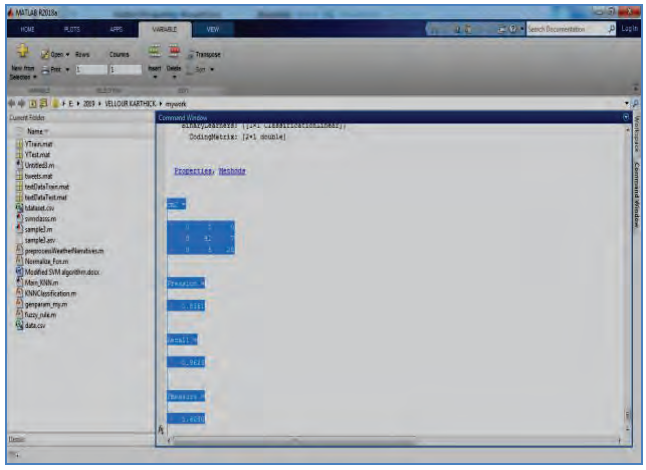

Figure 7. Classification Parameters

Figure 8 to Figure 11 show the accuracy, precision, recall and time period of the proposed method in contrast to the method without BAT optimization.

It is seen that the scheme with feature extraction using Bag of Words (BoW) algorithm and optimization using BAT algorithm yield better results.

DOI: 10.32377/cvrjst 1912

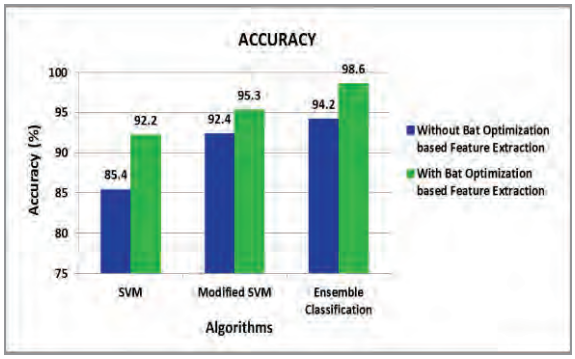


Figure 8. Accuracy

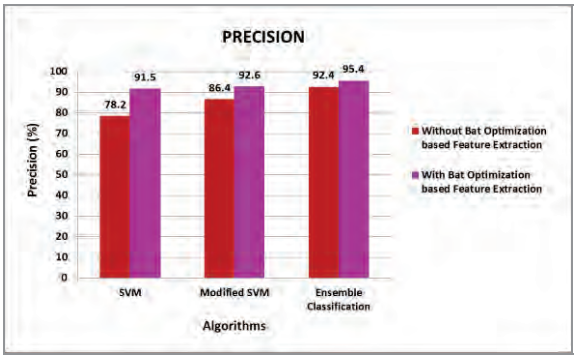


Figure 9. Precision

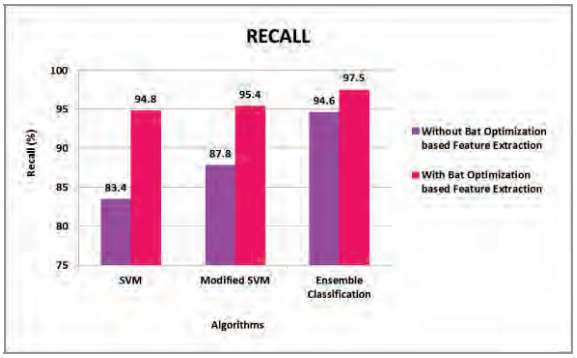


Figure 10. Recall

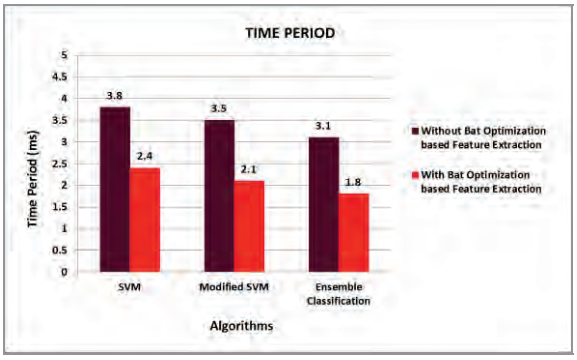


Figure 11. Time Period

## VIII. Conclusions

A novel method is proposed to classify customer reviews taken from Twitter. The Bag of Words (BoW) algorithm is used to extract relevant features. In addition, the data is classified using modified Support Vector Machine (SVM) and ensemble classification. Further, the results are optimized using BAT algorithm which improves the classification accuracy.

## References

[1] Kalra, V., & Agrawal, R. "Challenges of Text Analytics in Opinion Mining", Advances in Data Mining and Database Management, vol .1, no. 2, pp. 268-282, 2019.

[2] Ramteke, J., Shah, S., Godhia, D., & Shaikh, A., "Election result prediction using Twitter sentiment analysis", International Conference on Inventive Computation Technologies (ICICT), vol. 1, no. 1, pp. 45-56, 2016.

[3] Fang, X., & Zhan, J., "Sentiment analysis using product review data", Journal of Big Data, vol. 2, no. 1, pp. 67-78, 2015.

[4] Wang, H., & Castanon, J. A. "Sentiment expression via emoticons on social media", IEEE International Conference on Big Data (Big Data), vol. 1, no. 1, pp. 78-86, 2015.

[5] Ghosh, M., & Sanyal, G., "An ensemble approach to stabilize the features for multi-domain sentiment analysis using supervised machine learning", Journal of Big Data, vol. 5, no. 1, pp. 12-23, 2018.

[6] Singh, P., "Sentiment Analysis Using Tuned Ensemble Machine Learning Approach", Advances in Data and Information Sciences, vol. 1, no. 1, pp. 287-297, 2018.

[7] Shrote, K. R., & Deorankar, A., "Review based service recommendation for big data", 2nd International Conference on Advances in Electrical, Electronics, Information, Communication and Bio-Informatics (AEEICB), vol. 1, no. 2, pp. 34-43, 2016.

[8] Nhlabano, V., & Lutu, P., "Impact of Text Pre-Processing on the Performance of Sentiment Analysis Models for Social Media Data", International Conference on Advances in Big Data, Computing and Data Communication Systems (icABCD), vol. 1, no. 2, pp. 65-74, 2018.

[9] Patil, M., & Darokar, M. S., "A Supervised Joint Topic Modeling Process Using Sentiment Analysis", Journal of Advances and Scholarly Researches in Allied Education, vol. 15, no. 2, pp. 720-725, 2018.

[10] Kaur, G., "Text Mining Based Approach to Customer Sentiment Analysis Using Machine Learning", Journal of Advances and Scholarly Researches in Allied Education, vol. 15, no. 6, pp. 58-65, 2018.

[11] Jiang, Z., Li, L., & Huang, D., "A general protein-protein interaction extraction architecture based on word representation and feature selection", International Journal of Data Mining and Bioinformatics, vol. 14, no. 3, pp. 276-291, 2016.

[12] Salloum, S. A., Al-Emran, M., & Shaalan, K., "Mining social media text: extracting knowledge from Facebook", International Journal of Computing and Digital Systems, vol. 6, no. 02, pp. 73-81, 2017.

[13] Shang, J., Liu, J., Jiang, M., Ren, X., Voss, C. R., & Han, J., "Automated phrase mining from massive text corpora", IEEE Transactions on Knowledge and Data Engineering, vol. 30, no. 10, pp. 1825-1837, 2018.

[14] Ramesh, B., & Sathiaseelan, J. G. R., "An advanced multi class instance selection based support vector machine for text classification", Procedia Computer Science, vol. 57, pp. 1124-1130, 2015.

[15] Vijayarani, S., Dhayanand, S., & Phil, M., "Kidney disease prediction using SVM and ANN algorithms", International Journal of Computing and Business Research (IJCBR), vol. 6, no. 2, 2015.

[16] Dadgar, S. M. H., Araghi, M. S., & Farahani, M. M., "A novel text mining approach based on TF-IDF and Support Vector Machine for news classification", IEEE International

Conference on Engineering and Technology (ICETECH), pp. 112-116, 2016.

[17] Mohammad, A. H., Alwada'n, T., & Al-Momani, O., "Arabic text categorization using support vector machine", Naïve Bayes and neural network, GSTF Journal on Computing (JoC), vol. 5, no. 1, pp. 108, 2016.

[18] Rana, S., & Singh, A., "Comparative analysis of sentiment orientation using SVM and Naive Bayes techniques", 2nd IEEE International Conference on Next Generation Computing Technologies (NGCT), pp. 106-111, 2016.

[19] Ali, F., Kwak, K. S., & Kim, Y. G., "Opinion mining based on fuzzy domain ontology and Support Vector Machine: A proposal to automate online review classification", Applied Soft Computing, vol. 47, pp. 235-250, 2016.

[20] Niu, D., & Dai, S., "A short-term load forecasting model with a modified particle swarm optimization algorithm and least squares support vector machine based on the denoising method of empirical mode decomposition and grey relational analysis", Energies, vol. 10, no. 3, pp. 408, 2017.

[21] Jadav, B. M., & Vaghela, V. B., "Sentiment analysis using support vector machine based on feature selection and semantic analysis", International Journal of Computer Applications, vol. 146, no. 13, 2016.

[22] Sabbah, T., Selamat, A., Selamat, M. H., Al-Anzi, F. S., Viedma, E. H., Krejcar, O., & Fujita, H., "Modified frequency-based term weighting schemes for text classification", Applied Soft Computing, vol. 58, pp. 193-206, 2017.

[23] Abidine, B. M. H., Fergani, L., Fergani, B., & Oussalah, M., "The joint use of sequence features combination and modified weighted SVM for improving daily activity recognition", Pattern Analysis and Applications, vol. 21, no. 1, pp. 119-138, 2018.

[24] Ren, Y., Zhang, L., & Suganthan, P. N., "Ensemble classification and regression-recent developments, applications and future directions", IEEE Computational intelligence magazine, vol. 11, no. 1, pp. 41-53, 2016.

[25] Yijing, L., Haixiang, G., Xiao, L., Yanan, L., & Jinling, L., "Adapted ensemble classification algorithm based on multiple classifier system and feature selection for classifying multi-class imbalanced data", Knowledge-Based Systems, vol. 94, pp. 88-104, 2016.

[26] Pan, B., Shi, Z., & Xu, X., "Hierarchical guidance filtering-based ensemble classification for hyperspectral images", IEEE Transactions on Geoscience and Remote Sensing, vol. 55, no. 7, pp. 4177-4189, 2017.

[27] Gomes, H. M., Barddal, J. P., Enembreck, F., & Bifet, A., "A survey on ensemble learning for data stream classification", ACM Computing Surveys (CSUR), vol. 50, no. 2, pp. 23, 2017.

[28] Ju, C., Bibaut, A., & van der Laan, M., "The relative performance of ensemble methods with deep convolutional neural networks for image classification", Journal of Applied Statistics, vol. 45, no. 15, pp. 2800-2818, 2018.

[29] Kang, M., Ahn, J., & Lee, K., "Opinion mining using ensemble text hidden Markov models for text classification", Expert Systems with Applications, vol. 94, pp. 218-227, 2018.

[30] Heraguemi, K. E., Kamel, N., & Drias, H., "Multi-swarm bat algorithm for association rule mining using multiple cooperative strategies", Applied Intelligence, vol. 45, no. 4, pp. 1021-1033, 2016

[31] Alomari, O. A., Khader, A. T., Al-Betar, M. A., & Abualigah, L. M., "MRMR BA: a hybrid gene selection algorithm for cancer classification", J Theor Appl Inf Technol, vol. 95, no. 12, pp. 2610-2618, 2017.

[32] Alomari, O. A., Khader, A. T., Al-Betar, M. A., & Abualigah, L. M., "Gene selection for cancer classification by combining minimum redundancy maximum relevancy and bat-inspired algorithm", International Journal of Data Mining and Bioinformatics, vol. 19, no. 1, pp. 32-51, 2017.

[33] Sivic, J., & Zisserman, A., "Efficient visual search of videos cast as text retrieval", IEEE transactions on pattern analysis and machine intelligence, vol. 31, no. 4, pp. 591-606, 2008.

[34] Harris, Z. S., "Distributional structure", Word, vol. 10, no. 2-3, pp. 146-162, 1954.

[35] Ko, Y., "A study of term weighting schemes using class information for text classification", 35th International ACM SIGIR conference on Research and Development in Information Retrieval, pp. 1029-1030, 2012.

[36] Dietterich, T. G., "Ensemble learning, The handbook of brain theory and neural networks", MA Arbib, vol. 2, pp. 110-125, 2002.

[37] Yang, X. S., "A new metaheuristic bat-inspired algorithm", In Nature inspired cooperative strategies for optimization, pp. 65-74, Springer, Berlin, Heidelberg, 2010.

[38] Richardson, P., "Bats", Natural History Museum, London, 2008.

E-ISSN 2581 - 7957
P-ISSN 2277 - 3916

CVR Journal of Science and Technology, Volume 19, December 2020
DOI: 10.32377/cvrjst 1913

# Shape Recovery of Stationary and Rotating Object using Spatio-Temporal Images

M.Vasavi[1] and Dr. A. Murugan[2]

[1]Asst. Professor, CVR College of Engineering/CSE Department, Hyderabad, India
Email: m.vasavi@cvr.ac.in

[2]Assoc. Professor, SRM Institute of Science & Technology/ CSE Department, Kattankulanthur, India
Email: murugana@srmist.edu.in

***Abstract:*** **It is propose in this paper a method to find multi dimensional shape of a stationary object in a particular space. A spatio-temporal image is collection of sub-images considered in a given space and time. The projections of multi-dimensional image are taken as intensity values. Analyzing intensity values will discover the position of stationary object and tracking. The analysis report with stationary images shows the effectiveness of this method.**

***Index Terms:*** **Spatio-temporal image, intensity values, stationary object.**

## I. Introduction

Multi dimensional objects are used in designing, archeology and computer graphics. Laser technology is very expensive for multi-object trajectory. Images which are ordinary and related to passive methods will be easier to handle.

The sub-images of a stationary image taken by camera are advisable instead of normal movable images. Each stereo vision gives a one-side projection only. Previous methods on image [1,2] cannot discover real and inverted images. Methods which extract features of an image and locate them in a space [3]. In [1, 2, 3] the surface intensity point features are discovered, if they change in space then it is not discovered.

To find out the intensity value of a sub image in change of space utilizes original feature value or information. Our method first frames the spatio-temporal image and then finds the intensity values of each projection as values. After getting projection values then the shape of the image can be easily translated.

## II. Methodology

Sub images are captured at equal intervals of time values using the camera. Intensity value of each stationary image is known. Then a spatio-temporal image is created with a constant angle representing the space and at a constant time slot. The object will be considered in three cases.

Case 1:-image taken at angle where intensity values are changing with temporal data.

Case 2:-image taken at angle where intensity values are always constant at any temporal data.

Case3:- For image moving or rotating in space will have x-intensity values at various temporal‘t’ values.

If the object is moving, then the captured image will be having any one sub image as cross sectional parallel to the original image values. For our study captured image taken the sub image parallel to the image plane and the image features are compared with the parallel intensity values. The rotation of the object amplitude is the radius of the surface point intensity. The real and inverted image is important to be detected which will be discussed in the next section.

## III. Real and Inverted Image Detection

The rotation axis is taken as the projection area of the image at t=t0, that is the total area of the image represented with sine curve intensity levels taken at t=t0.

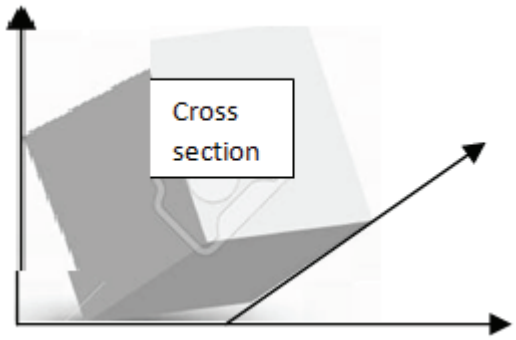


Figure1. Rotating object with captured devices

Image considered with projection points along the line at t=t0 as reference points and identify the intensity values at the cross section that is the reference point. Let the projection point be (t0, angular value) and its intensity values are noted at each angular value (0 to 360). Considering any point of projection in the image and if the selected value passes through the (t0, angular point) it is represented by the following equations.

$$t = v\sin(\theta(t) - \theta) + v$$

or

$$t = v\cos(\theta(t) - \theta) + (t - v)$$

E-ISSN 2581 - 7957
P-ISSN 2277 - 3916

CVR Journal of Science and Technology, Volume 19, December 2020
DOI: 10.32377/cvrjst 1913

Where t is the reference point at angular value θ, as the value of the project matches with the actual intensity values the curve is generated at t-v values and if the project matches only start and end point then a curve is generated at v values.

The intensity values of each projection are almost equal for our example image. So, in evaluation the real projection points and intensity values are passing through the point (t0, angular value[0 to 360]) . The summation of each difference is actually used as visible projection points. The strategy is taken as matching projection to intensity values of image at all angular values each projection point matches corresponding v values from equation of t. The match values are computed as follows.

$$Z = \exp\left( \sum - \frac{(\text{intensity } (t, \theta) - t0)}{2v - (t - \theta)} \right)$$

After calculating the match values at all angular points or projected points (0 to 360) , the radius of rotation of the projection point is taken as {v,[angular point/(each projected point-match point value) ]} represented as below.

$$\text{Angular arc value } (Z) = \arg \min\left[\int_{v0}^{v1} \exp\{-(intensity(t,\theta)\frac{t}{2v} - d\theta)\right.$$

After calculating the match values at all angular points or projected points (0 to 360) , the radius of rotation of the projection point is taken as {v,[angular point/(each projected point-miss match point value) ]} represented as below.

$$\text{Angular arc value } (Z) = \arg \max\left[\int_{v0}^{v1} \exp\{-(intensity(t,\theta)\frac{t}{2v} - d\theta)\right.$$

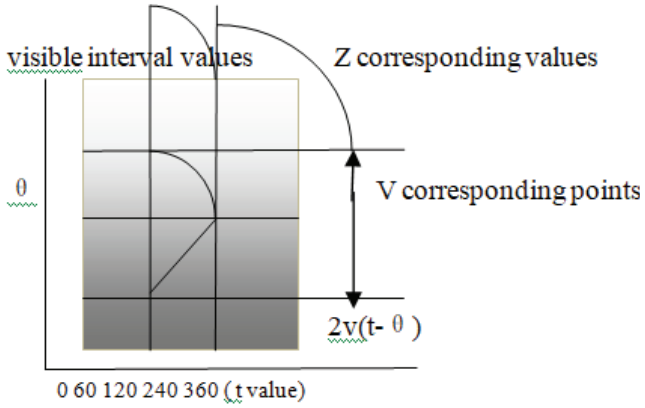


Figure 2. Intensity values Z and v at t values.

As per the integration values of v defined along the projection of each candidate r, θ and v along with the desired interval from the captured device is noted. The visible interval value depends on the local surface values as per t values noted in above figure.

If the surface normal passes along the radius values of projection the symmetric curve is visible otherwise and asymmetric curve as cos with arg max is visible and it is not in range of the angular projections. Since points of images are not know the orientation or surface value as x-axis or y-axis in our study computation have taken projection as the image base is on x-axis. Suppose specifically stating the radius is purely perpendicular to the visible interval values that y-axis, the study is as follows:

Case 1:-image taken at angle where intensity values are changing with temporal data.(y-axis as base value that is t value)

Case 2:-image taken at angle where intensity values are always constant at any temporal data.(y-axis as visible value that is θ values (0 to 360))

Case3:- For image moving or rotating in space will have x-intensity values at various temporal‘t’ values.( only considering the z values computing with match values of rotation)

Matching values of the radius to the angular rotation is given as

M(x)=arg min[max{(Z,v)}]

Where the Z and v values are taken as intersecting values of projection to intensity values in all three cases visualized can have M(x). If the object is real and inverted, a surface point can be seen for an angular period (0 to 360). So the image is shorter than the visible points taken into account to the real image. It should be decided to take a real and inverted image or convex image.

Probability projection point to the noted intersection point taken as follows:

P(z)=v-[∑{p(v)} +(t-intersecting point at angular valueθ)]

If the equation is considered with the three cases taken have according to the visible intensity values resulting with the probability of each projection to image is different.

## IV. Possibilites of Image Capturing

Case 1: image taken at angle where intensity values are changing with temporal data.(y-axis as base value that is t value)

Considering the image as parallel to the y-axis so the angle of incidence will be taken as intensity values changing at each θ values. Here data points also consider the time interval for each image intensity value recording. So, any one either time or intensity value will be taken as the x-axis.

Y-axis is image base value
X-axis is either time or intensity values.

E-ISSN 2581 - 7957
P-ISSN 2277 - 3916

CVR Journal of Science and Technology, Volume 19, December 2020
DOI: 10.32377/cvrjst 1913

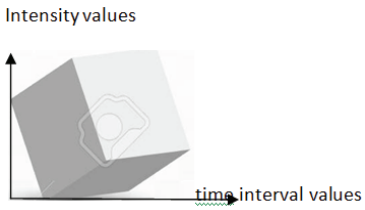


Figure 3. Time and intensity values image

Case 2: Image taken at angle where intensity values are always constant at any temporal data.(y-axis as visible value that is values (0 to 360))

In this considering image at x-axis resting on and the intensity values are at y-axis the temporal values will be taken with corresponding intensity values as pair {(0,t0), (60,t1), (120,t3)…… up to 360 angular values}. The recording values will be depending on pair-wise selection in optimized taken first from pair and then taking x-axis value correspondingly.

y-axis is optimized pair wise intensity values at angular and temporal data.

x-axis is image base values.

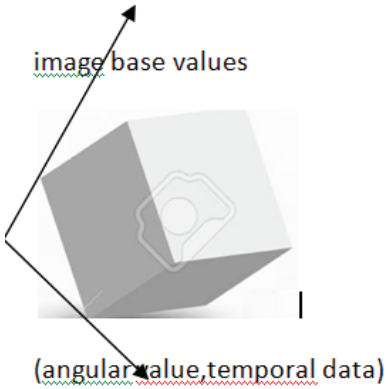


Figure 4. Base and temporal angular values of image

Case3: For image moving or rotating in space will have x-intensity values at various temporal‘t values. (only considering the z values computing with match values of rotation)

In this considering the image is not constant and rotation with radius values at equal intervals of temporal is taken into consideration. X-axis is taken as intensity values at t and y-axis taken as radius value at match intensity of z.

x- axis is intensity values

y-axis is the z values

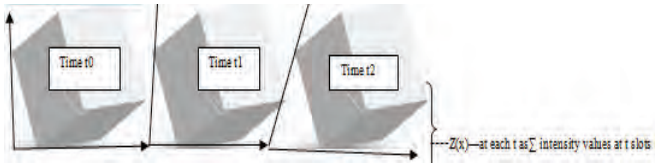


Figure 5. Temporal values with intensity of image

## V. Experimental Results

Experimental results by using original images. Figure is the cube captured by camera. An image of pixel size 480 X 640 pixels and the total number of images taken is 10 per each rotation.

Figure6. Original image

The visible solid image is as taken at angular section ∏/2. The 3-D surface points are solid lines with horizontal sections of the object surface with less intensity level values. Shape of the image is best recovered with real and inverted characteristics of the image, then convex. Some features like edge projections with less intensity values are missing.

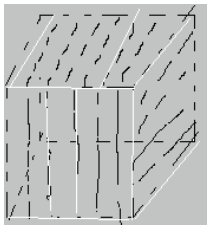

Figure 7. Captured image with Z and v values computing

The white surfaces are noted output for our given image at values z and v. Visualization of output have given black shading to make user to understand the intensity of image to be clear at all visible time values.

## VI. Conclusions

In this paper, presented a method to recover 3-dimenional shape of the object which is constant and also rotating at equal interval of temporal values. To get clear and dense image data points taken match intensity values at each rotation of object at angular values. This is an absolute vision recording with a max and min of size intensity of matching window. If image is matched the matching window will be suitable to spot all white cells in recording. If image is mismatch, then matching window will not be

suitable at any edge of white cells in recording. Stating the image for recovering this has led the ability for revering fine local shapes.

Although the shape is quite featureless as some image measurements are missing, future task might include developing the way to deal with a surface with no intensity change values.

## REFERENCES

[1] j.c.carr,w,r,fright.A.H.Gee,R.W.Prager and k.j Dalton, 3d shape reconstruction using volumn intersection techniques, ICCV, pp.1095-1100,2015.
[2] R.Cipolla and A.Black, the dynamic analysis of apparent contour, 3rd ICCV , pp.616-623 2019.
[3] P.Giblin and R.Weiss: Reconstruction of surface from profile, 1st ICCV, pp, 136-144 2017.
[4] A. Laurentini, How far 3D shapes can be understood from 2Dsihuette,IEEE trans,PAMI,16(2),pp.163-177,2020
[5] Shape recovery of roatating object using weighted voting of spacio-temporal images, Masatoshi Okutomi,shigekisugimoto, graduate school of information science and engineering,0-7695-0750-2020-IEEE.
[6] A portable three-dimensional digitizer, proc. Int. conf. recent advances in 3D imaging and Modeling, pp-197-204,2017,H.P.sawhney, J.Olienis, A.R.Hanson.
[7] R.Szeliski :Rapid octree construction from image sequence, CVGIP: image understanding , 58(1):23-32, july 2020.
[8] R.Szeliski and R.Weiss: robust shape recovery from occluding contours using a linear smoother in image understanding workshop, pp.939-948, april 2018.

E-ISSN 2581 - 7957
P-ISSN 2277 - 3916

CVR Journal of Science and Technology, Volume 19, December 2020
DOI: 10.32377/cvrjst 1914

# Memetic Particle Gravitation Optimization Algorithm-based Optimal Cluster Head Selection in Wireless Sensor Networks (WSNs)

Dr. Sengathir Janakiraman[1] and Dr. Rakesh Kumar Godi[2]
[1]Assoc. Professor, CVR College of Engineering/ IT Department, Hyderabad, India
Email: dr.sengathir@cvr.ac.in
[2]Assoc. Professor, CVR College of Engineering/ IT Department , Hyderabad, India
Email: drrakeshkumargodi@cvr.ac.in

***Abstract:*** **Wireless Sensor Networks (WSNs) consist of millions of sensor nodes that operate cooperatively for attaining the objective of sensing and transmitting information to the base station for necessary decision making processes. In WSNs, the problem of hotspot or energy hole is a major issue that arises when the number of sensor nodes in close proximity of the base station decreases rapidly and results in a network partitioning. This issue of energy holes is feasible in the network only when the difference between the energy consumptions of the sensor nodes are quite large and which has the capability of minimizing the network lifespan. This limitation of WSNs needs to be handled through the potential selection of cluster heads with maximized energy efficiency. In this paper, Memetic Particle Gravitation Optimization Algorithm-based Optimal Cluster Head Selection scheme is proposed for handling the issue of the energy hole in order to sustain energy stability and prolonged network lifetime in WSNs. This MPGOA-OCHS scheme facilitates cluster head head selection by integrating the merits of Centralized Particle swarm Optimization (CPSO) and Gravitational search algorithm (GSA) in order to maintain balance between the rate of intensification and diversification in the cluster head selection process. The simulation results proved that the proposed MPGOA-OCHS scheme is predominant in residual energy by 22.21% and prolonged network lifetime by 16.39%, compared to the baseline schemes.**

***Index Terms:*** **Wireless Sensor Networks, Memetic Particle Optimization Algorithm, Gravitational Optimization Algorithm, Energy Hole.**

## I. Introduction

Wireless Sensor Networks (WSNs) include a number of sensor nodes deployed in a wide area to monitor the surroundings. The Internet of Things (IoT) is the prime and vital technology. Much research is done in each area. Initially, WSNs were used only in the defence, but now they finding their applications in various areas like monitoring of healthcare, environment, tracking objects, traffic control, smart homes and cities, etc., This is made possible due to their reduced size, price and sturdiness to withstand the tough conditions and hostile environments. They include a number of sensor nodes to sense the phenomena in a particular region. The device includes several units viz., sensing, computing and communicating unit. The nodes are arbitrarily deployed to collect and process the accumulated data and convey to the Base Station (BS) in a single hop or multiple hops. The BS connects with the administrator through the internet or General Packet Radio Service (GPRS). As sensor nodes are battery powered, they cannot be changed or revitalized. Hence, ensuring energy efficiency is the demand of the hour and needs to be considered while designing a WSN. Energy in a network directly relates to network lifetime. Many techniques are proposed to enhance the lifespan of a network. Designing efficient routing and clustering mechanisms reduce energy consumption and improves network lifetime. Further, as sensors are arbitrarily deployed, there are chances for them to be closely placed thus transmitting redundant data. This can be avoided by aggregating the data collected from the sensors that are in proximity.

Clustering involves data aggregation and concurrently reduces the amount of energy consumed. Cluster Heads (CHs) may be selected based on the residual energy and nodes may be assigned to the CHs. An energy hole or hot spot may be formed in a WSN, wherein the sensor nodes that are close to the BS die soon creating network partitions. The variance in the amount of energy consumed in WSN deals with the reduction of network lifetime. Unequal clustering supports circumventing early node demises and extends the lifespan of the network by reducing the amount of energy consumed. A diversified number of clustering approaches were propounded in the literature over the decades, but each one of the cluster head selection schemes has their own limitations. In this context, metaheuristic algorithms-based clustering schemes are considered to be highly suitable for clustering processes that prolongs the network lifetime.

In this paper, Memetic Particle Gravitation Optimization Algorithm-based Optimal Cluster Head Selection scheme is proposed for resolving the problem of hot-spot for the purpose of prolonging network lifetime and maintaining energy stability in WSNs. This MPGOA-OCHS scheme included the potentialities of the Centralized Particle swarm Optimization (CPSO) and Gravitational search algorithm (GSA) for sustaining the tradeoff between the rate of intensification and diversification involved in the process of cluster head selection. The simulation experiments of the proposed MPGOA-OCHS scheme is conducted using Matlab R2018a with respect to number of alive nodes, the number of dead nodes, throughput and packet delivery rate under the impact of different densities of sensor nodes and number of rounds.

E-ISSN 2581 - 7957
P-ISSN 2277 - 3916


DOI: 10.32377/cvrjst 1914

## II. Related Work

An improved Breeding Artificial Fish Swarm Algorithm (IBAFSA)-based cluster head selection scheme was proposed by Sengottuvelan and Prasath [9] for sustaining energy and network lifespan. This IBAFSA scheme was proposed for maintaining the balance between diversification and intensification during the process of cluster head selection. The simulation results of IBAFSA confirmed optimal performance in throughput by 19.31% and network lifespan by 17.28%, compared to the classical LEACH and GA algorithms. A Particle Swarm Optimization (PSO)-based clustering scheme was proposed by Rao et al [10] for attaining better network stability. This PSO approach used an objective function that considered the parameters of residual energy, sink distance, intra-cluster distance for energy efficient cluster head selection process. It utilized the merits of a weight function that aids in the formation of the cluster with the cluster member nodes joining their associated cluster head nodes. The result of this PSO-based clustering approach proved best results in alive nodes by 23.81% and throughput by 18.79%, compared to ACO and ABC-based clustering approaches.

A Fuzzy Logic and Harmony Search (FLHS) algorithm-based cluster head selection scheme was proposed by Agrawal and Pandey [15] for lengthening the network lifetime. This FLHS handled the issue of hotspot through the unequal clustering process independent of the network settings considered for implementation. The results of FLHS were confirmed to improve the network lifetime and energy stability with different sensor nodes by 19.32% and 21.78%, respectively.

## III. Proposed Memetic Particle Gravitation Optimization Algorithm-Based Optimal Cluster Head Selection (MPGOA-OCHS)

The proposed Memetic Particle Gravitation Optimization Algorithm-based Optimal Cluster Head Selection (MPGOA-OCHS) was proposed by integrating the benefits of Particle Swarm Optimization (PSO) and Gravitational search algorithm (GSA). This proposed MPGOA-OCHS scheme mutually handles the limitations of CPSO and GSA for maintaining the tradeoff between the diversification and intensification during the cluster head selection process. This cluster head selection approach enhances the capabilities of individual search with rapid convergence rate. The two core strategies utilized in MPGOA targets on diversity enhancement and hybrid operation for preventing impotent sensor nodes from being selected as cluster heads. GSA included the operator of improvement as similar to the differential evolution crossover operator, while CPSO aims in individual exchange of solutions between the sub-populations for attaining maximized diversity and intensification, respectively. The method of the roulette wheel is utilized for accomplishing solution exchanges between CPAO and GSA.

In this section, the detailed view of CPSO and GSA are presented in order to depict the process of integrating them in the cluster head selection process.

### *A. Centralized Particle Swarm Optimization*

Particle Swarm Optimization (PSO) algorithm is a stochastic-based swarm intelligent algorithm proposed through the inspiration derived from the flocking characteristics of birds. In the PSO algorithm, the randomly initialized potential solutions are determined based on the positions and velocities of 'K' particles represented in the space of 'D' dimensions. The positions and velocities of 'K' particles are presented in '$d_S$' dimensions in order to facilitate potential solutions that are initialized randomly. The particle solution 'i' in iteration 't' is presented in Equation (1)

$$S_{(i)}^{(t)} = \left\{S_{(i,1)}^{(t)}, S_{(i,2)}^{(t)}, \ldots\ldots S_{(i,D_{SP})}^{(t)}\right\} \quad (1)$$

with i=1,2,3,….n

Then, the global and local point of optimality is utilized for updating the current solution of each and every particle is calculated based on Equation (2) and (3)

$$V_{(i,j)}^{(t+1)} = I_w . V_{(i,j)}^{(t)} + C_p . r_{nd(1)} \left(P_{(i,j)}^{(t)} - S_{(i,j)}^{(t)}\right) + S_p\, r_{nd(2)} \left(P_{(Gl-Best)}^{(t)} - S_{(i,j)}^{(t)}\right) \quad (2)$$

$$S_{(i,j)}^{(t+1)} = S_{(i,j)}^{(t)} + V_{(i,j)}^{(t+1)} \quad (3)$$

Where '$S_{(i)}^{(t)}$' and '$V_{(i,j)}^{(t)}$' represents the position and velocity of each 'i' particle (search agent) explored in 'd' dimension. '$I_w$' is the inertial weight that impacts the speed of convergence with '$P_{Gl-Best}^{(t)}$' and '$P_{(i,j)}^{(t)}$' depicting the global and local optimum point pertaining to the best and current best position of the search agent among all the search agents at time 't'. In addition, the constants '$S_p$' and '$C_p$' represent the social and cognitive parameters. In this case, the social and cognitive parameters are initialized to 0.5, respectively. The random variables '$r_{nd(1)}$' and '$r_{nd(2)}$' is considered to range between the value of 0 and 1, respectively.

Furthermore, the primitive PSO is improved into a centralized PSO approach by adding an individual solution ($S_{(Center,j)}^{(t+1)}$) with maximized centrality into the original population presented in Equation (4).

$$S_{(Center,j)}^{(t+1)} = \frac{\sum_{i=1}^{n-1} S_{(i,j)}^{(t)}}{n-1} \quad (4)$$

### *B. Gravitational Search Algorithm (GSA)*

Gravitational search algorithm (GSA) is a population-based meta-heuristic approach developed based on the inspiration developed from mass interactions and laws of gravity. The search agent in the GSA systems is the mass aggregates that are utilized attaining mutual cooperation based on laws of motion and Newtonian gravity. The search agents used for identifying the cluster heads are randomly generated by GSA with the solution consisting of position and velocity possessed by them. In the process of cluster

E-ISSN 2581 - 7957
P-ISSN 2277 - 3916


DOI: 10.32377/cvrjst 1914

head selection, GSA calculates the fitness values and updates the position and velocity of every search agent based on the existing population present in the search space. In this scenario, the search agent (representing the significant solution for the complete set of 'n' agents) position in an iteration 't' is defined based on Equation (5).

$$S_{(i)}^{(t)} = \left\{S_{(i,1)}^{(t)}, S_{(i,2)}^{(t)}, \ldots\ldots S_{(i,D_{SP})}^{(t)}\right\} \quad (5)$$

with i=1,2,3,….n

The aforementioned equation depicts the position of the search agent determined through the dimensions with as the maximum dimensions used

The coefficient of gravitation in an iteration is calculated based on Equation (6).

$$G_{Coeff}^{(t)} = G_{Coeff\,(0)}^{(t)} + \exp\left(-\propto \frac{t}{t_{max}}\right) \quad (6)$$

Where '$\propto$' is the constant of shrinking.

Then, the individual masses (possible solutions) and the overall mean mass (average mean solutions) are computed using the worst agent ($Worst_{Fit\,(t)}$) and best agent ($Best_{Fit\,(t)}$) based on Equation (7) and (8), respectively.

$$a_{(t)}^{(i)} = \frac{Fit_{(t)}^{(i)} - Worst_{Fit(t)}}{Best_{Fit(t)} - Worst_{Fit(t)}} \quad (7)$$

$$OA_{Mean\,(t)}^{(i)} = \frac{m_{(t)}^{(i)}}{\sum_{i=1}^{n} m_{(t)}^{(i)}} \quad (8)$$

Further, the complete force imposed on each agent, by all the other agents is randomly weighted and its influence is determined based on Equation (9).

$$T_{Force\,(i,j)}^{(t)} = \sum r_{nd(j)} * \frac{\left(OA_{Mean(i)-ip}^{(t)} * OA_{Mean(i)-op}^{(t)}\right)}{ED_{(i,r)}^{(t)} + \xi_{DE}} \left(S_{(Center,j)}^{(t)} - S_{(i,j)}^{(t)}\right) \quad (9)$$

Where, '$ED_{(i,j)}^{(t)}$' represents the Euclidean distance between an agent 'i' and the other agents 'op' influencing its selection with '$\xi_{DE}$' as the constant used for preventing division by zero exception.

Finally, the acceleration towards which the cluster head selection is attained at iteration 't' is computed based on Equations (10) and (11).

$$ACC_{(i,j)}^{(t)} = \frac{T_{Force\,(i,j)}^{(t)}}{OA_{Mean(t)}^{(i)}} \quad (10)$$

$$T_{Force(i,j)}^{(t)} = \sum_{K-Best(sa)} r_{nd\,(j)} * \frac{\left(OA_{Mean(i)-ip}^{(t)} * OA_{Mean(i)-op}^{(t)}\right)}{ED_{(i,r)}^{(t)} + \xi_{DE}} \quad (11)$$

In this scenario, the agent 'K-Best(sa)' is the agent which possesses the greatest mass (solutions containing sensor nodes with maximized energy and has the possibility of being selected as cluster head) is presented in Equation (12).

$$K - Best(sa) = \left(\beta + \left(1 - \frac{t}{t_{max}}\right)(1 - \beta n)\right) \quad (12)$$

In the subsequent iteration, the agents' solution space gets updated based on Equation (13) and (14).

$$V_{(i,j)}^{(t)} = r_{nd\,(i)} * V_{(i,j)}^{(t)} + ACC_{(i,j)}^{(t)} \quad (13)$$

$$S_{(i,j)}^{(t+1)} = S_{(i,j)}^{(t)} + V_{(i,j)}^{(t)} \quad (14)$$

### *C. Integration Of CPSO And GSA For Cluster Head Selection*

Finally, the integration of CPSO and GSA is achieved by initializing the solution of each individual system randomly. Then, CPSO is utilized for estimating the center agent and particle of the center. Further, GSA and CPSO are run simultaneously for attaining global optimality for enhancing the potentialities of exploration and exploitation for determining better solutions. Further, the diversity is improved through the use of crossover attributed by Differential Evolution algorithm. In addition, roulette wheel selection is included for selecting the individuals from the GSA and CPSO for better cluster head selection process.

## IV. Simulation Results and Discussion

The simulation experiments of the proposed MPGOA-OCHS scheme and the baseline FLHS-OCHS, HEOA-OCHS and BAFSA schemes are conducted using Matlab R18a. These simulation experiments are conducted for evaluating the potential of the proposed MPGOA-OCHS scheme based on percentage improvement in throughput, percentage sustenance in energy stability, the percentage improvement in network lifetime and percentage improvement in resisting energy holes with different number of sensor nodes.

Figure 1 and 2 presents the percentage improvement in throughput and energy stability with the number of sensor nodes changed in the environment. The percentage improvement in throughput and energy stability facilitated by the proposed MPGOA-OCHS scheme is confirmed to be improved with a systematic increase in sensor nodes, since the dynamic searching ability of CPSO aided in sustaining the tradeoff between intensification and diversification process. The percentage improvement in throughput enabled by the proposed MPGOA-OCHS scheme is improved by 8.42%, 10.54% and 12.96%, compared to the benchmarked FLHS-OCHS, HEOA-OCHS and BAFSA schemes. The percentage improvement in energy stability enabled by the proposed MPGOA-OCHS scheme is improved by 7.12%, 9.64% and 11.88%, compared to the benchmarked FLHS-OCHS, HEOA-OCHS and BAFSA schemes.

E-ISSN 2581 - 7957
P-ISSN 2277 - 3916

CVR Journal of Science and Technology, Volume 19, December 2020
DOI: 10.32377/cvrjst 1914

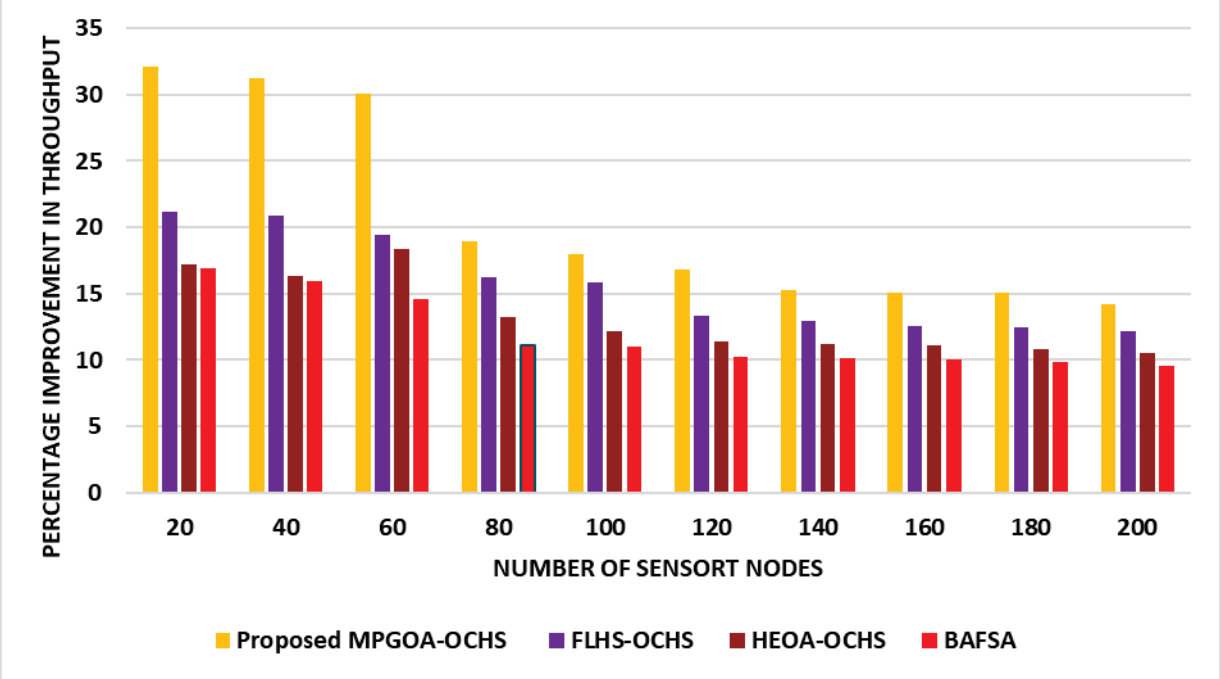


Figure 1. Proposed MPGOA-OCHS-Percentage improvement in throughput with different sensor nodes

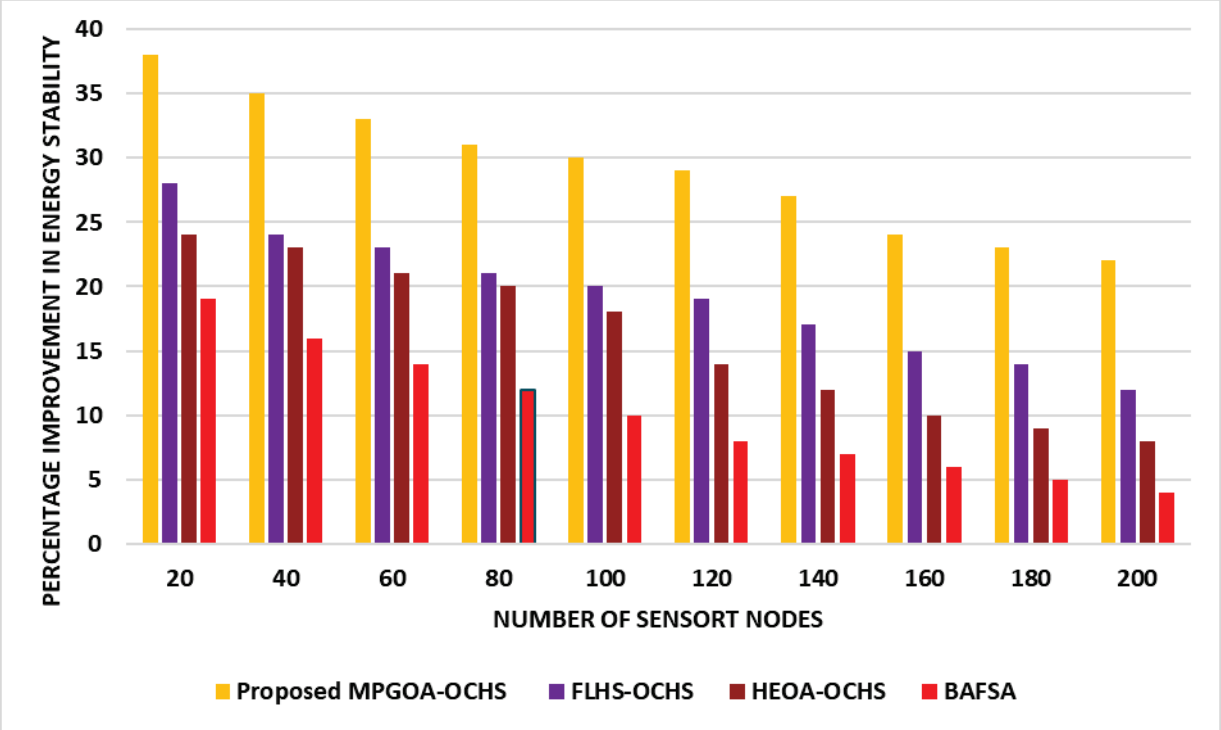


Figure 2. Proposed MPGOA-OCHS-Percentage improvement in energy stability with different sensor nodes

E-ISSN 2581 - 7957
P-ISSN 2277 - 3916

CVR Journal of Science and Technology, Volume 19, December 2020
DOI: 10.32377/cvrjst 1914

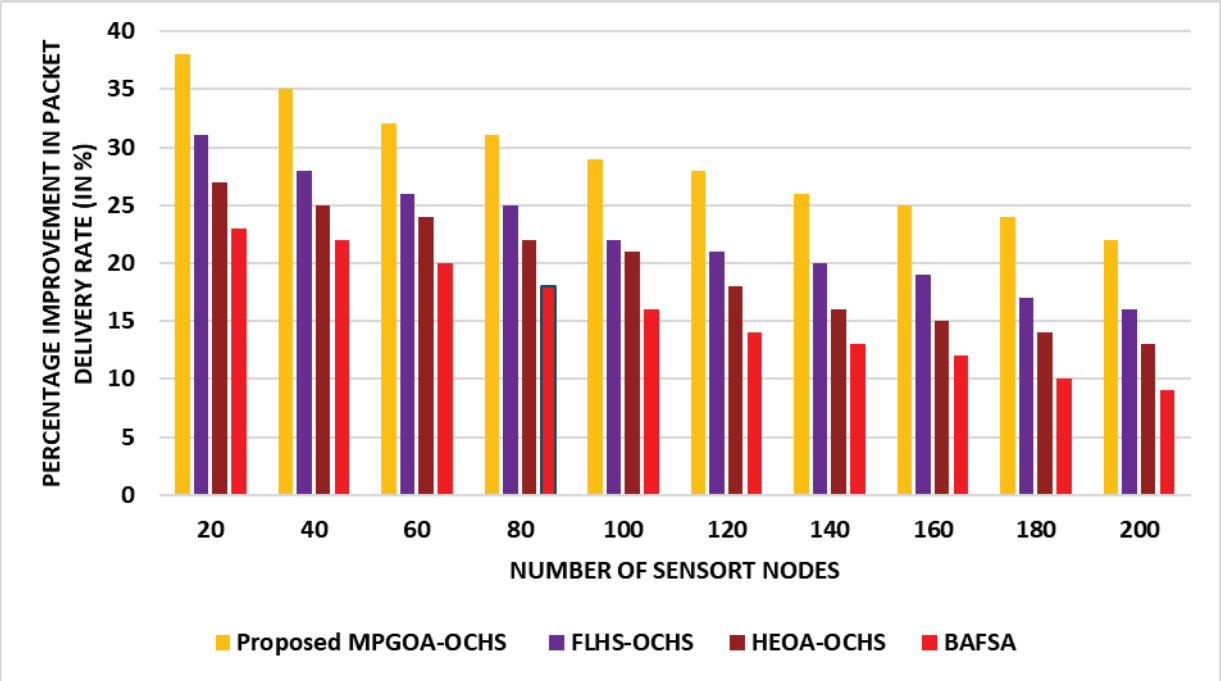


Figure 3. Proposed MPGOA-OCHS-Percentage improvement in packet delivery rate with different sensor nodes

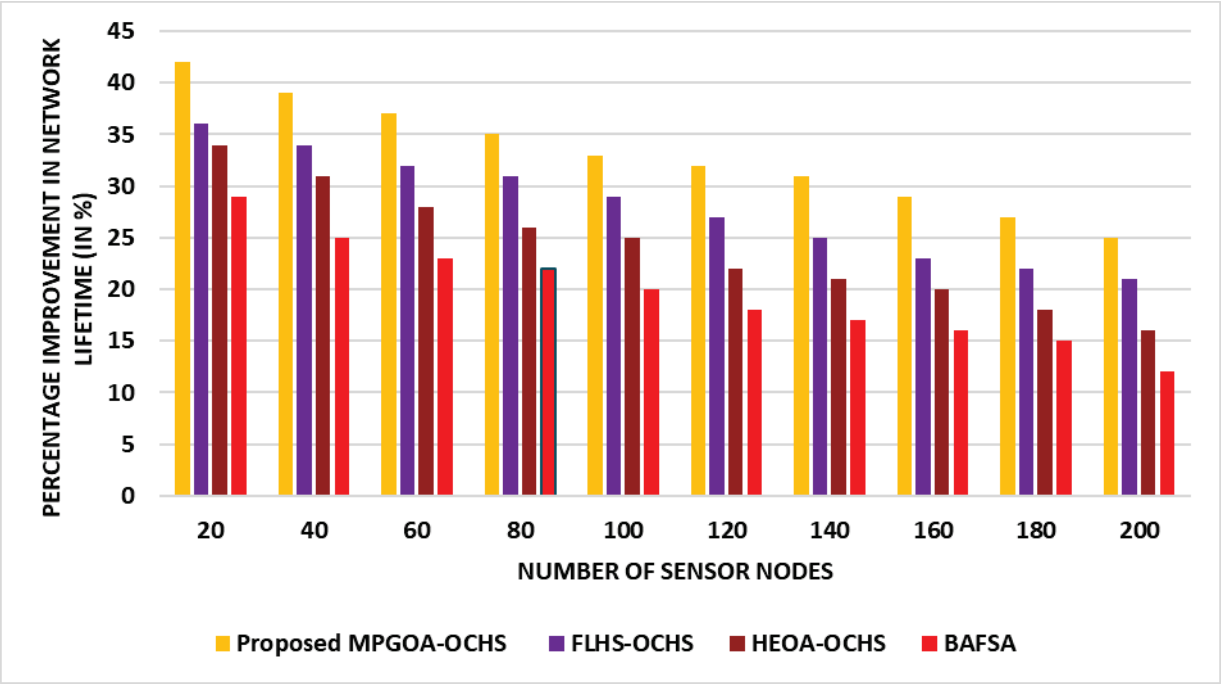


Figure 4. Proposed MPGOA-OCHS-Percentage improvement in network lifetime with different sensor nodes

Figure 3 and 4 demonstrates the percentage improvement in packet delivery rate and network lifetime with the number of sensor nodes increased in the environment. The percentage improvement in packet delivery rate and network lifetime attained by the proposed MPGOA-OCHS scheme is determined to be minimized with a corresponding increase in the sensor nodes. This predominant performance of the proposed MPGOA-OCHS scheme visualized in terms of packet delivery rate and network lifetime is mainly due to the sustenance attributed between the rate of intensification and diversification during the clustering process. The percentage improvement in packet delivery rate facilitated by the proposed MPGOA-OCHS scheme with varying sensor nodes is improved by 8.21%, 10.82% and 12.34%, compared to the benchmarked FLHS-OCHS, HEOA-OCHS and BAFSA schemes. The percentage improvement in lifetime attained by the proposed MPGOA-OCHS scheme is improved by 9.36%, 10.94% and 12.18%, compared to the benchmarked FLHS-OCHS, HEOA-OCHS and BAFSA schemes.

E-ISSN 2581 - 7957
P-ISSN 2277 - 3916

CVR Journal of Science and Technology, Volume 19, December 2020
DOI: 10.32377/cvrjst 1914

Further, the proposed MPGOA-OCHS scheme and the benchmarked approaches are explored based on the number of alive and dead sensor nodes visualized with the number of increasing rounds. The number of alive nodes maintained by the proposed MPGOA-OCHS scheme with increasing rounds is identified to be enhanced due to its capability of preventing worst fitness sensor nodes from being selected as cluster heads. The number of sensor nodes is also considerably minimized as the frequency of cluster head selection is completely minimized to the maximum level.

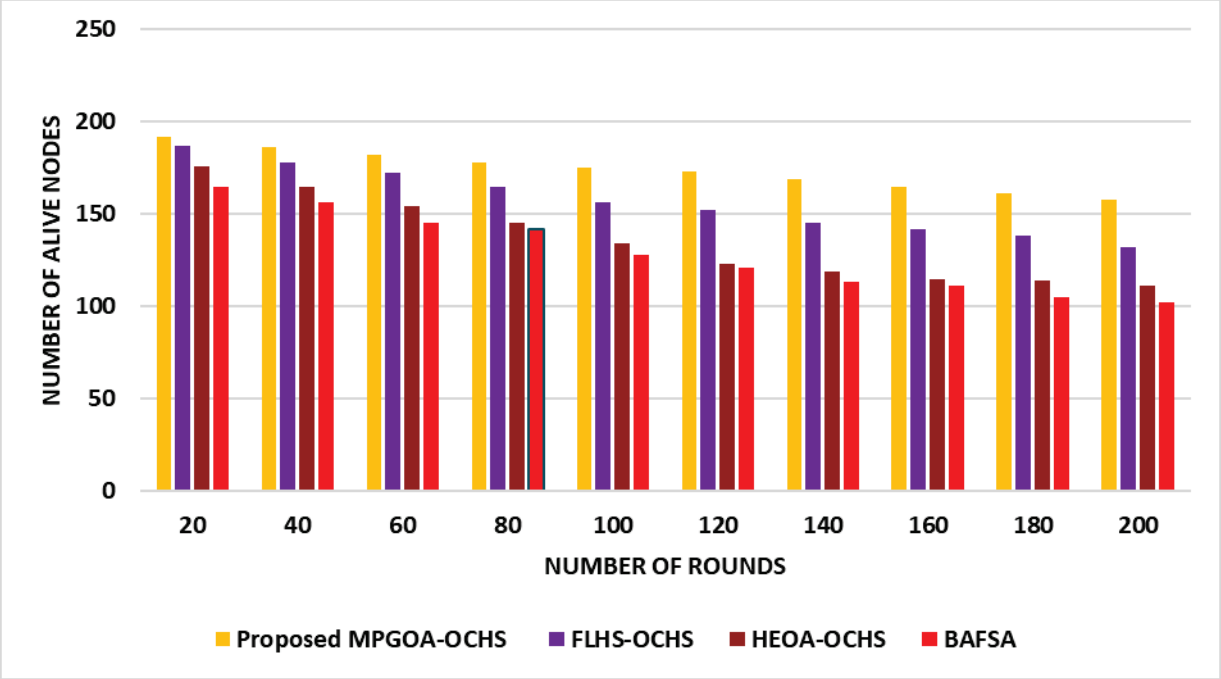


Figure 5. Proposed MPGOA-OCHS-number of alive nodes with different sensor nodes

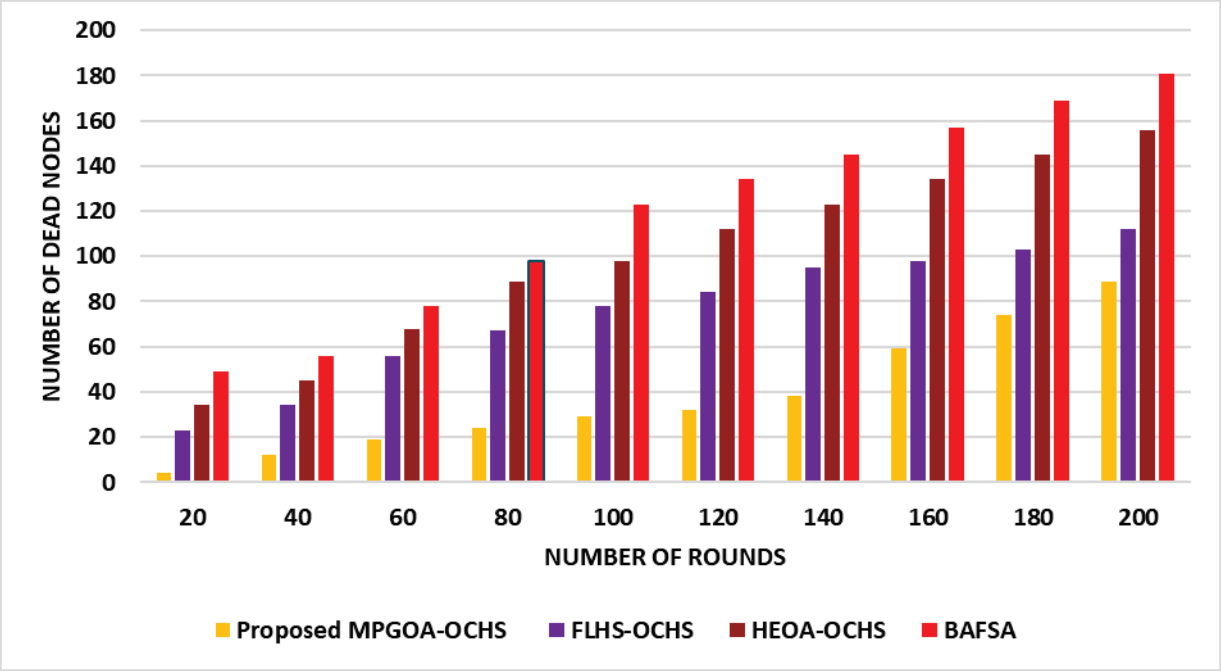


Figure 6. Proposed MPGOA-OCHS-number of dead nodes with different sensor nodes

The number of alive nodes sustained by the proposed MPGOA-OCHS scheme is improved by 9.31%, 11.54% and 13.47%, compared to the benchmarked FLHS-OCHS, HEOA-OCHS and BAFSA schemes. The number of dead nodes prevented from death by the proposed MPGOA-OCHS scheme is improved by 9.32%, 10.41% and 12.74%, compared to the benchmarked FLHS-OCHS, HEOA-OCHS and BAFSA schemes.

## V. Conclusions

In this paper, MPGOA-OCHS scheme was proposed for sustaining energy stability and prolonging network lifetime by addressing the issue of energy holes in WSNs. This proposed MPGOA-OCHS scheme attains maximized diversity through the use of crossover attributed by Differential Evolution algorithm. In addition, roulette wheel selection is included for selecting the individuals from the GSA and CPSO for better cluster head selection process. The percentage improvement in throughput enabled by the proposed MPGOA-OCHS scheme is improved by 8.42%, 10.54% and 12.96%, compared to the benchmarked FLHS-OCHS, HEOA-OCHS and BAFSA schemes. The percentage improvement in energy stability enabled by the proposed MPGOA-OCHS scheme is improved by 7.12%, 9.64% and 11.88%, compared to the benchmarked FLHS-OCHS, HEOA-OCHS and BAFSA schemes.

## References

[1] T. M. Behera, S. K. Mohapatra, U. C. Samal, M. S. Khan, M. Daneshmand and A. H. Gandomi, "Residual Energy-Based Cluster-Head Selection in WSNs for IoT Application," in IEEE Internet of Things Journal, vol. 6, no. 3, pp. 5132-5139, June 2019.

[2] N. Shivappa and S. S. Manvi, "Fuzzy-based cluster head selection and cluster formation in wireless sensor networks," in IET Networks, vol. 8, no. 6, pp. 390-397, 11 2019.

[3] R. K. Poluru and L. K. Ramasamy, "Optimal cluster head selection using modified rider assisted clustering for IoT," in IET Communications, vol. 14, no. 13, pp. 2189-2201, 11 8 2020.

[4] S. Lata, S. Mehfuz, S. Urooj and F. Alrowais, "Fuzzy Clustering Algorithm for Enhancing Reliability and Network Lifetime of Wireless Sensor Networks," in IEEE Access, vol. 8, pp. 66013-66024, 2020.

[5] K. A. Darabkh, J. N. Zomot and Z. Al-qudah, "EDB-CHS-BOF: energy and distance-based cluster head selection with balanced objective function protocol," in IET Communications, vol. 13, no. 19, pp. 3168-3180, 3 12 2019.

[6] N. Hemavathi, M. Meenalochani and S. Sudha, "Influence of Received Signal Strength on Prediction of Cluster Head and Number of Rounds," in IEEE Transactions on Instrumentation and Measurement, vol. 69, no. 6, pp. 3739-3749, June 2020.

[7] S. Murugaanandam and V. Ganapathy, "Reliability-Based Cluster Head Selection Methodology Using Fuzzy Logic for Performance Improvement in WSNs," in IEEE Access, vol. 7, pp. 87357-87368, 2019.

[8] Shankar, T., Shanmugavel, S., & Rajesh, A. (2016). Hybrid HSA and PSO algorithm for energy efficient cluster head selection in wireless sensor networks. Swarm and Evolutionary Computation, 30(3), 1-10.

[9] Sengottuvelan, P., & Prasath,N. 2016). BAFSA: Breeding artificial fish swarm algorithm for optimal cluster head selection in wireless sensor networks. Wireless Personal Communications, 94(4), 1979-1991.

[10] Rao, P. C., Jana, P. K., Banka, H. (2016). A particle swarm optimization based energy efficient cluster head selection algorithm for wireless sensor networks. Wireless Networks, 23(7), 2005-2020.

[11] Dattatraya, K. N., & Rao, K. R. (2019). Hybrid based cluster head selection for maximizing network lifetime and energy efficiency in WSN. Journal of King Saud University - Computer and Information Sciences, 2(1), 56-68.

[12] Lavanya, N., & Shankar, T. (2020). Hybrid based energy efficient cluster head selection using camel series elephant herding optimization algorithm in WSN. International Journal of Advanced Computer Science and Applications, 11(5), 23-35.

[13] Prahadeeshwaran, S., & Priscilla, G. (2018). A hybrid elephant optimization algorithm-based cluster head selection to extend network lifetime in wireless sensor networks (WSNs). EAI Endorsed Transactions on Energy Web, 3(1), 165677.

[14] Rambabu, B., Venugopal Reddy, A., & Janakiraman, S. (2019). Hybrid artificial bee colony and monarchy butterfly optimization algorithm (HABC-mboa)-based cluster head selection for WSNs. Journal of King Saud University - Computer and Information Sciences, 2(1), 34-45.

[15] Agrawal, D., & Pandey, S. (2020). Optimization of the selection of cluster-head using fuzzy logic and harmony search in wireless sensor networks. International Journal of Communication Systems, 2(1), e4391.

E-ISSN 2581 - 7957
P-ISSN 2277 - 3916

CVR Journal of Science and Technology, Volume 19, December 2020
DOI: 10.32377/cvrjst 1915

# Performance Prediction of Task Workloads in Work-Stealing Runtimes for NUMA Multi-core Architectures

J. Yashasree[1], A. Mallareddy[2] and Dr. B. Vikranth[3]
[1]Asst. Professor, CVR College of Engineering/CSIT Department, Hyderabad, India
Email: yashasree123@gmail.com
[2]Assoc. Professor, CVR College of Engineering/IT Department, Hyderabad, India
Email: malla.reddy@cvr.ac.in
[3]Professor, CVR College of Engineering/IT Department, Hyderabad, India
Email: b.vikranth@cvr.ac.in

***Abstract:*** **Work stealing is a popular load balancing technique which is successfully adapted by various user level task parallel runtime systems such as Cilk, TBB etc. On the other hand, processor manufacturers are working on releasing processors with more than one socket on chip, to overcome the memory wall problem. If work stealing based run-time systems are ported onto such multi-socket machines, it may lead to performance issues. This paper has attempted to study the impact of such multi-socket multi-core architectures on performance of work stealing based run-times. In this paper, a work stealing parameter called remote steal count is introduced specially for assessing work stealing run-times on multi-socket architectures. This paper also proposes a simple regression model between work stealing parameters and performance of task-based applications. This model is helpful to predict the performance impact of task parallel applications while porting them into multi-socket hardware environment.**

***Index Terms:*** **Multi-core, Multi-socket, Non-Uniform Memory Architecture, Load balancing, Work Stealing, worker threads, Regression.**

## I. INTRODUCTION

### *A. Features of Modern Multi-Core Architecures*

Modern High-Performance Computing processor consists of more than one integrated memory controller (IMC) on a chip to fill the gap between fast growing speeds of CPU and compatible data delivery rates of memory units [1]. Introducing more than one such IMC serves the data needs of threads pinned to cores belonging to different chips simultaneously. By deploying these multiple DRAM controllers, the memory bandwidth is improved and contention for single memory controller hub can be reduced [2]. The processors cores are grouped and deployed in a socket. These processors are High Performance Server processors such as Intel Xeon or AMD Opteron. The processors are connected with high speed links such as Quick Path Interconnect (QPI) links [2] [3] from Intel or Hyper transport links from AMD. These links allow more than one socket to be deployed in a single pack on high performance servers. The presence of multiple memory controllers make these processors behave as Non Uniform Memory Architecture (NUMA). A dual socket Xeon E5-2620 series processor architecture which is studied in this paper as an experimental platform is presented in Fig. 1.

Figure 1. Dual socket Xeon E5 2620 processor [4]

It can be observed from the Fig 1 that it is a two-socket (2 NUMA nodes) architecture since, two separate memory controllers (MC) are attached to individual sockets. It means that all the six cores present in a socket can access the memory bank's memory through the local memory controller. If these cores need to access any data from memory attached to a remote socket, they experience more memory latency. A thread which is pinned onto a CPU core, can access data from a memory bank connected to its local memory controller at a faster rate than that of a remote memory bank connected to different sockets. The ratio of the remote memory access latency to the local memory access latency is called NUMA ratio ($R_{NUMA}$) and is given by

$$R_{NUMA} = \frac{T_{RemoteAccess}}{T_{LocalAccess}} \quad (1)$$

CVR Journal of Science and Technology, Volume 19, December 2020
DOI: 10.32377/cvrjst 1915

where $T_{LocalAccess}$ represents the local memory access time and $T_{RemoteAccess}$ represents the memory access time on remote memory node. It is obvious that remote memory access latency is greater than local memory access time.

In the experimental setup, Intel's Memory Latency Checker [5] program is executed for calculating the memory latency values of local and remote memory accesses. These values are presented in TABLE I. This table clearly shows that a thread is pinned to one of the cores on socket 0. The latency involved in accessing a data item from socket 0 is 77.3 nano seconds whereas if the data item is located on socket 1 memory module, the latency is 124.7 nano seconds. The other way around is also approximately the same.

TABLE I.
. LOCAL AND REMOTE ACCESS LATENCIES IN XEON E5-2620

| socket | 0 | 1 |
|---|---|---|
| 0 | 77.3 nS | 124.7 nS |
| 1 | 122.8 nS | 75.0 nS |

$R_{NUMA}$ factor is computed substituting the values of from TABLE I. $R_{NUMA}$ is considered as the average of remote latency accesses by socket 0 and socket 1 which yield 1.625 for Xeon E5 2620 architecture.

### *B. Effect of NUMA architectures on Work Stealing run-time environment*

Work stealing algorithm is a popular load balancing approach used in many user level run-time systems such as Cilk [6], Intel Threading Building Blocks (TBB) [7], Wool [8] and few implementations of OpenMP [9]. The common approach followed in work stealing is: during the initialization of the run-time system, a new worker thread is created which is associated with each processor core at hardware level. Associated with each worker thread, there is a task queue that contains the tasks spawned by the application program. These tasks are added to the queue. Each worker thread pops out one task at a time and executes the body of the task. Since the tasks arrive randomly as the user program instantiates tasks, the queues associated with worker threads may contain different counts of tasks, thereby causing imbalance in the load. Keeping the goal of balancing the load among worker threads as final objective, work-stealing strategy designates the worker thread which is under loaded as a *thief worker.* The thief worker attempts to *steal* tasks from another worker's queue. The worker from which one or more tasks are stolen is called a *victim worker*. If work stealing technique is applied in NUMA multi-core architectures:

- Identity affinity must be guaranteed. Individual worker thread is pinned to a processor core belonging to a particular node.
- If underlying hardware is NUMA, the memory locality of these worker queues is important since it is frequently accessed by the associated worker thread. In other words, the worker queue must be bound to the memory node(socket) where the worker thread is pinned to. Worker threads access these task queues in almost fully distributed way except in the instance of stealing occurrence i.e. regular job of the worker thread is to pop tasks from its own queue and execute the job on its processor. If locality of these queues is not considered, and if the worker thread and its task queue are mapped to different nodes due to the default first-touch policy of Linux [10] the overall performance may be affected due to increased remote memory access.

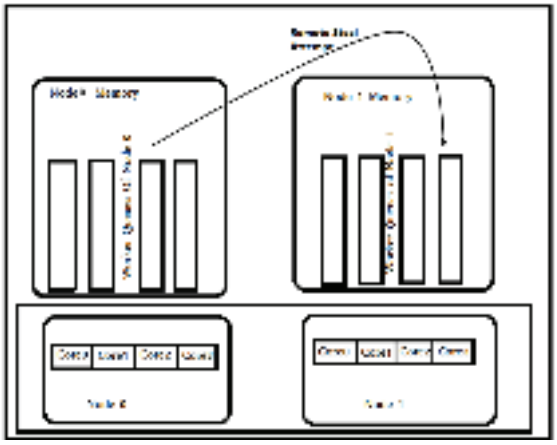

Figure 2. A thief worker attempting to steal task from remote node

- If a thief and victim are pinned to two different cores belonging to different sockets, the delays involved in stealing introduce additional performance overhead because of NUMA.

In this paper, the concept of remote stealing is analyzed, and a technique is proposed to predict the remote stealing attempts based on our experimental results.

### *C. Related Work*

The effect of scheduling different threads that access different data and shared data is analyzed in [11] but the processors considered here are single socket machines with multiple cores. This approach is confined to cache miss values when data is shared among multiple threads on a multi core processor when more than one core has common last level cache. Threads that access shared data that is bound to different NUMA nodes and its effects is analyzed in [1]. Machine learning based performance prediction of applications on single socket multi-core processors by using the cache level parameters is done in [12]. Comparison and performance analysis of different data structures as task-queues in work stealing run-time systems is done in [13]. This proposed model in this paper is inspired by [12] but our work is confined to prediction of task parallel application's execution times on work stealing run-time systems with multi-socket processors. To the best of our knowledge, the work carried out is unique and the proposed model is useful in studying the effect of remote steal attempts on overall performance of an application.

### *D. Organization of the paper*

Section II of this paper describes the motivation of the work behind the proposed strategy. In Section III, the experimental setup and the procedure followed in order to obtain work stealing parameters is elaborated. The mathematical model is proposed in Section III based on the empirical analysis. Section IV contains the concluding points of the proposed strategies in the paper.

E-ISSN 2581 - 7957
P-ISSN 2277 - 3916

CVR Journal of Science and Technology, Volume 19, December 2020
DOI: 10.32377/cvrjst 1915

## II. Motivation

The work-stealing strategy proposed is also called as randomized work-stealing [14] since it follows a technique for choosing a victim by generating a random number. The random number generated indicates the victim worker. If the architecture on which the work stealing runtime is deployed has a multi-socket NUMA architecture, the processors are divided into equal portion on different sockets. In our experimental platform (Xeon E5-2620), there are two sockets each, with its own memory banks. A total of 12 cores are arranged as 6 cores per socket. All the 6 cores of the socket can access its local memory bank at low latency. If the work stealing is randomized, the random victim chosen by the algorithm may refer to a worker with remote socket affinity.

- In randomized work stealing strategy, whenever a worker thread finds no tasks in its own task queue, it becomes a thief, and it can randomly choose a worker queue as a victim for stealing tasks. But if randomly chosen worker thread is pinned to a core belonging to a different node, it is a remote steal attempt. This scenario is depicted in Fig. 2.
- As a result of random stealing, unrelated tasks stolen from other workers brought to execution on local worker thread may result in performance isolation problems [11].

## III. Experimental Results

### *A. Platform description*

MATMUL benchmark program was executed on a hardware platform with dual socket Xeon-E52620 processor where each socket has 6 cores (12 hyper threads). Hyper threading was intentionally disabled in BIOs while carrying out our experimentation to ensure that cache contention effects are minimized on the performance. The physical memory of the hardware platform is a total of 16 GB, where each socket is attached with its own integrated memory controller connected to 8GB RAM. The work-stealing layer of target experimental platform consists a total of 12 worker threads pinned to each core.as shown in Fig.3**.** Separate worker queues are associated with each worker thread. Dispatcher module is responsible for initial static-distribution of the tasks equally among all the worker queues. The actual load imbalance occurs because of run-time characteristics of tasks, since each task may execute for different quantum of time when it is scheduled on to a worker thread. These worker threads behave as software level virtual processors, within the work stealing infrastructure.

To analyze the remote work stealing effects, MATMUL benchmark [16] implemented using work stealing runtime is executed on the target experimental platform. The size of matrix is taken as 8192×8192 for the following reasons:

- The size of matrix is intentionally taken as 8192 to be greater than the kernel supported virtual memory page size, to ensure that the data section of the program occupies multiple pages in virtual memory system. Consideration of a large matrix also increases the possibility of pages mapping across multiple nodes of NUMA architecture.
- Huge number (8192×8192) of tasks must be generated quickly so that the worker queues filled quickly causing a load imbalance in terms of tasks thereby causing considerable number of task-stealing attempts by the worker threads.

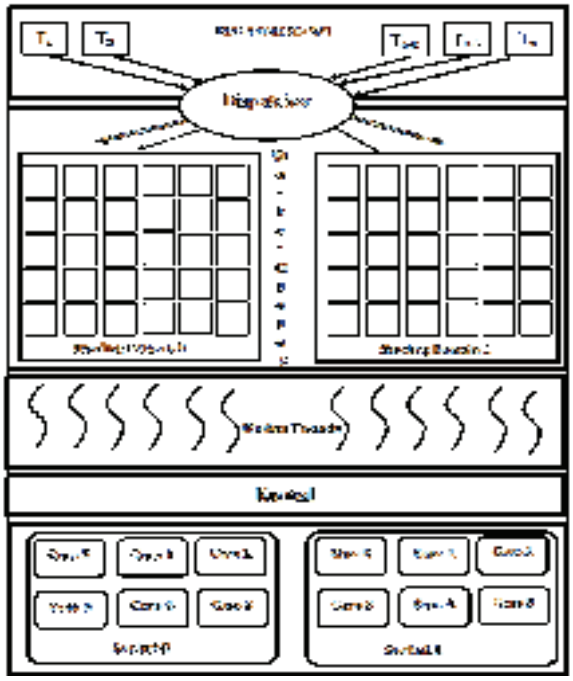

Figure 3. Modular Architecture of Experimental Platform

The MATMUL workloads are run using randomized work stealing policy with the additional feature of *thread to CPU pinning* policy. Remote steal count is measured for varying number of worker threads. It is ensured that the number of worker threads is even, such that two different halves of worker threads are bound to two different sockets during the execution of experiments. For instance, the first entry on the TABLE II represents the case with only two worker threads. In such a case, one thread has been explicitly bound on to a core belonging to one node and the other worker thread onto a different core belonging to different node. Explicit control of thread affinity is made possible using *sched_setaffinity* control functions of Linux environment.

While analyzing the remote steal attempts, special *work stealing parameters* were introduced in the source code to find the values of the following interested counters:

- *Remote Steal Attempts:* counts how many randomly generated victim indexes are leading to refer a worker thread on remote nodes.
- *Remote False Steals* count how many randomly generated victim indexes are leading to a failure to select a proper victim.

The common approach followed in randomized work stealing to choose a victim is:

$$victim\_id = random\ (seed)\ \%\ ncpus \qquad (2)$$

Where *ncpus* represents the number of processors or hardware-threads in the machine. On a multi-socket NUMA

CVR Journal of Science and Technology, Volume 19, December 2020
DOI: 10.32377/cvrjst 1915

multicore machine, n is the count of CPUs on all nodes. For instance, if the target platform is with 2 sockets where each socket has 6 processors, randomized work stealing strategy generates the victim index in range *[0:11]*. Among these generated indexes, the indexes generated in range [6:11] will result in a remote memory access. In the run-time's source code, a new parameter *Remote Steal Attempts* is used to count such remote event occurrences. Sample average values are presented in TABLE II after running the experiment for 10 times. It can be observed from the TABLE II that, 50% of the steal attempts are remote. Techniques to minimize the value of false steal count were proposed in [15]. Similar approaches can be useful for NUMA multi-core runtime; the second counter Remote False Steals can be minimized.

TABLE II.
REMOTE STEAL MISS RATIOS IN RANDOMIZED WORK STEALING

| Number Of Worker Threads | Average Remote Steal Count | Average Local Steal Count |
|---|---|---|
| 2 | 23 | 21.6 |
| 4 | 41 | 49 |
| 6 | 46 | 54 |
| 8 | 56 | 55 |
| 10 | 66 | 56 |
| 12 | 61 | 45 |
| 14 | 123 | 88 |
| 16 | 243 | 235 |
| 18 | 334 | 401 |
| 20 | 354 | 473 |
| 22 | 226 | 312 |
| 24 | 102 | 77 |

### *B. Model for performance prediction*

To investigate the effect of remote steal attempts on the performance of the workload, the MATMUL benchmark [16] has been executed for 50 times on dual socket architecture. Sample values of this experiment are presented in TABLE III. Unlike considering different number of worker threads as shown in TABLE II, this time, the number of threads is confined to the number of cores (i.e. 12 cores with 12 worker threads) to maintain identity affinity. The remote *tasks-steal-attempt*s parameter is obtained from the experiments and respective execution times are noted. Using these results, an effort is put to study the impact of remote stealing attempts on overall performance of the task parallel matrix multiplication application.

TABLE III.
SAMPLE VALUES OF REMOTE STEAL ATTEMPTS ON EXECUTION TIME

| S. No | No of worker threads | Local Steals count | Remote Steal count | Execution Time |
|---|---|---|---|---|
| 1 | 12 | 90 | 81 | 1867 |
| 2 | 12 | 99 | 74 | 1966 |
| 3 | 12 | 75 | 51 | 1835 |
| 4 | 12 | 86 | 86 | 1848 |
| 5 | 12 | 47 | 20 | 1781 |

While proposing the mathematical model, Pearson Correlation Coefficient Calculator is used on the obtained data, the value of R was 0:9123 and it is a strong positive relationship between remote steals and execution time. The relationship is presented in the Fig. 4. The results of regression analysis are presented below where $X$ represents the remote steal count and $\hat{y}$ indicates the execution time experienced by the MATMUL benchmark application.

Sum of X = 3555

Sum of Y = 91885

Mean X = 71.1

Mean Y = 1837.7

Sum of squares (SSX) = 127796.5

Sum of products (SP) = 205740.5

Regression Equation = $\hat{y} = bX + a$

b = SP/SSX = 205740.5/127796.5 = 1.60991

a = MY - bMX = 1837.7 - (1.61*71.1) = 1723.2356

$$\hat{y} = 1.60991X + 1723.2356 \quad (3)$$

It can be observed from (1) and (3) that the *b* value 1.6099 is approximately equal to $R_{NUMA}$ value 1.625 of (1). This is very important conclusion which shows the strong relationship between $R_{NUMA}$ factor and the performance. Fig. 4 shows the predictive model of performance given the number of remote steal counts as input. The error value between predicted performance (50 values) and emperical performance (50 values) is computed using root mean square method that yeilded error value 5.1683. This is a insignificant error with respect to execution time factor and the model is apt for prediction of performance.

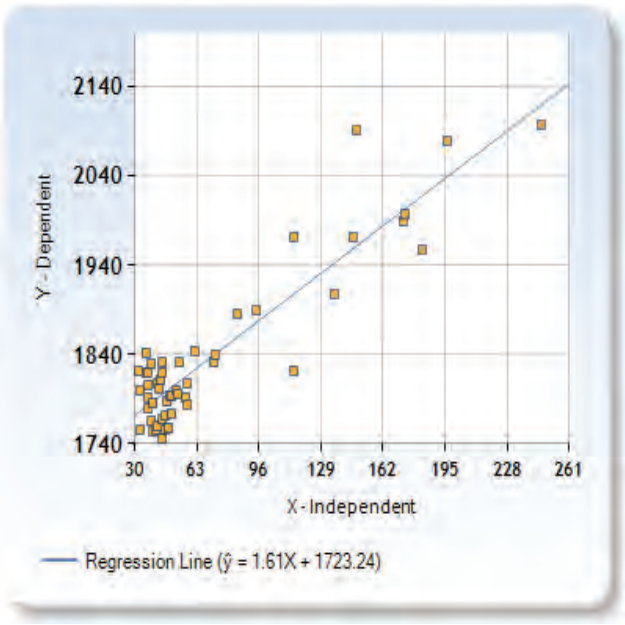


Figure 4. Regression relationship between remote steal count and execution time

CVR Journal of Science and Technology, Volume 19, December 2020
DOI: 10.32377/cvrjst 1915

## IV. Conclusions

In this paper, the impact of multi-socket multi-core architectures on randomized work stealing load balancing algorithm implementation is analyzed. This paper also proposes a linear regression model to predict the performance of task-based application, based on the work stealing parameter called remote steal count. The proposed model confirms the dependency of performance of an application on $R_{NUMA}$ value of the target architecture.

## References

[1] Z. &. G. T. R. Majo, " Memory system performance in a NUMA multicore multiprocessor", in In Proceedings of the 4th Annual International Conference on Systems and Storage , (2011, May)..

[2] A. B. R. A. M. A. R. J. Dimitrios Ziakas, "Intel R quickpath interconnect architectural features supporting scalable system architectures", in IEEE 18th Annual Symposium on High Performance Interconnects, 2010.

[3] D. E. A. Ziakas, "Intel® quickpath interconnect architectural features supporting scalable system architectures.", 2010.

[4] "IntelR . Xeon E5 2620v3 processor architecture", Intel,2014.[OnlineAvailable: ProcessorE5-2620-v3-15M-Cache-2.40-GHz.

[5] K. K. A. T. W. V Viswanathan, ". Intel memory latency checker", Intel Technology Journal, 2015.

[6] C. F. J. B. C. K. Robert D Blumofe, "Cilk: An efficient multithreaded runtime system. Journal of parallel and distributed", Journal of parallel and distributed computing, vol. 37, no. 1, pp. 55-69, 1996.

[7] C. Pheatt, "Intel R threading building blocks," Journal of Computing, vol. 23, no. 4, pp. 298-298, 2008.

[8] K.-F. Faxén, "Wool-a work stealing library", 2009.

[9] F. F. N. G. B. N. R. &. W. P. A. .. Broquedis, "Dynamic task and data placement over NUMA architectures: an OpenMP runtime perspective", 2009.

[10] M. D. D. H. A. G. H. Martin J Bligh, " Linux on NUMA systems”., volume 1, in In Proceedings of the Linux Symposium, Pages:89-102, 2004.

[11] F. G. S. K. A. Y. S. Dhruba Chandra, " Predicting inter-thread cache contention on a chip multi-processor architecture”., pages 340-351. IEEE, 2005 in 11th IEEE International Symposium on High-Performance Computer Architecture HPCA-11. , 2005.

[12] A. N. A. R. W. Jitendra Kumar Rai, "Using machine learning techniques for performance prediction on multi-cores. In Applications and Developments in Grid, Cloud, and High Performance Computing", Applications and Developments in Grid, Cloud, and High Performance Computing. IGI Global, pp. 259-273, 2013.

[13] B. Vikranth, "Performance Analysis of Load Balancing Queues in User Level Runtime Systems for Multi-Core Processors", CVR Journal of Science and Technology, vol. 11, pp. 87-90, 2016.

[14] Robert D Blumofe and Charles E Leiserson, " Scheduling multithreaded computations by work stealing", Journal of the ACM (JACM), vol. 46, no. 5, pp. 720-748, 1999.

[15] B. R. W. A. C. R. R. Vikranth, "Topology aware task stealing for on-chip NUMA multi-core processors", in Procedia Computer Science, Barcelona, 2013.

[16] J. P. P. A. P. S. C. Burkardt, "MATMUL: An Interactive Matrix Multiplication Benchmark," IETE Journal, p. 640, 1995.

[17] I. Panourgias, " Numa effects on multicore, multi socket systems", The University of Edinburgh, 2011.

E-ISSN 2581 - 7957
P-ISSN 2277 - 3916

CVR Journal of Science and Technology, Volume 19, December 2020
DOI: 10.32377/cvrjst 1916

# Analysis of Powder-Mixed EDM Process Characteristics of Tungsten Carbide alloy by using GRA Technique

Jagdeep Singh[1], Manjeet Kharub[2] and Sarat Kumar Sahoo[3]
[1]Asst. Professor, Lovely Professional University/ Mechanical Engg. Department, Punjab, India
Email: erjagdeep88@gmail.com
[2]Asst. Professor, CVR College of Engineering/ Mechanical Engg. Department, Hyderabad, India
Email: manjeetkharub@gmail.com
[3]Asst. Professor, CVR College of Engineering/ Mechanical Engg. Department, Hyderabad, India
Email: saratkumar222@gmail.com

***Abstract:*** **Abrasive electrical discharge machining of tungsten carbide is performed by using a powder of graphite and alumina mixed in working fluid. Taguchi method is used to predict the optimal choice of EDM parameters like current, powder, pulse on time and pulse off time. After experiments, it has been found that adopted parameters significantly affect the response characteristics like metal removal rate and tool wear rate. Taguchi technique with the grey relational analysis was for optimizing machining operations with multi-process parameters. Optimum process parameter is determined with the help of Taguchi technique using grey relational grade as the performance index. Response table is used to optimize the process parameters. Further, an analysis of variance (ANOVA) study is performed to show the significance and percentage contribution of each factor in the study.**

***Index Terms:*** **EDM, Electrical, Discharge, Machining, ANOVA, GRG, Optimization**

## I. Introduction

Electric discharge machining (EDM) process is an unconventional machining process, where the material removal occurs due to a spark between the tool and workpiece dipped in a dielectric fluid [1]. The spark causes a temperature of about 10,000˚C, which is sufficient to melt and vaporize the material, enabling the process to machine High Strength Temperature Resistant (HSTR) materials and alloys. [1,2]. Being capable of producing intricate geometrical shapes, the process finds its applications in the manufacturing of automotive, aerospace, surgical components and mold & dye-making industry. Although the process has widespread industrial applications, yet it faces limitations due to its low machining efficiency and poor surface finish [3,4].

Therefore, to overcome the limitations mentioned above, several studies have been carried out by several researchers - particularly for better control over the machining parameters. Nowadays, due to advances in technology, and an overall hybrid process called “Powder Mixed Electrical Discharge Machining (PMEDM)” process is being used to overwhelm the limitations of conventional EDM [1, 5]. In PMEDM, the material in powder form is mixed in the dielectric fluid to decrease its insulating strength and increase the spark gap distance between the electrode & workpiece, which allows uniform flushing of debris [6]. Due to this, the process becomes more stable, thereby improving the machining rate and surface finish. Further, the surface produced via PMEDM is found to be having high resistance to corrosion and abrasion. Although the powder mixed EDM process possesses better result than traditional processes, still it lacks swift acceptance in industries. In recent literature, many studies have shown future analysis of process parameters, as a future scope. So, this study is an attempt to optimize various process parameters. Material removal rate (MRR) and tool wear rate (TWR) were taken as output parameters whereas pulse-on, pulse-off, current and powder were taken as input variables.

## II. Background and Review

The first study on powder-mixed EDM was published in 1980. The addition of powder particles into dielectric fluid produced better surface finish and machining rate compared to conventional EDM [7]. Research and industrial experts have been continuously working on its parameters to reach an optimum level with respect to various materials. For instance, Kansal et al. [8] executed research development using additives/powders with the EDM process. Mahdavinejad and Mahdavinejad [9] examined the variability of EDM process through machining of WC–Co composite by varying compositions. Sharma and Singh [1] applied RSM optimization technique to optimize process parameters during the EDM process of WC-Co composite. Kung et al. [3] used the RSM technique for optimization of the input variables of WC in powder EDM process and revealed that Al powder mixed in dielectric fluid enhances the efficiency of the EDM process.

It is observed from the above literature reviews, that much work has been undertaken by a number of researchers to explore the PM-EDM of different materials, but very few authors have studied the EDM or PM-EDM of WC material, which prompts the current research to execute the powder mixed EDM of tungsten carbide [10]. For this study, input parameter settings were taken with the help of Taguchi’s L27 orthogonal array design. To find the optimum processing parameter, the grey relational grade technique was applied.

E-ISSN 2581 - 7957
P-ISSN 2277 - 3916

CVR Journal of Science and Technology, Volume 19, December 2020
DOI: 10.32377/cvrjst 1916

## III. Experimental Details

Metal powders are added in the dielectric fluid. In order to avoid the powder being mixed with the filtering system, a transparent bath is used. For the enhanced circulation of the powder in the dielectric fluid, a stirrer is used for shaking the powders constantly in the box, and the rpm is controlled by a heavy-duty regulator. Experiments were executed on CNC electric discharge machine. Tungsten carbide was used as workpiece material with composition, W-65.50%, Ti-15.47%, Co-10.07%, Nb-4.69% and Cu-3.66%. Copper was used as a tool electrode, and EDM oil was used as a working fluid.

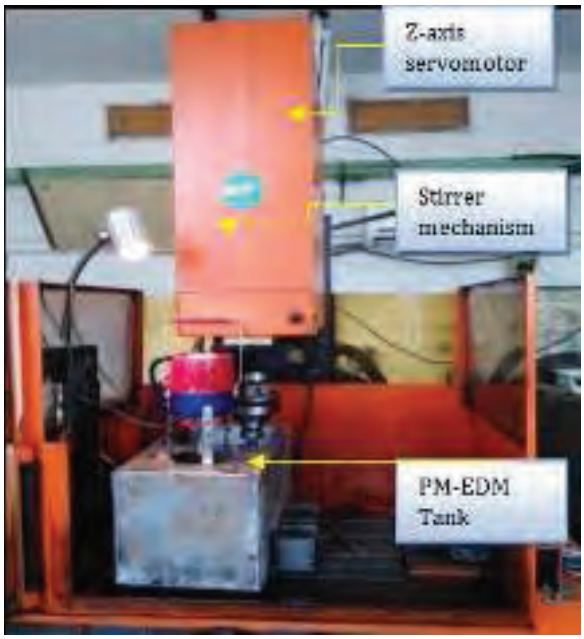


Figure 1. Experimental setup (Model no. T-3822)

Material removal rate (MRR) and tool wear rate (TWR) of the powder EDM process was studied by taking four input parameters, i.e. pulse-on, pulse-off, current and powder.

The input parameters and their levels are shown in Table. 1. The fixed input parameters used in this experiment are:

open circuit voltage (135 ± 5%);

- polarity (+);
- copper tool;
- machining time (10 min);
- powder concentration (15 gm/l).

Four factors and three levels were taken into consideration based on pilot experimentation and literature review. Taguchi's $L_{27}$ orthogonal array was applied to this experiment, as shown in Table 2. Grey relational analysis was used to determine the appropriate selection of machining parameters for experimenting. To evaluate the PM-EDM machining performance, MRR and TWR were calculated after each experiment by using equation 1.

$$\text{MRR or TWR} = \frac{Wi-Wf}{\rho \times t} \times 1000 \text{ mm}^3/\text{min} \quad (1)$$

$w_i$, $w_f$ = Initial and Final weight of the sample respectively, $t$ = Period of trials, $\rho$ = Density of sample, MRR and TWR were measured using a digital weighing machine with least count 0.001 gm.

## IV. Results and Discussions

In this section, the data of MRR and TWR obtained from 27 experiments as tabulated in Table.2 were analyzed by using Grey Relational Analysis (GRA) technique followed by response tables. At last, ANOVA analysis for mean was performed to show the significant factors and their contributions to the study. Figures 2 shows that MRR and TWR increase with an increase in pulse-on time and current, whereas it decreases with an increase in pulse off time.

TABLE I.
Process Parameters and their Levels

| Factors | Process Parameter | 1 | 2 | 3 |
|---|---|---|---|---|
| A | Pulse-on time (μs) | 30 | 50 | 70 |
| B | Pulse-off time (μs) | 20 | 35 | 50 |
| C | Current (A) | 3 | 5 | 7 |
| D | Powders | CP | AP | * |
| CP = graphite Powder; AP = aluminum oxide Powder; 1,2,3 = levels; simple EDM = *, 1. | | | | |

With the increase in input discharge energies (pulse-on time and current), the temperature between both the electrodes increases, which helps to melt and evaporate vast amounts of material out from the electrodes, hence increase MRR & TWR. With the mixing of graphite powder and alumina powder MRR increases as compared to simple EDM process. Graphite seems to be most useful to improve material removal rate for PM-EDM of WC. Alumina powder gives low TWR as compared to simple EDM and carbon powder.

Response table for mean data and GRG grade for MRR & TWR are shown in Table 3. For MRR, higher-the-better response characteristic is taken. So a higher value from the response tables has been selected. For TWR, lower-the-better response characteristic is considered. Therefore, the lower value from the response table has been selected. According to response tables, the powder is the most effective process parameter followed by pulse-on time, pulse-off time and current—Star (*) in response table highlights the most significant values. Grey relational grade co-efficient provides the optimum process sequence. The GRG ranking provides a ranking of the alternatives, in which higher values determines a better alternative. ANOVA analysis for GRA grade is shown in Table 5. It

E-ISSN 2581 - 7957
P-ISSN 2277 - 3916

CVR Journal of Science and Technology, Volume 19, December 2020
DOI: 10.32377/cvrjst 1916

concludes that powder (71.87%) was found to be the most contributing factor for overall performance, followed by the pulse-on time (5.46%) and pulse-off time (3.61%). The rest of the terms were found insignificant.

TABLE II.
TAGUCHI L27 OA EXPERIMENTAL DESIGN AND NORMALIZED VALUES [$X^*(K)$]

| Sl. no. | Pulse-on Time, (µs) | Pulse-off Time, (µs) | Current, (A) | Powder | MRR, ($mm^3$/min) | TWR, ($mm^3$/min) | MRR [$X^*(k)$] | TWR [$X^*(k)$] |
|---|---|---|---|---|---|---|---|---|
| 1 | 30 | 20 | 3 | CP | 1.569 | 0.0825 | 0.4028 | 0.7592 |
| 2 | 30 | 20 | 5 | AP | 1.401 | 0.0667 | 0.2895 | 0.9533 |
| 3 | 30 | 20 | 7 | * | 1.302 | 0.1084 | 0.2227 | 0.4410 |
| 4 | 30 | 35 | 3 | AP | 1.322 | 0.0629 | 0.2362 | 1.0000 |
| 5 | 30 | 35 | 5 | * | 1.105 | 0.085 | 0.0897 | 0.7285 |
| 6 | 30 | 35 | 7 | CP | 1.637 | 0.0911 | 0.4487 | 0.6536 |
| 7 | 30 | 50 | 3 | * | 0.972 | 0.0883 | 0.0000 | 0.6880 |
| 8 | 30 | 50 | 5 | CP | 1.538 | 0.0809 | 0.3819 | 0.7789 |
| 9 | 30 | 50 | 7 | AP | 1.541 | 0.0734 | 0.3839 | 0.8710 |
| 10 | 50 | 20 | 3 | CP | 1.968 | 0.1156 | 0.6721 | 0.3526 |
| 11 | 50 | 20 | 5 | AP | 1.681 | 0.0841 | 0.4784 | 0.7396 |
| 12 | 50 | 20 | 7 | * | 1.519 | 0.1381 | 0.3691 | 0.0762 |
| 13 | 50 | 35 | 3 | AP | 1.583 | 0.0754 | 0.4123 | 0.8464 |
| 14 | 50 | 35 | 5 | * | 1.323 | 0.1018 | 0.2368 | 0.5221 |
| 15 | 50 | 35 | 7 | CP | 2.162 | 0.1270 | 0.8030 | 0.2125 |
| 16 | 50 | 50 | 3 | * | 1.219 | 0.0975 | 0.1667 | 0.5749 |
| 17 | 50 | 50 | 5 | CP | 1.931 | 0.1103 | 0.6471 | 0.4177 |
| 18 | 50 | 50 | 7 | AP | 1.702 | 0.0842 | 0.4926 | 0.7383 |
| 19 | 70 | 20 | 3 | CP | 2.062 | 0.1194 | 0.7355 | 0.3059 |
| 20 | 70 | 20 | 5 | AP | 1.841 | 0.0948 | 0.5864 | 0.6081 |
| 21 | 70 | 20 | 7 | * | 1.742 | 0.1433 | 0.5196 | 0.0123 |
| 22 | 70 | 35 | 3 | AP | 1.729 | 0.0873 | 0.5108 | 0.7002 |
| 23 | 70 | 35 | 5 | * | 1.654 | 0.1367 | 0.4602 | 0.0934 |
| 24 | 70 | 35 | 7 | CP | 2.454 | 0.1443 | 1.0000 | 0.0000 |
| 25 | 70 | 50 | 3 | * | 1.565 | 0.1315 | 0.4001 | 0.1572 |
| 26 | 70 | 50 | 5 | CP | 2.343 | 0.1324 | 0.9251 | 0.1462 |
| 27 | 70 | 50 | 7 | AP | 1.842 | 0.0971 | 0.5870 | 0.5799 |
| [$X^*(K)$] = Normalized Values for kth experiment | | | | | | | | |

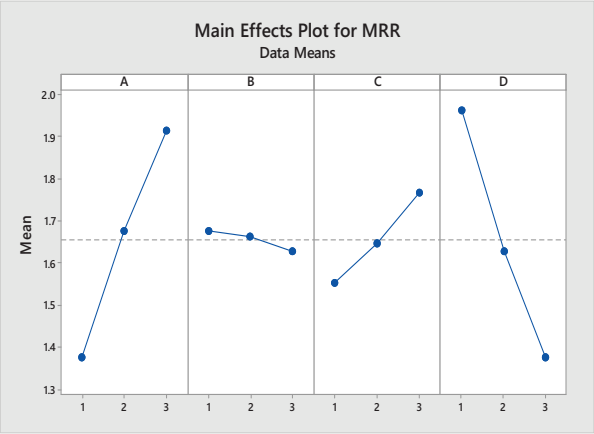


Figures 2. Effect for MRR

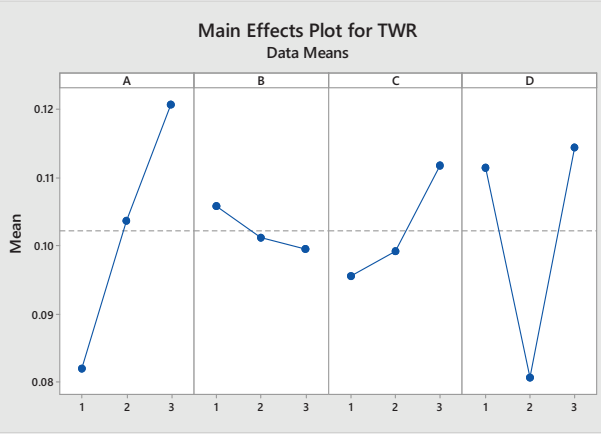


Figures 3. Effect for TWR

TABLE III.
DEVIATION VALUES [ΔXI(K)], GREY RELATIONAL CO-EFFICIENT [€I(K)], GREY RELATIONAL GRADE, RANKING

| Sl. no. | MRR [$\Delta X_i(k)$] | TWR [$\Delta X_i(k)$] | MRR [$€_i(k)$] | TWR [$€_i(k)$] | GRG [$\eta_j$] | Rank |
|---|---|---|---|---|---|---|
| 1 | 0.5972 | 0.2408 | 0.4557 | 0.6749 | 0.5653 | 11 |
| 2 | 0.7105 | 0.0467 | 0.4131 | 0.9146 | 0.6639 | 3 |
| 3 | 0.7773 | 0.559 | 0.3915 | 0.4721 | 0.4318 | 23 |
| 4 | 0.7638 | 0 | 0.3956 | 1.0000 | 0.6978 | 1 |
| 5 | 0.9103 | 0.2715 | 0.3545 | 0.6481 | 0.5013 | 19 |
| 6 | 0.5513 | 0.3464 | 0.4756 | 0.5907 | 0.5332 | 16 |
| 7 | 1 | 0.312 | 0.3333 | 0.6158 | 0.4746 | 20 |
| 8 | 0.6181 | 0.2211 | 0.4472 | 0.6934 | 0.5703 | 9 |

CVR Journal of Science and Technology, Volume 19, December 2020
DOI: 10.32377/cvrjst 1916

| | | | | | | |
|---|---|---|---|---|---|---|
| 9 | 0.6161 | 0.129 | 0.4480 | 0.7949 | 0.6215 | 4 |
| 10 | 0.3279 | 0.6474 | 0.6039 | 0.4358 | 0.5199 | 18 |
| 11 | 0.5216 | 0.2604 | 0.4894 | 0.6575 | 0.5735 | 8 |
| 12 | 0.6309 | 0.9238 | 0.4421 | 0.3512 | 0.3967 | 27 |
| 13 | 0.5877 | 0.1536 | 0.4597 | 0.7650 | 0.6124 | 6 |
| 14 | 0.7632 | 0.4779 | 0.3958 | 0.5113 | 0.4536 | 22 |
| 15 | 0.197 | 0.7875 | 0.7174 | 0.3883 | 0.5529 | 13 |
| 16 | 0.8333 | 0.4251 | 0.3750 | 0.5405 | 0.4578 | 21 |
| 17 | 0.3529 | 0.5823 | 0.5862 | 0.4620 | 0.5241 | 17 |
| 18 | 0.5074 | 0.2617 | 0.4963 | 0.6564 | 0.5764 | 7 |
| 19 | 0.2645 | 0.6941 | 0.6540 | 0.4187 | 0.5364 | 15 |
| 20 | 0.4136 | 0.3919 | 0.5473 | 0.5606 | 0.5540 | 12 |
| 21 | 0.4804 | 0.9877 | 0.5100 | 0.3361 | 0.4231 | 24 |
| 22 | 0.4892 | 0.2998 | 0.5055 | 0.6252 | 0.5654 | 10 |
| 23 | 0.5398 | 0.9066 | 0.4809 | 0.3555 | 0.4182 | 25 |
| 24 | 0 | 1 | 1.0000 | 0.3333 | 0.6667 | 2 |
| 25 | 0.5999 | 0.8428 | 0.4546 | 0.3724 | 0.4135 | 26 |
| 26 | 0.0749 | 0.8538 | 0.8697 | 0.3693 | 0.6195 | 5 |
| 27 | 0.413 | 0.4201 | 0.5476 | 0.5434 | 0.5455 | 14 |
| ΔXI(K)= Deviation values, €I(K)= Grey relational co-efficient | | | | | | |

TABLE IV.
RESPONSE TABLE FOR MEANS

| Level | A | B | C | D |
|---|---|---|---|---|
| 1 | 0.5622 | 0.5183 | 0.5381 | 0.5654 |
| 2 | 0.5186 | 0.5557 | 0.5420 | 0.6012* |
| 3 | 0.5269 | 0.5337 | 0.5275 | 0.4412 |
| Delta | 0.0436 | 0.0374 | 0.0145 | 0.1600 |
| Rank | 2 | 3 | 4 | 1 |


Figure 4. Overall performance based on GRA grade

TABLE V.
ANOVA TABLE FOR GRA METHOD

| Factors | DOF | Adj SS | Adj MS | F-Value | P-Value | % of Contribution |
|---|---|---|---|---|---|---|
| $T_{ON}$ | 2 | 0.009642 | 0.004821 | 7.32 | 0.025 | 5.461033 |
| $T_{OFF}$ | 2 | 0.006372 | 0.003186 | 4.84 | 0.056 | 3.608971 |
| Current | 2 | 0.001014 | 0.000507 | 0.77 | 0.504 | 0.574309 |
| Powder | 2 | 0.126890 | 0.063445 | 96.31 | 0.000 | 71.86792 |
| $T_{ON}$ × $T_{OFF}$ | 4 | 0.000569 | 0.000142 | 0.22 | 0.920 | 0.32227 |
| $T_{ON}$ × Current | 4 | 0.007148 | 0.001787 | 2.71 | 0.132 | 4.048482 |
| $T_{ON}$ × Powder | 4 | 0.020969 | 0.005242 | 7.96 | 0.014 | 11.87642 |
| Error | 18 | 0.003952 | 0.000659 | | | 2.238333 |
| Total | 26 | 0.17656 | | | | 100 |

CVR Journal of Science and Technology, Volume 19, December 2020
DOI: 10.32377/cvrjst 1916

## V. Conclusions

Witnessing the increasing application of powder-mixed EDM processes, this study has been conducted to optimize its process parameters. This work investigates results of powder mixed EDM of tungsten carbide by using GRA technique. GRA method has been used to determine the significant factors and the optimum machining conditions to enhance the performance of EDM. Graphite and alumina powders are used in working fluid, whereas graphite powder seems suitable for high MRR. Alumina powder has been found suitable for low TWR. Alumina powder has been found to be the primary governing factor for these response characteristics.

## References

[1] Sharma R K, Singh J (2014) "Effect of powder mixed electrical discharge machining (PMEDM) on difficult to machine materials - A systematic literature review", Journal for Manufacturing Science and Production, 14(4), 233–255.

[2] S. K. Sahoo, A. Bara, A.K. Sahu, S.S. Mahapatra, D.S. Kiran, G.S. Teja, E.S. Teja and S.P. Reddy, Analysis and Optimization of Wire EDM Process Parameters by using GRA Methodology; Materials Science Forum, Trans Tech Publications, Scientific.Net, 969 (2019), pp. 678-684.

[3] Kung K Y, Horng J T, Chiang K T (2009) "Material removal rate and electrode wear ratio study on the powder mixed electrical discharge machining of cobalt-bonded tungsten carbide", Int Jour of Adv Manuf Tech, 40(1–2): 95–104.

[4] Khundrakpam, N. S., Brar, G. S., & Deepak, D. (2016). Experimental investigation on EDM processes by tool rotating speed. *Bonfring Int. J. Ind. Eng. Manag. Sci*, *6*(4), 171-173.

[5] Kansal H K, Singh S, Kumar P (2005) "Parametric optimization of powder mixed electrical discharge machining by response surface methodology", Journal of Materials Processing Technology, 169, 427–436.

[6] Sharma R K, Singh J (2016) "Determination of multi-performance characteristics for powder mixed electric discharge machining of tungsten carbide alloy", Proc IMechE Part B: J Engineering Manufacture, 230 (2), 303–312.

[7] Zhao W S, Meng Q G, Wang Z L (2002) "The application of research on powder mixed EDM in rough machining", Journal of Material Processing Technology, 129, 30-33.

[8] Kansal H K, Singh S, Kumar P (2007) "Technology and research developments in powder mixed electric discharge machining", Journal of Materials Processing Technology, 184, 32–41.

[9] A.K. Sahu, P.P. Mohanty, S.K Sahoo, Electro discharge machining of Ti-alloy (Ti6Al4V) and 316LStainless Steel and Optimization of process parameters by Grey relational analysis (GRA) method, Advances in 3D Printing & Additive Manufacturing Technologies, Springer, 2017, pp. 65-78.

[10] Mahdavinejad R.A., Mahdavinejad A. ED machining of WC–Co. Journal of Materials Processing Technology, 2005, 162–163, 637–643.

[11] Pragya Shandilya, Arun Kumar Rouniyar and D Saikiran, Multi-objective parametric optimization on machining of Inconel-825 using wire electrical discharge machining, J Mechanical Engineering Science, SAGE, 234(2020), pp. 4056–4068.

E-ISSN 2581 - 7957
P-ISSN 2277 - 3916

CVR Journal of Science and Technology, Volume 19, December 2020
DOI: 10.32377/cvrjst 1917

# Study of Condensation on PDMS Substrates for Enhanced Solar Still

M. Udaya Kiran[1], Sk. Mohammad Shareef[2] and A.L.N. Arun Kumar[3]
[1]Asst. Professor, CVR College of Engineering/Mechanical Engg. Department, Hyderabad, India
Email: udaysteve@gmail.com
[2]Asst. Professor, CVR College of Engineering /Mechanical Engg. Department, Hyderabad, India Email: shareefshaik4@gmail.com
[3]Asst. Professor, CVR College of Engineering /Mechanical Engg. Department, Hyderabad, India
Email: aln.arunkumar@gmail.com

***Abstract:*** **Condensation surfaces are found in many applications from solar stills to phase change heat exchangers, solar condensers etc. In all these applications, it is important to increase the condensation efficiency by engineering the surface which yields better condensation properties that are suitable for targeted needs. In the current project, we envisage such an effort where metal elastomeric composite substrates are employed to increase condensation efficiency.**

**We use Polydimethylsiloxane (PDMS) as a choice of elastomer and Aluminum particulates as the choice of the metallic inclusions. Write after preparing the substrates of different portions of metallic particulate inclusions and condensations, tests are carried out on each substrate separately. Here we prepare a few substrates by varying the Aluminium metallic particle mass fraction over five decades from $10^{-6}$ to $10^{-8}$. The substrates thus obtained are used in condensation tests. From the measurements, a dew condensation rate was calculated. The tests were repeated four to five times to ensure repeatability of the measurements. Care was also taken to ensure that all the measurements were obtained in the same atmosphere.**

**The dew condensation rate was studied by varying the Aluminium mass fraction in the substrate. A non-monotonic behavior was observed wherein high condensation rates were obtained for an Aluminium mass fraction of approximately $5*10^{-4}$ g. For all other mass fractions, the condensation rates are less than this above condition. Therefore, it can be concluded that this is an optional mass fraction for which dew condensation efficiency was the highest**

***Index Terms:*** **Elastomer, PDMS, Condensation, Mass fraction, Substrates, Dew**

## I. Introduction

It is needless to mention that water, a compound of Hydrogen and Oxygen is a precious natural gift, which is very essential for survival of humankind including animals. Nowadays pure water is a rare substance. There are so many ways to produce potable water for example water purifiers, water treatment in plants like sedimentation, filtration etc. However, all these processes need some external power supply and not everybody can afford those systems. In some remote areas there is no availability of electrical power source also. One of the alternatives to get potable water is by using solar stills. Even though production rates are low it is viable because of low initial cost and it does not need electricity. Solar still is a low-tech way of distilling water with the help of heat of the Sun, to be precise the heat and humidity of the soil, and relative cool of plastic.[1]

Further, dew can be collected from the atmosphere using hydrophobic substrates and used for drinking purposes. Dew is a commonly occurring natural phenomenon where the humid air condenses on a substrate and transforms into liquid water. Colleting of water from atmosphere which is in the form of Dew is not a new idea, some experiments have been done and some are going on. The main problem in harvesting Dew water from the atmosphere is setting up of the process is difficult and not effective; sometimes it is expensive, considering the output obtained.

### *A. Formation of dew*

Dew is a natural phenomenon where humid air condenses on a substrate and finally transforms into liquid water [2]. Dew can be a potential source of water. Dew is a surface phenomenon. In some cases, dew is an unfavorable phenomenon. On plant leaves it develops spores, mainly fungus spores, which are undesirable for the process of photosynthesis. It lowers the transmission of light by more than 50% when it forms on greenhouse shields and affects the yield of agricultural production [3]. Studying and controlling of Dew is found in medicine for sterilization processes, agriculture field and in Nano-electronics to know and control vapor decompositions.

The formation of dew is essentially a problem of phase transition, the presence of other gases like nitrogen or air do not affect fundamental problems of condensation. The surface properties of the substrate can modify the conditions of formation of liquid phase. With desired geometrical conditions of the substrates the growth of the dew is controlled [4]. Another important thing is wetting properties of the substrate. The wetting properties decide whether the condensation is either drop wise or film wise

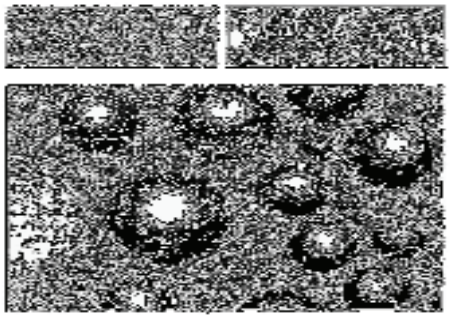

Figure 1. Self-similar growth of a pattern of droplets condensing on hydrophobic glass.

E-ISSN 2581 - 7957
P-ISSN 2277 - 3916

DOI: 10.32377/cvrjst 1917

The pattern at t=1s (a) after condensation started, is equivalent to the one at t=6s (b). In (c)att=25s, new families of droplets have nucleated between the initial drops. Source: D. Beysens / C.R. Physique 7 (2006) 1082-1100.

There are some other cases where the growth of the drops is favorable. The key role of the growth of the drops is its perimeter. If the temperature gradients are higher, accommodation of molecules of water is also high. The temperature gradients due to thermal release of energy at the substrate surface are parallel to the liquid-vapor interface leading to flows of Marangoni effects [5]. This will increase the growth pattern. The very small drops of critical radii coalesce with each other until they form a stable drop. This leads to distributions of drops on the substrate at a later stage. On the substrate, continuous nucleation and evaporation leads to surface diffusion that feeds drop at its perimeter [6].

## II. Experiments

The substrates were prepared by mixing prescribed amounts (by mass) of Aluminium powder in a known amount of PDMS, while the elastomer was in the pre-cured state. Then the liquid was poured on a flat surface and allowed to cure for some time. The experiments consist of preparation of hydrophobic surface using Sylgard 184: Silicone elastomer with very little amounts of Aluminum metal powder inclusions. Quantitatively calculate the condensation rate on those surfaces and finally calculate the humidity in the atmosphere. The condensation tests involved measuring the true weights using microbalance. We then place the substrates on a block of ice for definite time and allow the dew to condense on the top surface of the substrate by lowering of the substrate temperature. Then the masses of the substrates are measured before and after placing on the ice block. This process is repeated, and all the dry weights and wet weights are noted down for further comparisons. All these experiments are conducted in same environmental conditions.

### *A. Hydrophobic Surfaces*

Preparation of Surfaces : The super hydrophobic surfaces are created by using SYLGARD 184: Silicone elastomer, which is supplied as two-part liquid component kit comprising of Part A/Part B (Lot-matched base/Curing agent) to be mixed in a 10:1 ratio by weight or volume. The mixing can be done either manually or automatically by any mixing equipment and the final mixture is dispensed to form a desired shape of substrate. When the two liquid components are mixed thoroughly, the mixture cures to be a flexible elastomer.

When ten parts of base material mixed to one part of curing agent and are thoroughly mixed and agitate gently to reduce the amount of air introduced. Allow the mixture to set for 30 minutes before using. This may be adequate for removal of the air introduced during the mixing process. For best curing results, glassware and glass or metal stirring implements are used. The mixing should be done smoothly so that excess air is not introduced into the final mixture.

Curing reaction starts with the mixing, which leads to gradual increase in viscosity, followed by gelation and finally converting into a solid elastomer, which is transparent in nature. This mixture should be used within two hours after mixing. For preparing surface, pour the mixture on a flat surface and leave it for some time to form final elastomer substrate. Usually at room temperature, it takes 48 hours to give final silicone elastomer surface and at higher temperatures, the time taken to give the final elastomer is reduced as follows.

- ~48 hours at room temperature
- 45 minutes at 100°C (212°F)
- 20 minutes at 125°C (257°F)
- 10 minutes at 150°C (302°F)

For preparing a flat surface, the mixture should be poured on a flat surface and allowed to move freely without any obstructions. After two days simply peeling it off gives a plain transparent sheet of silicone elastomer as shown in Figure 2. By preparing surfaces with different proportions of very little amount of Aluminium powder along with base and curing agent, quantitatively find out the condensation rate on each surface of different Aluminium proportions

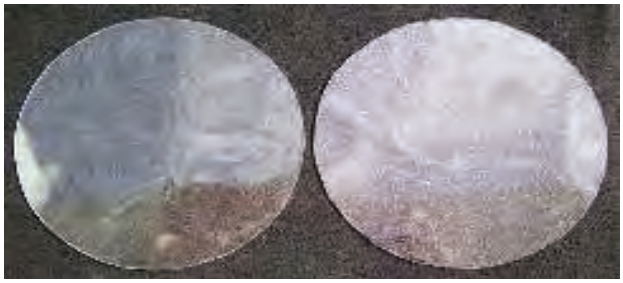

Figure 2. Plain PDMS substrate and PDMS with Aluminium particle inclusions.

### *B. Condensate measurements:*

Experimental Procedure.: All the measurements are taken using micro weighing machine, TB-215D Denver instrument. It is convenient for analytical balancing with large display and clear function keys. It gives reliable weighing results under normal ambient conditions. For getting good accurate results follow the manufacturer instructions.

To deliver exact results, the balance must warm up for at least 30 minutes after initial connection to AC power or a relatively long power outage to reach the required operating temperature. After the balance has been turned on, an automatic self-test of the balance's electronic circuitry is performed. At the end of the self-test, zero readout is displayed. Then the balance is ready to operate. Before taking any measurements, press TARE option to make the defined zero point or initial value. Tarring can be done within the entire weighing range of the balance.

By maintaining one surface of the substrate at lower temperature, by keeping it on an ice block and leaving the other surface to atmospheric conditions, the humidity present in the atmosphere condense on the surface that is open to atmosphere and finally gives water droplets. For this to happen, there must be a temperature difference and the substrates are kept on ice block and left for some time. The procedure for measuring the condensate on each surface is as follows.

E-ISSN 2581 - 7957
P-ISSN 2277 - 3916


DOI: 10.32377/cvrjst 1917

First, dry weight of each material is measured with the use of a micro weighing machine. Then the materials are placed on an ice block and left there for some time about five minutes. Then measure the wet weight. Subtracting the wet weights and dry weights of the substrates gives condensate weights. This is repeated and all the values are tabulated. This procedure is followed for all other elastomer surfaces made up of different mass fractions of Aluminum inclusions. All the weight measurements are done with help of micro weighing machine. And all the measurements are taken in similar ambient conditions.

### *C. Relative Humidity:*

Dew condensation rates on different substrates with different amounts of Aluminum metal powder inclusions are tabulated and humidity calculations are done by using wet bulb and dry bulb temperatures. By taking these dry and wet bulb temperatures and with the help of psychometric chart the percentage of relative humidity present in the room is determined. While taking the condensation measurements for the different concentrations of Aluminium powder included elastomer substrates, these dry bulb and wet bulb temperatures are taken in the surroundings.

## III. Results and Discussions

### *A. Dew on plain metal surface and PDMS Surface:*

By taking two metal pieces of same dimensions (here Aluminium metal plates) and comparing the dew formation on both plates, one is plain metal surface and other is a PDMS surface, it is observed that dew formation on PDMS surface is higher than on the plain metal surface. By pouring the elastomer mixture on surface of flat metal plate and allowing it to cool for about 48 hours at normal room temperature, the mixture gets solidified and gives a PDMS surface on metal plate. For comparing dew on these surfaces, both plates are maintained at lower temperature so that dew is formed on surface of the plates. For this, both plates are placed in a refrigerator for some time and after taking them out they are kept in atmosphere until dew is formed on the surface. When observed dew formation on metal with PDMS surface is higher than plain metal surface as shown in Figure 3.

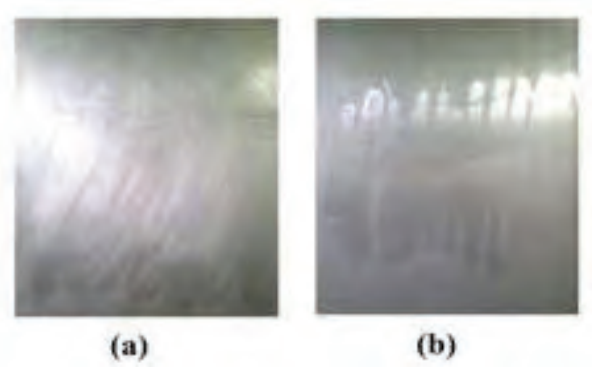


Figure 3 Dew formation on substrates (a) Plain metal surface (b) Plain PDMS surface

### *B. Dew measurement on different PDMS Substrates:*

As dew formation on any substrate is controlled by surface properties and the wetting properties of the surface, PDMS surfaces are used with different amounts of Aluminium metal powder inclusions. These substrates are compared with each other quantitatively for dew formation. After preparing PDMS substrates with different amounts of Aluminium metal inclusions, condensate weights are measured with the help of micro weighing machine.

Dew water on substrates with different Aluminium metal inclusions is measured. All the measurements are taken by same micro weighing machine and each substrate is prepared with 20 grams of Silicone base material. The surface areas of all substrates are equal, and diameter of each material is 120 mm. The nucleation of metal in PDMS substrates cools faster and results in a good condensation on the substrate. Condensation of dew and formation of water droplets can be seen in following Figure 4.

Figure 4. Dew formation on PDMS substrates.

**1. Dew water condensation on substrates with 0.001, 0.002, 0.004 and 0.01 grams of Aluminium metal inclusions. Test time: 5 minutes**

I. Substrate 1: 20 g.Silicone + 0.001 g. Al powder.

TABLE I.

| Test No. | Dry weight, g | Weight after condensation, g | Condensate Water weight, g |
|---|---|---|---|
| 1 | 10.1826 | 10.4100 | 0.2274 |
| 2 | 10.1822 | 10.4030 | 0.2208 |
| 3 | 10.1818 | 10.3907 | 0.2089 |
| 4 | 10.1820 | 10.4050 | 0.2230 |
| 5 | 10.1819 | 10.4325 | 0.2506 |

E-ISSN 2581 - 7957
P-ISSN 2277 - 3916

CVR Journal of Science and Technology, Volume 19, December 2020
DOI: 10.32377/cvrjst 1917

II. Substrate 2: 20 g. Silicone + 0.002 g. Al powder.

TABLE II.

| Test No. | Dry weight, g | Weight after condensation, g | Condensate Water weight, g |
|---|---|---|---|
| 1 | 10.4046 | 10.6374 | 0.2328 |
| 2 | 10.4038 | 10.6369 | 0.2331 |
| 3 | 10.4038 | 10.6301 | 0.2263 |
| 4 | 10.4032 | 10.6345 | 0.2313 |
| 5 | 10.4033 | 10.6607 | 0.2574 |

III. Substrate 3: 20 g. Silicone + 0.004 g. Al powder.

TABLE III.

| Test No. | Dry weight, g | Weight after condensation, g | Condensate Water weight, g |
|---|---|---|---|
| 1 | 11.2543 | 11.4946 | 0.2403 |
| 2 | 11.2537 | 11.4693 | 0.2156 |
| 3 | 11.2539 | 11.4613 | 0.2074 |
| 4 | 11.2538 | 11.4772 | 0.2234 |
| 5 | 11.2540 | 11.4950 | 0.2410 |

IV. Substrate 4: 20 g. Silicone + 0.01 g. Al powder. (Test time: 5 minutes)

TABLE IV.

| Test No. | Dry weight, g | Weight after condensation, g | Condensate Water weight, g |
|---|---|---|---|
| 1 | 11.3696 | 11.6250 | 0.2554 |
| 2 | 11.3696 | 11.6148 | 0.2449 |
| 3 | 11.3698 | 11.5847 | 0.2149 |
| 4 | 11.3700 | 11.5899 | 0.2199 |
| 5 | 11.3693 | 11.6125 | 0.2432 |

From Table I to Table IV, data gives weights of condensed water for the substrates with 0.001, 0.002, 0.004 and 0.01grams of Aluminium metal included silicone elastomer substrates. Here only very few amounts of metal inclusions are added to maintain the transparency of the substrates to use them for the solar still applications. And from the values it is understood that with increase in metal inclusions, the condensate weight is also increased as expected.

**2. Dew water condensation on substrates with 0.000, 0.008, 0.005, 0.01, 0.015, 2.00 and 5.00 grams of Aluminium inclusions is as follows.**

I. Substrate 1: 20 g. Silicone + 0.000 g. Al powder. (Test time: 5 minutes)

TABLE V.

| Test No. | Dry weight, g | Weight after condensation, g | Condensate Water weight, g |
|---|---|---|---|
| 1 | 12.137 | 12.2697 | 0.1327 |
| 2 | 12.1344 | 12.2442 | 0.1098 |
| 3 | 12.1348 | 12.2475 | 0.1127 |
| 4 | 12.136 | 12.2518 | 0.1158 |
| 5 | 12.1356 | 12.2566 | 0.121 |

II. Substrate 2: 20 g. Silicone + 0.005 g. Al powder. (Test time: 5 minutes)

TABLE VI.

| Test No. | Dry weight, g | Weight after condensation, g | Condensate Water weight, g |
|---|---|---|---|
| 1 | 11.9855 | 12.0937 | 0.1082 |
| 2 | 11.9813 | 12.0804 | 0.0991 |
| 3 | 11.981 | 12.0873 | 0.1063 |
| 4 | 11.9831 | 12.0849 | 0.1018 |
| 5 | 11.9827 | 12.0854 | 0.1027 |

III. Substrate 3: 20 g. Silicone + 0.008 g. Al powder. (Test time: 5 minutes)

TABLE VII.

| Test No. | Dry weight, g | Weight after condensation, g | Condensate Water weight, g |
|---|---|---|---|
| 1 | 11.7074 | 11.8198 | 0.1124 |
| 2 | 11.7037 | 11.8432 | 0.1395 |
| 3 | 11.7033 | 11.8189 | 0.1156 |
| 4 | 11.7037 | 11.823 | 0.1193 |
| 5 | 11.7051 | 11.824 | 0.1189 |

E-ISSN 2581 - 7957
P-ISSN 2277 - 3916

CVR Journal of Science and Technology, Volume 19, December 2020
DOI: 10.32377/cvrjst 1917

### IV. Substrate 4: 20 g. Silicone + 0.01 g. Al powder. (Test time: 5 minutes)

TABLE VIII.

| Test No. | Dry weight, g | Weight after condensation, g | Condensate Water weight, g |
|---|---|---|---|
| 1 | 12.5335 | 12.6451 | 0.1116 |
| 2 | 12.5296 | 12.6622 | 0.1326 |
| 3 | 12.5299 | 12.676 | 0.1461 |
| 4 | 12.529 | 12.6773 | 0.1483 |
| 5 | 12.5288 | 12.6691 | 0.1403 |

### V. Substrate 5: 20 g. Silicone + 0.015 g. Al powder. (Test time: 5 minutes)

TABLE IX.

| Test No. | Dry weight, g | Weight after condensation, g | Condensate Water weight, g |
|---|---|---|---|
| 1 | 11.1329 | 11.2232 | 0.0903 |
| 2 | 11.1293 | 11.2545 | 0.1252 |
| 3 | 11.1286 | 11.2421 | 0.1135 |
| 4 | 11.1295 | 11.2393 | 0.1098 |
| 5 | 11.1288 | 11.2464 | 0.1176 |

### VI. Substrate 6: 20 g. Silicone + 2.0 g. Al powder. (Test time: 5 minutes)

TABLE X.

| Test No. | Dry weight, g | Weight after condensation, g | Condensate Water weight, g |
|---|---|---|---|
| 1 | 12.3042 | 12.4087 | 0.1045 |
| 2 | 12.3014 | 12.4168 | 0.1154 |
| 3 | 12.3004 | 12.3942 | 0.0938 |
| 4 | 12.301 | 12.3962 | 0.0952 |
| 5 | 12.3016 | 12.409 | 0.1074 |

### VII. Substrate 7: 20 g. Silicone + 5.0 g. Al powder. (Test time: 5 minutes)

TABLE XI.

| Test No. | Dry weight, g | Weight after condensation, g | Condensate Water weight, g |
|---|---|---|---|
| 1 | 12.358 | 12.4617 | 0.1037 |
| 2 | 12.3568 | 12.4571 | 0.1003 |
| 3 | 12.3561 | 12.441 | 0.0849 |
| 4 | 12.357 | 12.4732 | 0.1162 |
| 5 | 12.3565 | 12.451 | 0.945 |

From the above set of tables, the values of dry weights, wet weights and condensate weights are calculated and compared for the different values of Al particle inclusions.

### *C. Relative humidity measurement:*

The relative humidity varies from 52% to 46% within the span of two hours. Where dry bulb temperatures are 32 $^0$C to 33 $^0$C and wet bulb temperature is 24 $^0$C. From the measurements of relative humidity, by calculating mass fraction of Al for each substrate.

TABLE XII.

| S. No. | Mass fraction of Aluminium | Mean condensation rate, g/s | Standard deviation, g/s |
|---|---|---|---|
| 1 | 0 | 344.92 | 0.87 |
| 2 | 0.0002499 | 364.17 | 4.67 |
| 3 | 0.0003998 | 374.67 | 12.33 |
| 4 | 0.0004998 | 407.0 | 4.33 |
| 5 | 0.000749 | 369.08 | 2.67 |
| 6 | 0.0909091 | 344.0 | 2.33 |
| 7 | 0.2 | 341.08 | 1.77 |

E-ISSN 2581 - 7957
P-ISSN 2277 - 3916

CVR Journal of Science and Technology, Volume 19, December 2020
DOI: 10.32377/cvrjst 1917

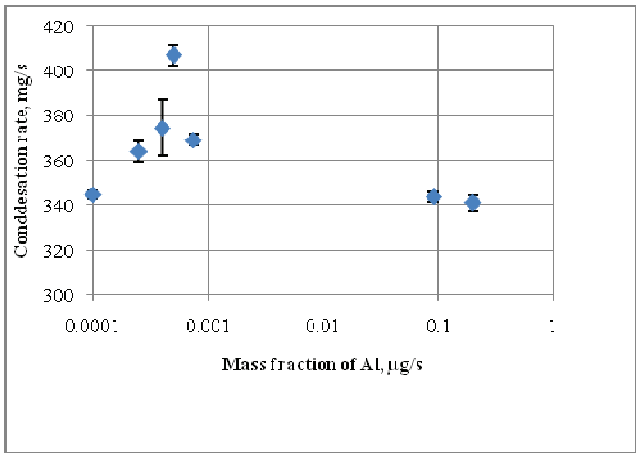


Figure 5. Condensation rate to the mass fraction of Aluminium

From the above graph, the rate of condensation on silicone substrate is gradually increasing and then decreasing with the addition of Aluminium powder to the silicone elastomer. For the weight of 0.010 g. Aluminium powder the substrate is giving more condensed water. From 0 g. to 0.010 g., condensation rate is gradually increasing. And with more amounts of Aluminium powder inclusion, condensation rate is decreasing.

## IV. Conclusions

### *Summary*

The objective is to understand the working of a solar still and to improve its efficiency by using alternative PDMS surfaces. By replacing conventional transparent glass surfaces with these PDMS substrates with small amounts of metal inclusions, better condensation rates are possible. And without changing any wetting properties of the surfaces there is a possibility of getting good amount of distilled water without using any electrical or mechanical power. A sheet of polyethylene, assuming that there is no evaporation and that all the condensed water flows into a vessel, should yield approximately 1liter per square meter surface area under the meteorological conditions. Hence, practical utilization of dew contained in the air is possible. Further by including small amounts of metal inclusions in these PDMS substrates, the condensation rate is varying and for a particular amount of inclusions, condensation is the maximum depending on the ambient conditions.

### *Future Work*

It is found that the condensation efficiency of water is higher with partial introduction of Aluminium nucleation sites. And aslo it is observed that the condensation efficiency is a non-monotonic function of the Aluminium mass fraction in the substrate, where peak condensation efficiencies were observed at a critical mass fraction of Aluminium.

Future work can take advantage of these conclusions by building a solar still that uses PDMS / Al substrates as condensation surface and manifest higher condensation efficiencies than either pure PDMS or pure Aluminium surfaces. In addition, the partial introduction of Al into PDMS maintains the transparency characteristics of the surface, allowing sunlight to pass through the substrate.

## References

[1] Prof. Alpesh Mehta “Design of solar distillation system”. *International journal of advanced science and technology*, vol 29, April 2011.

[2] D. Beysens, "The formation of dew" *Atmospheric Research* 39 (1995) 215-237.

[3] Jaffrin, A., Makhlouf S., Scotto la Massese C., Bettachini,A. ansVoisin, R., 1989.Sigsbee, R.A., 1969. “Vapor to condensed-phase heterogeneous nucleation. In: A.C” Zettlemoyer (Editor), Nucleation. Marcel Decker, New York, pp. 151-224.

[4] Platten, J.K.and Legros, J.C. “Convection in liquids”. Springer, Heidelberg.

[5] Family, F.and Meakin, P., “Scaling of the droplet-size distribution in vapor-deposited thin films.” *Phys. Rev. Lett.,* 61: 428-431.

[6] V.S. Nikolayev, D. Beysens, A. Gioda, I. Milimouk, E. Katiushin, J.P. Morel. “Water recovery from dew”. TB-215D, *Pinnacle series Analytical and precision balances*.

E-ISSN 2581 - 7957
P-ISSN 2277 - 3916

CVR Journal of Science and Technology, Volume 19, December 2020
DOI: 10.32377/cvrjst 1918

# Modelling and Analysis of Brake Drum using ANSYS Workbench

C. Sai Kiran[1], M. Ravi Kumar[2], P. Srinivas Reddy[3] and T. Venkatesh[4]
[1]Asst. Professor, CVR College of Engineering/Mechanical Engg. Department, Hyderabad, India
Email: csaikiran001@gmail.com
[2]Asst. Professor, CVR College of Engineering/Mechanical Engg. Department, Hyderabad, India
Email: marripallyravikumar@gmail.com
[3]Asst. Professor, CVR College of Engineering/Mechanical Engg. Department, Hyderabad, India
Email: srinivasrdd87@gmail.com
[4]Asst. Professor, CVR College of Engineering/Mechanical Engg. Department, Hyderabad, India
Email: venkatesh2711991@gmail.com

***Abstract:*** **In this paper, a brake drum was modelled and analyzed which is useful for slowing or completely stopping a moving vehicle. Brake drum is a critical part of the safety system, which is used to prevent the motion of vehicle. The purpose of the work is to find a suitable brake drum material which will be able to stop the vehicle within a minimum distance in case of emergency. Brake drum is modelled in CREO software and analysis of brake drum was performed on three different materials i.e., Grey cast iron, Aluminum alloy and Carbon ceramics by using ANSYS software. Total deformation and Von-mises stress analysis help to predict the brake drum failure when an internal pressure acts on it.**

***Index Terms:*** **Brake drum, CREO, ANSYS, Von-mises stress.**

## I. Introduction

A brake is a device which inhibits the motion of a vehicle. Brake absorbs kinetic energy of the vehicle and decelerates the vehicle motion. Brake drum is connected to the wheels of an automobile for slowing or stopping the vehicle. A brake drum is one type of a brake, which uses friction caused by the set of brake shoes, pressed against a rotating drum. Capacity of any brake device depends on the unit pressure between the braking surface and coefficient of friction.

Sankara et al. [1] has modelled a brake drum design to withstand high temperature and thermal stresses when brakes are applied. The brake drum is modelled in Solidworks2016 software. Structural and thermal analysis is performed in ANSYS workbench software. After modelling the brake drum, pressure of 1.5 MPa and 90 degrees temperature is applied for carbon steel and grey cast iron material. Von-mises stress and total deformation values are observed in the results.

Meenakshi and suman [2] has designed a brake drum for a two-wheeler through reverse engineering approach. Six different materials for brake drum are considered and different stresses, deformation values, rise in temperature on different braking time and heat transfer rate values are obtained. The brake drum is modelled by using CAD software and analyzed in ANSYS workbench 14.5 software. In the results, deflection and stress induced in the brake drum with gradual and sudden braking is observed.

Raju et al. [3] has designed a 3D model of brake drum by using AutoCAD software. In brake drum, kinetic energy is converted into friction and the heat is to be dissipated into the atmosphere. Steady state and transient analysis are performed on brake drum by considering three different materials by using ANSYS software. Steady state analysis was performed to validate the temperature distribution of the brake drum. To determine the thermal flux for different time intervals, transient analysis is performed.

Sagar and dabade [4] have modelled a brake drum using UG-NX 8.5 software. By using analysis software, transient thermal analysis has performed on the brake drum and brake drum has been modified based on the results.

Venkataramana [5] has been modelled and analyzed the brake drum by using ANSYS APDL 10 software. Brake drum of tata indica car and tata nano car is considered for performing thermal and structural analysis.

Anup and sabarish [6] have modelled a brake drum using Pro/ENGINEER software. Structural and thermal analysis is performed by considering the shoe pressure on the brake drum.

Gowthami and balaji [7] has designed a 3D model of brake drum by using AutoCAD software. Thermal flux and steady state conditions are applied for three different materials in ANSYS by applying one Newton pressure. After observing the results for three different materials, aluminium is proved as a better material than other brake drum materials.

Yang et al. [8] has modelled a brake drum using Solidworks software. Modal analysis of brake drum is performed by using ANSYS workbench software. Modal analysis is performed for first 12 natural frequencies to understand deformations for twelve different mode shapes.

Rambabu et al. [9] has focused on designing a standard brake drum by using weight reduction approach. All the different parts of brake drums are designed and assembled in 3D CAD modelling software. Hexahedral finite element model of brake drum is prepared by using CAE processing software. The design iterations are solved by using non-linear/linear finite element solver.

Chiranjeevi and sreenivasulu [10] have modelled a brake drum by using AutoCAD software. Steady state and transient analyses were performed by using Ansys 10.0

E-ISSN 2581 - 7957
P-ISSN 2277 - 3916

CVR Journal of Science and Technology, Volume 19, December 2020
DOI: 10.32377/cvrjst 1918

software. In analysis, four cyclic braking conditions to determine the thermal deformations and peak temperature developed in the brake drum.

Sinha and gurumeet [11] have created a brake drum model with fins by using Creo parametric software. CFD analyses are performed by considering different materials for brake drum. CFD is performed to determine heat flux, heat transfer coefficient and heat transfer rate by using Ansys Fluent software.

Bakoet al. [12] has developed a modified brake drum model which has extended fins along its circumference by using Solidworks 2013 software. These fins on the brake drum help to improve the heat dissipation rate from the surface of brake drums. The results of stress plot, displacement plot, strain plot and thermal plot are compared with modified finned brake drum and normal brake drum.

Abdul et al. [13] has designed the brake drum by using CATIA V5 software. By considering different loading conditions, structural analysis is performed by using ANSYS software.

### *A. Different Types of Brake Drum*

Brake drum is connected to either rear wheel of a vehicle or to every wheel of a vehicle. A brake drum is coupled with a spring, which is to be internally expanded or contract the brake shoe.


Figure 1. Brake Drum and its Parts

Brake drum is represented in Fig. 1. The main parts of a brake drum are brake shoes, wheel cylinder and shoe holding spring. Brake drums are mainly divided into three types depending on the brake shoes pressing the brake drum:

1. Twin leading shoe type.
2. Leading/trailing shoe type.
3. Duo-servo type.

Twin leading shoe type consists of two leading shoe and two wheel cylinder. In twin leading shoe type, the piston is expanded in both directions and applies equal pressure. This type is mainly used for front brakes of small and medium sized trucks.

In leading/trailing shoe type, two different brake shoes are used. The brake shoes are pressed in the same direction as the rotation of the brake drum, which applies greater pressure on the brake drum. This type is mainly used for the rear brakes of the passenger cars.

In duo-servo type, the primary and secondary brake shoe is linked together by an adjuster. Strong pressure from servo of the primary brake shoe is transmitted to the secondary brake shoe by the link and large braking force is generated. This type is mainly used for parking brakes on the passenger cars.

### *B. Working Principle of a Brake Drum*

Whenever a brake pedal is pressed by the driver, then the brake booster or servo system helps the master cylinder to send the brake oil to the wheel cylinder. Piston is expanded in the wheel cylinder and it will apply pressure on the two curved brake shoes. These two curved brake shoes will be pressed against the inner surface of a rotating brake drum. This contact pressure will create the necessary friction, which enables to slow down or stop the moving vehicle. Therefore, it is very important to design all the components of the brake drum such a way that it can efficiently dissipate the heat to the atmosphere. The working principle of a brake drum is shown in Fig.2.

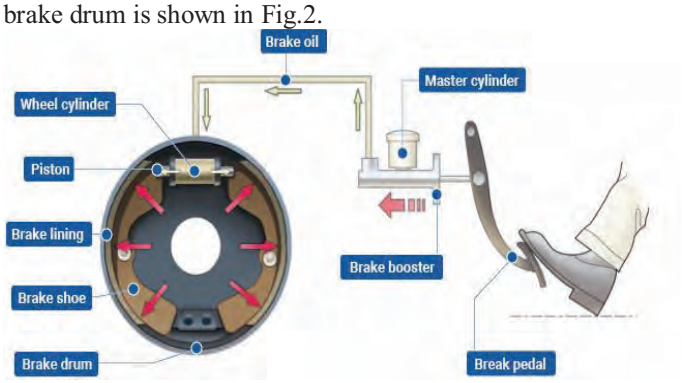


Figure 2. Working Principle of a Brake Drum

### *C. Brake Drum Material*

Brake drums are generally made of materials which are strong enough to withstanding pressure on it and to dissipate heat effectively to atmosphere. Grey cast iron, aluminum alloy and carbon ceramics are the materials selected for brake drum as shown in Table I.

TABLE I.
MATERIAL PROPERTIES FOR DIFFERENT MATERIALS OF BRAKE DRUM

| S. No | Properties | Grey Cast Iron | Aluminum Alloy | Carbon Ceramics |
|---|---|---|---|---|
| 1. | Density (Kg/m$^3$) | 7,200 | 2,800 | 2,450 |
| 2. | Elastic Modulus (GPa) | 110 | 68 | 30 |
| 3. | Poisson's Ratio | 0.28 | 0.33 | 0.27 |
| 4. | Thermal conductivity (w/mK) | 54 | 170 | 40 |
| 5. | Coefficient of thermal expansion ($10^{-6}$/K) | 10.5 | 23 | 2.8 |

## II. MODELLING AND FINITE ELEMENT ANALYSIS

### *A. Brake Drum Model*

All the different parts of the brake drum are modelled separately as per the standard dimensions using CREO

E-ISSN 2581 - 7957
P-ISSN 2277 - 3916

CVR Journal of Science and Technology, Volume 19, December 2020
DOI: 10.32377/cvrjst 1918

parametric 2.0 software and all the individual parts of the brake drum are assembled in the CREO parametric 2.0 software as shown in Fig. 3

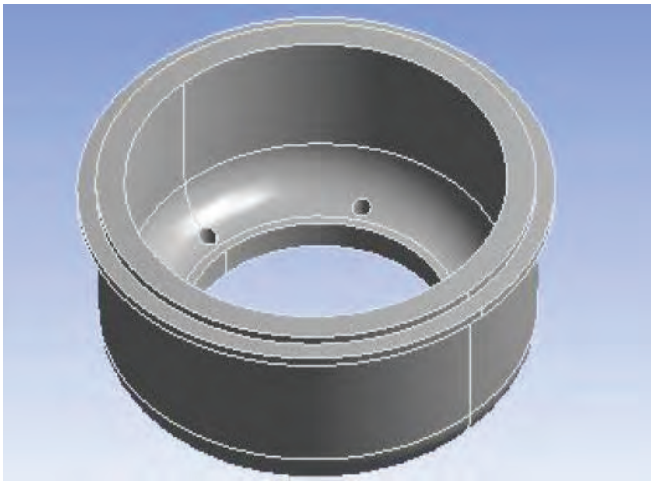

Figure 3. Assembled Model of Brake Drum in CREO

### B. Elememt Type

The element type selected for brake drum is SOLID 186. It is a 20-node higher order solid element which has three degrees of freedom per node. The three degrees of freedom are nodal x, y and z translations.

It exhibits quadratic displacement behavior and have spatial orientation. SOLID 186 support large strain capabilities, plasticity, large deflection, hyper elasticity, stress stiffening and creep. SOLID 186 have capability for simulating deformations of incompressible elastoplastic materials and incompressible hyper-elastic materials.

### C. Meshing

In meshing, the created 3D model is divided into the certain number of divisions or elements for accurate analysis result. By applying meshing on the model, we can determine the effectiveness and efficiency of any analysis. An automated mesh is generated on the created model which is shown in Fig. 4.

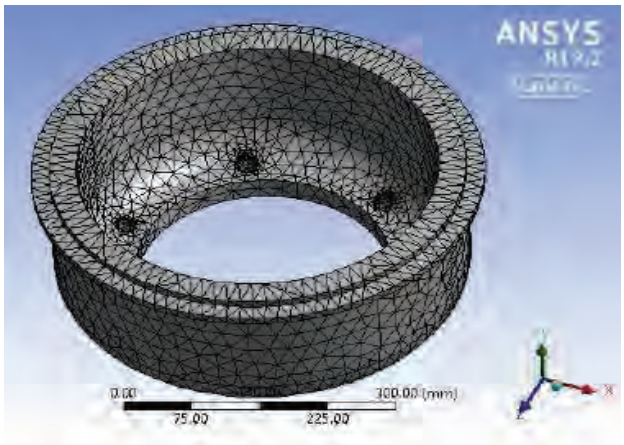


Figure 4. Meshing of Brake Drum

In the automatic mesh, the mesh applied was a fine mesh for achieving precise and accurate results. Instead of using a fine mesh on all the components of the model, coarse mesh was applied on larger area and fine mesh was applied only on the area of higher stress concentration.

### D. Applying Loads

On bottom of the brake drum, a fixed support is assigned to withstand the pressure acting on the brake drum as shown in Fig. 5.

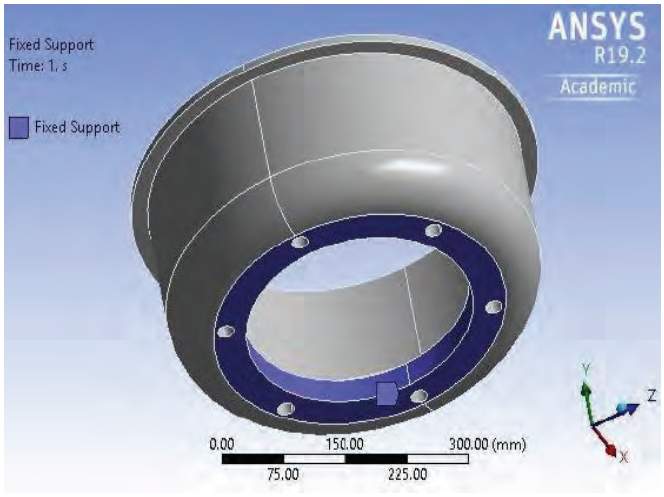


Figure 5. Fixed Support on Bottom of Brake Drum

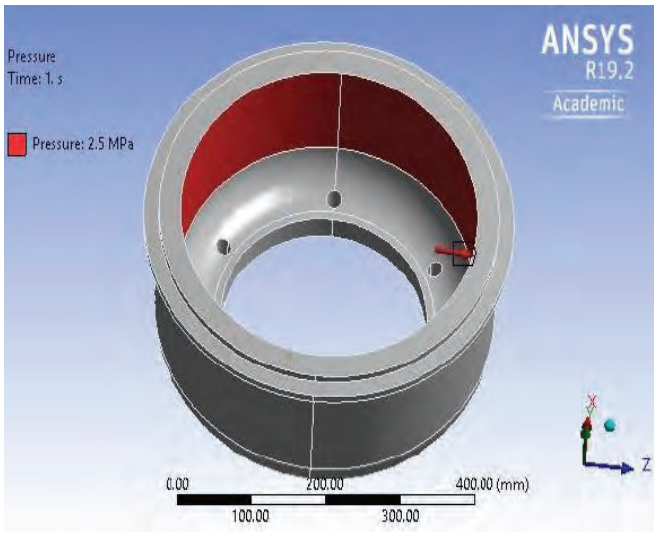


Figure 6. Applying Internal Pressure on Brake Drum

Brake shoe applies internal pressure of 2.5 MPa on the brake drum. For applying the load on the brake drum, the maximum pressure a driver can apply is calculated applied on the brake drum as shown in Fig. 6.

## III. Results and Discussions

After assigning fixed support on bottom and applying internal pressure on the brake drum, structural analysis is performed on the brake drum for three different materials in ANSYS workbench to determine the total deformation and von-mises stress. The following results were observed in the analysis.

E-ISSN 2581 - 7957
P-ISSN 2277 - 3916

CVR Journal of Science and Technology, Volume 19, December 2020
DOI: 10.32377/cvrjst 1918

### *A. Total Deformation of Brake Drum*

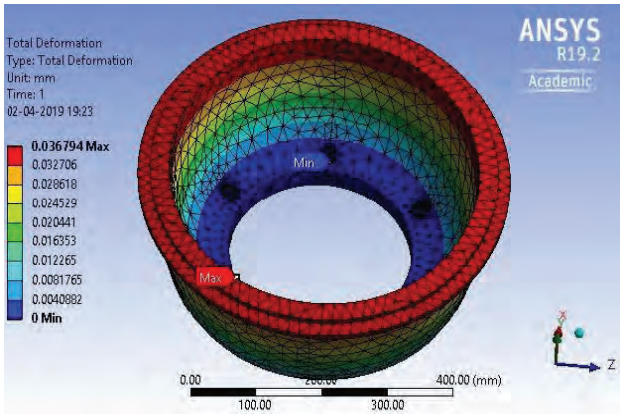


Figure 7. Total Deformation of Grey Cast Iron Material

After performing structural analysis by applying the load on brake drum for grey cast iron material, a maximum total deformation of 0.036 mm is observed from the Fig. 7.

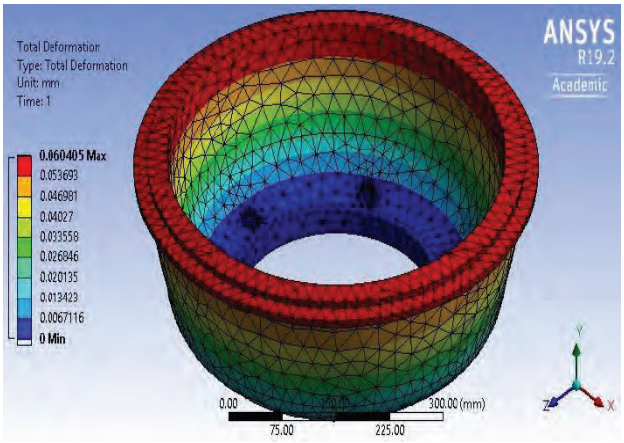


Figure 8. Total Deformation of Aluminum Alloy Material

After performing structural analysis by applying the load on brake drum for aluminum alloy material, a maximum total deformation of 0.06 mm is observed from the Fig. 8.

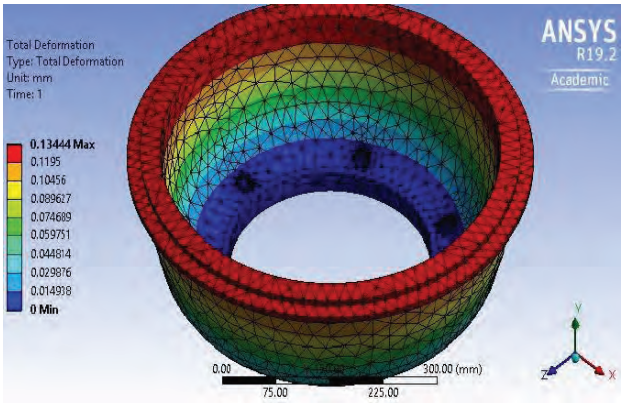


Figure 9. Total Deformation of Carbon Ceramics Material

After applying the load on brake drum, structural analysis is performed on carbon ceramics material. A maximum total deformation of 0.133 mm is observed from the Fig. 9.

### *B. Von-mises Stress of Brake Drum*

After performing structural analysis by applying the load on brake drum for grey cast iron material, maximum von-mises stress of 20.2 MPa and minimum von-mises stress of 0.002 MPa are observed from the Fig. 10.

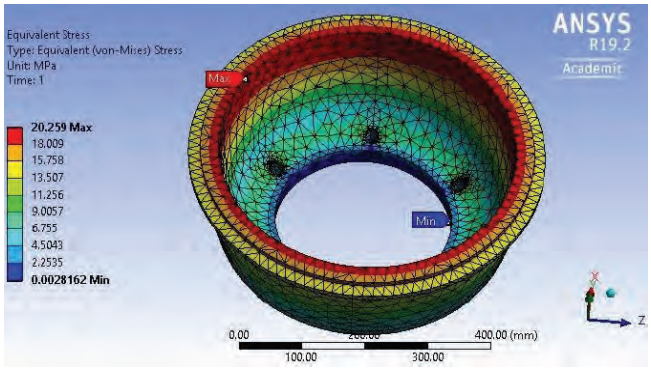


Figure 10. Von-mises Stress of Grey Cast Iron Material

After applying the load on brake drum for aluminum alloy material, maximum von-mises stress of 20.36 MPa and minimum von-mises stress of 0.001 MPa are observed from the Fig. 11.

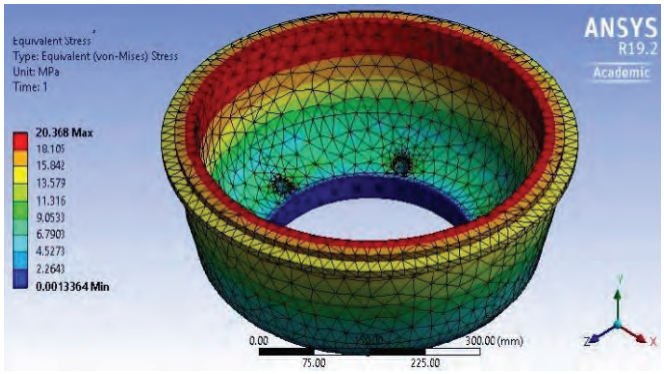


Figure 11. Von-mises Stress of Aluminum Alloy Material

After applying the load on brake drum for carbon ceramics material, maximum von-mises stress of 20.236 MPa and minimum von-mises stress of 0.003 MPa is observed from the Fig. 12.

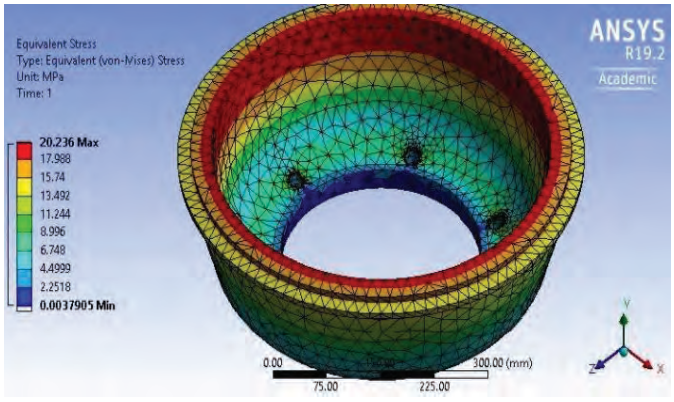


Figure 12. Von-mises Stress of Carbon Ceramics Material

CVR Journal of Science and Technology, Volume 19, December 2020
DOI: 10.32377/cvrjst 1918

The graph of total deformation for three different materials is observed from the Fig. 13.

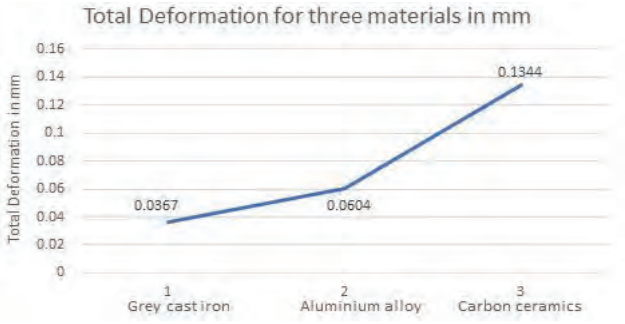


Figure 13. Total Deformation Graph for Different Materials

The graph of von-mises stress for three different materials is observed from the Fig. 14.

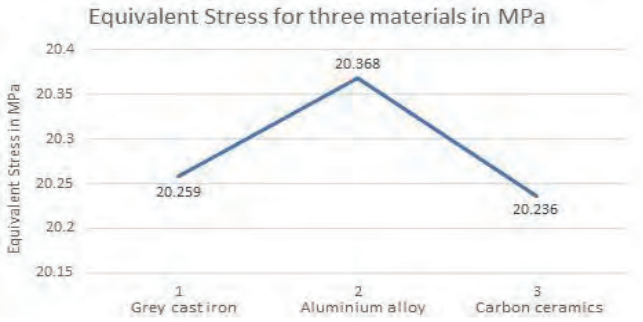


Figure 14. Equivalent Stress Graph for Different Materials

The results of total deformation in mm and Equivalent stress in MPa for three different brake drum materials are represented in Table II.

TABLE II.
RESULTS COMPARISON FOR BRAKE DRUM MATERIAL

| Material | Total Deformation (mm) | Equivalent Stress(MPa) |
|---|---|---|
| Grey Cast Iron | 0.0367 | 20.259 |
| Aluminum Alloy | 0.0604 | 20.368 |
| Carbon Ceramics | 0.1344 | 20.236 |

## IV. CONCLUSIONS

In this paper, Creo parametric 2.0 software is used for modelling the brake drum and analysis of brake drum with an internal pressure of 2.5MPa is analyzed by using ANSYS workbench software.

From the results, it is observed that the maximum total deformation is observed in carbon ceramics because of presence of carbon and the minimum total deformation is observed in grey cast iron material. Maximum von-mises stress is observed in aluminium alloy and the minimum von-mises stress is observed in carbon ceramics material. The values of von-mises stress and total deformation of the brake drum obtained are within their allowable values. Therefore, modelled brake drum design is safe based on the strength and rigidity criteria.

## REFERENCES

[1] K. Sankara Narayanan, J. L. Miren Kishan, Ben Mathew Augustine and D. Vijayaganapathy, "Parametric modelling of brake drum and dynamic analysis for different materials," *International Journal of Pure and Applied Mathematics*, vol. 120, Issue 6, ISSN 1314-3395,pp. 3919-3931, June 2018.

[2] Meenakshi Kushal and Suman Sharma, "Optimization of design of brake drum of two wheeler through approach of reverse engineering by using ansys software," *IOSR Journal of Mechanical and Civil Engineering (IOSR-JMCE)*, vol. 12, Issue 4, e-ISSN 2278-1684, p-ISSN: 2320-334X.pp. 70-75, August 2015.

[3] P Lakshminarayana Raju, P Hussain, A Ramanjaneya Reddy, B Sidda Reddy and S Sudhakar Babu, "Design and analysis of a brake drum by using finite element method," *International Journal of Mechanical Engineering Research and Technology*, vol. 2, Issue 2,ISSN 2454-535X, pp. 51-72, May 2016.

[4] Sagar N. Taleand B. M. Dabade, "Customization & analysis of brake drum," *Journal of Basic and Applied Engineering Research*, vol. 3, Issue 7, p-ISSN 2350-0077, e-ISSN 2350-0255,pp. 575–579, June 2016.

[5] P Venkataramana, "Design of a brake drum using finite element method," *International Journal of Mechanical Engineering and Robotics Research*, vol. 2, Issue 2, pp. 101–105, April 2013.

[6] Anup Kumar, and R. Sabarish, "Structural and thermal analysis of brake drum," *Middle-East Journal of Scientific Research*, vol. 20, Issue 8, ISSN 1190-9233, pp. 1012–1016, 2014.

[7] K. Gowthamiand K. Balaji, "Designing and analysis of brake drum," *International Journal for Research in Applied Science & Engineering Technology*, vol. 4, Issue 9, ISSN 2321-9653,pp. 135–142, September 2016.

[8] Dan Yang,Zhen Yu, Leilei Zhangand Wentao Cheng, "Modal analysis of automobile brake drum based on ansys workbench," *Advances in Computer Science Research*, vol. 75, pp. 608–612, 2017.

[9] D. Rambabu, R. Gopinath, U. Senthil Rajan and G. B. Bhaskar, "Weight reduction of a standard brake drum: a design approach," *International Journal of Engineering & Technology*, vol. 3, Issue 2, pp. 201–207, 2014.

[10] M. Chiranjeevi and B. Sreenivasulu, "Thermal analysis of brake drums at various temperatures,"*Iconic Research and Engineering Journals*, vol. 2, Issue 5, ISSN 2456-8880, pp. 79–82, November 2018.

[11] Yogeshwar Sinha and Gurmeet Singh Gahir, "Modeling and analysis of brake drum with extended fins on the circumference of drum to improve heat dissipation: a CFD approach,"*Research Journal of Engineering Sciences,* vol. 7, Issue 5, ISSN 2278 – 9472, pp. 1–6, May 2018.

[12] Bako Sunday, Usman Aminu, Paul O. Yahaya and Mohammed B. Ndaliman, "Development and analysis of finned brake drum model using solidworks simulation," *International Journal of Innovative Research in Science, Engineering and Technology*, vol. 4, Issue 5, ISSN2319 - 8753, pp. 3651–3658, May 2015.

[13] Mohammed Abdul Aleem, Asrar Ahmed Saad, Abdul Sohail, Shaik Mohammed Siraj and M. Raghunath Reddy, "Design and analysis of drum brakes," *International Journal of Advanced Technology and Innovative Research*, vol. 10, Issue 4, ISSN2348-2370, pp. 348–354, April 2018.

E-ISSN 2581 - 7957
P-ISSN 2277 - 3916

CVR Journal of Science and Technology, Volume 19, December 2020
DOI: 10.32377/cvrjst 1919

# Performance and Emission Characteristics of Diesel Engine by Semi Ellipsoidal Arc Grooves on Piston Crown

Sk. Mohammad Shareef[1], A.L.N. Arun Kumar[2], T. Venkatesh[3] and M. RaviKumar[4]
[1]Asst. Professor, CVR College of Engineering/Mechanical Engg. Department, Hyderabad, India
Email: shareefshaik4@gmail.com
[2]Asst. Professor, CVR College of Engineering/Mechanical Engg. Department, Hyderabad, India
Email: aln.arunkumar@gmail.com
[3]Ast. Professor, CVR College of Engineering/Mechanical Engg. Department, Hyderabad, India
Email: venkatesh2711991@gmail.com
[4]Asst. Professor, CVR College of Engineering/Mechanical Engg. Department, Hyderabad, India
Email: marripallyravikumar@gmail.com

***Abstract:*** **Direct injection diesel engines are very useful in heavy duty vehicles as well as light duty vehicles. Direct injection diesel engine emits significant amount of pollutants such as HC, CO, NOx and soot etc., which are harmful to the environment. These pollutants formed due to improper combustion in combustion chamber. In the present experimental attempt is made to study the performance and emission characteristics of diesel engine by adding the semi ellipsoidal arc grooves on piston crown. The tests are performed at two, three and five groves on piston crown of diesel engine [ 2EGP,3EGP and 5EGP]. The grooves on the piston crown creates turbulence and proper mixing of air and fuel in combustion chamber which helps to create proper combustion and leads to decrease the formation of pollutants as compared to normal diesel engine. From the experimental investigations, it is concluded that three ellipsoidal grooves arc pistons [3EGP] has less emissions and high performance than that of other type of pistons.**

***Index Terms:*** **Ellipsoidal arc grooves, Piston crown, Diesel engine, Performance and Emissions**

## I. Introduction

It is well-known that in DI diesel engines swirl motion is required for proper mixing of fuel and air. Moreover, the efficiency of diesel engines is often improved by increasing the burn rate of fuel air mixture. This can be achieved in two ways, one by designing the combustion chamber and two by providing the intake system so it can create a swirl motion to the incoming air.

In this experimental work is conducted on single cylinder 4-stroke DI diesel engine with semi hemispherical bowl [1],[2],[8] in the piston to study the effect of groves on fluid flow and on the engine performance.

Experiments are carried out to measure the performance and emission characteristics of two, three and five ellipsoidal groves on piston crown. The result of grooves on piston head and optimum number of grooves for better performance is discussed. It is observed from the experiments, is that three ellipsoidal grooves (3EGP) is better than two and five ellipsoidal grooves (2EGP, 5EGP) for conventional engine.

## II. Literature Survey

J.Li et.al [1] has conducted simulation work using CFD on different types combustion chamber i.e. hemispherical combustion chamber (HCC), shallow depth combustion chamber (SCC) and omega combustion chamber (OCC).This project conclude that at low speed SCC is favorable and at high speed hemispherical combustion is favorable.

Nimesh. A. Patel et al [2] has conducted test on direct diesel engine by varying injection pressures and piston bowl geometry to reduce the emissions and performance of engine. In this study, hemisphere combustion chamber with circular arc on the periphery of the piston crown at $120^0$ is used for test and compared these results with hemispherical open type combustion chamber. The results show that Break thermal efficiency, exhaust gas temperature and $No_x$ is increased and break specific fuel consumption, HC emissions and CO emissions are decreased.

Venkata Ramesh Mailla et al [3] has conducted experiment on direct injection diesel engine by changing the combustion chamber design by using different blends of Jathropa Mythyl ester as alternative fuel and results are shown.

Md Nurun Nabi et al [5] has studied the performance of diesel engine and production of biodiesel from linseed oil. The performance characteristics like thermal efficiency, break thermal efficiency and emissions characteristics like CO, HC and $NO_x$ are calculated and shown in results.

A Swayamkumari et al [6] has done research on direct injection diesel engine for calculating the performance and emissions characteristics by using sunflower oil as biodiesel and the results are shown.

Sk. Gouse Ahamed et al [7] has conducted experiment on direct injection diesel engine by using apricot seed oil as bio diesel. Mechanical efficiency break thermal efficiency, CO, NOx and HC emissions are calculated and shown in results.

Banapurmath NR et al [8] has calculated the emissions characteristics and performance characteristics of direct injection diesel engine by changing the different shapes of piston geometry using mahua and neem oil as biodiesel.

CVR Journal of Science and Technology, Volume 19, December 2020
DOI: 10.32377/cvrjst 1919

B Naveen Kumar et al [9] has conducted experiment on diesel engine by changing the piston shape as toroidal using olive oil as biodiesel and results are calculated.

Y Shyamala et al [10] has conducted experiment on four stroke direct injection diesel engine by changing the combustion chamber as shallow depth combustion chamber using olive oil as biodiesel and results are calculated.

## III. Piston Modification

### *A. Piston Modifications*

The design of the combustion chamber and the fluid flow within the chamber are necessary for complete combustion. The main goal from the design of chamber geometry is to optimize the mixing of the fuel and air, before and during ignition, and to improve the flow of the exhaust products once combustion is complete.

The piston crown of 80 mm diameter of normal engine is changed by producing semi ellipsoidal arc grooves. In this work, two, three and five semi ellipsoidal arc grooves at $180^0$, $120^0$, $72^0$ on the pistons [2] with different widths of 10mm, 8mm and 6mm were created on three pistons of 80 mm diameter and continuing the depth of 3 mm prepared by CNC machine**.** The experiments were carried out with these pistons and their performance and emissions are compared with normal diesel engine [4].

### *B. Three types of semi-elliptical arc grooves*

a) Two groove elliptical piston

b) Three groove elliptical piston

c)Five groove elliptical piston

Figure 1. Two, Three and Five grooves elliptical piston

Fig.1 shows that two, three and five grooves elliptical pistons which are prepared by CNC machines used in diesel engine to find performance and emissions characteristics.

## IV. Experimental Setup

The experimental set up consists of KIRLOSKAR engine, DC alternator with resistance heaters, Rota meter, and digital RPM indicator fuel tank along with immersion heater, thermocouples, and manometer. The engine which is supplied by KIRLOSKAR make AV1 model diesel engine (crank started) of 5HP (3.7kW) capacity single cylinder water cooled diesel and the specifications are given in Table-II. For the measurement of emissions five-gas-analyzer is used. The fuel used for present work is diesel. The level of lubricating oil in the sump was checked periodically. Constant water flow was maintained through the engine to reduce the overheating of engine. All the readings were taken under steady running conditions.

E-ISSN 2581 - 7957
P-ISSN 2277 - 3916

CVR Journal of Science and Technology, Volume 19, December 2020
DOI: 10.32377/cvrjst 1919

TABLE I.
ENGINE SPECIFICATIONS

| Particulates | Specifications |
|---|---|
| Model | AV1 |
| Make | KIRLOSKAR |
| Engine type | Single cylinder, four strokes, Water cooled Compression ignition engine |
| Bore | 80 mm |
| Stroke | 110 mm |
| Speed | 1500 rpm |
| Rated power | 5HP |

Table I. Shows the Engine specifications which are used in this work.

### *A. Nomenclature*

i. Normal: Normal piston with pure diesel.
ii. 2EGP: Two semi ellipsoidal arc groove piston with pure diesel.
iii. 3EGP: Three semi ellipsoidal arc groove piston with pure diesel.
iv. 5EGP: Five semi ellipsoidal arc groove piston with pure diesel.

## V. RESULTS AND DISCUSSIONS

The performance of the engine is measured in the form of brake specific fuel consumption, brake thermal efficiency and mechanical efficiency. The exhaust emissions of the engine are measured in percentage of HC, $NO_x$, and CO [4]. The results acquired by the piston with grooves are compared with the normal piston.

### *A. Break Thermal Efficiency*

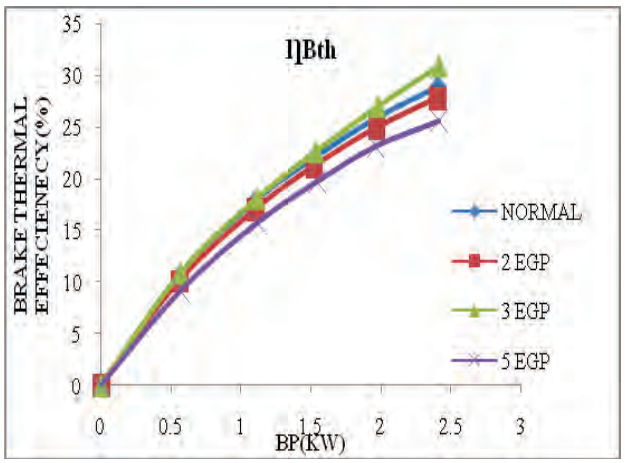


Figure 2. Brake power Vs Brake thermal efficiency with diesel

Fig.2 represents the variation of brake thermal efficiency with load for different Pistons with pure diesel. It is clear from the graph that 3EGP high break thermal efficiency as compared to other pistons. The brake thermal efficiency is found to increase by 6.27% for Normal piston with pure diesel of engine.

### *B. Break Specific fuel consumption*

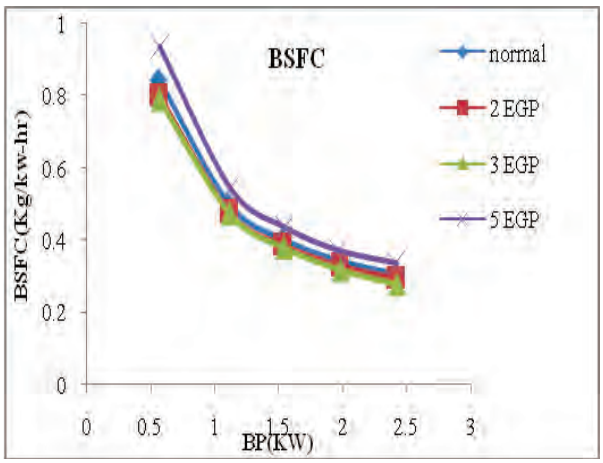


Figure 3. Brake power Vs Brake specific fuel consumption with Diesel

Fig.3 represents the variation of brake Specific fuel consumption with Diesel for different pistons of conventional engine. It is observed from graph that 3EGP has lower BSFC compare to other pistons. The BSFC is reduced about 10% compare to Normal piston.

### *C. Mechanical Efficiency*

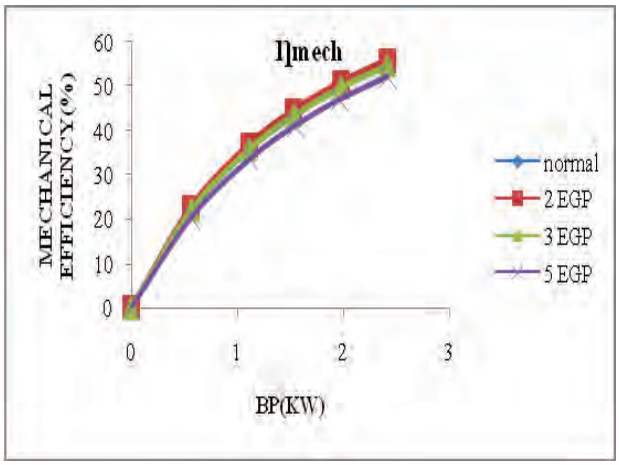


Figure 4. Brake power Vs Mechanical efficiency with Diesel

Fig.4 represents the variation of Mechanical efficiency with load for different Pistons. It is clear from the graph that 2EGP has slightly high mechanical efficiency compared to 3EGP piston in conventional engine.

E-ISSN 2581 - 7957
P-ISSN 2277 - 3916

CVR Journal of Science and Technology, Volume 19, December 2020
DOI: 10.32377/cvrjst 1919

### *D. Hydrocarbons Emissions*

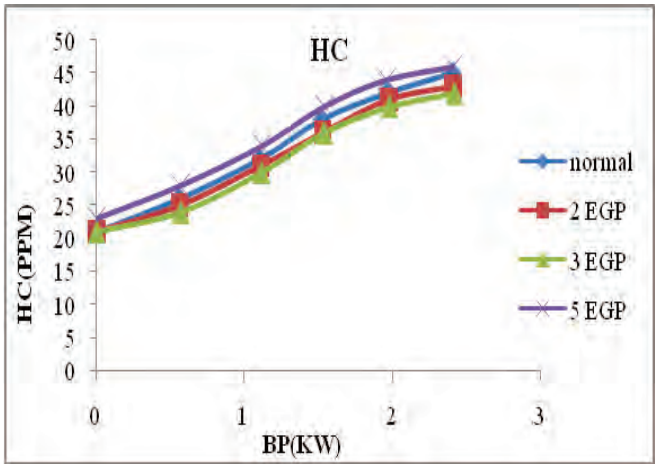


Figure 5. Brake power Vs HC emissions with Diesel

Fig.5 shows the HC emissions of diesel engine for different pistons. It shows that HC emission for 3EGP has less compare to other pistons because of proper atomization of fuel and air inside the combustion chamber.

### *E. Nitrogen Oxides ($NO_x$)*

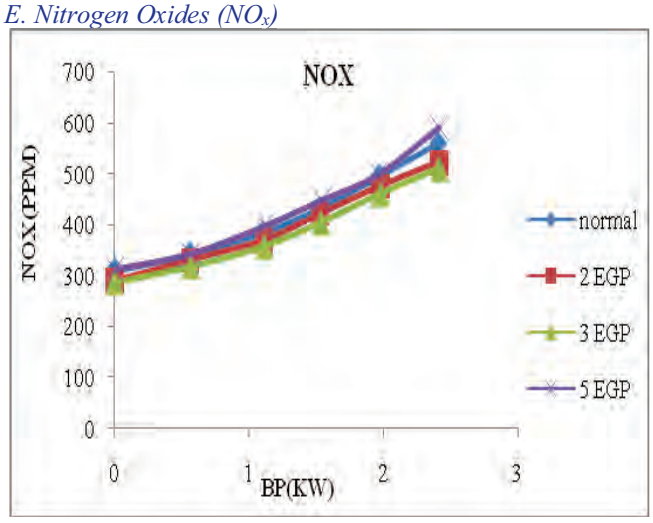


Figure 6. Brake power Vs $NO_x$ emissions with Diesel

Fig.6 shows the variation of $NO_x$ emissions with load for different pistons. It is clear from the graph that 3 EGP has low $NO_x$ emissions compared to other pistons in conventional engine.

### *F. Carbon Monoxide(CO)*

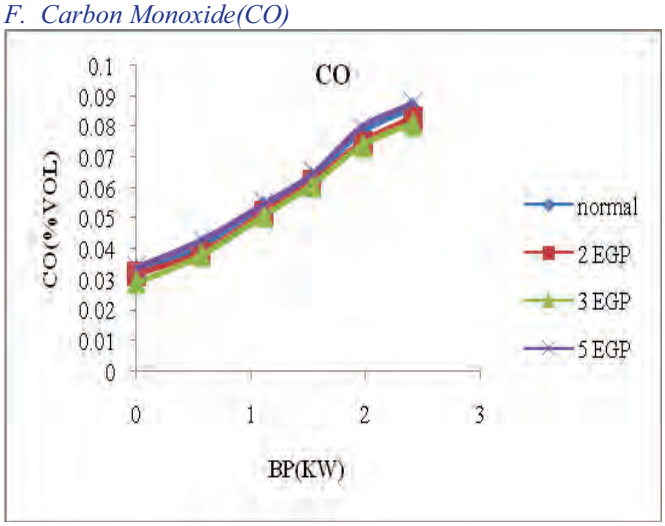


Figure 7. Brake power Vs CO emissions with diesel.

Fig.7 shows the variation of CO emissions with other pistons. It is observed that 3EGP is lower CO emissions than compared to 2EGP, 5EGP and normal piston.

TABLE II.
ENGINE PERFORMANCE CHARACTERISTICS

| S.NO | Brake thermal efficiency (%) | BSFC (Kg/kw-hr) | Mechanical Efficiency (%) |
|---|---|---|---|
| **Normal Piston** | 21.22 | 0.40 | 43.27 |
| **2 EGP** | 22.07 | 0.38 | 44.61 |
| **3EGP** | 22.64 | 0.36 | 43.43 |
| **5EGP** | 19.69 | 0.43 | 41.24 |

Table.II shows the comparison of characteristics of engine i.e. brake thermal efficiency, BSFC and mechanical efficiency using normal, 2EGP, 3EGP and 5EGP. It clearly shows that three ellipsoidal arc groove piston [3EGP] having high brake thermal efficacy and low BSFC as compared to other pistons, but the mechanical efficiency is slightly less than the two ellipsoidal arc groove piston.

TABLE III.
EMISSIONS CHARACTERISTICS

| S.NO | HC (PPM) | $NO_x$(PPM) | CO (% Vol) |
|---|---|---|---|
| **Normal Piston** | 38 | 432 | 0.063 |
| **2 EGP** | 36 | 422 | 0.062 |
| **3EGP** | 34 | 404 | 0.061 |
| **5EGP** | 40 | 422 | 0.065 |

Table.III shows comparing of engine emissions i.e. HC, NOx and CO using normal, 2EGP,3EGP and 5EGP.It clearly shows that three ellipsoidal arc groove piston has

CVR Journal of Science and Technology, Volume 19, December 2020
DOI: 10.32377/cvrjst 1919

low HC, NOx and CO emissions compared to other type of pistons.

## V. Conclusions

- Break thermal efficiency is increased by 6.27% by changing the normal piston with three semi elliptical arc groves piston.
- Break Specific fuel consumption is decreased by 10% for 3EGP piston compare to normal piston.
- HC emissions are reduced by 10.5% by changing the piston from normal to 3EGP.
- $NO_x$ emissions are reduced 6.48% by changing the piston from normal to 3EGP.
- The CO emissions are reduced by 4% (3EGP) for modified pistons by compared to normal piston

From the above conclusions, three ellipsoidal grooves piston (3EGP) is better than the normal, two and five grooves piston (Normal,2EGP and 5EGP).

## References

[1] J. Li, and W.M. Yang, "Effects of Piston Bowl Geometry on Combustion and Emission Characteristics of Biodiesel Fueled Diesel Engines" Journal of Fuel, Volume 120, (2014) Pp 66–73.

[2] Nimesh A. Patel and Vinaykumar Sharma, "Effect of Piston Geometry on Diesel Engine Performance and Emission Characteristics with Varying Injection Pressure" Ijsrd - International Journal for Scientific Research & Development| Vol. 3, Issue 03, 2015 | Issn (Online): 2321-0613.

[3] Venkata Ramesh Mamilla, "Effect of Combustion Chamber Design on A Di Diesel Engine Fuelled With Jatropha Methyl Esters Blends with Diesel" *Journal of Procedia Engineering*, Volume 64, (2013) Pp 479 – 490.

[4] V. Ganesan, "Internal Combustion Engines". 4th Edition, *Tata Mcgraw Hill Education Private Limited*.

[5] Md.nurun nabi and Sm Najmulhoque, "Biodiesel Production from Linseed Oil and Performance Study of a Diesel Engine with Diesel Bio-Diesel", *Journal of Mechanical Engineering*, 2008, 39(1), Pp: 40-44.

[6] A. Swarnakumari, C.H. Penchalayya and A.V. Sita Rama Raju, "Performanc Evaluation of Diesel Engine with Sunflower Oil", *Journal of Engineering Studies and Research*, Volume 19(2013) No.2.

[7] Shaik Gouse Ahammad, Gajjala Vasavi and Shaik Mohammad Shareef "Performance and Emissions Characteristics of Direct Injection Diesel Engine Fueled with Apricot Seed Biodiesel and Diesel", *Global Journal of Engineering Science and Research Managemen*t, ISSN 2349-4506 PP 62-68.

[8] Banapurmath NR, Chavan AS, Bansode S, Sankalp Patil, Naveen G, Sanketh Tonannavar , Keerthi Kumar and Tandale "Effect of Combustion Chamber Shapes on the Performance of Mahua and Neem Biodiesel Operated Diesel Engines" MS2, *Journal of Petroleum & Environmental Biotechnology,* DOI: 10.4172/2157-7463.1000230, Volume 6,Issue 4 pp 1-7.

[9] B. Naveen Kumar and Dr. Smt. G. Prasanthi "Experimental Investigation of Toroidal Combustion Chamber (Piston Bowl) For Four-Stroke Single Cylinder Di Diesel Engine Fuelled With Blends of Olive Oil", *International Journal of Advance Engineering and Research Development* Volume 4, Issue 11, PP 705-712.

[10] Y. Syamala and Dr. Smt. G. Prasanthi, "Experimental investigation of shallow depth combustion chamber (piston bowl) for four stroke single cylinder DI Diesel engine fuelled with blends of olive oil" *International Journal of Advanced Scientific Research and Management*, Vol. 2 Issue 11, PP 88-94.

E-ISSN 2581 - 7957
P-ISSN 2277 - 3916

CVR Journal of Science and Technology, Volume 19, December 2020
DOI: 10.32377/cvrjst 1920

# Parametric Optimization of Submerged Arc Welding using Taguchi Method on P91 Steel

Vidyanand Kumar[1], Dr. Manjeet Kharub[2] and Neeraj Kumar Jha[3]
[1]Asst. Prof, CVR College of Engineering/Mechanical Engg. Department, Hyderabad, India
Email: vidyanandk75@gmail.com
[2]Asst. Prof, CVR College of Engineering/Mechanical Engg. Department, Hyderabad, India
Email: manjeetkharub@gmail.com
[3]Assoc. Prof, CVR College of Engineering/Mechanical Engg. Department, Hyderabad, India
Email: neerajjha.me@gmail.com

***Abstract:*** **Welding is one of the fabrication processes use to join metals permanently. Submerged arc welding (SAW) is one of the fusion welding process in which continuously fed consumable wire electrode is used for welding purpose. Selection of welding parameter plays an important role on weld quality. The main aim of our work in this paper is to investigate the influence of welding parameters like feed rate of wire electrode, welding speed and stick out distance on the weld bead of modified 9Cr-1Mo steels (P91). In this study parameters are optimized by Taguchi L9 orthogonal array (OA) experimental design and other statistical tool Analysis of Variance (ANOVA) techniques. Percentage contributions of individual parameter are validated by using ANOVA technique. The experimental results were analyzed by using statistical software Minitab 17. Further variation in hardness in weld zone and microstructure of welds are investigated.**

***Index Terms:*** **SAW, ANOVA, S/N ratio, P91, Optimization**

## I. Introduction

American Welding Society (AWS) defines welding as a permanent joining of metals or non-metals produced by heating the materials to a suitable temperature with or without the application of pressure along with or without the use of filler material. Welding is more economical joining methods as compared to casting and riveting. Welding is used for the fabrication of sheet metal, joining of ferrous and non-ferrous metal, automobile and aircraft industries. It has been preferred owing to its capability to produce joints at low unit production, extremely reliable and works under severe conditions [1]. The characteristic of the weld zone is mainly affected by some important control process parameters such as welding speed, welding current, voltage, stick out distance, electrode wire feed rate. Welding quality like weld bead size or geometry, penetration, and hardness of different zone play an important role in the fabrication industry. Estimation of perfect parameters for sound weld joints is a very complex process. Some researchers have made several attempts to estimate the optimum process parameters for smooth and quality weld. Commonly used are welding are as follow:

*Arc welding* is a type of welding process which uses an electric arc to generate heat for the joining purpose. It creates an arc between electrode and work metal that electrode may be consumable or non-consumable. Contamination of air particles and elements like oxygen, helium, and nitrogen is considered as the biggest problem in arc welding. Many times this contamination results in poor weld surfaces.

*Friction welding* involves mechanical deformation of specimens in order to achieve a strong joint. As the process does not require melting, melting-solidification and other heat related defects are eliminated. However, this process is preferred for low melting points metals.

*Friction stir welding (FSW)* is also called the solid-state welding. It joins the workpiece through mechanical deformation. The process used to join previously reported non-weldable aluminum grades. It can produce joints with approximate 30% to 50% stronger than simple arc welding. However, the process is found much slower than others, limiting its application.

*Flash welding (FW)* this process is used to produce butt joints through the application of arc welding along with pressure. This is capable to produce weld joint which are equal in strength of base metal. However, this process wastes comparatively much material during the flushing process. Further, it is used for zinc and its alloy, cast iron and lead.

In addition of above described welding commonly used welding process are Gas Metal Arc Welding (GMAW), Gas Tungsten Arc Welding (GTAW), Plasma Arc Welding (PAW), Laser Beam Welding (LBW), Electron Beam Welding (EBW), Diffusion Welding (DFW), this study is focused on submerged arc welding.

Submerged arc welding (SAW) is one of the most commonly used welding methods in these decades. SAW is a semiautomatic welding process firstly used in the 1930s to make good quality welds. The SAW process turned out as the best welding process, especially because of high rate of deposition, high depth of penetration and neat quality of weld [2]. Thus, it is applied in pipe making, ship building, structures (beams, girders etc.), pressure vessels, nuclear and power plants etc [2].

Weld quality has been considered an important parameter in its applications. According to experts welding quality including strength, appearance, durability and reliability are strongly characterized by process parameters [3]. Vinodh & Bharathi [4], pointed out that various welding process parameters like amperage setting, arc voltage, feed rate of consumable wire electrode, speed of welding, weld angle and the electrode standoff distance affect weld quality to a great extent. Process parameters play an important role in determining the mechanical properties of the welded specimen [6]. So, the selection of proper parameters is an

E-ISSN 2581 - 7957
P-ISSN 2277 - 3916

CVR Journal of Science and Technology, Volume 19, December 2020
DOI: 10.32377/cvrjst 1920

important task for sound and qualitative weld joint. Therefore, the selection of the optimal welding process parameters combination is very essential for obtaining desired qualities in weldments [4]. Many experts have emphasized that by the use of control systems the guesswork can be eliminated in the selection of welding parameters. In order to optimize process parameters the statistical Taguchi design method has been widely used by many researchers [5,6]. For instance, multiple regression methods or techniques are employed to obtain the empirical model for different arc welding processes by Murugan et al. [7]; Ravindra & Pramar [8]. A mathematical programming optimization technique was implemented for optimization of the welding flux composition and it was found accountable for weld metal characteristics as a function of welding flux level [10]. In their study, Hsiao et al. [11] analyzed the optimal process parameters of plasma arc welding by the Taguchi method with Grey relational analysis with input parameters as Torch stand-off, welding current, welding speed, and plasma gas flow rate (Argon). Similarly, Hakan et al. [12], used the Taguchi based Grey relational analysis for parametric optimization of Friction stir welding [12]. Usually, welding parameters for a given welding process are preferred based on experimental outcomes, welder's experience, welding standards and empirical laws [9].

In present study selected parameters are as follows:

a) Input
   i. Wire feed rate;
   ii. Welding speed; and
   iii. Stick out distance based on previous research on SAW;

b) Output
   i. Penetration depth;
   ii. Weld bead width;
   iii. Weld zone hardness.

## II. Experimentation

Modified 9Cr-1Mo steels (P91) steel is selected over other materials because of its distinct properties and its application. It is widely used in thermal power plant applications in view of its excellent creep strength, corrosion and oxygen resistance, toughness and reasonable cost. This steel is especially used in steam boilers, pressure vessel, steam popes and so many engineering application. The chemical composition of the specimen used in this study is presented in Table I. This steel pertains to be in the category of ferritic/martensitic steel. It's critical characteristics are its stability at high temperature and creep resistance.

Bead on plate type techniquees of size 100x50x8 mm dimension were prepared for welding by submerged arc welding set up at constant current and voltage. Bead on plate not a butt welding of two different plates, in this welding has been done on the surface of plate without any joint preparation. Many research articles are using this technique because there is no chance of distortion in the welded plate for study purposes. Welding process parameters and their range are selected based on the number of trial runs experiment on 8 mm thickness of P91 steel as given in Table II.

TABLE I.
CHEMICAL COMPOSITION OF P91 STEEL

| Components | Cr | Mo | C | Mn | Si | V | Nb | Fe |
|---|---|---|---|---|---|---|---|---|
| Weight % | 8.91 | 0.98 | 0.09 | 0.42 | 0.31 | 0.21 | 0.07 | rest |

TABLE II.
PROCESS PARAMETERS AND THEIR LEVELS

| Process Parameter | Level 1 | Level 2 | Level 3 |
|---|---|---|---|
| Wire feed rate (mm/min) | 150 | 200 | 250 |
| Welding speed (mm/min) | 60 | 75 | 90 |
| Stick out (mm) | 20 | 22 | 24 |

The experiments were outlined by L9 orthogonal array, experimental plan for the welding process characteristics with L9 orthogonal array and experimental outcomes for the weld bead geometry using L9 orthogonal array which can be observed in Table III. The experiments were conducted by taking a bead on 100 X 50 X 8 mm P91 steel plates.

After removal of slag the job was allowed to cool, then specimens were cut, polished and etching was done in the direction of the cross section of the weld to weld zone, heat affected zone and base metal regions. After that, the polished samples were etched by a chemical solution containing 1 gm Picric acid with 5 ml HCl and 100 mL Ethanol. To measure the responses, average values of the penetration, reinforcement width and heights were taken using a digital vernier caliper of least count 0.02mm.

TABLE III.
L9 ORTHOGONAL ARRAY DESIGN AND RESPONSE OUTPUT

| S.no. | Wire feed rate | Welding speed | Stick out | Penetration(mm) | Bead width(mm) | HAZ(mm) | HV |
|---|---|---|---|---|---|---|---|
| 1 | 150 | 60 | 20 | 3.6 | 14.25 | 1.2 | 265 |
| 2 | 150 | 75 | 22 | 3.25 | 14.12 | 1.1 | 271 |
| 3 | 150 | 90 | 24 | 3.2 | 13.52 | 1.08 | 255 |
| 4 | 200 | 60 | 22 | 4.9 | 14.55 | 1.29 | 260 |
| 5 | 200 | 75 | 24 | 4.4 | 14.30 | 1.21 | 268 |
| 6 | 200 | 90 | 20 | 4.3 | 14.13 | 1.15 | 252 |
| 7 | 250 | 60 | 24 | 6.5 | 14.65 | 1.35 | 270 |
| 8 | 250 | 75 | 20 | 6.0 | 14.35 | 1.22 | 264 |
| 9 | 250 | 90 | 22 | 6.1 | 14.20 | 1.18 | 265 |

## III. Analysis

In this section analysis of responses are presented, it makes the understanding of relationship between process parameters electrode feed rate, welding speed and electrode stick out distance and output response penetration, weld bead width, hardness of weld zone of submerged arc welding. In order to evaluate optimal process parameters the Taguchi method has been used as a statistical measure. Taguchi provides the minimum set of experiment and signal to noise ratios which are logarithmic functions of desired response that serve as objective functions during optimization of process parameters. The S/N ratio developed by Dr. Taguchi is a benchmark to choose control levels that best suit with noise. The S/N ratio considers mean as well as variability. It is the ratio of the mean (signal) to the standard deviation (noise). The standard S/N ratios usually taken are, nominal-is-best (NB), lower-the-better (LB) and higher-the-better (HB)[13]. In present investigation, the output

E-ISSN 2581 - 7957
P-ISSN 2277 - 3916


DOI: 10.32377/cvrjst 1920

responses are bead width, depth of penetration, heat affected Zone and hardness of weld zone. In this study for penetration, bead width and hardness HB is selected whereas LB is selected for heat affected zone.

Further, a statistical analysis of variance (ANOVA) has been applied to inspect the statistical process parameters. The optimal combination of the characteristics has been determined by ANOVA and S-N analysis.

### *A. Analysis of Variance (ANOVA)*

ANOVA is used to identify the SAW parameters that significantly affect the multiple performance characteristics. ANOVA Table IV (A-D) consists of degrees of freedom, sums of squares, the F-ratios corresponding to the ratios of two mean squares, and the contribution proportions from each of the control factors.

TABLE IV (A).
ANOVA FOR PENETRATION

| Welding Parameter | DOF | Sum of square | Mean square | F- ratio | Contributed % |
|---|---|---|---|---|---|
| Wire feed rate | 2 | 12.4172 | 6.20861 | 1719.31 | 97.16 |
| Welding speed | 2 | 0.3372 | .016861 | 46.69 | 2.63 |
| Stick out | 2 | 0.0172 | 0.00861 | 2.38 | 0.13 |
| Error | 2 | 0.0072 | 0.00361 | R-Sq(adj)=99.98% | |
| Total | 8 | 12.7789 | R-Sq= 100 % | | |

TABLE IV (B).
ANOVA FOR BEAD WIDTH

| Welding Parameter | DOF | Sum of square | Mean square | F- ratio | Contributed % |
|---|---|---|---|---|---|
| Wire feed rate | 2 | 0.32807 | 0.16403 | 8.16 | 39.73 |
| Welding speed | 2 | 0.42987 | 0.21493 | 10.69 | 52.06 |
| Stick out | 2 | 0.02747 | 0.01373 | 0.68 | 3.32 |
| Error | 2 | 0.04020 | 0.2010 | R-Sq(adj)=80.52% | |
| Total | 8 | 0.82560 | R-Sq=95.13% | | |

TABLE IV (C).
ANOVA FOR HAZ

| Welding Parameter | DOF | Sum of square | Mean square | F- ratio | Contributed % |
|---|---|---|---|---|---|
| Wire feed rate | 2 | 0.024422 | 0.012211 | 1099.00 | 41.85 |
| Welding speed | 2 | 0.032822 | 0.016411 | 1477.00 | 56.24 |
| Stick out | 2 | 0.001089 | 0.000544 | 49.00 | 1.86 |
| Error | 2 | 0.000022 | 0.000011 | R-Sq(adj)=99.85% | |
| Total | 8 | 0.058356 | R-Sq=99.96 % | | |

TABLE IV (D).
ANOVA FOR HARDNESS

| Welding Parameter | DOF | Sum of square | Mean square | F- ratio | Contributed % |
|---|---|---|---|---|---|
| Wire feed rate | 2 | 104.22 | 52.11 | 4.55 | 27.50 |
| Welding speed | 2 | 118.22 | 59.11 | 5.17 | 31.19 |
| Stick out | 2 | 133.56 | 66.78 | 5.83 | 35.25 |
| Error | 2 | 22.89 | 11.44 | R-Sq(adj)=82.71% | |
| Total | 8 | 378.89 | R-Sq=89.98% | | |

### *B. Mathematical Modeling*

Multiple linear regression models were developed for penetration, bead width, HAZ (heat affected zone), Vickers hardness (HV) by using Minitab17 software. The responsible variables are penetration, bead width, HAZ and hardness whereas the predictors are wire feed rate, welding speed and stick out distance. The equations of the best suited model for tensile and bending strengths are given below:

- Penetration= -0.21+ 0.02850 Wire feed rate- 0.01556 Welding speed+ 0.0167 Stick out (1)
- Bead width= 15.167+ 0.00437 Wire feed rate- 0.01778 Welding speed- 0.0217 Stick out (2)
- HAZ= 1.181+ 0.001233 Wire feed rate- 0.004778 Welding speed+ 0.00583 Stick out (3)
- HV= 255.2+ 0.0267 Wire feed rate- 0.256 Welding speed+ 1.00 Stick out (4)

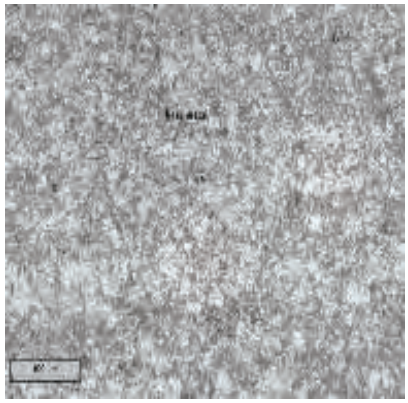

Figure 1(a). Base metal

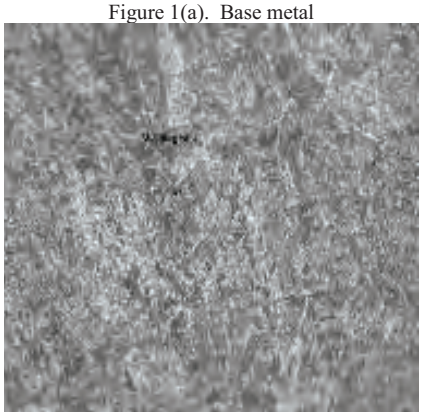

Figure 1 (b). Welding zone

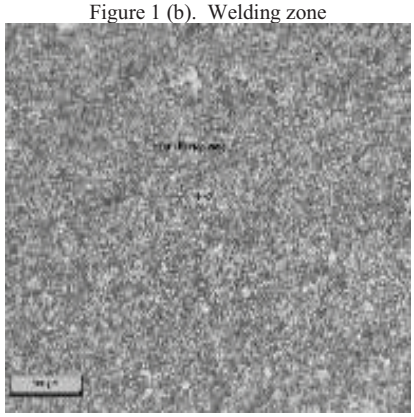

Figure 1(c). HAZ

### *C. Study of microstructure*

The study gives a view of the material characteristics in the grain growth at the weld region, HAZ and in the base metal portion. Observation of microstructure shows a little inclusion near the HAZ region and also differences in grain sizes which are developed during the process of welding.

E-ISSN 2581 - 7957
P-ISSN 2277 - 3916

CVR Journal of Science and Technology, Volume 19, December 2020
DOI: 10.32377/cvrjst 1920

Figure 1(a) to Figure 1 (c) presents the structure of base metal, weld zone and HAZ.

## IV. Results and Discussion

The analysis is performed by MINITAB 17. The main effect plots for S/N ratio can be seen in Fig. 2 and Fig. 3. Figures indicate the alteration of discrete response with the three criterions i.e. wire feed rate, welding speed and stick out individually. In the plots, the x-axis represents the value of each process criteria at three levels and y-axis the response value. Horizontal line represents the mean value of the response. The main effects plots are applied to obtain the optimal design situations to find out the optimum response surface.

Effect of process parameters on penetration shows that penetration is mainly affected by wire feed rate and it has a contribution of 97.17% from ANOVA analysis presented in table IV(A). It decreases with increase in welding speed and slightly increases with stick out distance.

Contribution of process parameters on bead width, it is mainly affected by welding speed and it has a contribution of 52.07% from ANOVA analysis as shown in table IV(B). Wire feed rate has also a significant effect on bead width.

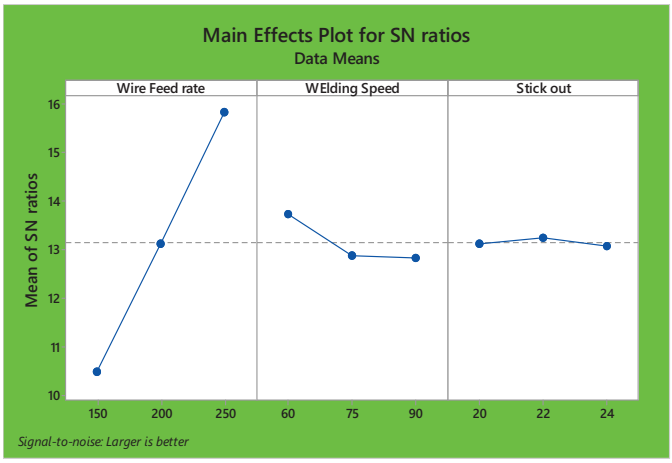


Figure 2. Main effect plot for penetration

Effect of process parameters on HAZ. Both wire feed rate and welding speed have significant effect with a contribution of 41.85% and 56.24% respectively. Stick out distance has a negligible contribution with 1.86% as presented in table IV(C). Effect of process parameters on hardness of weld zone, shows that wire feed rate, welding speed and stick out has significant effect as shown in table IV(D).

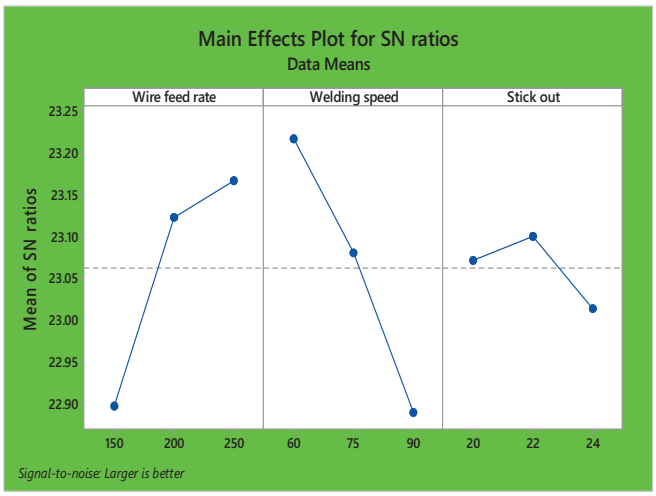


Figure 3. Main effect plot for bead width

Fig. 2 shows the main effect plot for penetration. The plot reveals that penetration increases with wire feed rate. It also shows decrease in penetration with increase in welding speed and stick out distance is non-significant in penetration. Fig. 3 shows the main effect plot for bead width with parameters involved. It shows that response value increases with wire feed rate and decreases with welding speed and slightly increases and then decreases with electrode stick out distance.

Fig. 4 shows the main effect plot for the heat affected zone. From this plot it is clear that HAZ decreases with electrode wire feed rate, increases with welding speed and decreases with stick out distance. Fig. 5 shows that the response first decreases and then increases with wire feed rate, there is an increment and decrement with welding speed. With stick out distance it shows an increment and slightly decreases the hardness of weld zone.

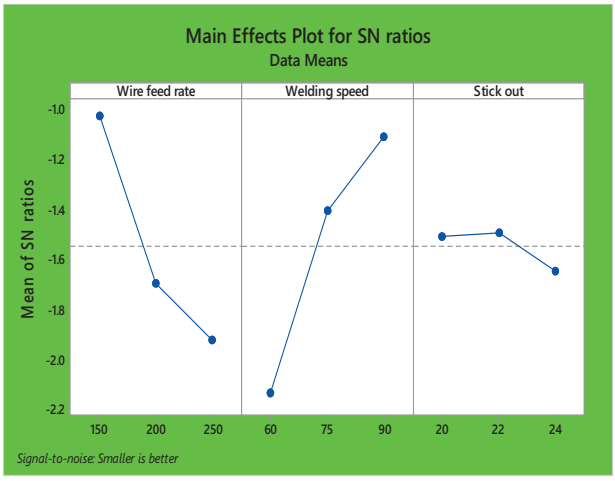


Figure 4. Main effect plot for HAZ

Welding parameters (feed rate, speed, and stick out distance) need to be in perfect combination to obtain sound weld bead. With increase in wire feed rate the deposition should be high, whereas welding speed controls the volume of molten metal (deposition per unit volume). It influences the bead width and penetration significantly and stick out distance maintains the burn-off rate. For perfect output there

CVR Journal of Science and Technology, Volume 19, December 2020
DOI: 10.32377/cvrjst 1920

should be an optimum combination of welding speed and stick out distance.

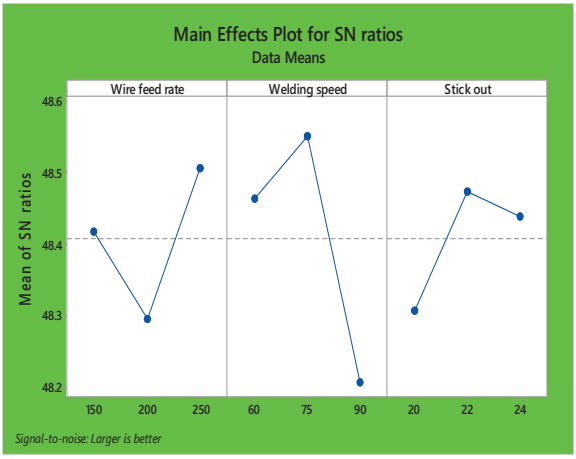


Figure 5. Main effect plot for Hardness

## V. Conclusions

Optimal parametric conditions and main effect plot have been obtained for each response separately by Taguchi method. Using, Analysis of variance (ANOVA) it is found that wire feed rate (96.16% contribution) and welding speed (56.24%) have the highest impact on penetration and heat affected zone, respectively. Further the influence of stick out on penetration, bead width and HAZ has been obtained. It is found that stick out has greater influence on hardness (35.25% contribution) on hardness of weld zone

1. Penetration is greatly influenced by wire feed rate and optimal parameters for maximum penetration according to main effect plot are wire feed rate (250 mm/min), welding speed (60 mm/min) and stick out (22 mm).
2. As shown in the main effect plot optimum condition for maximum bead width is wire feed rate (250 mm/min), welding speed (60 mm/min) and stick out (22 mm). Bead width is greatly affected by welding speed.
3. Heat affected zone is a function of wire feed rate and welding speed and optimal condition for LB, parameters are wire feed rate(250 mm/min), welding speed (60 mm/min) and stick out (25 mm).
4. Hardness is a function of wire feed rate, welding speed and stick out distance.
5. Regression equations were developed based on the experimental values of penetration, bead width, HAZ and hardness of weld zone of submerged arc welded joints of P91 steel. The developed models can be used to predict the responses at 95% confidence level.

## References

[1] P.D. Houldcroft (1989), Submerged Arc Welding Abington Publishers, U.K.
[2] S. Vinodh, S.K. Bharathi and N. Gopi, "Parametric Optimization of SAW Using Taguchi Method," Design of Exp. in Prod. Engi. DOI 10.1007/978-3-319-23838-8_8,2016.
[3] B. Anirban and S. Singla, "Mechanical properties and metallurgical characterization of dissimilar welded joints between AISI 316 and AISI 4340", Trans. of the Indian Insti. Of Met., Doi 0.1007/s12666-016-0879-7, April 2016.
[4] S. Vinodh, S.K. Bharathi and N. Gopi,"Parametric Optimization of SAW Using Taguchi Method," Design of Exp. in Prod. Engi., DOI 10.1007/978-3-319-23838-8_8, 2016.
[5] E.M. Anawa and A.G. Olabi, "Using Taguchi method to optimize welding pool of dissimilar laser-welded components", Optics & Laser Technol., vol. 40, pp. 379–388, March 2008.
[6] J. E. R. Dhas and S. Kumanan,"Optimization of parameters of submerged arc weld using non-conventional techniques",Appl. Soft Comp., vol. 11, pp. 5198-5204, Dec 2011.
[7] N.Murugan, R.S.Paramar, S.K.Sud, "Effect of submerged arc process variables on dilution and bead geometry in single wire surfacing",Journal of materials Processing Technology, vol. 37,pp.767-780, 1993.
[8] J.Ravindra, R.S.Pramar, Mathematical models to predict weld bead geometry for flux cored arc welding. Met.Construct.192, pp. 31R-35R.,1987.
[9] I.S.Kim, C.E.Park, Y.G.Cha, J.Jeong and J.S.Son, A study on development of a new algorithm for predicting process variables in GMA welding processes. JSME Int.442(2001), pp.561-566.
[10] Adeyeye D Ademola and O.A Fes Festus. Weld metal property optimization from flux ingredients through mixture experiments and mathematical programming approach. Material research. 2009; 12(03), pp 339-343.
[11] Hsiao, Y. F., Tarng, Y. S., and Huang, W. J., "Optimization of plasma arc welding parameters by using the taguchi method with the grey relational analysis", Materials and Manufacturing Processes,Vol. 23, No. 1, 2008, pp. 51-58.
[12] Hakan, A., Bayram, A., Ugur, E., Kazancoglu, Y., and Onur, G., "Application of Grey relational analysis and taguchi method for the parametric optimization of friction stir welding process",Materials and Technology, Vol. 44, No. 4, 2010, pp. 205-211.
[13] Pradeep Deshmukh, M. B. Sorte, "Optimization of Welding Parameters Using Taguchi Method for Submerged Arc Welding On Spiral Pipes", International Journal of Recent Technology and Engineering (IJRTE) ISSN: 2277-3878, Volume-2, Issue-5, November 2013, 50-54.

E-ISSN 2581 - 7957
P-ISSN 2277 - 3916

CVR Journal of Science and Technology, Volume 19, December 2020
DOI: 10.32377/cvrjst 1921

# Modelling of a Banana Fiber Extraction Machine

Mada Rukmi Sai Rupa Sri [1] and N. Ankitha[2]
[1]Asst. Professor, CVR College of Engineering/Mechanical Engg. Department, Hyderabad, India
Email: mada.rukmini@gmail.com
[2]Asst. Professor, CVR College of Engineering/Mechanical Engg. Department, Hyderabad, India
Email: graceankitha@gmail.com

***Abstract:*** **The paper details the modelling and analysis of natural fiber extraction machine to extract high quality natural fibers from the banana pseudo stems. Manual extraction of banana fiber produces good quality fiber, but it is a time-consuming process. Labor expenses are quite high, and output is low. Hence efficient extraction of banana fiber can only be possible through a machine. Machines existing in present scenario for extracting banana fiber are manually operated and cannot be referred for mass production. The impurities are present in rolled fiber. The efficiency of existing machines is average. It consumes time and the process is not safe. This paper describes the model of machine to be designed for extracting banana fiber from the banana stem. The machine is to be designed in a very simple way such that it can be used by everyone, as the mechanism is very simple.**

***Index Terms:*** **Pseudo stem, extraction, mass production, efficiency.**

## I. Introduction

Natural fibers such as jute, coconut, banana, and sugarcane extracts are the upcoming promising fibers within the area of composites as well as handcrafted products. Most developing countries like India are in the verge to grow these natural fiber plants due to the favorable climatic conditions. There are several methods of extracting natural fibers from its source, but the mechanical way of extracting fibers is commonly used for reducing the amount of time and efforts put for it. The mechanisms and therefore the design features for extracting fibers should be developed in such a way that the natural properties of the fibers are not lost and comprising the value factor suitable for this system. Natural fibers offer several advantages in comparison to synthetic fibers in terms of low production cost, tenuity, renewability, ecofriendly, availability, budget friendly, nonhazardous and simply available [1] [3] [10]. For a better understanding of the properties of natural fiber materials, it is essential to know the physical, mechanical and chemical properties. The strength characteristics of fiber depends on the properties, fibrillary structure, lamellae matrix, method of processing and chemical modifications [9]. Due to these factors they're well-known to the composites field. The disadvantage of natural fibers is that the moisture absorption and the poor compatibility between fiber and the matrix .in the composites. But the importance of these fibers is highlighted by various government schemes to provide employment in this domain [10].

Banana tree is a symbol of prosperity and fertility and thus it is frequently used in all the Indian festivals for serving food or as a cooked dish. Almost every part of banana tree is employed for some economical or medicinal purposes. Banana fiber is extracted by crushing its pseudo stem for obtaining the pulp. Pseudo stem [2] is the part of the tree which is disposed after it bears fruits only once. It is produced above the ground by the true stem which lies underground. It looks like a trunk and is formed by the leaf sheaths which are tightly packed. The fiber is extracted by splitting the stem into strips, crushing it under rollers, washing it for the residual removal and later drying it for the production. The design of this fiber extracting machine considers the factors such as the detangling and pulp cleaning for its direct usage in the applications like textiles or paper making [6] [7].

Banana fiber is used as a raw material in the following industries:

- Paper Industries
- Cardboard Industries
- Plywood Industries
- Handicraft Items- Cap –Purse-Bag
- Rope Making
- Handloom Industries
- Banana Yarn – Textile Use

Banana fiber has its own physical and chemical characteristics [3] [8] and many other properties that make it a fine quality fiber.

- Banana fiber is finer than any other naturally produced fibers.
- The chemical composition of banana fiber is cellulose, hemicellulose, and lignin, which makes it a highly strong fiber.
- It has smaller elongation.
- It appears shiny depending upon the extraction & spinning process.
- It is lighter in weight.
- Also, it has strong moisture absorption quality. It absorbs as well as releases moisture very fast.
- It is bio- degradable and has no negative effect on environment and thus can be categorized as eco-friendly fiber.
- It can be spun through almost all the methods of spinning including ring spinning, open-end spinning, bast fiber spinning, and semi-worsted spinning among other.

E-ISSN 2581 - 7957
P-ISSN 2277 - 3916

CVR Journal of Science and Technology, Volume 19, December 2020
DOI: 10.32377/cvrjst 1921

Figure 1. Pseudo stem of banana tree

## II. Problem Statement

The pseudo stem is chopped off from the original stem once the fruits on it are harvested. It can bear the fruits only once and hence disposed after single harvest. The disposal of these stems creates a lot of biogas which goes waste. To avoid this and the rising interest in natural fibers gives a way to extract the fiber from these stems [3] [10] [11]. These fibers possessing good mechanical properties and being economical are widely used in many applications including fiber composites. These fibers can be thick and thin. Thick fibers are mainly used for handicrafts whereas the latter is used in textile industry. Table I shows the composition of fiber highlighting the properties that are very useful for various applications [12].

TABLE I.
Chemical Composition of Banana Fiber

| Property | Value |
|---|---|
| Tenacity | 29.98 g/denier |
| Fitness | 17.15 denier |
| Moisture regain | 13% |
| Elongation | 6.54 |
| Total cellulose | 81.8% |
| Alpha cellulose | 61.5% |
| Residual gum | 41.9% |
| Lignin | 15% |

## III. Extraction of fiber

There are two methods used for the extraction of the fiber [7].

### *A. Manual way of extraction*

Fiber is extracted from the leaf sheath or pseudo stem of banana plant by decortication of the sheath. The pseudo stem is the aerial stem that is seen above the core part of banana stem. It is created by closely packed leaf sheaths embedded within the growing tip. Each leaf incorporates a banana leaf sheath forming a part of pseudo stem petiole and lamina [2]. It is hectic to extract the fiber by segregating the fiber from the pulp manually or by machines. It is often extracted chemically, as an example boiling in NaOH solution. Though Manual extraction of the banana fiber produces a better quality of fiber but it is much time consuming.

### *B. Mechanical way of extraction*

By employing a finest fiber extractor machine, an oversized amount of fiber is obtained which can produce an additional income. The Banana Fiber Extractor Machine is the exclusive form invented [4] for the extraction of fiber from waste portions of Banana like stems, leaf stalks and peduncle. The manual (or) semi mechanical extraction of Banana Fiber is tedious, time consuming, and damages the fiber. It's an economical portable device developed for the good cause about the farming community and self-employed women group. Cost of the Machine varies basing on the iron and steel rates [4]. 100% safety in machine operation with less maintenance cost. Many schemes were introduced by government for encouraging the practical usage of these machines.

## IV. Modelling of Parts in CATIA

The 3D model of the machine is designed in CATIA. The major components designed are as follows:

### *A. Frame*

All the parts of the machine are mounted on this frame structure with the suitable arrangement. According to the bearing size bore holes are drilled for their proper alignment during the assembly and proper lubrication provisions are also provided. Figure 2 shows the frame modelled. The frame is designed with a height of 750mm and length of 750mm. Width of the machine is taken as 400mm.

Figure 2. Frame

### *B. Bearing*

Bearings are used to reduce the friction between parts which have relative motion between them [6]. Ball bearings as in figure 3 are used in this machine to reduce the motor friction. These can also be easily replaced when they deform or squish under heavy loads. Bearing 6202 type is used for this [8].

E-ISSN 2581 - 7957
P-ISSN 2277 - 3916

CVR Journal of Science and Technology, Volume 19, December 2020
DOI: 10.32377/cvrjst 1921

Figure 3. Bearing

### C. Belt

Belts provide mechanical link between two rotating shafts. The shaft on the motor and the other on the roller drum are connected by this and slippage of belt over these shafts is taken care of. A32 power loom belt is used in the mechanism.

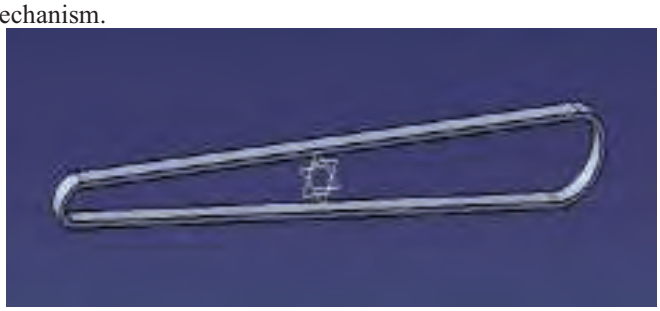

Figure 4. Belt

### D. Motor

This part provides the initial motion of the machine. An AC type motor used for the speeds and driving force to the roller [5]. A motor of capacity 1hp with single phase is used for the running of the machine.

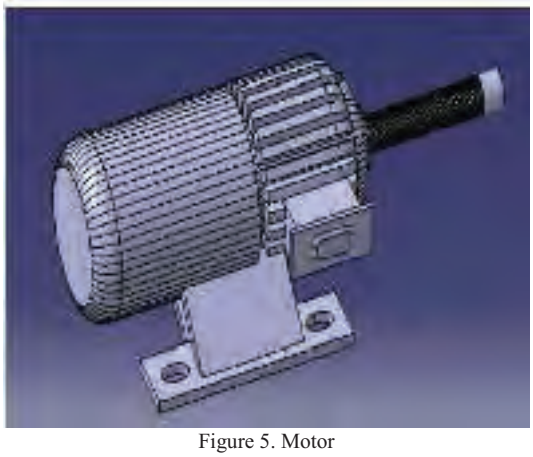

Figure 5. Motor

### E. Pulley

Pulley transmits the power from motor to the roller drum with belt attached to it. Two pulleys are used for this purpose. One of them is fixed which provides deviation for the force on the rope or belt moving on its circumference. The second pulley is a movable pulley which offers a greater mechanical advantage when the rope or belt is passed over its circumference. Both the pulleys are designed with a diameter of 300mm.

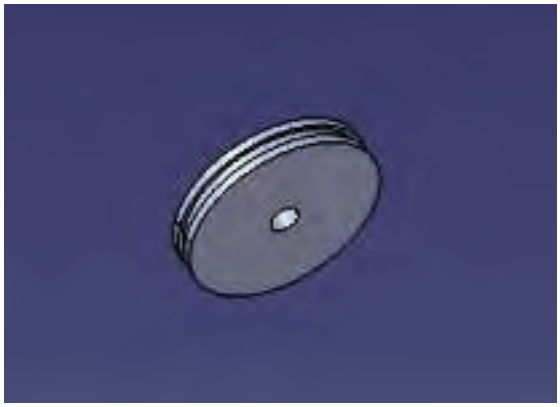

Figure 6. Pulley

### F. Feeding roller

The feeding roller is used to insert the banana pseudo stem, which is placed in between operator and in front of roller drum. This roller ensures the stem is inserted fully and safety to the operator during the stem insertion in to the roller. The dimensions of roller design are 400mm in length and 50mm in width.

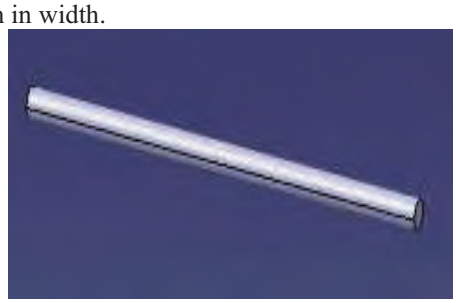

Figure 7. Feeding roller

### G. Supporter

It is used for holding the motor on the frame. The motor is held fixed on the machine with the help of this supporter shown in figure 8. This is designed in such a manner that the vibrations occurring at larger speeds of motor does not interrupt the working of the machine and the roller drum functions smoothly during the crushing process.

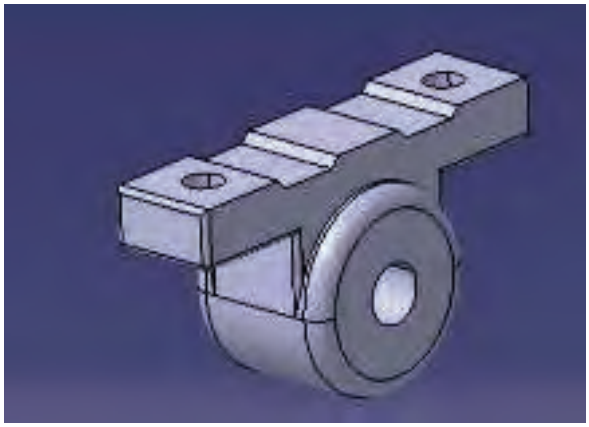

Figure 8. Supporter

E-ISSN 2581 - 7957
P-ISSN 2277 - 3916

CVR Journal of Science and Technology, Volume 19, December 2020
DOI: 10.32377/cvrjst 1921

### *H. Roller drum*

Roller or crusher is the most important elements in this machine. It provides necessary crushing load on the pseudo stem such that the pulp is separated from the stem leaving only the fiber. Type of the roller used mainly affect the quality of fiber. The standard of fiber depends on the design of the roller. When compared with square tooth roller, the crushing line saw roller separates a finer quality of banana leaf sheath. So dual saw rollers are used in this machine and one square tooth roller or rasp bar roller. The diameter, length and number of cutting blades on the roller are 300mm, 350mm and 12 blades respectively.

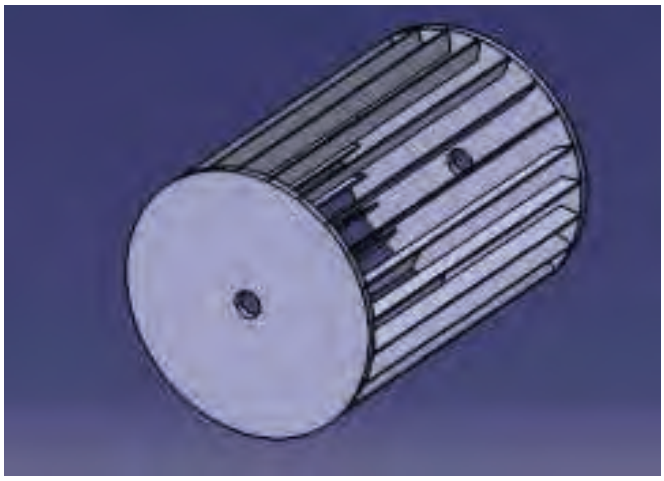

Figure 9. Roller drum

## V. Assembly of Parts

Assembly of these parts to form the machine can be carried out in two formats. One of the models has the motor and roller drum placed on the frame and the length of the belt connecting these is small [3][6]. After the crushing process, the pulp must be taken away from the machine by the operator and not letting it fall on the motor. The other version of this machine has the motor placed at the bottom while the roller is placed on the top. This model offers an advantage of the pulp falling away from the motor without any human intervention. The length of the belt connection the shafts is large and hence slacking or sagging must be taken care of. Any one of these formats can be used for the construction of machine. Both give the same output with respect to the fiber extraction.

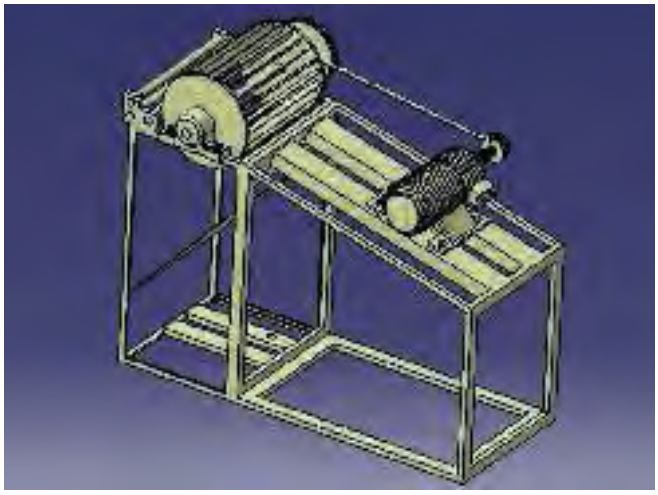

Figure 10. Assembly 1

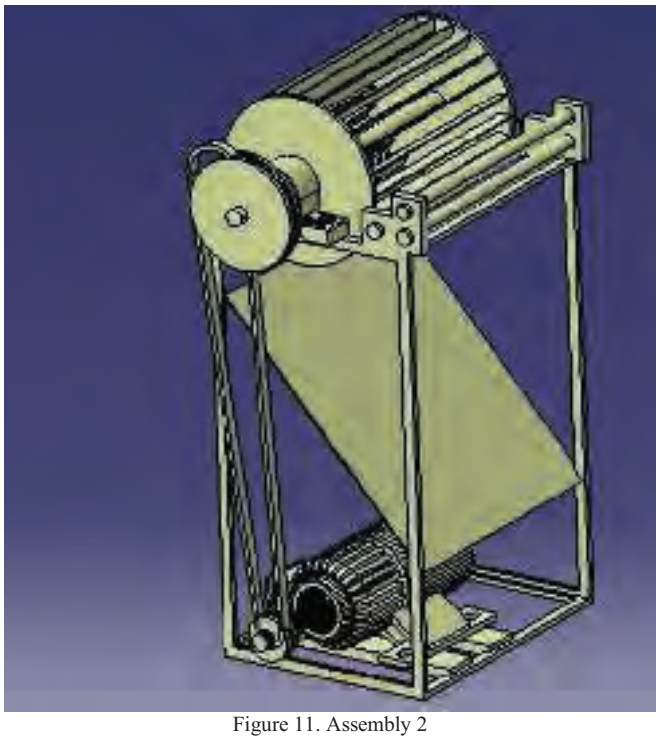

Figure 11. Assembly 2

## VI. Analysis on Roller Drum

Structural analysis is carried out on roller drum as it is the part that bears maximum load during the fiber extraction process. Loads are applied on the roller at different speeds and the deformation and von misses stress are analyzed.

EN 8 carbon steel [6] with improved strength over mild steel, through-hardening medium carbon steel is used for the roller. It is also machinable in any condition. The analysis was carried out in ANSYS workbench. Figures show the deformation and von misses' effects at 1000 rpm. The analysis was also carried out at 2000 rpm and 3000 rpm.

E-ISSN 2581 - 7957
P-ISSN 2277 - 3916

CVR Journal of Science and Technology, Volume 19, December 2020
DOI: 10.32377/cvrjst 1921

Figure 12. Meshing of roller drum

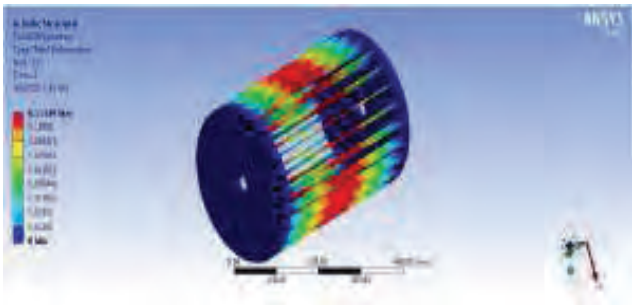

Figure 13. Total deformation

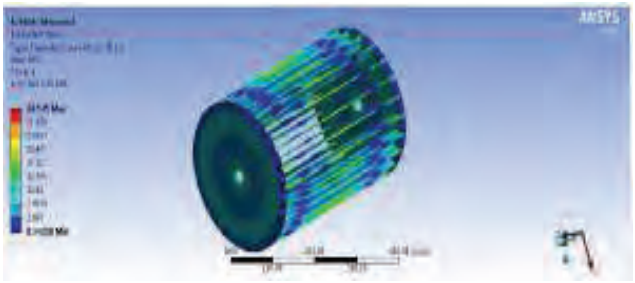

Figure 14. Von misses stress

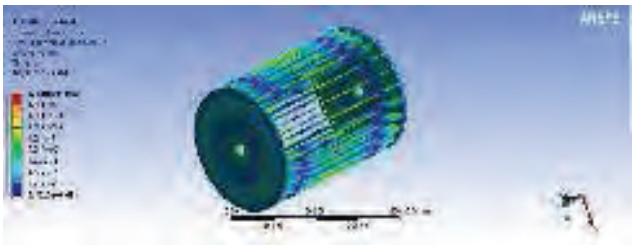

Figure 15. Von misses strain

## VII. Conclusions

Table II shows the deformation and von misses stress & strain values of roller drum at 1000rpm, 2000rpm and 3000rpm. Even at high speed conditions the deformation and von misses' values are optimal, thus resulting in a good working condition of machine at heavy loads.

TABLE II.
Results of Structural Analysis of Roller Drum

| Material | Speed (RPM) | Deformation (mm) | Stress (N/mm$^2$) | Strain |
|---|---|---|---|---|
| EN 8 Steel | 1000 | 0.11349 | 30.545 | 0.001546 |
| | 2000 | 0.45397 | 122.18 | 0.000618 |
| | 3000 | 0.66523 | 179.04 | 0.000906 |

The fabrication can be carried out with the same steel as it is economical and of higher efficiency. The fabrication cost is also less with the parts chosen for the machine, hence reducing the process cost. Purified form of fiber is obtained by this design and enzyme treatment can be done on the fiber for its usage directly in the production of various products. The design offers advantage in terms of compactness and easy dissembling.

## References

[1] D. Saravanabavana and G. C. Mohan Kumar, *Conceptual design features and eco methods for the extraction of natural fibers in the materialistic earth*, ISBN: 978-981-087721-7, pp. 461- 471, 2011.

[2] Dr. S. K. Dey and Dr. K. K. Satapathy, A combined technology package for extraction of pineapple leaf fiber an agro waste, utilization of biomass and for application in textiles, 2013.

[3] Bandi sruthi and Chand Bhadshah, Energy conservation drives for efficient extraction and utilization of banana fiber. IJETER, vol.3, pp. 489- 491, 2015.

[4] Kishan naik, R. P. Swamy, and Prem Kumar Naik, Design and fabrication of areca fiber extraction machine, 2014.

[5] L. A. Pothan, T. Sahu, and Neelakantan. Short banana fiber reinforced polyester composites; mechanical, failure and aging characteristics- reinforced plastic and composites, 16(8), pp. 744 -765, 1997.

[6] Suhaib A Sheik and N. P. Awate, A design and development of banana fiber extraction machine, ISSN 2277 9655, 2011.

[7] S. N. Kunte and A. B. Amale, A structure modification of banana fiber extraction machine, March 2016.

[8] Vadivel Vijay Kumar, Solomon and Santosh Kumar, A Review paper on Design and Fabrication of Banana Fiber Extraction Machine and Evaluation of Banana Fiber Properties, IJAREEIE, ISSN: 2320- 3765, Vol. 6, pp. 1513-1518, March 2017.

[9] Satyanarayana, K. G., K. Sukumaran, A. G. Kulkarni, S. G. K. Pillai, and P. K. Rohatgi, , Fabrication and Properties of Natural Fiber-Reinforced Polyester Composites, Journal of Composites, Vol. 4, pp. 329–333.

[10] Satyanarayana, K. G., K. Sukumaran, P. S. Mukherjee, C. Pavithran, and S. G. K. Pillai, Natural Fiber– Polymer Composites, J Cement and Concrete Composites, Vol. 2, pp. 117–136.

[11] Laly A. Pothana, Zachariah Oommenb, and Sabu Thomas, Dynamic Mechanical Analysis of Banana Fiber Reinforced Polyester Composites, Composites Science and Technology, Vol. 3, pp. 283–293, 2003.

[12] Mansur M. A. and M. A. Aziz, (1983), Study of Bamboo-Mesh Reinforced Cement Composites, International Cement Composites and Lightweight Concrete, Vol. 5, pp. 165– 171.

E-ISSN 2581 - 7957
P-ISSN 2277 - 3916

CVR Journal of Science and Technology, Volume 19, December 2020
DOI: 10.32377/cvrjst 1922

# Structural Analysis of Centrifugal Compressor Impeller using ANSYS

T. Venkatesh[1], A.L.N. Arun Kumar[2], Sk. Mohammad Shareef[3] and P. Lava Kumar[4]
[1]Asst. Professor, CVR College of Engineering/Mechanical Engg. Department, Hyderabad, India
Email: venkatesh2711991@gmail.com
[2]Asst. Professor, CVR College of Engineering/Mechanical Engg. Department, Hyderabad, India
Email: aln.arunkumar@gmail.com
[3]Asst. Professor, CVR College of Engineering/Mechanical Engg. Department, Hyderabad, India
Email: shareefshaik4@gmail.com
[4]Asst. Professor, CVR College of Engineering/Mechanical Engg. Department, Hyderabad, India
Email: kumar.lava7023@gmail.com

***Abstract:*** **In this present work, compressor impeller has been analyzed with different materials to increase the efficiency of turbocharger. The research work has been done by using CREO and ANSYS software. The modelling of compressor impeller has been done by using CREO software. The variation of deformations, strains and stresses of the compressor impeller using different materials has been determined by ANSYS software. A structural analysis is used to carry out the displacements, strains, and stresses of compressor impeller. The compressor impeller of turbocharger of diesel engine will be recommended based on the results.**

***Index Terms:*** **centrifugal compressor impeller, Creo, Ansys, structural analysis, different materials, stresses, deformations, strains.**

## I. Introduction

Turbocharger is the device which is used to increase the efficiency of the diesel engine. Centrifugal compressors are used in turbochargers to increase the mass flow rate of fluid through the runner. Inlet, impeller/rotor, and diffuser are the main components of the centrifugal compressor. In this study, different materials are selected for the analysis those are copper alloy, incoloy alloy-286, titanium alloy and stainless-steel alloy. In this work, the modeled is created in CREO and this modeled is used for analyzing in ANSYS software by selecting different materials. The deformations, strains and stresses are evaluated for different materials at different conditions.

Farah Elida selama et. al. [1] has conducted simulation work using ANSYS-CFX on centrifugal pump impeller for determine the performance. By increasing the speed of the impeller, the efficiency of the centrifugal pump is shown in the results.

Dr. S. Shankar et. al. [2] has conducted analysis work on compressor impeller using ANSYS - CFX to determine the inner flow characteristics of radial flow pump by changing the number of blades. In the results, the performance and efficiency of the compressor by changing blades is discussed.

S. Rajendran et. al [3] has carried out simulation work on impeller of centrifugal pump using ANSYS-CFX to understand the complex interflows in centrifugal pumps and numerical solution of the three-dimensional flow is shown in results.

Bhanumik B. Patel et. al [4] has conducted design and flow analysis of impeller by using ANSYS-CFX. The model is created using SOLIDWORKS software and it is used in ANSYS by changing the blade angles. CFD software also used to determine the heads, which are shown in results.

Ajith M S et al [5] has carried out analysis work of centrifugal pump impeller using ANSYS FLUENT. In this work, impeller is designed by head, speed, and discharge. The impeller analysed by forward and backward vanes in CFD and velocity and variation of pressure distribution are shown in results.

Alpesh Kumar R et al [6] has conducted experimental study and simulation work using CFD of centrifugal pump impeller. In this work, internal flow of centrifugal pump is observed by ANSYS-CFX and characteristics curves like head, rate of flow, efficiency are calculated and compared these results with experimental work.

P. Gurupranesh et. al [7] has carried out analysis of centrifugal pump impeller in CFD to increase the performance. In this project, model is created by SOLIDWORKS, this model is used for CFD by changing the vane profiles to increase the performance. The values of increased efficiency and head are shown in results.

Satish M et al [8] has conducted stress analysis using ANSYS on the impeller of centrifugal pump by changing speed. In this project, stresses developed in impeller and deformation developed in impeller is calculated using ANSYS by changing speed. The safe speed levels are shown in results.

D. Ramesh Kumar et al [9] has carried out design and analysis of impeller of turbocharger. In this project, a model is created in CATIA and analysis is carried out in ANSYS and structural analysis is carried out by selecting the different materials for the impeller. By observing the structural results, best material is selected which is shown in results.

B James Prasad Rao et al [10] has conducted design and analysis work on turbocharger impeller by changing the materials by applying different loads on impeller. In this project, the structural analysis (stress, strain, and deformation) are calculated and those are shown in results.

E-ISSN 2581 - 7957
P-ISSN 2277 - 3916

CVR Journal of Science and Technology, Volume 19, December 2020
DOI: 10.32377/cvrjst 1922

## II. Materials Selection

For structural analysis of compressor impeller Copper alloy, Incoloy alloy-286, Titanium alloy and Stainless steel are selected. The properties of materials like young's modules, the ratio of poison and density are in Table.1

### *A. Modeling*

Compressor impeller model is created in CREO software and is saved in IGS format. This model is imported in ANSYS for structural analysis.

Fig.1 shows the 3D impeller model which is used for analysis.

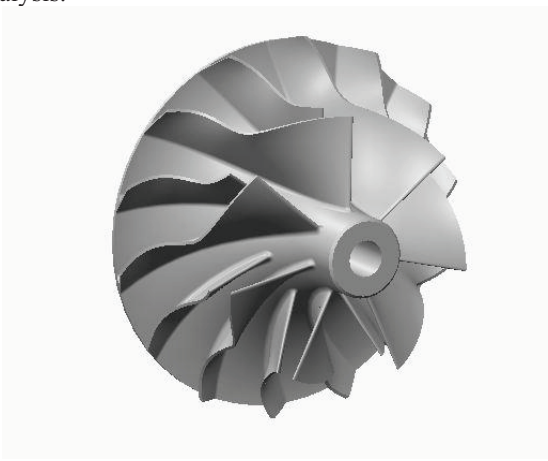

Figure 1. 3D Model of Compressor impeller

## III. FEM Analysis

Static structural analysis is selected in ANSYS for different materials to identify the deformations, Von-Mises strain, and Von-Mises stresses at different loading conditions.

### *A. Meshing*

The geometry which is created in SOLIDWORKS is imported in ANSYS is meshing by tetrahedron method which is shown in Fig.2.

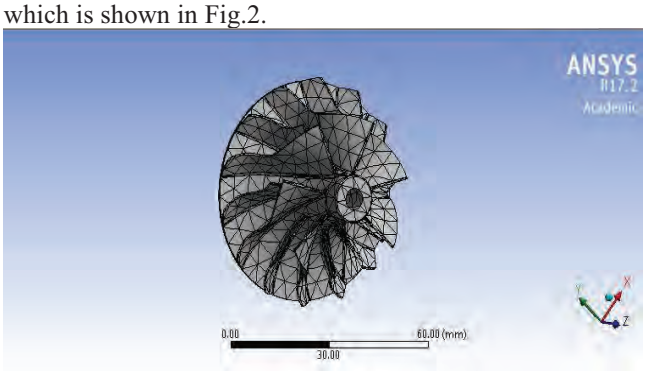


Figure 2. Meshed impeller.

### *B. Boundary Conditions:*

Centrifugal compressor impeller domain is considered. Rotating frame of reference with a rotational speed of 735 rpm. The working fluid through the impeller is water at 27 C. The hub is fixed in the compressor impeller.

## IV. Results and Discussions

For compressor impeller four materials are used to carry out the investigation in static structural analysis by changing the loads.

### *A. Structural analysis of copper alloy material*

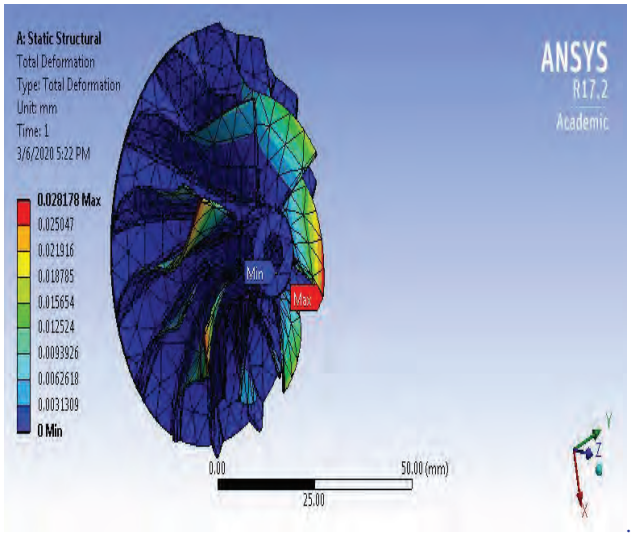


Figure 3. Total deformation of copper alloy.

Fig.3 shows the variations in total deformation on compressor impeller. From the above figure, minimum total deformation is zero and maximum total deformation is 0.028178 mm.

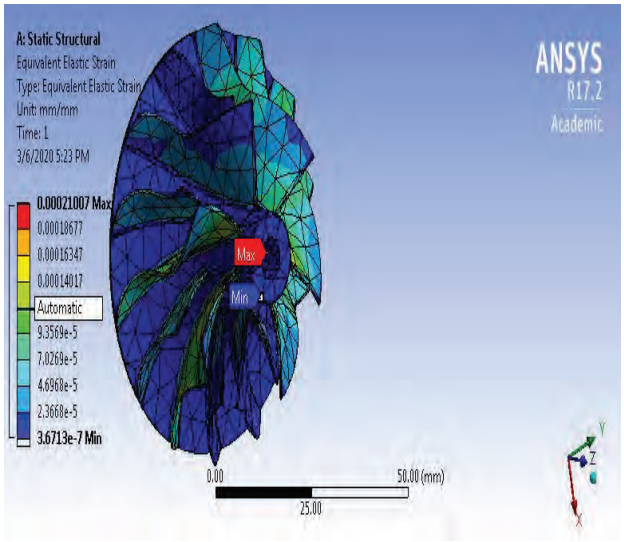


Figure 4. Equivalent elastic strain of copper alloy.

Fig.4 shows the elastic strain distribution in copper alloy material. It is observed that the maximum value of elastic strain is 0.0002107.

E-ISSN 2581 - 7957
P-ISSN 2277 - 3916

CVR Journal of Science and Technology, Volume 19, December 2020
DOI: 10.32377/cvrjst 1922

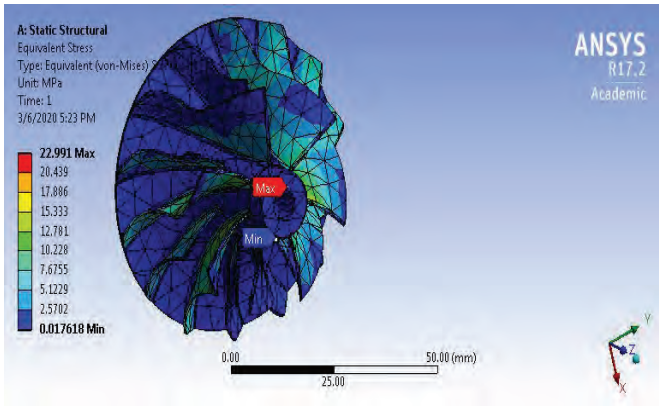


Figure 5. Von-mises stresses for copper alloy.

Fig.5 shows that von-mises stresses for copper alloy and it is observed that the maximum value is 22.991Mpa.

### *B. Structural analysis of Incoloy alloy-286 material*

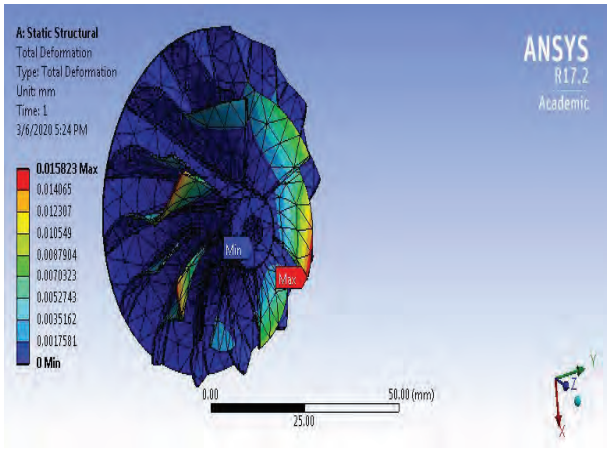


Figure 6. Total deformation of Incoloy alloy-286 impeller.

Fig.6 shows the variation of total deformation on compressor impeller. It is observed that the maximum deformation value is 0.0158 mm.

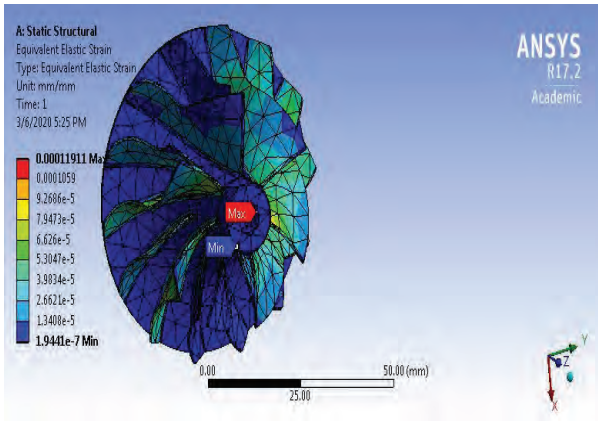


Figure 7. Equivalent elastic strain of Incoloy alloy-286.

Fig.7 shows the variation of equivalent elastic strain of impeller. It is observed that the maximum value is 0.0001191.

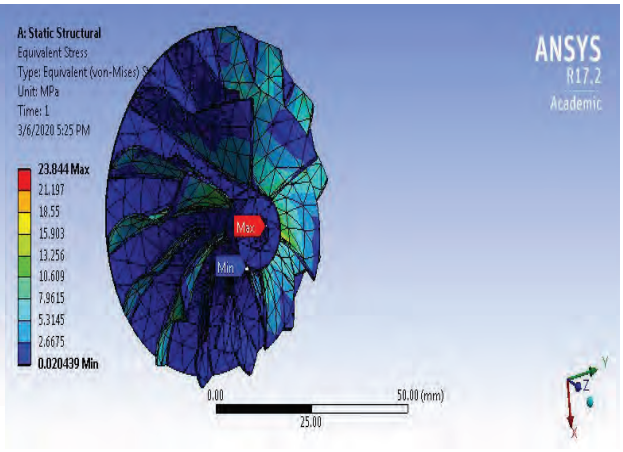


Figure 8. Von-mises stresses for Incoloy alloy-286.

Fig.8 shows that von-mises stresses for Incoloy alloy-286 and it is observed that the maximum value is 23.884Mpa.

### *C. Structural analysis of Titanium alloy material*

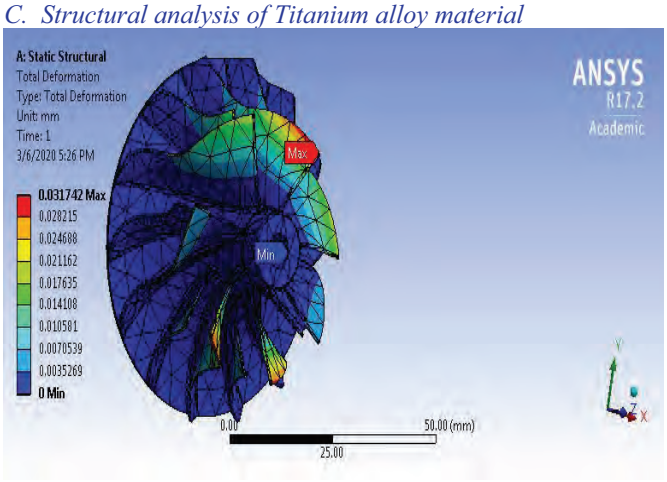


Figure 9. Total deformation of Titanium alloy.

Fig.9 shows the variations in total deformation on compressor impeller. From the above figure, minimum total deformation is zero and maximum total deformation is 0.03174 mm.

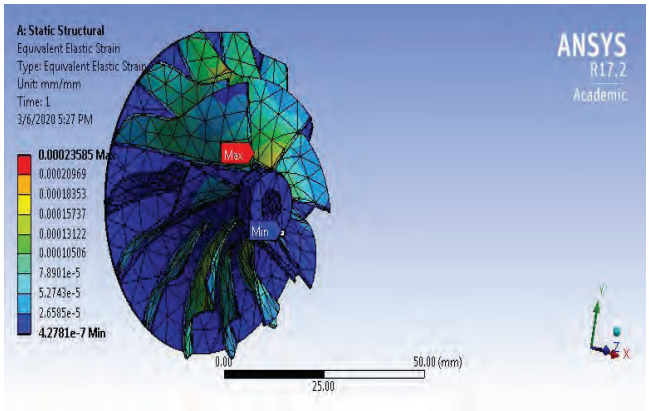


Figure 10. Equivalent elastic strain of titanium alloy.

Fig.10 shows the elastic strain distribution in Titanium alloy material. It is observed that the maximum value of elastic strain is 0.000235

E-ISSN 2581 - 7957
P-ISSN 2277 - 3916

CVR Journal of Science and Technology, Volume 19, December 2020
DOI: 10.32377/cvrjst 1922

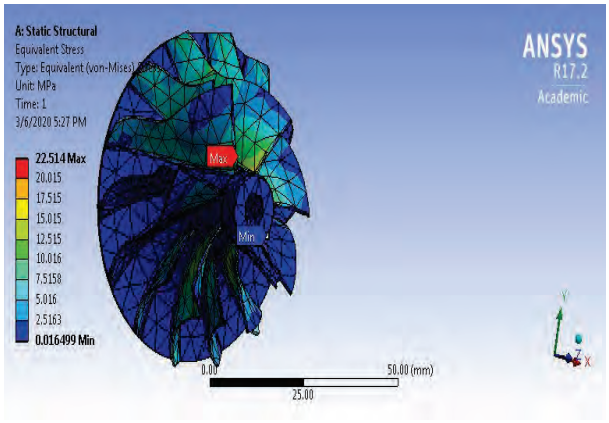


Figure 11. Von-mises stresses for titanium alloy.

Fig.11 shows that von-mises stresses for Titanium alloy and it is observed that the maximum value is 22.514Mpa.

### C. *Structural analysis of Stainless-Steel alloy material*

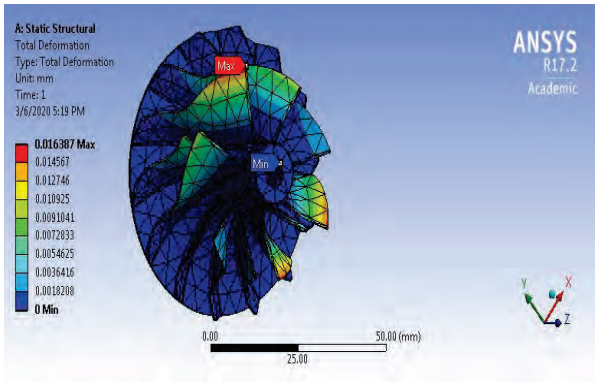


Figure 12. Total deformation of Stainless-steel alloy.

Fig.12 shows the variations in total deformation on compressor impeller. From the above figure, minimum total deformation is zero and maximum total deformation is 0.01638mm.

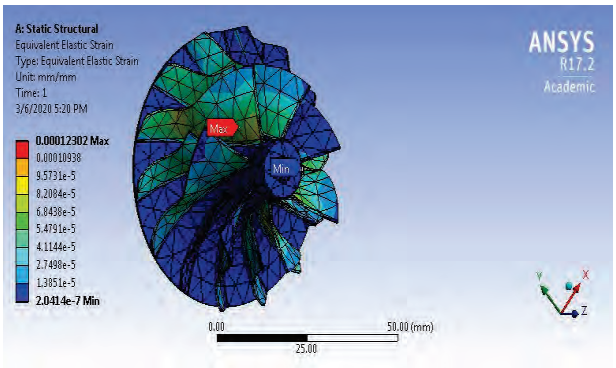


Figure 13. Equivalent elastic strain of Stainless-Steel alloy.

Fig.13 shows the elastic strain distribution in Stainless-steel alloy material. It is observed that the maximum value of elastic strain is 0.000123.

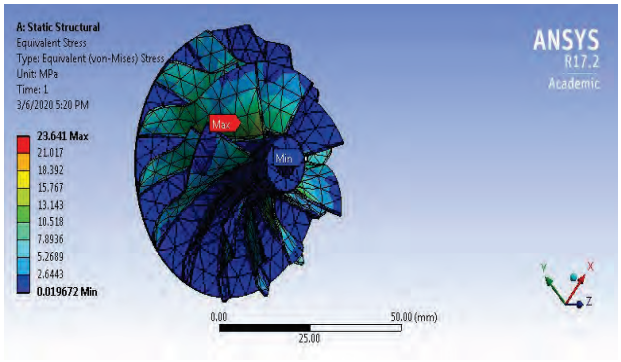


Figure 14. Von-mises stresses for Stainless-Steel alloy.

Fig.14 shows that von-mises stresses for Stainless-Steel alloy and it is observed that the maximum value is 23.641Mpa.

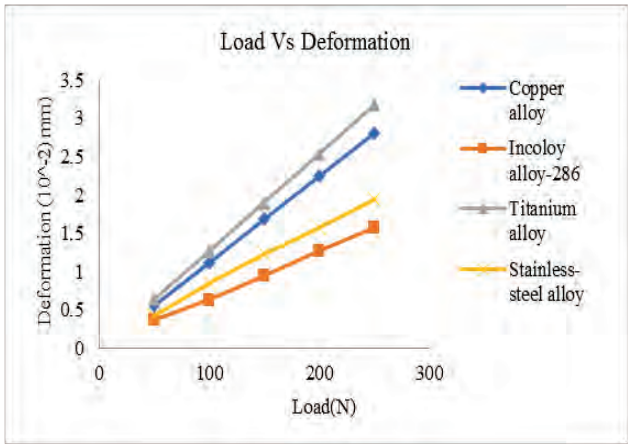


Figure 15. Load Vs Deformation for different materials

Fig.15. shows the variation of total deformation for different materials at different loads. From the above figure, the maximum deformation is for copper alloy material and minimum deformation is for Incoloy alloy-286.

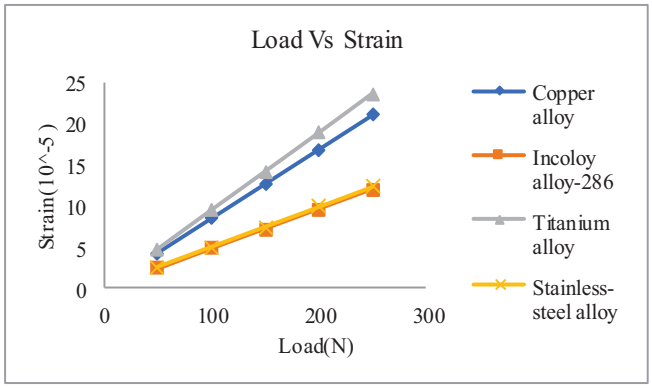


Figure 16. Load Vs Strain for different materials

Fig .16 shows the variation of strain with respect to different loads for different materials. From the above figure, copper alloy has more value of strain than other material and Incoloy alloy-286 has less strain than other materials.

CVR Journal of Science and Technology, Volume 19, December 2020
DOI: 10.32377/cvrjst 1922

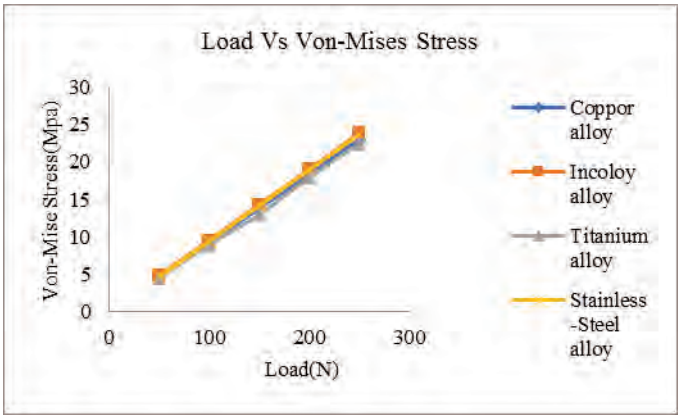


Figure 17. Load Vs Von-Mises Stress for different materials

Fig.17 shows the variation of Von-Mises stress for different materials at different load conditions. From the above figure, it is observed that Incoloy alloy-286 and Copper alloy have more von-mises stresses and Titanium alloy has less stresses than that of other materials.
Table II shows the total deformation, Strain and Von-mises stress for different materials.

## V. Conclusions

- From the results and discussions, it is clearly shown that Incoloy alloy-286 has minimum total deformation, i.e. 44.4% less than that of copper alloy,50.7% less than titanium alloy and 4.2 % less than stainless steel alloy.
- Strain values for Incoloy alloy-286 are 46.6% less than that of copper alloy, 52.5% less than titanium alloy and 0.08% less than stainless steel alloy.

But while comparing the Von-mises stresses, Incoloy alloy has less difference than Titanium alloy.
So, finally, Incoloy alloy -286 will give good results than others.

## References

[1] "Design and Analysis of Centrifugal Pump Impeller for Performance Enhancement" by Farah Elida Selama, Twan Hariz Iskandar Wan Izhan, Journal of Mechanical Engineering, Vol SI 5(2), 36-53, 2018.
[2] "Analysis of Centrifugal Pump Impeller Using ANSYS" by Deepak E P, Dr. S.Sankar, Tedy Thomas, Sreejith K.V, International Journal of Innovative Research in Science, Engineering and Technology, Vol. 7, Issue 5, May 2018 PP 5021-5026.
[3] "Analysis of a centrifugal pump impeller using ANSYS-CFX" by S.Rajendran and Dr.K.Purushothaman , International Journal of Engineering Research & Technology (IJERT) Vol. 1 Issue 3, May – 2012 ISSN: 2278-0181.
[4] "Design and Flow Through CFD Analysis of Enclosed Impeller" by Ashish J. Patel, Bhaumik B. Patel, International Journal of Engineering Research & Technology (IJERT) ISSN: 2278-0181, Vol. 3 Issue 7, July – 2014.PP 1366-1373.
[5] "Design and Analysis of Centrifugal Pump Impeller Using Ansys Fluent" by Ajith M S, Dr Jeoju M Issac, International Journal of Science, Engineering and Technology Research (IJSETR), Volume 4, Issue 10, October 2015 PP-3640-3643
[6] "CFD Analysis and Experimental Study on Impeller of Centrifugal Pump" by Alpesh kumar R, Patel Neeraj Dubey, IJSRD - International Journal for Scientific Research & Development Vol. 3, Issue 02, 2015 ISSN (online): 2321-0613 PP-1447-1451.
[7] "CFD Analysis of centrifugal pump impeller for performance enhancement" by P.Gurupranesh, R.C.Radha,N.Karthikeyan, IOSR Journal of Mechanical and Civil Engineering (IOSR-JMCE) e-ISSN: 2278-1684, p-ISSN: 2320-334X PP 33-41.
[8] "Study of Stresses Developed on the Impeller of Centrifugal Pump at Different Speed using Ansys" by Mr. Satish M. Rajmane, Dr. S. P. Kallurkar, International Journal of Engineering Research & Technology (IJERT) ISSN: 2278-0181 ICIATE - 2017 Conference Proceedings PP 1-7
[9] "Design and Analysis of Turbocharger Impeller in Diesel Engine" by D. Ramesh Kumar B. Shanmugasundaram P. Mohanraj International Journal of Advance Mechanical and Mechanics Engineering Volume 1 Issue 1 PP- 2-15.
[10] "Design And Analysis Of Turbochargers" by B.James Prasad Rao, E.Venkata Reddy, V. Mallikarjuna, International Journal of Engineering Research-OnlineVol.4., Issue.2., 2016 (Mar-Apr) PP-302-312.

E-ISSN 2581 - 7957
P-ISSN 2277 - 3916

CVR Journal of Science and Technology, Volume 19, December 2020
DOI: 10.32377/cvrjst 1923

# Energy Audit Along with Energy Saving Implementations for HVAC Systems

P. Srinivas Reddy
Asst. Professor, CVR College of Engineering/Mechanical Engg. Department, Hyderabad, India
Email: srinivasrdd87@gmail.com

***Abstract:*** **The main objective of this work involves performance of energy audit at a retail store. The focus is on energy and power saving ideas on Heat Ventilation & Air Conditioning (HVAC) systems. Energy audit includes monitoring of daily energy consumptions from different electronic devices and gives the scope for energy savings ideas and implementations at workplace. The other objective is to find any possible energy saving implementations for the energy audit. As a result, we have developed an idea regarding set temperature controlling sensor module.So that the temperature of HVAC remains same regardless how much temperature change we make through remote or controller. This helps us in saving the compressor's work, amount of usage of refrigerant, power consumption and the most important advantage is human safety.**

***Index Terms:*** **HVAC, energy audit, energy saving implementations.**

## I. Introduction

Energy is of many types like primary and secondary energy. The key primary and the secondary energy sources are shown in Figure1.

Matteo Dongellini et al. [1] has carried out preliminary energy audit on eight big industrial buildings of a car manufacturing company in Bologna State. They developed a model to estimate various energy effects on primary energy consumption in the buildings and performance of HVAC systems.

Malkiat Singh et al. [2] has developed a basic model for load management in industries and explained an example of lighting in the industries.

Primary sources are principally regenerated in industrial utilities into secondary energy sources. For instance, coal, oil or gas regenerates into steam and electricity. Across the world, commercialized fuels are predominant supplies not only for economic production but also for several household works of general population. Anupama Gupta et al. [3] has focused on various rules of management of energy i.e. auditing and various processes involved in saving of energy and cost analysis. S.U.Kulkarni [4] has concentrated on energy management related to small and medium industries. They considered an industrial unit and have done energy audit analysis related to lighting and harmonic. P.Kiranmai et al. [5] has discussed usage of energy in a standard manner. According to him and energy auditing is one effective program. Study mainly related to aspects of energy economics, money saving on electricity amounts and emissions of the green house.

M. S. Sujatha et al. [6] has developed a modern method to overcome under frequency load shedding problems by the implementation of "ANFIS" controller to calculate quantity of load shed. JianZhang. [7] They clearly mentioned how energy can be saved by using various latest energy audit and energy management methods. Tarun B Patel. [8] they focused mainly on small companies' energy auditing, process of audit and how it should be carried out in companies. AhilaC.P. [9] they have considered a ladies hostel and have done energy auditing for that particular hostel and made calculations related to Power consumption, cost analysis and other facilities like water. Shashank Shrivastava. [10] has carried out energy audit in a particular industry and improved the efficiency. To improve efficiency, they collected data of pumps, water, and lighting. They removed losses in it.

Figure 1 represents various stages involved in energy generation. In the initial stages various sources of energy available are identified, and then from the earth crust energy sources are extracted. This is materialized by using various methods. In the next stage processing or preparation takes place. Finally, it is converted into energy.

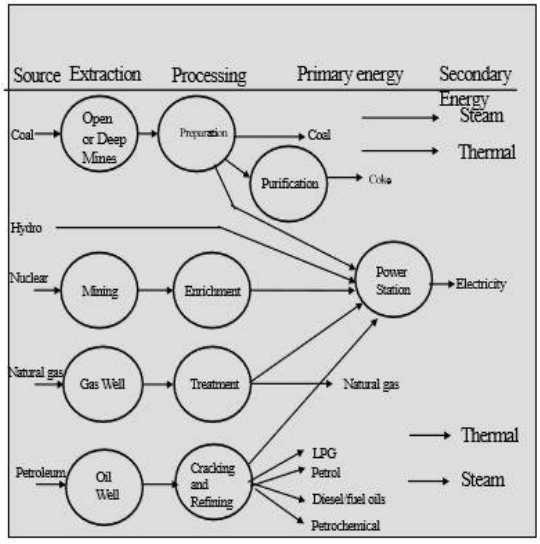


Figure 1. Various sources

(Source: BP2018, Statistical Review of World Energy)

Figure 2 represents about energy consumption taking place around the world. It also shows a particular type like

E-ISSN 2581 - 7957
P-ISSN 2277 - 3916

CVR Journal of Science and Technology, Volume 19, December 2020
DOI: 10.32377/cvrjst 1923

oil, natural gas, nuclear energy, hydroelectricity, and coal utilization globally.

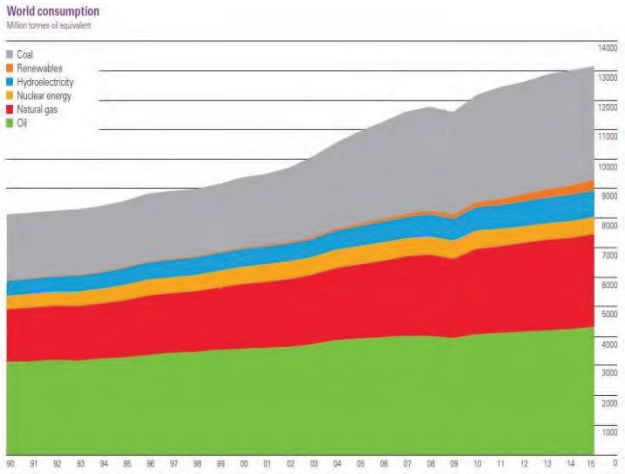


Figure 2. Global Primary Energy Consumption
(Source: BP2018, Statistical Review of World Energy)

The pollutants which damage the atmosphere are (SO2), (NOX), (CO) and (CFC) etc. In chemical and fertilizers industries poisonous gases which are emitted will damage the Environment. The Input and output of process is shown in figure 3.

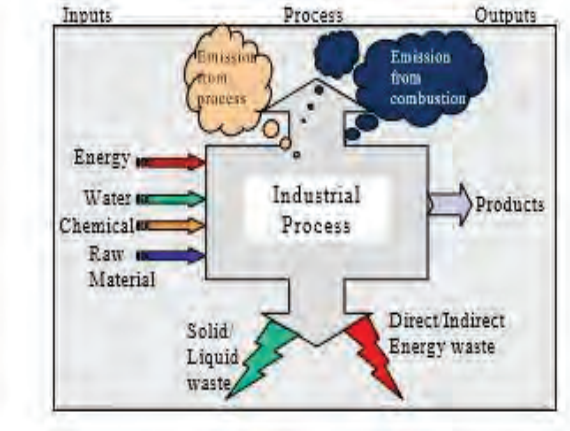


Figure 3. Input and Output of Process.
(Source: researchgate.net)

Figure 3 shows the various input parameters taken and finally the products which we obtain. The principle pollutants made by industrial, domestic and traffic sources are sulfur dioxide, N oxides, material, CO, ozone, hydrocarbons, benzene, 1, 3-butadiene, poisonous organic small pollutants, lead, and significant metals.Human activities and combustion of fossil fuels have created the blanket of greenhouse gases (water vapor, carbonic acid gas, methane, ozone etc.) round the earth thicker.

## II. Energy Conservation

Promotion of energy potency can contribute to energy conservation is thus an integral part of energy conservation promotional policies. Energy potency is usually viewed as a resource possibility like coal, oil, or fossil fuel.

Energy conservation protects the resources and reduces pollution as an example, replacement of ancient lightweight bulbs with Compact Fluorescent Lamps (CFLs). It means that one uses solely 1/4th of the energy to lightweight an area. Pollution levels conjointly scale back by an equivalent quantity. Figure 4 is the best example of energy conservation. In this figure one can see the difference in $Co_2$ emission by using 60W Incandescent lamp and 15W fluorescent lamp.


Figure 4. Energy Conservation Example.
(Source: researchgate.net)

The commercial sector accounts for a 40% of worldwide primary energy demand and around constant share of carbonic acid gas emissions. The advantages of energy conservation for varied players are shown in Figure 5.

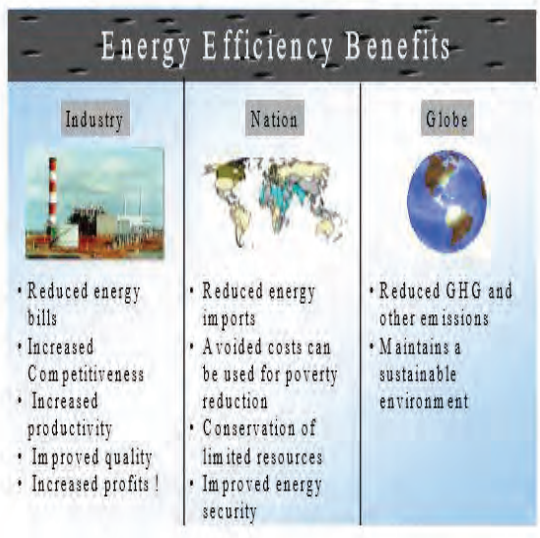


Figure 5. Energy Efficiency Benefits.
(Source: Energy Auditing and Demand Side Management (10EE842))

E-ISSN 2581 - 7957
P-ISSN 2277 - 3916

CVR Journal of Science and Technology, Volume 19, December 2020
DOI: 10.32377/cvrjst 1923

## III. Energy Management and Audit

To appreciate and maintain optimum energy acquisition and utilization, throughout the organization, to scale back energy costs / waste whereas not moving production.

Energy audit is that the key to a scientific approach for decision-making at intervals is the house of energy management. Energy Audit will facilitate to grasp loads of (some word is missing) regarding the ways in which energy and fuel are used in any trade. First objective of energy audit is to see ways that to cut back energy consumption per unit of product output or to lower in operation prices.

Energy audit provides a "benchmark" (Reference point) for managing energy within the organization and additionally provides the premise for designing a more practical use of energy throughout the organization.

The sort of energy audit to be performed depends on perform and kind of business, depth to that final audit is required.

Preliminary energy audit is a quick process to identify the problems. It uses existing, or simply obtained knowledge.

### Phase I (Pre-Audit Phase)

The engineer will perform the following activities: discuss economic aspects related to the audit, analyze the foremost energy consumption knowledge with the relevant personnel, get web site drawings wherever required and instruments needed for finishing audit.

### Phase II (Audit Phase)

The data to be obtained in this phase will contain energy consumption based on a kind of energy, instrumental and material information, development of compressed gas and steam, usage of co-generation systems, energy management procedures and awareness programs.

The audit team ought to collect the subsequent baseline data: nowadays, to be at the forefront of any trade it's imperative to own a correct energy management system established. Strain to be sooner than your competitors include constant work towards eliminating waste, increasing potency and up fight. The energy audit could be a valuable partner on the road to achieve energy potency. Several corporations merely pay their bills and place up with the high prices of energy. However, increasing range of corporations understands the importance of understanding energy consumption and begins operating to eliminate inessential prices.

These savings will then be reinvested back in potency with the prospect to continuous improvement that successively results in improved economic and environmental results.

## IV. Ten Step Methodology

Table I represents the methodology of auditing. The auditing is divided into three phases. In first phase works related to plan and organize. In the second phase works related to data gathering and drawing process flow diagrams and energy diagrams. Finally, in the third phase post auditing will be done. In this phase, works carried out related to preparing schedule, action plan and follow-up.

TABLE I.
Methodology of Auditing

| Step No. | Plan of Action | Purpose/Results |
|---|---|---|
| Step1 | **Phase I:** Plan and organize, Walk through Audit and Informal Interview with Energy Manager, Production/Plant Manager. | (1) Resource planning,<br>(2) Establish/organize an Energy audit team.<br>(3) Organize Instruments & time frame.<br>(4) Macro Data Collection<br>(5) Familiar with all activities.<br>(6) Fresh observation & Evaluation of present operation and practices. |
| Step2 | Conduct of brief meeting / awareness program with all divisional heads and persons concerned (2-3 hrs.). | (1) Building up cooperation.<br>(2) Issue questionnaire for each department.<br>(3) Orientation, awareness creation. |
| Step3 | **Phase II:** Primary data gathering, Process Flow Diagram, & Energy Utility Diagram. | (1) Historic data analysis, Baseline data collection.<br>(2) Prepare process flow charts.<br>(3) All service utilities system diagram (Example: Single line power distribution diagram, water, compressed air & steam distribution).<br>(4) Design, operating data and schedule.<br>(5) Yearly Energy Bill and energy consumption shape. |
| Step4 | Conduct survey and monitoring. | Measurements:<br>Motor survey, Insulation, and Lighting survey with portable instruments for collection of more and accurate data. Confirm and compare operating data with design data. |
| Step5 | Conduct of detailed trials /experiments for selected energy guzzlers. | Trials/Experiments:<br>(1) 24 hours power monitoring.<br>(2) Load variations trends in pumps, fan compressors etc.<br>(3) Boiler/Efficiency trials for (4 – 8 hours).<br>(4) Furnace Efficiency trials Equipment's Performance experiments etc. |
| Step6 | Analysis of energy use. | Energy and Material balance & energy loss/waste analysis. |
| Step7 | Identification and development of Energy Conservation (ENCON) opportunities. | Identification& Consolidation ENCON measures:<br>(1) Conceive, develop, and refine ideas.<br>(2) Review the previous ideas suggested by unit personal.<br>(3) Review the previous ideas.<br>(4) Use various techniques.<br>(5) Contact contractors for new idea. |
| Step8 | Cost benefits analysis. | (1) Assess technical feasibility, economic viability and prioritization of ENCON options for implementation.<br>(2) Pick up Value projects.<br>(3) Take measures. |

| | | |
|---|---|---|
| Step9 | Reporting & Presentation to the Top Management. | Give Presentation to Management. |
| Step10 | **Phase III: Post Audit Phase** Implementation and Follow-up. | Related to ENCON<br>(1) Action plan, Schedule for starting.<br>(2) Follow-up and regular review. |

## V. Energy Saving Implementations

Energy saving implementations based on the energy audit for HVAC systems involves arrangement of sensor module between the HVAC indoor and outdoor unit. With this module, one can control the set temperatures, shut down the compressor and can break the signal coming from the indoor unit of HVAC. This entire sensor module has three main units:

1. Input Unit
2. Data Controller Unit
3. Operating Unit

**Technology (Microcontroller ESP 32)**

ESP32 is a series of low-cost, low-power system on a chip micro and controllers with integrated Wi-Fi and dual-mode Bluetooth.

Figure 6 represents the type of microcontroller used in energy auditing process. The micro controller used here is ESP32 type.

Figure 6. ESP32 Microcontroller.
(Source: Calcutta Electronics.com)

**Arduino software (IDE):** The Arduino IDE employs the program argued to convert the potential code into a document in number representation system writing that is loaded into the Arduino board by a loader program in the board's firmware. The details and coding part of Arduino software sample is shown in Figure 7.It is less expensive software and easy conversion tool which is used by mainly electrical and mechanical engineers in industries, specially industries related to energy systems there are very limited companies which are developing this software in India.


Figure 7. Arduino IDE Coding.
(Source: researchgate.net)

**Eagle Software:** EAGLE stands for simply Applicable Graphical Layout Editor and is developed by CAD Soft pc GmbH.Schematics area unit keep in files with SCH extension, elements area unit outlined in device libraries with LBR extension. Figure 8 represents the Eagle software details related to a circuit design. This software is mainly used in Energy saving processes for developing circuit design.

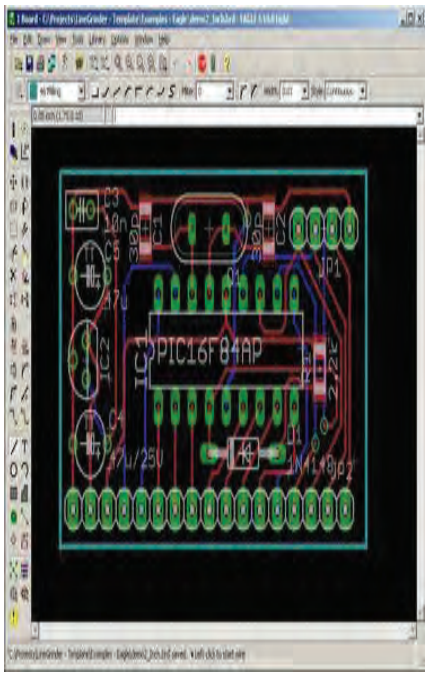


Figure 8. Eagle Software for Circuit Design

E-ISSN 2581 - 7957
P-ISSN 2277 - 3916

CVR Journal of Science and Technology, Volume 19, December 2020
DOI: 10.32377/cvrjst 1923

**Block diagrams: without Module and with Module**

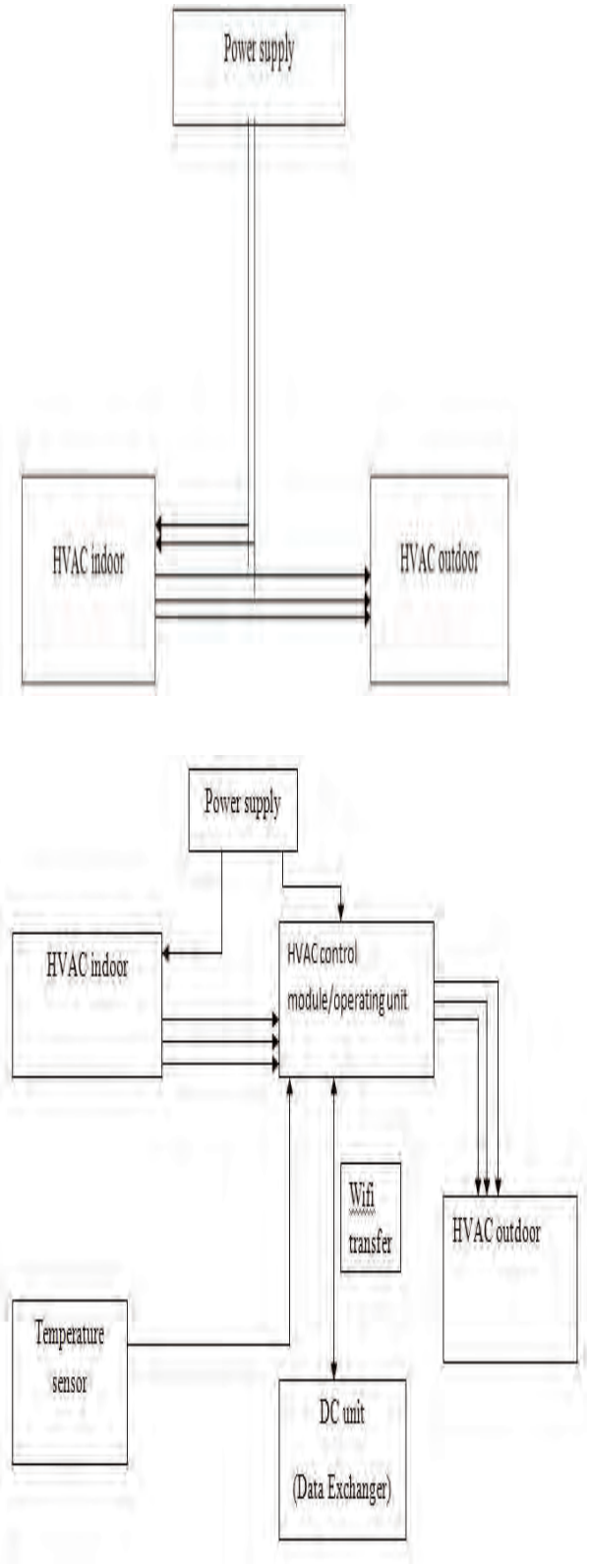


Figure 9. Block Diagrams with Module and without Module

Figure 9 represents the block diagrams related to, with module and without module.

The figure clearly shows how the process takes place with the installation of module and without the installation of module.

## VI. Results

Table II represents the energy audit report without using module in it and, have taken weekly readings at different times of a day and noted down the energy consumed at a particular time of a day by using energy meter readings.

TABLE II.
Energy Audit Report Without Module Unit

| Days Count/Time | Set Temperature of AC unit in 0c | | | Ton of Refrigeration | | | Energy Meter Readings in KW-h |
|---|---|---|---|---|---|---|---|
| | AC1 | AC2 | AC3 | AC1 | AC2 | AC3 | |
| 1/11.30 am | 22 | 24 | 21 | 9.5 | 9.5 | 9.5 | 9636.11 |
| 2/1.45 pm | 21 | 22 | 20 | 9.5 | 9.5 | 9.5 | 9661.63 |
| 3/12.30 pm | 21 | 22 | 22 | 9.5 | 9.5 | 9.5 | 9667.63 |
| 4/4.30 pm | 22 | 19 | 21 | 9.5 | 9.5 | 9.5 | 9702.25 |
| 5/7.00 pm | 23 | 19 | 23 | 9.5 | 9.5 | 9.5 | 9736.63 |
| 6/2.10 pm | 21 | 22 | 20 | 9.5 | 9.5 | 9.5 | 9764.92 |
| 7/2.45 pm | 23 | 21 | 22 | 9.5 | 9.5 | 9.5 | 9789.37 |

For a week readings, the difference in energy meter readings for the first and the last is approximately 153 units.

Let, per unit is cost Rs.10 → For 153 units 1530 per week.

Table III represents the energy audit report by using module in it, and have taken weekly readings at different times of a day and noted down the energy consumed at a particular time of a day by using energy meter readings in this case the set temperature is constant.

TABLE III.
Energy Audit Report With Module Unit

| **Days (Count/ Time)** | **Set (T)** | **Set Temperature of AC unit in 0c** | | | **Ton of Refrigeration** | | | **Energy Meter Readings in KW-h** |
|---|---|---|---|---|---|---|---|---|
| | | **AC 1** | **AC 2** | **AC 3** | **AC 1** | **AC 2** | **AC 3** | |
| 1/11.30 am | 24 | 22 | 24 | 21 | 9.5 | 9.5 | 9.5 | 9837.14 |
| 2/1.45 pm | 24 | 21 | 22 | 20 | 9.5 | 9.5 | 9.5 | 9847.4 |
| 3/12.30 pm | 24 | 22 | 21 | 22 | 9.5 | 9.5 | 9.5 | 9859.95 |
| 4/4.30 pm | 24 | 22 | 19 | 21 | 9.5 | 9.5 | 9.5 | 9871.63 |
| 5/7.00 pm | 24 | 23 | 19 | 23 | 9.5 | 9.5 | 9.5 | 9881.45 |
| 6/2.10 pm | 24 | 21 | 22 | 20 | 9.5 | 9.5 | 9.5 | 9891.94 |
| 7/2.45 pm | 24 | 23 | 21 | 22 | 9.5 | 9.5 | 9.5 | 9905.56 |

For a week readings, the difference in energy meter readings for the first and the last is approximately 69 units.

Let, per unit is cost Rs.10 → For 69 units, Rs.690 per week.

Total Savings/Week = Rs.1530 – Rs.690 = Rs.840/week

CVR Journal of Science and Technology, Volume 19, December 2020
DOI: 10.32377/cvrjst 1923

## VII. Conclusions

Energy auditing is done mainly for energy saving purposes.

(1) By the installation of module unit, we can save large amount of energy consumption.
(2) The number of units per week can be reduced by using module
(3) The working life of refrigerant can be improved.
(4) The environment can be emission free.
(5) Percentage of usage of refrigerant reduces.

## References

[1] Matteo Dongellini, Cosimo Marinosci, GianLuca Morini." Energy Audit of an Industrial site: a Case Study," *68thConferenceof the Italian Thermal Machines Engineering Association*ATI2013 vol.45, pp424-433, 2014.
[2] Malkiat Singh, Gurpreet Singh, Harmandeep Singh."Energy Audit: A Case study to reduce Lighting Cost," *Asian Journal of Computer Science and Information Technology*vol.2, pp 119-122, 2012.
[3] Anupama Gupta, Pallavi Verma, and Richa Priyadarshani, "A Review on Energy Management and Audit", *International Journal of Advanced Research in Electrical, Electronics and Instrumentation Engineering*, Feb2015.
[4] S.U. Kulkarni, Kalpana Patil "Energy Audit of an Industrial Unit-A case study", *International Journal of Emerging Science and Engineering,* November *2013.*
[5] P.Kiranmai, M. Divya Krishna, and Dr. M.S. Sujatha, "Energy Auditing," *IOSR Journal of Electrical and Electronics Engineering*, 2016.
[6] M. S. Sujatha, Dr. Vijay Kumar, "Under frequency load shedding for energy management using ANFIS / case study*,"* International Journal of Electrical Engineering and Technology, volume 4, issue2, Mar-Apr 2013, 93-104.
[7] Jian Zhang, Yuchen Zhang etc., "How to reduce Energy Consumption by Energy Audits and Energy Management: The case of Province Jilin in China," IEEE, Technology Management in the Energy Smart World (PICMET), Jul-Aug, 2011, 1-5.
[8] Tarun BPatel, Ketan D Panchal, "An Effective implementation of Energy Audit Methodology-A Case Study," IJAIEM, volume 4, issue3, March 2015, 260-268.
[9] AhilaC.P, Jeha Femi. W.J, "Energy Audit in Ladies Hostel," IEEE, TENCON 2015-2015 IEEE Region 10 conference, Nov 2015, 1-12.
[10] Shashank Shrivastava, Sandip Kumar, "Improving Industrial Efficiency by energy Audit," IJSET, volume 2, issue4, April 2013, 291-294.

E-ISSN 2581 - 7957
P-ISSN 2277 - 3916

CVR Journal of Science and Technology, Volume 19, December 2020
DOI: 10.32377/cvrjst 1924

# Reliability Design and Maintenance Formulation for Dumpers used in Mining Industries

A. Suresh[1], Dr. G. Diwakar[2] and B. Appala Naidu[3]
[1]Asst. Professor, CVR College of Engineering/Mechanical Engg. Department, Hyderabad, India
Email: suri0341@gmail.com
[2]Professor, K L Deemed of University/Mechanical Engg. Department, Guntur, India
Email: diwakar4236@kluniversity.in
[3]Assoc. Professor, CVR College of Engineering/Mechanical Engg. Department, Hyderabad, India
Email: bnaidua@gmail.com

***Abstract:*** **In present day production systems, productivity is dependent on reliability of fewer but more sophisticated equipment and processes, particularly in Manufacturing and Material handling. As a key parameter of this I have found the reliability of the heavy moving machinery such as dumpers in the Singareni Colleries Godavarikani. For this the methodology of Reliability Centered Maintenance is taken as a part of that the Time Between Failures (TBF) and Time To Repair (TTR) for the same have been found and there by plotted the cumulative graphs between the Failure No Vs Cumulative TBF and also TTR. There from did the trend analysis; trend analysis is an aspect of technical analysis that tries to predict the future based on past data. Trend analysis is based on the idea that what has happened in the past gives Engineers an idea of what will happen in the future. There are three main types of trends: positive trend, negative trend and no trend. All the dumpers have been classified in the category of various trend categories so that the suitable maintenance plans have opted to increase the reliability of the heavy earth moving machinery. Hence based on the results obtained from the trend analysis the reliability of the dumpers can be found. That finally enhances the productivity of the system. This is not only limited to the coal mines but also can be applied or useful in all the company's or industries which can use any type of earth moving machinery.**

***Index Terms:*** **Heavy earth moving machinery, Reliability, Time between failures, Time to repair.**

## I. Introduction

The analysis on dumpers operated in Open Cast Project (OCP-III) mine of Singareni Collieries Company Limited (SCCL), Ramagundam are taken up with the following objectives.

1. To check whether the machines have come to their third stage of life cycle (Bathtub curve).
2. To identify the failure distribution and failure patterns of LHD vehicles [1,2,3].
3. To estimate the reliability characteristics of LHD vehicles.
4. To establish reliability oriented maintenance instead of time based preventive maintenance.
5. To optimize the overall maintenance cost.
6. To evaluate group behavior and hence to estimate contribution of each machine to the productivity/loss of production.
7. To evaluate reliability characteristics and failure behaviors of sub units so as to find which components are contributing to higher failures.
8. To establish suitable replacement policy for equipment and sub units.

### *A. Contribution of this Paper*

On the whole this Paper is expected to contribute in the following fashion.

1. The trend tests will help the maintenance and production managers to predict the behavior of machinery. More clearly the trend test indicates in which state the machine stands in its life cycle (Bathtub curve).
2. Maintenance/production managers can thus come to a decision to adopt suitable policy of maintenance such as contractual/preventive/OFCM/CBM etc. hence plan for suitable maintenance policies aimed at utmost reliability[4,5].
3. The TTT plots indicate whether the failures of a machine are increasing or constant or decreasing.
4. The TTT plots can also help in planning and scheduling the reliability oriented preventive maintenance.
5. The reliability growth plots can be used to check whether the machine reliability can be improved by the modifications suggested.
6. The analysis can help to arrive at a decision on replacement policy of the equipment.
7. The analysis of subunits can give an idea for the group replacement of the components or parts.

### *B. Limitations*

Calculation errors: In analysis and calculations wherever accuracy is not significant, figures are rounded off to the

CVR Journal of Science and Technology, Volume 19, December 2020
DOI: 10.32377/cvrjst 1924

nearest whole number. It may hence contain or appear as an error and is to be ignored as it is negligible [6,7].

Influencing Factors: Various factors can affect the performance of dumpers.

### *C. Assumptions*

Dumpers unavailability due to the natural disasters or any kind environmental impacts will be assumed as neglected. Hence in that particular case the dumpers are not treated as unavailable.

### *D. Procedure for RCM modelling*

Step 1: Identification and Definition of Problem or Setting the Hypothesis
Step 2: Collection of Relevant Data
Step 3: Removal of Inconsistencies and Errors in Data
Step 4: Trend Analysis and Correlation Tests
Step 5: TTT Plots to Examine Exponential Fit
Step 6: Fitting the Suitable Model
Step 7: Confirmation Tests and Goodness of Fit
Step 8: Reliability Centred Maintenance Planning and Scheduling

## II. METHODOLOGY

The field data is collected for the equipment categorized under repaired items in the form of Time between Failures (TBFs) and Time To Repair (TTRs). The data inconsistencies and errors are removed and the refined data is analyzed by both types of models viz. graphical and analytical models. However, more importance is given to graphical methods since it provides better simple understanding and can be easily reproduced. The graphical tests such as eye-ball analysis, cumulative plot test and serial correlation determine the presence of trend. The machines, which exhibit presence of strong trend, are further analyzed and fitted into non-homogeneous Poisson process (NHPP) models. Power law process (PLP) model, one of the most popular and commonly used NHPP models can be used for such study. If there is no trend, it confirms the independently and identically distributed (IID) assumption. The values obtained can be checked with some analytical tests such as Laplace test [8,9]. The machines free from trend are further graphically analyzed through total time on test (TTT) plots. The exponential fit that confirms homogeneous Poisson process (HPP) models can be known from this analysis, otherwise can be categorized as renewable process (RP) model which is in accordance with Weibull pattern. The goodness of fit (analytical) tests can confirm this. Thus, reliability characteristics and maintenance schedules can be estimated. Further, their reliability growth plots can also be drawn to estimate the improvements [10,11,12]. The reliability analysis and maintenance formulation are the key areas for enhancement of the dumpers performance. Further it is also to be understood that reliability is the key indicator of the dumper performance and also it has the influence over the other facets of the machine life cycle (MLC). Rahimdel, M et al have made an interesting research towards the betterment of the machines by analyzing the machine position in the MLC and also the cause and effects were found. Wang, R et al have used the failure mode effects and criticality analysis for understanding the failure criteria and their prioritization.

TABLE I.
CUMULATIVE PLOT TEST TABLE-C-379

| Failure no | TTR | CTTR | CAUSE | TBF | CTBF |
|---|---|---|---|---|---|
| 1 | 160 | 160 | oil leakage | 120 | 120 |
| 2 | 138 | 298 | Hoist | 192 | 312 |
| 3 | 2250 | 2548 | Differential | 1128 | 1440 |
| 4 | 12 | 2560 | Brakes | 96 | 1536 |
| 5 | 8 | 2568 | Hose | 1056 | 2592 |
| 6 | 72 | 2640 | Body | 696 | 3288 |
| 7 | 348 | 2988 | Brakes | 24 | 3312 |
| 8 | 36 | 3024 | Brakes | 48 | 3360 |
| 9 | 42 | 3066 | Brakes | 48 | 3408 |
| 10 | 12 | 3078 | Brakes | 24 | 3432 |

Similarly, the remaining tables for C-379, C-362, C-378, C-306, C-304, C-314.

E-ISSN 2581 - 7957
P-ISSN 2277 - 3916

DOI: 10.32377/cvrjst 1924

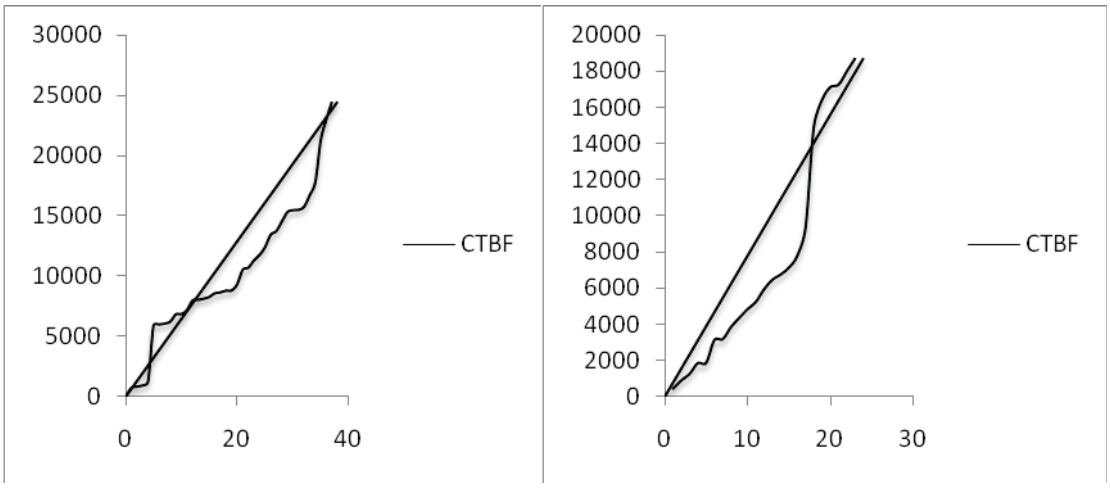


Figure 1. Cumulative Plot Test for C-379 and C-362 Dumpers

Similarly the remaining graphs for C-379, C-362, C-378, C-306, C-304, C-314, C-312, C-310, C-371, C-370, C-313, C-301, C-303, C-309, C-366, C-381, C-307, C-354, C-305, C-384, C-374, C-353, C-377, C-302, C-352, C-357, C-368, C-383, C-363, C-308

TABLE II.
TREND ANALYSIS TABLE

| Sl. No | Dumper No | Cumulative Trend Test | EyeBall Trend Test | Trend |
|---|---|---|---|---|
| 1 | C-361 | Weak +Ve Trend | No Trend | No Trend |
| 2 | C-369 | +Ve Trend | +Ve Trend | +Ve Trend |
| 3 | C-375 | No Trend | No Trend | No Trend |
| 4 | C-357 | No Trend | No Trend | No Trend |
| 5 | C-353 | Strong +Ve Trend | Strong +Ve Trend | +Ve Trend |
| 6 | C-374 | Weak +Ve Trend | No Trend | No Trend |

**Trend Analysis**

1. 20 Dumpers out of 36are not possessing any trend.
2. 10 Dumpers are showing a positive trend.
3. 06 Dumpers are showing a negative trend.

## III. TTT PLOTS BY MLE METHOD

TABLE III.
MLE METHOD FOR C-361

| F.NO | TBF | CTBF | OTBF | SI | I/N | PHI | SLOPE |
|---|---|---|---|---|---|---|---|
| 1 | 696 | 696 | 8 | 288 | 0.027027 | 0.011784 | 0.050595 |
| 2 | 120 | 816 | 24 | 848 | 0.054054 | 0.034697 | 0.123448 |
| 3 | 96 | 912 | 48 | 1664 | 0.081081 | 0.068085 | 0.217251 |
| 4 | 288 | 1200 | 72 | 2456 | 0.108108 | 0.100491 | 0.30909 |
| 5 | 4704 | 5904 | 72 | 2456 | 0.135135 | 0.100491 | 0.336117 |
| 6 | 72 | 5976 | 72 | 2456 | 0.162162 | 0.100491 | 0.363144 |
| 7 | 72 | 6048 | 96 | 3176 | 0.189189 | 0.129951 | 0.449091 |
| 8 | 168 | 6216 | 96 | 3176 | 0.216216 | 0.129951 | 0.476118 |
| 9 | 600 | 6816 | 120 | 3848 | 0.243243 | 0.157447 | 0.558137 |
| 10 | 17568 | 24384 | 144 | 4496 | 0.27027 | 0.183961 | 0.638192 |

Similarly, the remaining tables for C-379, C-362, C-378, C-306, C-304, C-314

E-ISSN 2581 - 7957
P-ISSN 2277 - 3916


DOI: 10.32377/cvrjst 1924

## IV. TTT Plots by KME Method

TABLE IV.
KME method for C-361

| F. NO | OTBF | LN(OTBF) | Ti(Beeta) | PRODUCT | CDF | PHI | SLOPE |
|---|---|---|---|---|---|---|---|
| 1 | 8 | 2.07944154 | 42.22425 | 87.80287 | 3E-05 | 4.1E-06 | 4E-05 |
| 2 | 24 | 3.17805383 | 305.0565 | 969.4859 | 0.00022 | 5.4E-05 | 0.0003 |
| 3 | 48 | 3.87120101 | 1062.268 | 4112.254 | 0.00075 | 0.00026 | 0.0013 |
| 4 | 72 | 4.27666612 | 2203.934 | 9425.488 | 0.00156 | 0.00057 | 0.0027 |
| 5 | 72 | 4.27666612 | 2203.934 | 9425.488 | 0.00156 | 0.00057 | 0.0027 |
| 6 | 72 | 4.27666612 | 2203.934 | 9425.488 | 0.00156 | 0.00057 | 0.0027 |
| 7 | 96 | 4.56434819 | 3699.033 | 16883.68 | 0.00261 | 0.00093 | 0.0045 |
| 8 | 96 | 4.56434819 | 3699.033 | 16883.68 | 0.00261 | 0.00093 | 0.0045 |
| 9 | 120 | 4.78749174 | 5527.468 | 26462.71 | 0.0039 | 0.00134 | 0.0066 |
| 10 | 144 | 4.9698133 | 7674.542 | 38141.04 | 0.00541 | 0.00181 | 0.009 |

Similarly the remaining tables for C-379, C-362, C-378, C-306, C-304, C-314, C-312, C-310, C-371, C-370, C-313, C-301, C-303, C-309, C-366, C-381, C-307, C-354, C-305, C-384, C-374, C-353, C-377, C-302, C-352, C-357, C-368, C-383, C-363, C-308

## V. Results of TTT Plotting by MLE and KME Methods

TABLE V.
List of Results

| Sl. No | Dumper No | MLE METHOD | KME METHOD | RESULT |
|---|---|---|---|---|
| 1 | C-361 | Deteriorating | Deteriorating | Deteriorating |
| 2 | C-375 | Deteriorating | Deteriorating | Deteriorating |
| 3 | C-357 | Deteriorating | Deteriorating | Deteriorating |
| 4 | C-372 | Deteriorating | Deteriorating | Deteriorating |
| 5 | C-383 | Deteriorating | Deteriorating | Deteriorating |
| 6 | C-352 | Improving | Improving | Improving |

**Characteristics of reliability designing and planning**

The following characteristics have been chosen for reliability designing and planning for maintenance of repairable equipment as these are found more suitable and meaningful [13,14,15].

**T (Mode)**

It is the most frequent probable Time Between Failure in a sample space of time domain.

$$T(mode) = \alpha * (1 - 1/\beta)^{1/\beta}$$

**T (Median)**

It is the median Time Between Failure of an equipment among the sample space of time domain about a Weibull Distribution at Reliability (R) = 0.5

$$T(median) = \alpha * (-\ln 0.5)^{1/\beta}$$

**T (Optimal)**

It is an optimal Preventive Maintenance interval for a machine to be observed at a certain reliability value.

$$T(optimal) = \alpha*(1/(\beta - 1))^{1/\beta}$$

**T (Characteristic)**

The life (period) of equipment in which 63.2 % of Weibull failures will occur. It is independent of shape parameter and reliability.

$T(Char) = \alpha$ [It's value is equal to alpha ($\alpha$)].

**B1 Life**

It is the time at which 1 percent of the population will have failed at a reliability of 0.99.

$$B1\ life = \alpha * (-\ln 0.99)^{1/\beta}$$

**B.1 Life**

It is the time at which 0.1 percent of the population will have failed at a reliability of 0.999.

$$B.1\ life = \alpha * (-\ln 0.999)^{1/\beta}$$

E-ISSN 2581 - 7957
P-ISSN 2277 - 3916

CVR Journal of Science and Technology, Volume 19, December 2020
DOI: 10.32377/cvrjst 1924

## VI. Summary of Results

TABLE VI.
SUMMARY OF RESULTS

| Sl. No | D. No | α | β | T (Mode) | T (Median) | T (Optimal) | T (Char) | B1 Life | B.1 Life |
|---|---|---|---|---|---|---|---|---|---|
| 1 | C-361 | 2613.05 | 1.8 | 1665.58 | 2131.657 | 3475.86 | 2613.05 | 202.88 | 56.31 |
| 2 | C-375 | 454.733 | 1.05 | 26.079 | 320.959 | 755.88 | 454.733 | 5.73 | 0.64 |
| 3 | C-357 | 1237.11 | 1.62 | 683.79 | 987.17 | 2153.9 | 1237.11 | 72.81 | 17.58 |
| 4 | C-352 | 1847.66 | 2.26 | 667.58 | 783.78 | 936.62 | 1847.66 | 95.24 | 30.2 |
| 5 | C-374 | 1288.85 | 1.68 | 752.3 | 1036.23 | 1621.43 | 1288.85 | 83.37 | 21.11 |
| 6 | C-383 | 609.6 | 1.3 | 198.09 | 459.97 | 1532.14 | 609.6 | 17.71 | 3.01 |

## VII. Scheduling

The number of working hours after which the dumper should be taken for minor and major overhauling for increased efficiency of the dumper are given below.

TABLE VII.
SCHEDULING OF DUMPERS

| Sl. No | Dumper. No | Major Overhauling | Minor Overhauling |
|---|---|---|---|
| 1 | C-361 | 3475.86 | 2613.05 |
| 2 | C-375 | 755.88 | 454.733 |
| 3 | C-357 | 2153.9 | 1237.11 |
| 4 | C-352 | 936.62 | 940.67 |
| 5 | C-374 | 2321.43 | 1288.85 |
| 6 | C-383 | 1532.14 | 609.6 |

The available hours as well as utilized hours for dump trucks are less.

The availability of dumpers for production / the dumpers on roll at any point of time is 28 to 30 out of 36 (85T dumpers), at Ramagundam open cast project. This should be improved.

It is observed that about 35 – 40 % of the time is lost in attending machine breakdowns. A critical analysis of machine failures were taken into consideration, to locate the areas that require additional attention in maintenance, ordering spares and other requirements. Out of these the Spare Parts management area should be concentrated to strengthen the maintenance activity.

At the Ramagundam OC-III project, the reporting system is so poor, it was found difficult to analyze typical types of faults. Sometimes the reported failure could not be ascertained for want of confirmation from workshops. Hence with available data only reliability/availability analysis was carried out on 36 nos. of 85T trucks. The

## VIII. Results and Discussions

The purpose of this study is to collect data relating to transporting equipment operating in a group of coal mines, record keeping should be made perfect in directly usable form.

At last, it is advised that the company must emphasize Research and Development particularly, to perform research in reliability studies pertaining to the maintenance department.

It is better to establish a separate cell to evaluate reliability, schedule maintenance intervals, costing maintenance planning, study inventory policies, logistic studies etc. Such a department may be established with highly experienced, qualified and intellectual engineers and managers. If required this department may be centralized to oversee all the machines operated in various units/quarries/OCPs/UG mines of SCCL so that the transferability, interchangeability can be increased in the interest of enhancing the overall productivity. Further, the company should adopt by sponsoring some research scholars and make tie up with academicians such as professors to help in studying in this direction.

analyze data and evaluate the performance of dump trucks using the techniques of reliability engineering. Further the study is aimed at locating areas that need special attention, so that the availability and utilization of transport equipment can be improved in addition to enhancing the machine life.

In today's economic climate, it is extremely important to minimize both capital and operating costs in any mining project. In an open cast project loading and hauling are the expense areas, the later costing as good as 30 to 50% of total mining cost. There is a concentrated effort to reduce haulage costs as well as limiting the haulage fleet size so that overall capital and operating costs are minimized.

The results of the trend analysis have given the nature and direction of the dumpers performance and also it has the laid arena for the total time on test. The complete analysis over the time horizon has also yielded the dumpers ability for the work to be performed.

### *A. Summary of Results*

**Trend Analysis**

1. 20 Dumpers out of 36 do not possess any trend.
2. 10 Dumpers are showing a positive trend.
3. 06 Dumpers are showing a negative trend.

## IX. Conclusions

The conclusions drawn from the aforesaid discussion of results after thorough analysis and scrutiny are summarized in the paragraphs to follow.

### *A. Investigation on Machine Condition*

The fundamental objective with which this research work has been started is to find the machine condition. The Dumpers are chosen for this purpose as they are assumed to have high a failure rate. The failure periods are time independent and not contradicting IID assumption. They are found to have increasing failure rates even though there is no evidence of Trend. Thus the assumption with which it started has been found true and hence it can be concluded that they are on the thresholds of the third stage (Old age/Worn out failures) of Machine Life Cycle i.e. BathTub Curve.

### *C. Reliability Characteristics*

Various Reliability Characteristics such as $T_{(mode)}$, $T_{(average)}$, $T_{(optimal)}$, $T_{(median)}$, B1 life, B.1 life, Scale Parameter (α) and Shape Parameter (β) of Weibull MLEs are estimated. These characteristics will be highly useful guidelines for scheduling the maintenance activity and to deriving the suitable maintenance policy.

### *D. Maintenance Schedule*

The present Preventive Maintenance is modified with reliability orientation. The existing Yearly, Half Yearly, Quarterly and Monthly Maintenance are substituted by Complete overhauling (C), Major Overhauling (M), minor overhauling (m) and Inspection (I). The frequency of dumper maintenance is arranged based on the machine conditions and MTBF or Failure Rate (and other Reliability Characteristics). The detailed proposed schedule chart is provided for quick reference. However, a little flexibility is taken in preparing the schedule in view of accommodating the complete and uniform overhauling of the dumpers and distributing the maintenance force evenly. This could be altered according to the practical demands and availability.

The performance of dump trucks in opencast coal mines are evaluated using the conventional statistical techniques and the performance when compared to the set norms of CMPDI with respect to available hours and utilized hours were found to be not up to the mark expected. The mines chosen for evaluation of transport equipment are working in a harsh environment with gradients of 1 in 10, with limited workshop facilities and trained personnel, the mining technology is different (old), in the sense open cast mining of already developed mines in a bored and pillar system. Further, it is found that the maintenance department is giving less importance to reliability orientation than production orientation.

### *B. TTT Plotting*

1. 16 numbers of Dumpers out of 20 no trend are deteriorating.
2. 04 numbers of Dumpers out of 20 no trend are Improving.

### *E. Further Scope*

The present study is confined to a small no. of equipment i.e. 36, 85T trucks. Collection of data is not only a time consuming task but it is also challenging because proper collection of data is possible only when failure and repair logs are maintained accurately. Equipment performance depends among other things than its age also. Failure/repair data, properly collected, analysed and stored can be used by the management for a(a) maintenance planning, (b) spare parts provision and (c) ordering new equipment depending upon the life of the project. Right now, cost of maintenance, equipment wise is not readily available for evaluation of effectiveness of maintenance. There is a need to provide a PC at the mine workshops to log the information and store for retrieval. The log sheets should properly be planned and the reporting system has to be perfected. It is observed that there is vast scope for improving machine utilized hours in case of 85T dumpers by reducing the idle hours by properly reorganizing the interfacing activities and maintenance plans.

Performance of mine not only depends upon production equipment like shovels/dumpers but very much affected by availability and utilization of service equipment like dozers, scrapers, graders and other equipment. An integrated study of availability of all the equipment in a mine can only be improved by the enhanced utilization of the production equipment in spite of their availability.

## REFERENCES

[1] Vilarinho, S., Lopes, I. and Oliveira, O.A. (2017), "Preventive maintenance decisions through maintenance optimization models: a case study", 27th International Conference on Flexible Automation and Intelligent Manufacturing, FAIM2017, Procedia Manufacturing 11, Modena, June 27-30, pp. 1170-1177.

[2] Sinha, R.S. and Mukhopadhyay, A.K. (2015), "Reliability centered maintenance of cone crusher- a case study", International Journal of System Assurance Engineering and Management, Vol. 6 No. 1, pp. 32-35.

[3] Navas, M.A., Sancho, C. and Carpio, J. (2017), "Reliability analysis in railway repairable systems", International Journal of Quality & Reliability Management, Vol. 34 No. 8, pp. 1373-1398, available at: https://doi.org/10.1108/IJQRM-06-2016-0087

[4] Mohammadi, M., Rai, P. and Gupta, S. (2016), "Improving productivity of dragline through enhancement of reliability inherent availability and maintainability", Acta Montanistica Slovaca, Vol. 21 No. 1, pp. 1-8.

[5] Fan, Q. and Fan, H. (2015), "Reliability analysis and failure prediction of construction equipment with time series models", Journal of Advanced Management Science, Vol. 3 No. 3, pp. 203-210.

[6] Campbell, J.D., Jardine, A.K.S. and McGlynn, J. (2017), Asset Management Excellence: Optimizing Equipment Life-Cycle Decisions, 5nd ed., Taylor and Francis Group, LLC, Boca Raton, FL.

[7] Balaraju, J., Govinda Raj, M. and Murthy, C.S.N. (2018), "Estimation of Reliability based maintenance time intervals of load haul dumper in an underground coal mine", International Journal of Mining and Environment, Vol. 9 No. 3, pp. 761-770, doi: 10.22044/jme.2018.6813.1508.

[8] Barabady, J. and Kumar, U. (2018), "Reliability analysis of mining equipment – a case study of a crushing plant at jajarm bauxite mine in Iran", Reliability Engineering and System Safety, Vol. 103 No. 4, pp. 647-653.

[9] Bala, R.J., Govinda, R.M. and Murthy, C.S.N. (2018), "Reliability analysis and failure rate evaluation of load haul dump machines using weibull distribution analysis", Journal of Mathematical Modeling of Engineering Problems, Vol. 5 No. 2, pp. 116-122.

[10] Allahkarami, Z., Sayadi, A.R. and Lanke, A. (2016), "Reliability analysis of motor system of dump truck for maintenance management", Current Trends in Reliability Availability Maintainability and Safety, Lecture Notes in Mechanical Engineering, Springer International Publishing, pp. 681-688, available at: https://doi.org/10.1007/978-3-319-23597-4

[11] Wang, R., Sha, N., Gu, B., & Xu, X. (2014). Statistical analysis of a Weibull extension with bathtub-shaped failure rate function. Advances in Statistics, 2014, 1–15. https://doi.org/10.1155/2014/304724

[12] Zhang, T., Li, W., & Dwight, R. (2016). Modeling failure data by 3-parameter Weibull distribution models. 11th International Conference on Reliability, Maintainability and Safety (ICRMS), 1–8. IEEE.

[13] Barabady, J., & Kumar, U. (2008). Reliability analysis of mining equipment: A case study of a crushing plant at Jajarm Bauxite Mine in Iran. Reliability Engineering & System Safety, 93, 647–653. https://doi.org/10.1016/j.ress.2007.10.006

[14] Harish Kumar, N. S., Choudhary, R. P., & Murthy, C. S. N. (2018). Failure rate and reliability of the KOMATSU hydraulic excavator in surface limestone mine. American Institute of Physics Conference Series, 1943 (020007), 1–9.

[15] Rahimdel, M. J., Hosienie, S. H., Ataei, M., & Khalokakaei, R. (2017). The reliability and maintainability analysis of pneumatic system of rotary drilling machines. Journal of the Institution of Engineers (India): Series D, 94(2), 105–111. https://doi.org/10. 1007/s40033-013-0026-0

E-ISSN 2581 - 7957
P-ISSN 2277 - 3916

CVR Journal of Science and Technology, Volume 19, December 2020
DOI: 10.32377/cvrjst 1925

# Influence of Bottom Ash as Partial Replacement for Fine Aggregate on the Properties of Hybrid Fiber Reinforced Cement Concrete

V. Nikhil[1] and V. Naveen[2]
[1]PG Scholar, CVR College of Engineering/Civil Engg. Department, Hyderabad, India
Email: vadlanikhil1695@gmail.com
[2]Asst. professor, CVR College of Engineering/ Civil Engg. Department, Hyderabad, India
Email: vuppunaveen22@gmail.com

*Abstract:* **The major problem the world is facing today is environmental pollution. In the construction industry mainly the production of Portland cement will cause the emission of CO2 which results in environmental pollution. On the other hand, the problem of depleting natural resources can be solved by the usage of industrial by-products obtained from the construction industry. concrete technology is heading towards an entirely new era by the use of Bottom ash, polypropylene fibers & Steel fibers in concrete. Concrete when mixed with fibers, give fibrous concrete. The mechanical property of fibrous concrete is superior to that of ordinary concrete. Bottom ash will be evaluated for use as supplementary Fine aggregate material in Fine aggregate based system, the performance of Bottom ash mixtures will be compared to controlled mixtures and mixtures incorporating Bottom ash as replacement for Fine aggregate.**

**In this present study, the effect of bottom ash on strength parameters and durability properties of hybrid fiber reinforced concrete are assessed. Fine aggregate is replaced with bottom ash by 5%,10%,15%,20%,25% and 30% in concrete specimens with 1% of hybrid fibers. Hybrid fiber (0.5 % of steel fibers and 0.5 % polypropylene fibers) were taken by total volume of concrete. The experimental studies show that bottom ash can be used in concrete as partial replacement for the fine aggregate without any effect on strength and durability.**

*Index Terms:* **Bottom ash, steel fibers, polypropylene fibers, strength parameters.**

## I. Introduction

The present research work was aimed to explore the possibility of use of low-calcium coal bottom ash as a construction material in place of the river sand. The appearance and particle size of coal bottom ash is similar to that of river sand. [1] The physical properties of coal bottom ash attract it to be used in concrete as fine aggregate either in partial or total replacement of river sand. In the literature published during the last decade, coal bottom ash has been targeted as fine aggregate in concrete. The published research data which is confined to strength properties only indicate that coal bottom ash is a viable material as sand replacement in concrete.[2] The present research study was motivated by the ecological concerns over the disposal of coal bottom ash and scarcity of natural sources of river sand in the country. The ultimate objective of the present research study was to explore the feasibility of use of low-calcium coal bottom ash either in partial or total replacement of natural river sand in manufacturing of concrete. [5-8]

## II. Literature Review

Kiran M Sannakki & Sanjith[1] Present study investigates the effect of coal bottom ash as partial replacement to sand in concrete. Compressive strength characteristics of M40 grade concrete were studied with bottom ash varying from 0% (Conventional concrete), 10%, 20%, and 30% replacement and at different curing periods. Analysis of results showed that maximum strength of 49.56 N/mm2 by replacing 20% of bottom ash as replacement fine aggregate Sand quarrying is done to extract sand for construction purposes. The workability of concrete decreased with the increase in bottom ash content due to the increase in water demand, which is nullified by increasing the content of super plasticizer. The compressive strength and Split Tensile strength for 7, 14 and 28 days were increased up to 20% replacement and after that gradually decreased for further replacement.

Kylasnath M, Ranjan Abraham [2], the study was carried out to evaluate the suitability of utilizing bottom ash as a partial replacement to fine aggregate in high strength concrete (M60 grade). Experiments were conducted by replacing fine aggregate with bottom ash in varying percentages 0%, 5%, 10%, 15%, 20%, 25% and 30%. Mechanical properties such as compressive strength, splitting tensile strength and flexural strength were evaluated. Test results indicated that bottom ash is suitable for improving the mechanical properties of concrete. Increase in water demand was incorporated by increasing the content of superplasticizer. The optimum replacement percentage of fine aggregate with bottom ash was found to be 20%. Compressive strength for 3, 7 and 28 days were increased up to 20% replacement and after that gradually decreased for further replacement. Bottom ash mix showed about 3.9%, 4.2% and 6.5 % increase in the 3-day, 7 day and 28 day compressive strength as compared to control mix

M. Purushothaman[3] & RM. Senthamarai[4], this paper reports the results of an experimental program to investigate the effect of using thermal power station bottom ash as a

E-ISSN 2581 - 7957
P-ISSN 2277 - 3916

CVR Journal of Science and Technology, Volume 19, December 2020
DOI: 10.32377/cvrjst 1925

replacement of natural fine aggregate on the properties of High-performance concrete (HPC). A Total of 10 mixes were prepared for these tests. Out of which five are Bottom ash Concrete (BAC) and five are Conventional Concrete mixes (CC). BAC mixes were evaluated for compressive, tensile and flexural strengths development for the concrete ages of 7 days,28 days,56 days and 90 days and the results were compared with those of CC mixes. The incorporation of 10% silica fume and 40% bottom ash in concrete results in significant improvements in its mechanical properties of BAC compared to the control mix. It should be noted that further research work is needed to explore the effect of bottom ash as fine aggregates on the durability properties of concrete.

Ramesh kanagavel, Arunachalam Kalidass [5], Mechanical properties of hybrid fibre reinforced quaternary concrete Quaternary blending cement concrete with fibres is studied in terms of compressive, split tensile, and flexural strength properties, and impact resistance. Fly ash, rice husk ash, and limestone powder are used as partial replacement of cement. Steel, carbon, and polypropylene fibres, are used in different fractions. The results show that the steel-carbon and steel-carbon-polypropylene hybrid fibre reinforced concretes perform better with regard to compressive, split tensile, and flexural strength properties, and impact resistance. There is a positive synergy in SCPHFRC mixes at the 0.5 % volume fraction of steel fibres, compared to SCHFRC mixes. However, this synergic effect disappears at the 1 % and 1.5 % volume fraction of steel fibres along with carbon and PP fibres. SCHFRC mixes perform better than SCPHFRC mixes at the 1 % and 1.5 % volume fraction of steel fibres. Mono CFRC mixes performed poorly with respect to impact load. SCHFRC and SCPHFRC specimens resisted high impact loads prior to complete failure. The specimens with steel-carbon-PP hybrid fibres exhibited the highest impact resistance and the maximum percentage of increase in the post crack resistance of about 69.8 % in the S3C1P1 mix, compared to the control concrete at 28 days. In the S3C1P1 mix, the energy required to produce the first crack increased by 5.82 times and the energy required for complete failure increased by 9.84 times, compared to the control concrete at 28 days.

## III. Experimental Study

### A. Cement

Ordinary Portland Cement of 53 grade conforming to IS:8112-1989 was used in the present study.

### B. Aggregates

The physical properties of Fine aggregate and Coarse aggregate used in the present study are presented in Table I.

TABLE I.
PHYSICAL PROPERTIES OF AGGREGATES

| Physical property | Fine aggregates | Coarse aggregates |
|---|---|---|
| Specific gravity | 2.70 | 2.72 |
| Fineness Modulus | 2.83 | 7.6 |
| Water Absorption | 1.7% | 0.9% |

- Fine aggregate conforming to grading zone II of Table 4 of IS 383.
- Coarse aggregate in the concrete mix was taken in proportion to 20mm passing.

### C. Water

Potable water was used in the preparation of concrete.
Water used for concrete conforms to IS:456-2000.

### D. Bottom ash

Coal bottom ash has angular, irregular, porous and rough surface textured particles. The particles of coal bottom ash range from fine sand to fine gravel. Coal bottom ash has appearance and particle size

TABLE II.
PHYSICAL PROPERTIES OF COAL BOTTOM ASH

| Sl. No | Properties | Value |
|---|---|---|
| 1 | Specific gravity | 2.66 |
| 2 | Water absorption | 1.52% |
| 3 | Fineness modulus | 2.55 |
| 4 | Maximum Size | 20mm |

distribution similar to that of river sand. Coal bottom ash is usually a well-graded material although variations in particle size distribution can be encountered from the same power plant.

### E. Chemical Admixture

Super plasticizer used in the present study was a conplast: SP-430. 1% to 1.5% Super plasticizer is taken by the weight of the binder in a concrete mix to increase workability.

### F. Steel fibers

Hooked end steel fibers of 0.4mm diameter and aspect ratio of 30 and 12mm length were used.

### G. Polypropylene fibers

Polypropylene fibers were formerly known as Steal the, these are micro reinforcement fibers and are 100% virgin homopolymer polypropylene graded monofilament fibers.

TABLE III.
PHYSICAL PROPERTIES OF POLYPROPYLENE FIBERS

| Sl.No | Parameter | Value |
|---|---|---|
| 1 | Appearance | Short cut staple fibre |
| 2 | Thickness | 20 Micron |
| 3 | Length | 6-12 mm |
| 4 | Colour | white |
| 5 | Specific gravity | 0.9 |

E-ISSN 2581 - 7957
P-ISSN 2277 - 3916

CVR Journal of Science and Technology, Volume 19, December 2020
DOI: 10.32377/cvrjst 1925

### *H. Mix proportion*

M40 grade is adopted and the mix proportion is 1:1.56:2.23 is obtained as per IS10262:2009.

- Cement = 437.6 kg/m$^3$
- Fine aggregate = 713 kg/m$^3$
- Coarse aggregate = 1099.12 kg/m$^3$
- Water = 191 kg/m$^3$

## IV. Test Results

### *A. Workability*

Slump test is performed to determine the workability of concrete. Normal conventional concrete with bottom ash as replacement.

TABLE IV.
WORKABILITY OF NC

| Mix | Fine aggregate % | Bottom ash % | Slump (mm) |
|---|---|---|---|
| Mix 1 | 100 | 0 | 68 |
| Mix 2 | 95 | 5 | 63 |
| Mix 3 | 90 | 10 | 60 |
| Mix 4 | 85 | 15 | 56 |
| Mix 5 | 80 | 20 | 53 |
| Mix 6 | 75 | 25 | 50 |
| Mix 7 | 70 | 30 | 45 |

- Conventional concrete with bottom ash as replacement along with 1% of hybrid fibers (0.5% of steel fibers +0.5 % of polypropylene fibers) and 1% to 1.5% of super plasticizer by weight of binder are added to concrete.

TABLE V.
WORKABILITY OF HFRC

| Mix | Bottom ash % | Hybrid Fibers % | Super Plasticizer % | Slump mm |
|---|---|---|---|---|
| Mix 1 | 0 | 1 | 0 | 55 |
| Mix 2 | 5 | 1 | 0 | 50 |
| Mix 3 | 10 | 1 | 0 | 49 |
| Mix 4 | 15 | 1 | 1 | 48 |
| Mix 5 | 20 | 1 | 1 | 46 |
| Mix 6 | 25 | 1 | 1.5 | 43 |
| Mix 7 | 30 | 1 | 1.5 | 41 |

### *B. Compressive strength*

Compressive strength of the concrete is obtained by casting and testing of cubes (size 100mm ×100mm × 100mm) after the curing period of 7 days and 28 days.

The obtained results are tabulated in below table

TABLE VI.
COMPRESSIVE STRENGTH OF NC AND HFRC (7 DAYS)

| Mix | B.A % | NCC avg 7 days strength | HFRC avg 7 days strength |
|---|---|---|---|
| Mix 1 | 0 | 33 | 36.5 |
| Mix 2 | 5 | 30 | 33.2 |
| Mix 3 | 10 | 33.2 | 35.8 |
| Mix 4 | 15 | 35.4 | 39.9 |
| Mix 5 | 20 | 33.7 | 38.4 |
| Mix 6 | 25 | 31.4 | 36.1 |
| Mix 7 | 30 | 30 | 35 |

Compressive Strength of NC and HFRC (28days)

| Mix | B.A % | NCC avg 28 days strength | HFRC avg 28 days strength |
|---|---|---|---|
| Mix 1 | 0 | 49.3 | 52.9 |
| Mix 2 | 5 | 43.9 | 48 |
| Mix 3 | 10 | 46 | 53 |
| Mix 4 | 15 | 48.6 | 54.2 |
| Mix 5 | 20 | 45.1 | 49 |
| Mix 6 | 25 | 42.8 | 46.1 |
| Mix 7 | 30 | 41 | 44 |

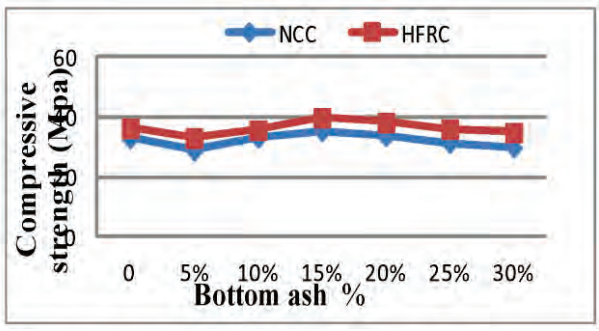


Figure 1. Average compressive strength of NC and HFRC at 7 days

E-ISSN 2581 - 7957
P-ISSN 2277 - 3916

CVR Journal of Science and Technology, Volume 19, December 2020
DOI: 10.32377/cvrjst 1925

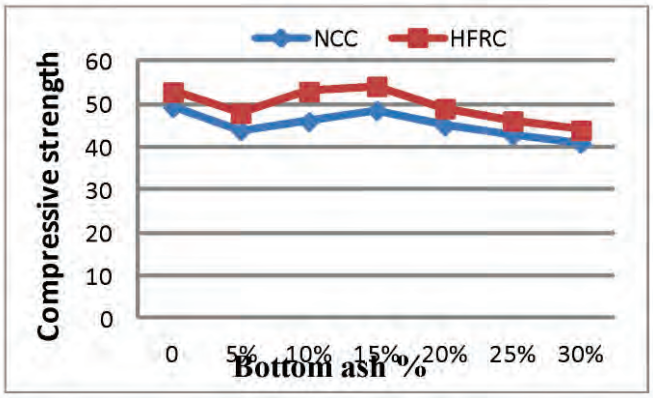


Figure 2. Average compressive strength of NCC and HFRC at 28 days

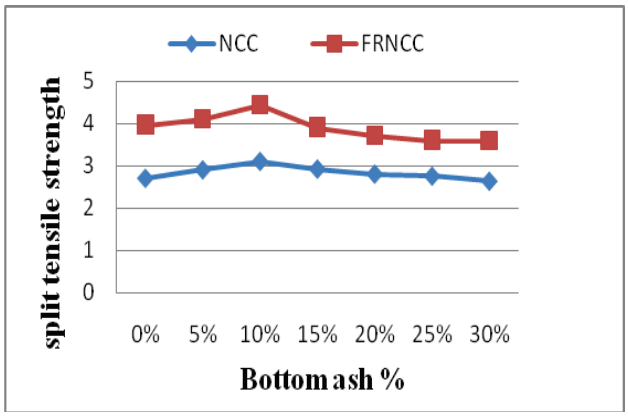


Figure 3. Average Split Tensile Strength of NCC and HFRC at 7 days

### C. *Split tensile strength*

Split tensile strength of the concrete is obtained by casting and testing of cylinders (size 300mm length and 150mm diameter) after the curing period of 7 days and 28 days.

The obtained results are tabulated in the table below.

TABLE VII.
SPLIT TENSILE STRENGTH OF NCC AND HFRC AT 7 DAYS.

| Mix | B.A % | NCC avg 7 days strength | HFRC avg 7 days strength |
|---|---|---|---|
| Mix 1 | 0 | 2.7 | 3.96 |
| Mix 2 | 5 | 2.9 | 4.1 |
| Mix 3 | 10 | 3.1 | 4.43 |
| Mix 4 | 15 | 2.92 | 3.9 |
| Mix 5 | 20 | 2.8 | 3.7 |
| Mix 6 | 25 | 2.75 | 3.6 |
| Mix 7 | 30 | 2.63 | 3.59 |

SPLIT TENSILE STRENGTH OF NCC AND HFRC AT 28 DAYS.

| Mix | B.A % | NCC avg 28 days strength | HFRC avg 28 days strength |
|---|---|---|---|
| Mix 1 | 0 | 3.94 | 5.95 |
| Mix 2 | 5 | 4.01 | 6.2 |
| Mix 3 | 10 | 4.3 | 6.42 |
| Mix 4 | 15 | 3.9 | 6.01 |
| Mix 5 | 20 | 3.82 | 5.86 |
| Mix 6 | 25 | 3.8 | 5.7 |
| Mix 7 | 30 | 3.75 | 5.62 |

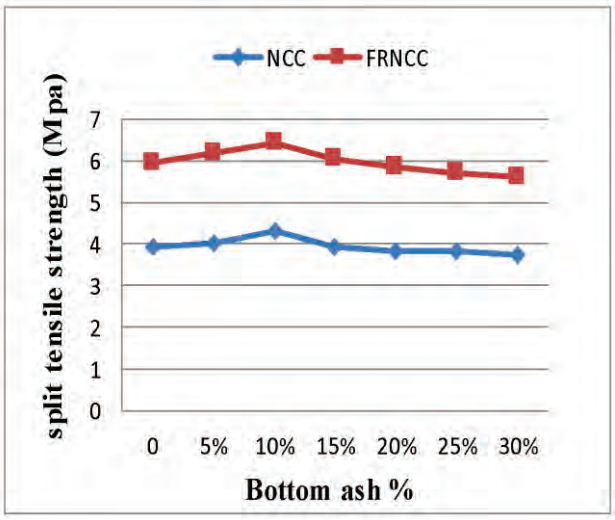


Figure 4. Average Split Tensile Strength of NCC and HFRC at 28 days

### D. *Flexural strength*

Flexural strength of the concrete is obtained by casting and testing of prisms (size 100mm ×100mm ×500mm) after the curing period of 7 days and 28 days.

The obtained results are tabulated in the table below.

TABLE VIII.
FLEXURAL STRENGTH OF NCC AND HFRC AT 7 DAYS

| Mix | B.A % | NCC avg 7 days strength | HFRC avg 7 days strength |
|---|---|---|---|
| Mix 1 | 0 | 3.9 | 5.95 |
| Mix 2 | 5 | 4.5 | 6.2 |
| Mix 3 | 10 | 4.7 | 6.65 |
| Mix 4 | 15 | 5.1 | 7.02 |
| Mix 5 | 20 | 4.8 | 6.8 |
| Mix 6 | 25 | 4.65 | 6.45 |
| Mix 7 | 30 | 4.3 | 6.1 |

E-ISSN 2581 - 7957
P-ISSN 2277 - 3916

CVR Journal of Science and Technology, Volume 19, December 2020
DOI: 10.32377/cvrjst 1925

FLEXURAL STRENGTH OF NCC AND HFRC AT 28 DAYS

| Mix | B.A % | NCC avg 28 days strength | HFRC avg 28 days strength |
|---|---|---|---|
| Mix 1 | 0 | 5.86 | 7.6 |
| Mix 2 | 5 | 6.82 | 8.62 |
| Mix 3 | 10 | 7.08 | 8.9 |
| Mix 4 | 15 | 7.3 | 9.55 |
| Mix 5 | 20 | 6.9 | 9.03 |
| Mix 6 | 25 | 6.76 | 8.7 |
| Mix 7 | 30 | 6.4 | 8.4 |

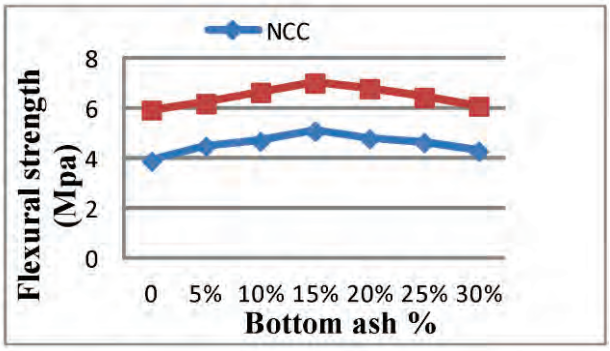


Figure 5. Average Flexural Strength of NCC and HFRC at 7 days

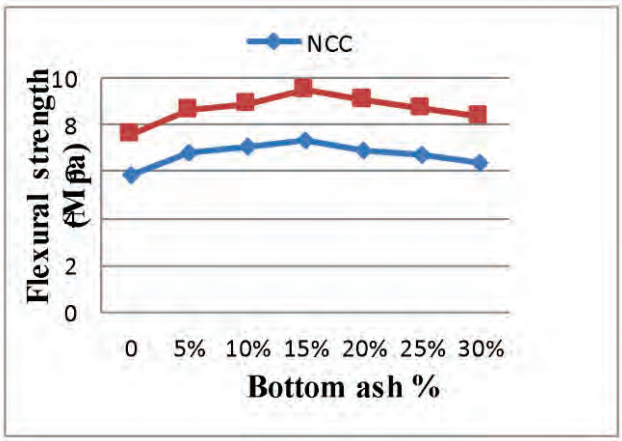


Figure 6. Average Flexural Strength of NCC and HFRC at 28 days

## I. *Durability*

Durability means the resistance to Physical or chemical deterioration of concrete resulting from interaction with the environment (Physical deterioration) or interaction between constituents (chemical deterioration) of concrete. Durability of concrete is related to its permeability. Permeability is the rate at which aggressive agents can penetrate to attack the concrete and the steel reinforcement. A durable concrete ensures corrosion resistance of embedded steel which in turn ensures a better longevity of the structure.

M40 concrete specimens were kept exposed to 5% solutions of sulfuric acid, hydrochloric acids and sodium sulphate. As specimens were continuously immersed in the solution for up to 28 days and 56 days and 98 days. The response of the specimens to the solutions was evaluated through change in appearance, weight, compressive strength and dimensions of solid diagonals.

Factors affected by acid attack on NCC and HFRC

a) Acid strength loss factor (ASLF) = Sr×(N/M),
Where Sr was a relative strength at N days (%), N is number of days at which the durability factor was required, M is number of days at which the exposure is to be terminated. A lower value of ASLF indicates greater stability towards acid attack.

b) Acid Attacking Factor (AAF) = (loss of acid length after immersion / original length) ×100%.
AAF is meant to indirectly measure the change in the length of diagonal (referred to as diagonal loss) in a typical concrete specimen after immersion in acids and sulphate for a certain period of time.

c) Acid weight loss factor (AWLF) = (Loss of weight of specimen after immersion / Original weight of specimen before immersion) ×100%

Higher value of the AWLF indicates that the weight loss was greater

**Acid Durability Loss Factors (ADLF)**

ADLF = ASLF × AAF × AWLF

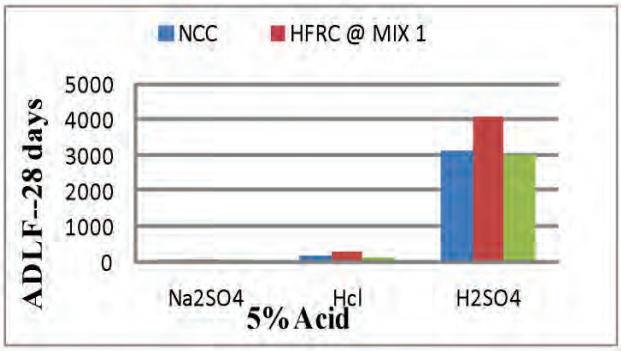


Figure 7. Acid Durability Loss Factors for NCC and HFRC at 28 days

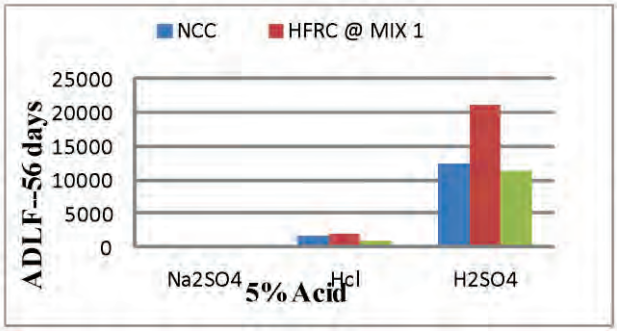


Figure 8 . Acid Durability Loss Factors for NCC and HFRCC at 56 days

CVR Journal of Science and Technology, Volume 19, December 2020
DOI: 10.32377/cvrjst 1925

TABLE IX.
ACID DURABILITY LOSS FACTORS FOR NCC AND HFRC AT 28 AND 56 DAYS

| Mix | Acid | Acid durability loss factors | |
|---|---|---|---|
| | | 28 days | 56 days |
| NHFC | $Na_2So_4$ | 5.4 | 41.73 |
| NC | | 10.63 | 75.70 |
| HFC | | 5.09 | 33.73 |
| NHFC | Hcl | 172.4 | 1628 |
| NCC | | 285.7 | 2106.6 |
| HFC | | 125.12 | 1024.3 |
| NHFC | $H_2So_4$ | 3131.5 | 12488.6 |
| NC | | 4099 | 21109 |
| HFC | | 3021 | 11362.14 |

## V. CONCLUSIONS

- The workability of fresh concrete is decreasing with increase in replacement of bottom ash.
- Test results states that compressive strength and flexural strength is achieved higher at 15% replacement of bottom ash in Normal conventional concrete (NC) and Hybrid fiber reinforced concrete (HFR).
- Split tensile strength is observed to be higher at 10% replacement of bottom ash in normal conventional concrete (NCC) and Hybrid fiber reinforced concrete (HFRC).
- With increase in period of immersion of the concrete in 5% of concentration of acid and sulphate like $Na_2SO_4$, HCL and $H_2SO_4$, there was damage of concrete near corners of cubes and such disruption in HFRC was less.
- When compared to Normal conventional concrete (NCC), the hybrid fiber reinforced concrete was
- found to be more durable against both acids and sulphate.

## REFERENCES

[1] Kiran Kumar M S1, Harish K S2, Vinay R B3, Ramesh M4, "Experimental study on partial replacement of fine aggregate by bottom ash in cement concrete", Volume: 05 Issue: 05 | May-2018.

[2] K.SathyaPrabha1, "Experimental Study on Properties of Concrete Using Bottom Ash with Addition of Polypropylene Fibre", Volume 5, Issue 8, August 2015.

[3] 1Abhishek Sachdeva,2 Gobind Khurana, "Strength Evaluation of Cement Concrete Using Bottom Ash as a Partial Replacement of Fine", Abhishek Sachdeva et al. 2015, Volume 3 Issue 6 Aggregates.

[4] P. Naga Gopi1, A. Sateesh2, "Experimental investigation of Cement Concrete with partially replacing the Fine Aggregate with Local available Soil and Adding coir and human hair Fibers" , Volume: 03 Issue: 06 | June-2016".

[5] 1Gagandeep,2Kshipra Gupta," effect of replacing fine aggregate with bottom ash in m30 grade of concrete with opc-43s cement", Volume 5, Issue 2 , Page No. 17-21 March-April 2017.

[6] P. Aggarwal∗ ,Y. Aggarwal, S.M. Gupta, "effect of bottom ash as replacement of fine aggregates in concrete", Asian journal of civil engineering (building and housing) vol. 8, no. 1 (2007).

[7] P.Ranapratap1, K.Padmanabham2, "effect of replacing fine aggregate with bottom ash in m40 grade of concrete with opc-53s cement", Volume: 05 Issue: 10 | Oct-2016.

[8] S.Sweetha1 E.Santhosh Kumar2, "Experimental Investigation on Replacement of Bottom Ash as Cement and Electronical Waste as Coarse Aggregate", International Journal of Advanced Research Trends in Engineering and Technology (IJARTET) Vol. 4, Issue 6, June 2017.

E-ISSN 2581 - 7957
P-ISSN 2277 - 3916

CVR Journal of Science and Technology, Volume 19, December 2020
DOI: 10.32377/cvrjst xxxx

# Template for the Preparation of Papers for Publication in CVR Journal of Science and Technology

First Dr. A. Author[1] and Second B. Author[2]
[1]Designation, Name of Institution/Department, City, Country
Email: first.author@hostname1.org
[2]Designation, Name of Institution/Department, City, Country
Email: second.author@hostname2.org

***Abstract:*** **These instructions give you basic guidelines for preparing camera-ready papers for CVR College journal Publications. Your cooperation in this matter will help in producing a high-quality journal.**

***Index Terms:*** **first term, second term, third term, fourth term, fifth term, sixth term**

## I. Introduction

Your goal is to simulate the usual appearance of papers in a Journal Publication of the CVR College. We are requesting that you follow these guidelines as closely as possible. It should be original work. Format must be done as per the template specified. Diagrams with good clarity with relevant reference within the text are to be given. References are to be cited within the body of the paper. Number of pages must not be less than five with minimum number of 4000 words and not exceeding eight pages. The journal is published in colour. Colours used for headings, subheadings and other captions must be strictly as per the template given in colour.

### *A. Full-Sized Camera-Ready (CR) Copy*

Prepare your CR paper in full-size format, on A4 paper (210 x 297 mm or 8.27 x 11.69 in). No header or footer, no page number.

*Type sizes and typefaces:* Follow the type sizes specified in Table I. As an aid in gauging type size, 1 point is about 0.35 mm. The size of the lowercase letter "j" will give the point size. Times New Roman has to be the font for main text. Paper should be single spaced.

*Margins:* Top and Bottom = 24.9mm (0.98 in), Left and Right = 16 mm (0.63 in). The column width is 86mm (3.39 in). The space between the two columns is 6mm (0.24 in). Paragraph indentation is 3.7 mm (0.15 in).

Left- and right-justify your columns. Use tables and figures to adjust column length. On the last page of your paper, adjust the lengths of the columns so that they are equal. Use automatic hyphenation and check spelling. Digitize or paste down figures.

For the Title use 24-point Times New Roman font, an initial capital letter for each word. Its paragraph description should be set so that the line spacing is single with 6-point spacing before and 6-point spacing after. Use two additional line spacings of 10 points before the beginning of the double column section, as shown above.

TABLE I.
TYPE SIZES FOR CAMERA-READY PAPERS

| Type size (pts.) | Appearance | | |
|---|---|---|---|
| | Regular | Bold | Italic |
| 6 | Table caption, table superscripts | | |
| 8 | Tables, table names, first letters in table captions, figure captions, footnotes, text subscripts, and superscripts | | |
| 9 | References, authors' biographies | Abstract | |
| 10 | Section titles, Authors' affiliations, main text, equations, first letters in section titles | | Subheading |
| 11 | Authors' names | | |
| 24 | Paper title | | |

Each major section begins with a Heading in 10-point Times New Roman font centered within the column and numbered using Roman numerals (except for REFERENCES), followed by a period, two spaces, and the title using an initial capital letter for each word. The remaining letters are in SMALL CAPITALS (8 point). The paragraph description of the section heading line should be set for 12 points before and 6 points after.

Subheadings should be 10 point, italic, left justified, and numbered with letters (A, B, …), followed by a period, two spaces, and the title using an initial capital letter for each word. The paragraph description of the subheading line should be set for 6 points before and 3 points after.

For main text, paragraph spacing should be single spaced, no space between paragraphs. Paragraph indentation should be 3.7mm/0.21in, but no indentation for abstract & index terms.

## II. Helpful Hints

### *A. Figures and tables*

Position figures and tables at the tops and bottoms of columns. Avoid placing them in the middle of columns. Large figures and tables may span across both columns. Leave sufficient room between the figures/tables and the main text. Figure captions should be centered below the figures; table captions should be centered above. Avoid placing figures and tables before their first mention in the

CVR Journal of Science and Technology, Volume 19, December 2020
DOI: 10.32377/cvrjst xxxx

text. Use the abbreviation "Fig. 1," even at the beginning of a sentence.

To figure axis labels, use words rather than symbols. Do not label axes only with units. Do not label axes with a ratio

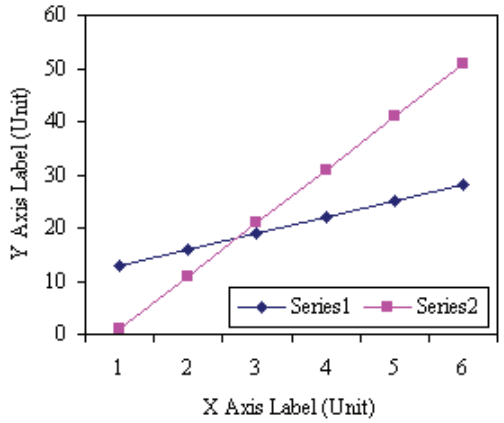


Figure 2. Note how the caption is centered in the column.

of quantities and units. Figure labels should be legible, about 8-point type.

All figures, tables and references must be cited in the text.

Please indicate the broad area/specializations into which the research paper falls, in the covering letter/mail to the Editor, so that reviewers with those specializations may be identified.

### B. References

Number citations consecutively in square brackets [1]. Punctuation follows the bracket [2]. Use "Ref. [3]" or "Reference [3]" at the beginning of a sentence:

Give all authors' names; use "et al." if there are six authors or more. Papers that have not been published, even if they have been submitted for publication, should be cited as "unpublished" [4]. Papers that have been accepted for publication should be cited as "in press" [5]. In a paper title, capitalize the first word and all other words except for conjunctions, prepositions less than seven letters, and prepositional phrases. Good number of references must be given.

**Latest references in the area must be included and every refence must be cited in the text of the research article.**

### C. Footnotes

Number footnotes separately in superscripts [1, 2, ···]. Place the actual footnote at the bottom of the column in which it was cited, as in this column. See first page footnote as an example.

### D. Abbreviations and Acronyms

Define abbreviations and acronyms the first time they are used in the text, even after they have been defined in the abstract. Do not use abbreviations in the title unless they are unavoidable.

### E. Equations

Equations should be left justified in the column. The paragraph description of the line containing the equation should be set for 6 points before and 6 points after. Number equations consecutively with equation numbers in parentheses flush with the right margin, as in (1). Italicize Roman symbols for quantities and variables, but not Greek symbols. Punctuate equations with commas or periods when they are part of a sentence, as in

$$a + b = c \ . \qquad (1)$$

Symbols in your equation should be defined before the equation appears or immediately following. Use "(1)," not "Eq. (1)" or "equation (1)," except at the beginning of a sentence: "Equation (1) is ..."

### F. Other Recommendations

Use either SI (MKS) or CGS as primary units. (SI units are encouraged.) If your native language is not English, try to get a native English-speaking colleague to proofread your paper. Do not add page numbers.

## III. Conclusions

The authors can conclude on the topic discussed and proposed, future enhancement of research work can also be briefed here.

## References

[1] G. Eason, B. Noble, and I. N. Sneddon, "On certain integrals of Lipschitz-Hankel type involving products of Bessel functions," Phil. Trans. Roy. Soc. London, vol. A247, pp. 529–551, April 1955.

[2] J. Clerk Maxwell, *A Treatise on Electricity and Magnetism*, 3rd ed., vol. 2. Oxford: Clarendon, 1892, pp.68–73.

[3] I. S. Jacobs and C. P. Bean, "Fine particles, thin films and exchange anisotropy," in *Magnetism*, vol. III, G. T. Rado and H. Suhl, Eds. New York: Academic, 1963, pp. 271–350.

[4] K. Elissa, "Title of paper if known," unpublished.

[5] R. Nicole, "Title of paper with only first word capitalized", *J. Name Stand. Abbrev.*, in press.

[6] Y. Yorozu, M. Hirano, K. Oka, and Y. Tagawa, "Electron spectroscopy studies on magneto-optical media and plastic substrate interface," *IEEE Transl. J. Magn. Japan*, vol. 2, pp. 740–741, August 1987 [Digests 9th Annual Conf. Magnetics Japan, p. 301, 1982].

[7] M. Young, *The Technical Writer's Handbook*. Mill Valley, CA: University Science, 1989.

[8] T. Ali, B.K. Subhash and R.C. Biradar, "A Miniaturized Decagonal Sierpinski UWB Fractal Antenna", PIERS C, vol. 84, pp. 161-174, 2018.

E-ISSN 2581 - 7957
P-ISSN 2277 - 3916



DOI: 10.32377/cvrjst xxxx

# In the next issue (vol. 20, June 2021)

1. ***Intelligent Aspect based Model for Efficient Sentiment Analysis of User Reviews*** — ***Prof. M. Deva Priya, R. Rithika***

2. ***Automation of Solar Panel Cleaning*** — ***A. Sairaj, Prof. K. Shashidhar Reddy***

3. ***FPGA Realization of Logic Gates using Neural Networks*** — ***R. Ganesh, D. Bhanu Prakash***

# ABOUT THE COLLEGE

CVR College of Engineering (A UGC Autonomous Institution) was established in the year 2001, and its Sixteenth batch of students graduated from the College. This college has been ranked **141** by **NIRF** among the Engineering institutions of the country for the fourth time in a row in the 101-150 range. The college also stands 3rd in Telangana for the 4th time consecutively.

The College was the **first** college in Telangana that was promoted by NRI technology professionals resident in the US. The NRI promoters are associated with cutting-edge technologies of the computer and electronics industry. They also have strong associations with other leading NRI professionals working for world-renowned companies like IBM, Intel, Cisco, Facebook, AT&T, Google and Apple who have agreed to associate with the College with a vision and passion to make the College a state-of-the-art engineering institution.

The college has many accomplishments and to name a few, it obtained **NBA Tier 1 accreditation for its UG Programs, NAAC 'A' grade , UGC autonomous status**, **National Employability Award** for seventh year in a row and received a very high rating by several ranking agencies including the most recent Education World ranking of third best college in Telangana and Outlook magazine, rating CVR CE, one among the **top 100 colleges in the country**, and **AAAA grade** from Careers 360.

The college has been sanctioned Rs.2.87 Crores from NEWGEN IEDC of the Department of Science and Technology. NEWGEN centre has been established to enable the staff and students to work on NEWGEN projects. 15 projects were completed in 2019-20 and 19 projects are lined up for the academic year 2020-21.

Faculty members are working on Rupees One crore worth projects with funding from AICTE, UGC and ISRO.

The students have brought home laurels by winning prizes in competitions outside the college. A batch of six students under the mentorship of Dr. Gaurav Sharma of the department of ECE won the FIRST prize of **Rs.1 Lakh** in the hardware version of the Smart India Hackathon in June 2019. A Group of three students of EIE and one student of IT have won the bronze cup along with a cash prize of **Rs. 50,000** in the Design contest by Mitsubishi Electric.

The college has been creating records year after year. With more than 100 companies visiting CVR and 930+ placements for the 2019-20 academic year, it is the highest among the peer group of colleges. The highest offer of **Rs. 30.25 Lakhs PA** was bagged by 7 students and close to 25 students got offers higher than **Rs. 10 Lakhs PA**. About 100 offers are higher than Rs. 6 Lakhs PA and another 60 offers are higher than Rs. 5 Lakhs PA. With this, CVR became the leading college in entire Telangana in terms of the offers with higher salaries. CVR has made huge progress in a short span of time and was preferred by the students and parents during the EAMCET counseling this year and is among the **top 3 colleges** in the state.

In keeping with the current global emphasis on green and eco-friendly energy generation, 360kW Solar PV plant has been installed on the campus to meet the power requirements of the college to a significant extent.

## CALL FOR PAPERS:

**Papers in Engineering, Science and Management disciplines are invited for Publication in our Journal. Authors are requested to mail their contributions to Editor, CVR Journal of Science and Technology (Email Id: journal@cvr.ac.in). Authors can also submit their papers through our online open journal system(OJS) www.ojs.cvr.ac.in or www.cvr.ac.in/ojs. Papers are to be written using a Standard Template, which may be obtained on request from the Editor. It is also available on the college website www.cvr.ac.in.**

# CVR JOURNAL OF SCIENCE AND TECHNOLOGY



## CVR COLLEGE OF ENGINEERING

(UGC Autonomous- Affiliated to JNTU Hyderabad)
Mangalpalli (V), Ibrahimpatnam (M),
R.R. District, Telangana - 501510
http://cvr.ac.in